

# **Use of Streamline Simulation in Large Scale Reservoir-Geomechanical Modeling of Reservoirs**

by

Behrooz Koohmarch Hosseini

A thesis submitted in partial fulfillment of the requirements for the degree of

Doctor of Philosophy

in

Petroleum Engineering

Civil and Environmental Engineering Department  
University of Alberta

© Behrooz Koohmarch Hosseini, 2015

## **Abstract**

The increasing demand for hydrocarbons and decreasing reserves have created the necessity to produce oil and gas more efficiently and economically. Increasingly, oil and gas companies are focusing on unconventional hydrocarbons; oil sands, shales and CBM. For this class of reservoir materials, the geomechanical response of the reservoir can play an important role in the recovery process. For naturally fractured, stress sensitive reservoirs or thermal recovery processes, geomechanical processes play an even greater role in efficient, economic recovery. For simulations of these processes, most research efforts have been focused on reservoir geomechanical simulations using conventional reservoir simulators coupled to geomechanical codes.

While coupled reservoir-geomechanics modeling has been recently widely studied in the literature, there is no applicable methodology implemented or proposed to mitigate the challenging computational cost involved with the inclusion of geomechanics in large multimillion-cell reservoirs. Past studies so far have focused on different coupling schemes, but not on the efficient and robust simulation workflows.

This research was conducted with the aim of development and application of various different strategies to include geomechanics into reservoir simulation workflows in large scale reservoirs and in a timely fashion process. The research was performed to allow the future simulators to perform high resolution reservoir-geomechanical simulations in a large scale (near field and far field) with long simulation time windows and lowest computational cost.

Initially, analytical proxies were developed and recommending for implementation in lieu of complex reservoir simulations. The analytical model was for prediction of heavy oil

geomechanical responses everywhere in the reservoir. The model adopted the use of the mathematical domain decomposition technique and a novel temperature front tracking developed in the very early stage of the research. As opposed to classical analytical models, the proxy predicted reservoir flow and mechanical behavior (on a synthetic case geometry with real hydraulic data) everywhere in the reservoir and in dynamic and transient flow regimes.

Subsequent research was aimed at reservoir-geomechanics coupled model order reduction by use of a numerical proxy. The proxy took advantage of streamline linear space behavior and power in decomposition of the reservoir domain into sub-systems (delineation/drainage areas). The combination of localization and linearization allowed predicting both mechanical and fluid flow responses of the reservoir with only solving the pressure equation in Cartesian underlying  $3D$  grids and the solution of saturation transport equation along only one streamline.

Following this, a streamline-based reservoir-geomechanics coupling was proposed and was implemented within a *Fortran-C++* based platform. The new developed technique was compared in terms of computational cost and results accuracy with the conventional hydromechanical coupling strategy that was developed on a *C++* based platform by use of collocated *FV-FEM* discretization scheme.

One of the final stages of the research explored different streamline-based reservoir-geomechanics coupling strategies for full-field reservoir simulations. Various coupling strategies including sequential coupling schemes and a semi-fully coupling scheme to embed geomechanics into streamline simulation workflow was developed and performed. Numerical software with advanced GUI was coded on *QT* programming language (*C++*

based) developed to couple mechanical simulator to streamline simulation engine. While streamline simulations were the center of the research, the last stage of research was conducted on numerical and physical stability, convergence and material balance errors of SL-based reservoir-geomechanics class of couplings. The results provided a solid foundation for proper selection of time-steps in SL-based coupling to ensure a numerically stable and physically robust hydromechanical simulation. As a result we showed that use of streamline simulation in both proxy forms and simulator forms have significant added value in full-field reservoir-geomechanics simulations.



## Preface

This dissertation is submitted for the degree of Doctor of Philosophy in Petroleum Engineering at the University of Alberta. The research described herein is original, and neither this nor any substantially similar dissertation was or is being submitted for any other degree or other qualification at any other university.

A version of **Chapter 3** was published in SPE Canadian Unconventional Resources Conference 2011 proceeding-OnePetro. A version of **Chapter 4** was submitted for publication in SPE peer reviewed Journal, SPE J. A version of **Chapter 5** was published in 9th International Geostatistics Congress proceeding 2012. . A version of **Chapter 6** was published in the proceeding of ARMA-47th U.S. Rock Mechanics-Geomechanics Symposium. A version of **Chapter 7** was published in the proceeding of SPE Heavy Oil Conference 2013-OnePetro. A combined version of **Chapter 6** and **Chapter 7** was submitted for publication in SPE Journal. A version of **Chapter 8** was published in the proceeding of ECMOR XIV (European Conference on the Mathematics of Oil Recovery), EAGE –EarthDoc library.

The most outstanding contributions of this dissertation are as follow: Inclusion of geomechanics into streamline simulation workflow and showing that the developed workflow was efficient, robust and effective for large-scale reservoir-geomechanics simulation, development of five different coupling strategies unique to streamline simulation workflow, providing longer coupling time steps ( by use of workflows) to avoid expensive geomechanical runs, and development of two different pressure field correctors/conditioner during forward cycles to mitigate the material balance errors. Finding the location of temperature front from saturation front at each time, and utilization of domain decomposition technique for full-field reservoir geomechanical solutions were novel as well.

I was the principal investigator, responsible for all major areas of concept formation, technical apparatus design, data collection and analysis, and manuscript composition. Dr. Chalaturnyk was the supervisory author on these papers and was involved throughout the concept formation and manuscript composition. The thesis explored and fully acknowledged the existing knowledge and references made at the end of each chapter. The personnel and institutions that financially and/or technically supported the research are acknowledged at the end of each chapter.

I spent about four months of my research work in Germany at University of Stuttgart (Department of Hydromechanics and Modeling of Hydrosystems) and shortly at the German Research Centre for Geosciences (GFZ) in Potsdam-Germany. The result of my work in Stuttgart contributed partly in formation of two chapters of my thesis.

*To my family and loved ones...*

## Acknowledgement

I would like to thank my intelligent supervisor, Dr. Rick Chalaturnyk that paved the path and enlightened the avenue of PhD for me. His advice, his encouragement for my research, his generous support, giving me the freedom of various ideas, and his nice attitude were indeed the key reasons to sustain my research thus far and stimulating. And finally thank you for the invaluable and applicable reservoir geomechanics knowledge that I gained over the last four years under your supervision and in your research group.

I would like to thank my family, parents, sisters and those without whose support and encouragement I could have not finished my Ph.D. I owe thanks to Parviz, Mitra, Bahareh, Banafsheh and Katherine for your unconditional support, energy and love, and thank you a lot for being beside me.

I would like to thank my examining committee members: Dr. Michael J. King (Texas A&M University), Dr. Alireza Nouri, Dr. Vinay Prasad, and Dr. Lijun Deng for their time, brilliant comments and valuable suggestions.

I am especially thankful to Rod Batycky (StreamSim Technologies) for his sustained support and technical discussions during the Ph.D., Dr. Holger Class (University of Stuttgart) for his support during my research visit in Germany.

I would also like to thank my colleagues and friends at university of Alberta for their direct or indirect supports and in particular all the students and staff of GeoREF-Reservoir Geomechanics research group.

My appreciations are extended to Helmholtz-Alberta-Innovative program, Foundation CMG Research Program in Reservoir Geomechanics for funding this research and to Itasca Consulting Inc. and StreamSim Technologies, Inc. for providing academic licenses and research code.

I would also express my thanks to Dr. Tony Settari, Daniel Moos, Robert Marsden, Marco R.Thiele, Tatyana Katsaga, and Adrian Herrera for their comments and fruitful discussions mainly on the current issues of reservoir geomechanics or streamline simulation.

## Table of Contents

Abstract.....	ii
Preface.....	v
<b>Chapter 1 : Introduction.....</b>	<b>1</b>
Introduction .....	1
Statement of Problem.....	3
Thesis Objective .....	5
Thesis Approach.....	5
Thesis Scope and Methodology .....	7
Structure of Dissertation .....	10
<b>Chapter 2 : Literature Survey .....</b>	<b>11</b>
<b>Chapter 3 : A New Analytical Approach To Investigate Heated Area in Thermal Recovery Techniques .....</b>	<b>23</b>
Introduction .....	23
Results and Discussions .....	34
Conclusions .....	37
Nomenclature.....	38
<b>Chapter 4 : A Domain Splitting-Based Analytical Model for Rapid Assessment of Hydro-thermo-geomechanical Responses of Large Scale Heavy Oil Reservoirs: A Steamflood Application .....</b>	<b>40</b>
Introduction .....	40
Domain Splitting Algorithm.....	46
Discussion.....	67
Conclusion.....	70
Nomenclature.....	70
<b>Chapter 5 : Reservoir-Geomechanics Model Order Reduction by Use of Streamline-Based Domain Decomposition and Linearization.....</b>	<b>72</b>
Introduction .....	72
Development of the Method for Linearization and Reduction of Reservoir Model .....	77
Inclusion of Geomechanics in the Proxy Development Workflow.....	82
Conclusion.....	94
<b>Chapter 6 : Inclusion of Geomechanics in Streamline Simulation for Hydromechanical Modeling of Underground CO<sub>2</sub> Storage.....</b>	<b>96</b>
Introduction .....	96
Model Geometry and Boundary Conditions.....	100
Discretization Scheme .....	103
Hydromechanical Coupling.....	108
Results and Discussions .....	111
Discussions.....	121
Conclusions .....	122
Acknowledgement.....	123
<b>Chapter 7 : Streamline-Based Coupled Geomechanics and Reservoir Simulation for Hydromechanical Modelling of CO<sub>2</sub> Storage in Saline Aquifers .....</b>	<b>125</b>
Introduction .....	125
Numerical Analysis.....	131
Comparison of the Coupling Strategies (Streamline-based vs. Box Method: FV-FEM).....	133
Discussion.....	142
Summary and Conclusions.....	143
Acknowledgement.....	145
<b>Chapter 8 : Streamline-based Reservoir Geomechanics Coupling Strategies for Full Field Simulations.....</b>	<b>146</b>
Introduction .....	146

Coupling Strategies.....	150
Results and Discussion.....	160
Conclusions .....	177
Acknowledgement.....	178
<b>Chapter 9 : On Stability and Material Balance of Full-Field Streamline-Based Reservoir</b>	
<b>Geomechanics Couplings.....</b>	<b>179</b>
Introduction .....	179
Stability and Convergence Study.....	182
Material Balance Error.....	190
Drained vs. Undrained.....	194
Compressible vs. Incompressible .....	197
Homogenous vs. Heterogeneous.....	199
Results and discussions.....	200
Conclusions .....	207
<b>Chapter 10 : Conclusion and Recommendations for Future Studies .....</b>	<b>209</b>
References.....	217

## List of Tables

### Chapter 3

Table 3-1-Main numerical simulation parameters-Hot water flooding .....	36
---	----

### Chapter 4

Table 4-1-Reservoir fluid and rock properties .....	60
---	----

### Chapter 5

Table 5-1-RMSE of state variables of the proposed method .....	89
--	----

Table 5-2- NRMS of state variables related to streamlines .....	89
---	----

### Chapter 6

Table 6-1-Reservoir hydraulic parameters .....	111
--	-----

Table 6-2-Reservoir mechanical parameters .....	111
---	-----

### Chapter 7

Table 7-1-Model dimensions .....	132
----------------------------------	-----

### Chapter 8

Table 8-1- Reservoir fluid and rock properties of Case 1 .....	160
--	-----

Table 8-2- Reservoir fluid and rock properties of Case 2 .....	161
--	-----

## List of Figures

### Chapter 1

Figure 1-1- Conceptual diagram explaining the combination and overlapping of the required approaches to include geomechanics in full field scale.

### Chapter 2

Figure 2-1-Schematic flowchart showing the successive steps of streamline simulation.....19

Figure 2-2-Conceptual sketch of sequential physical mechanisms of CO<sub>2</sub> storage -Zhdanov et al. (2013).....20

### Chapter 3

Figure 3-1- Temperature contours at different instances before breakthrough.....26

Figure 3-2- Graphical representation of saturation and temperature profile in a radial system when both heat and hot water flow mechanisms are convective. ....28

Figure 3-3- Water saturation and temperature front profiles in the hot waterflooding of sandpack... ....36

Figure 3-4- Temperature (b) and water saturation (a) distribution in a 1-D sandpack hot waterflood after 8 hours. ....36

Figure 3-5- Water saturation and temperature profiles in the steamflooding of sandpack. ....37

### Chapter 4

Figure 4-1-Temperature profile in space where heat flux mechanisms are both convective and conductive.....46

Figure 4-2-Temperature profile in space where heat flux mechanism is purely conductive .....46

Figure 4-3- Representation of zone 1 and geomechanical boundary conditions .....48

Figure 4-4-Representation of boundary conditions in Domain II.....54

Figure 4-5- Pressure profile changes, beyond steam chamber where geomechanical reservoir volume responses are taken into account. ....59

Figure 4-6-Pressure distribution (a) and temperature distribution (b) in a steamflood numerical simulation after 4 years of injection.....61

Figure 4-7-Pressure and temperature changes in time (a), and the individual volumetric strain changes due to temperature and pressure changes (b) .....62

Figure 4-8-Porosity changes due to volumetric strain changes in a steamflood case .....63

Figure 4-9-Dimensionless parameter  $\xi^*$  (ratio of temperature front distance to saturation front distance) versus porosity at different steam chamber temperatures.....64

Figure 4-10- Cross-sectional (x-z plane) representation of vertical displacement contour (a), horizontal stress contour (b), vertical displacement profile (c) and horizontal stress profile (d) versus distance .....65

Figure 4-11- Vertical displacement in meters along x horizontal-axis: validation of the analytical model with coupled numerical model in the middle of the reservoir.....66

### Chapter 5

Figure 5-1-Schematic description of flow simulator and definition of sub-systems.....77

Figure 5-2-Workflow and steps for SL\_based model order reduction of reservoir-geomechanics of large scale reservoirs.....85

Figure 5-3-Streamline configuration of the two-dimensional model (case I). Illustration of two drainage areas (operating regimes), represented by I2-P2 and I1-P1. ....87

Figure 5-4-Comparison between estimated pressure of reduced cells by proposed model and values of streamline simulator, Time step=3.....88

Figure 5-5-Comparison between estimated pressure of reduced cells by proposed model and values of streamline simulator, Time step=7.....88

Figure 5-6-Comparison between estimated pressure of reduced cells by proposed model and values of streamline simulator, Time step=10.....89

Figure 5-7-Model II: Permeability distribution mapped on 3D geo-model (left).Streamline distributions colored based on well-pair drainage areas (right).....90

Figure 5-8 -Matching results between simulation data and proposed linearized method's results for first grid of second streamline .....91

Figure 5-9- Representation of system decomposition into subdomains – model localization. ....	92
Figure 5-10-Representation of number of streamline per grid-cell as an index for selection of geomechanical coupling domain localization. ....	92
Figure 5-11-Pressure versus distance, representation of impact of pressure difference and pressure gradient and individual influence on the stress tensor components.....	93
Figure 5-12-Comparison of permeability changes due to changes in shear stress versus changes in principal stresses (after Chalaturnyk, 1996).....	94

## Chapter 6

Figure 6-1-Schematic of a reservoir target and CO <sub>2</sub> plume migration in a host geological formation (Zhdanov et al., 2013) .....	97
Figure 6-2- Conceptual sketch of sequential physical mechanisms of CO <sub>2</sub> storage .....	97
Figure 6-3-Schematic description of the model geometry and flow and geomechanical boundary conditions .....	102
Figure 6-4-Schematic of spatial discretization (Fully coupled Scheme) .....	105
Figure 6-5-Schematic of spatial discretization (decoupled Flow and Geomechanics) .....	106
Figure 6-6-Schematic of coupling strategy for sequential Streamline Based Flow &Geomechanical simulator.....	109
Figure 6-7-Cross-sectional CO <sub>2</sub> saturation map in different time steps of simulation: $t_1=100$ days, $t_2=200$ days, $t_3=300$ days, $t_4=400$ days, $t_5=700$ days $t_6=800$ days.....	113
Figure 6-8-Streamline configuration represented after 500 days (a) and 900 days (b) of injection.....	113
Figure 6-9-Evolution of CO <sub>2</sub> plume in the aquifer for the same model as before with coarse grids. $t_1=100$ , $t_2=200$ , $t_3=300$ , $t_4=400$ , $t_5=700$ , $t_6=800$ days. ....	114
Figure 6-10-Impact of grid refinement on computational load for pure streamline simulation .....	115
Figure 6-11- Representation of model top view: (a) shows signature of CO <sub>2</sub> after 900 days, and (b) shows the corresponding streamlines configuration for the same time of injection.....	116
Figure 6-12-Lateral view of 3D-model representing (a) CO <sub>2</sub> saturation map, and (b) shows corresponding streamline configuration after 1500 days of injection. Injection well is located in the middle of the domain. ....	117
Figure 6-13-Histogram of CO <sub>2</sub> saturation after 500 days of injection in a streamline-based hydromechanically coupled scheme (right) and in a coupled streamline simulation (left) .....	118
Figure 6-14-Permeability difference map between cycle 9 (900 days after injection) and cycle 1.....	118
Figure 6-15- Scatter-gram between porosity (in all cells) in cycle 1 -100 days vs. porosity values at cycle 9 .....	119
Figure 6-16-Scatter-gram between porosity (in all cells) in cycle 1 -100 days vs. porosity values at cycle 9 .....	119
Figure 6-17-Histogram of vertical displacement ( $u_{zz}$ in $z$ ) direction after 4 cycles (400 days of CO <sub>2</sub> injection).....	120
Figure 6-18-Histogram of $u_{xx}$ displacement in $x$ direction after 4 cycles (400 days of CO <sub>2</sub> injection) .....	120

## Chapter 7

Figure 7-1-Distribution of lateral displacement ( $u_x$ ) on $x$ - $z$ plane cross-section after 400 days of coupled simulation, from bottom to top of the reservoir .....	128
Figure 7-2-Distribution of vertical displacement ( $u_z$ ) on $x$ - $z$ plane cross-section after 400 days of coupled simulation, from bottom to top of the reservoir .....	128
Figure 7-3-Lateral displacements on top of the reservoir (left) and in the middle of the reservoir (right) on $x$ - $y$ plane, orthogonal to $z$ -axis at $t=400$ days .....	129
Figure 7-4- Lateral effective stress ( $S_{xx}$ : left ; $S_{yy}$ : right) on $x$ - $y$ plane in middle model cross-section $t=500$ d .....	130
Figure 7-5-Contour plot of effective lateral stress in $X$ direction ( $S_{xx}$ ), left and $S_{yy}$ , right on $x$ - $y$ plane in the middle of the reservoir at $t=500$ days. ....	130
Figure 7-6-Contour plot of effective vertical stress ( $S_{zz}$ ), on right and its distribution on left, both displayed on $x$ - $y$ plane in the middle of the reservoir at $t=500$ days .....	131
Figure 7-7-SL-Based reservoir-geomechanics, scaling behaviour for a homogenous reservoir. ....	133
Figure 7-8-Finite Volume-based reservoir-geomechanics scaling behaviour for a homogenous reservoir.....	135
Figure 7-9-Cumulative computational cost scaling behaviour (streamline-based hydromechanical coupling).....	136



Figure 7-10- Cumulative computational cost scaling behaviour: streamline-based hydromechanical coupling vs. finite-volume based hydromechanical coupling .....	137
Figure 7-11-CPU load behavior of streamline simulation in the course of forward simulation.....	138
Figure 7-12-Geomechanical simulation CPU run-time for each sub-interval of coupled simulation .....	139
Figure 7-13- FV-based fluid flow CPU run-time for each sub-interval of coupled simulation.....	140
Figure 7-14-Porosity distribution after 400 days of coupled simulation-LHS picture (finite-volume coupled simulation), RHS (SL-based coupled simulation) .....	141
Figure 7-15-Volumetric strain profile along x-axis on the middle $\bar{x}$ -plane cross section after 400 days.....	142

## Chapter 8

Figure 8-1-Schematic of coupling strategy for one-way streamline-based hydromechanical coupling with constant user forced- time steps. ....	152
Figure 8-2-Schematic of coupling strategy for sequential streamline-based hydromechanical coupling with constant user constrained time steps .....	154
Figure 8-3-Schematic of coupling strategy for sequential streamline-based hydromechanical coupling with staggered approach .....	155
Figure 8-4- Numerical time steps evolution for semi-fully coupling of streamline simulation-geomechanics.....	156
Figure 8-5-Schematic of full flight coupling scheme for sequential streamline-based hydromechanical coupling .....	158
Figure 8-6-Schematic of adaptive long time step coupling scheme for streamline-based geomechanical coupling- example on staggered technique .....	159
Figure 8-7- Comparison of streamline configurations along with mapped time of flights on streamlines at two different cycles: a) cycle 2 and b) cycle 9.....	162
Figure 8-8- Comparison of streamline configurations: a) coupled and b) uncoupled and well allocation factor maps: c) coupled and d) uncoupled after 4000 days.....	165
Figure 8-9- Impact of inclusion of geomechanics (through Approach 2) into streamline simulation on cumulative production data within 4000 days of production .....	165
Figure 8-10- Initial permeability distribution of the reservoir and well configuration (left), and updated permeability map due to reservoir geomechanical effects (right). ....	166
Figure 8-11-Left picture compares field oil rate by use of Approach 2 versus Approach 3 and right picture shows the top view of pressure field ratio of Approach 2 over Approach 3, at cycle 5 (400-500 days) .....	166
Figure 8-12-Comparison of production data in coupled system from Approach 2 vs. Approach 3. Left figure shows cumulative field oil production and right figure shows field water cut rate .....	167
Figure 8-13- Left figure shows pressure ratio and right figure shows saturation field ratio of Semi-fully coupled approach over Staggered approach (3). ....	168
Figure 8-14- Comparison of production data between Staggered Approach (3) vs Semi-fully coupled Approach.....	168
Figure 8-15- Comparison of total CPU run time of Staggered Approach (3) vs Semi-fully coupled Approach in model 1 within 1000 days of coupled simulation run with 10 cycles and 3 inner-cycles. ....	169
Figure 8-16- Convergence of field oil production and water cut rates by use of Approach 4 at 10 full flight cycles over 4000 days of coupled simulation. ....	170
Figure 8-17- Illustration of off-diagonal stress tensor component $\sigma_{xy}$ (top) and horizontal displacement along x axis (bottom) at four different time steps. ....	171
Figure 8-18-Vertical displacement history in the middle of the reservoir out of one way coupling. ....	172
Figure 8-19- Comparison of two different Approaches (2 and 3) at a coupling time step of 400 days (left) and 100 days (right). Representation of average reservoir pressure and reservoir gas injection rate. ....	173
Figure 8-20- Individual cyclic CPU run time of streamline versus geomechanics for different coupling strategies .....	174
Figure 8-21- Comparison of computational load involved in each coupling strategy on the 3D model with 2000 active cells on 20 cycles with coupling time step of 100 days.....	175

Figure 8-22-Comparison of streamline simulation CPU runtimes in Approach 3 (staggered) vs. Semi-fully coupled approach, with 20 cycles and 5 inner cycles (model size 20x20x10). .....	175
Figure 8-23-Comparison of computational load of Approach 3 (staggered) with Semi-fully coupled, on the 3D model with 2000 active cells on 20 cycles and 5 inner-cycles with coupling time step of 100 days.....	176
Figure 8-24-Example of linear scaling of coupled streamline-geomechanics run time (Approach 2, $\Delta T=100$ days) versus number of active grid-blocks for an incompressible CO <sub>2</sub> injection scenario.....	177

## Chapter 9

Figure 9-1-Representation of material balance error correction paths.....	192
Figure 9-2-Representation of streamline-geomechanics coupling workflows; comparison of optimized coupling scheme for drained (left) versus undrained (right) split methods. ....	197
Figure 9-3-Rate surface GOR gas oil ratio (top), surface oil rate (middle), cumulative reservoir gas production (bottom). ....	202
Figure 9-4-Convergence of the coupled system solution through Approach 3 appears to occur at around $\Delta t_{\text{coupling}}=150$ days (0.05 PVI). Representation of field GOR (left) and field oil rate (right).....	202
Figure 9-5-Convergence of field oil production and water cut rates by use of Approach 4 at 10 full flight cycles over 4000 days of coupled simulation. ....	203
Figure 9-6- Convergence of Approach 2 (left) at $DT=100, 200, 400$ days and convergence behavior of Approach 3 (right) at $DT=50, 100, 200, 400$ on average reservoir pressure.....	204
Figure 9-7-Uncoupled problem convergence study of model 3 on streamline standalone mode. a) in-place reservoir gas in time and b) average reservoir pressure. The comparison is performed on three progressive time steps equivalent to 0.01, 0.05 and 0.1 reservoir pore volume. ....	205
Figure 9-8-Convergence study of Approach 3 at progressive coupling time steps of 50, 100, 200 and 400 days when streamline global time steps are 0.1 pore volumes. Representation of reservoir gas injection rate (left) and average reservoir pressure (right) .....	206
Figure 9-9-Convergence study of Approach 3 at progressive coupling time steps of 200, 400 and 1000 days when streamline global time steps are 0.05 pore volumes. Representation of average in place reservoir pressure and cumulative mass water production at the model boundaries due to injection of supercritical CO <sub>2</sub> . ....	206
Figure 9-10-Convergence of reservoir gas injection rate by use of Approach 4 in 10 full flight cycles .....	207

## Chapter 10

Figure 10-1- Graphical User Interface Developed by QT Programming Language for hydromechanical coupling of Streamline simulation with C++ Geomechanical code .....	235
Figure 10-2-Schematic of interactive coupling between streamline simulation and geomechanical code.....	236
Figure 10-3-Schematic of interactive coupling between fluid flow simulation (FVE and FEM) and geomechanical code.....	236
Figure 10-4-Illustration of step 1 and 2. ....	237
Figure 10-5- Illustration of steps 3 and 4. ....	238
Figure 10-6-Representation of Step 5. ....	238
Figure 10-7-Illustration of steps 6, 7, 8. ....	239
Figure 10-8-Illustration of Step 10.....	239
Figure 10-9-Illustration of Step 11.....	240

# Chapter 1: Introduction

## Introduction

The increasing demand for hydrocarbons and decreasing reserves have created the necessity to produce oil and gas more efficiently and economically. Increasingly, oil and gas companies are focusing on unconventional hydrocarbons; oil sands, shales and coalbed methane (CBM). For this class of reservoir materials, the geomechanical response of the reservoir can play an important role in the recovery process. For naturally fractured, stress sensitive reservoirs or thermal recovery processes, geomechanical processes play an even greater role in efficient, economic recovery.

The origins of geomechanics in the oil and gas industry were in hydraulic fracturing, where the stimulation engineer wanted to know the wellbore pressures required to overcome formation stress and splitting the rock, and the likely extent and direction of the induced fracture. Later, geomechanics was applied in sand production problems, and wellbore stability issues (mainly due to stuck pipe in tight holes), and in over-pressure calculation and estimate of overburden shale formation pressure. And lately geomechanics has been applied in the production mechanisms. The major reservoir geomechanical response due to production was known as subsidence created by compacting reservoirs - probably one of the best-known examples of rock mechanical effects on “reservoir scale” behavior. There are some environmental and operational concerns associated with the subsidence problem such as risk of flooding, or platform integrity in offshore production sites, and major casing collapse in a compacting reservoir. Ekofisk and Valhall field in North Sea and Belridge in California and Goose Creek in Texas are some examples of where geomechanical changes due to (oil) production have led to pore reduction, collapse and reservoir compaction. The notable examples of this type of geomechanical impacts on a reservoir are: 8.5 meters of subsidence in Ekofisk, 0.4 meter in Groningen in Netherlands, 10 meters in Wilmington in California, and 400 mm per year in Belridge, San Joaquin Valley in California. Reservoir geomechanics also helps better understand stress state changes due to production, fault reactivation, and assists in the careful design of underground gas storage facilities where the reservoir may be over pressured (above the initial field pressure), and influence the integrity

of the caprock. It is well established that compaction may be a key drive mechanism in soft oil reservoirs (Fjær et. al., 2008).

The other major impact of geomechanics on reservoir dynamic performance is on production and recovery mechanism for both conventional and unconventional reservoirs. Injection into the reservoir or production from the field changes pore pressure in the reservoir. Pressure depletion (due to production) leads to changes in earth stresses; not only in effective stress, but also in the total stresses. Temperature changes in thermal recovery mechanisms can have the same impact and cause changes in the stress state. These stress changes control not only compaction and subsidence, but may also lead to changes in the fluid flow performance of the reservoir, mainly by changing the petrophysical properties of the reservoir. Permeability for instance may change significantly, and accordingly the preferential flow paths, may be altered as well.

Therefore, for both types of challenges (effect on production and recovery mechanism, and environmental risks), the reservoir geomechanical impacts have recently attracted increased attention. Therefore reservoir geomechanical responses are important information that needs to be taken into account for reservoir management and proper production optimization during life cycle development of a reservoir.

Production forecasts in petroleum reservoirs are most often computed by reservoir simulators, based on numerical solution of the equations for flow in porous media, and conventional simulators do not fully consider the compaction of the porous rock into account. However geomechanics is an important process to be modeled reliably, as it can have strong influence on pressure development, flow pattern and field production rate. For simulations of these processes, most research efforts have been focused on reservoir geomechanical simulations using conventional reservoir simulators coupled to geomechanical codes. Geomechanical models allow predicting reservoir compaction from pressure depletion, describing in situ stresses, rock mechanical parameters, among others, leading to production strategies to be optimized; and commercial simulators have been developed for this purpose, recognizing the impact of geomechanics on ultimate recovery.

Fully coupling of all these problems can be computationally cumbersome, particularly if the physics (fluid flow and geomechanics) are complicated and or the reservoir is large with multi-million grid-blocks. And sometimes due to computational cost of conventional

simulators (using finite difference or finite-volume techniques), it is not possible to work directly with them particularly for field (i.e., large scale) applications.

## Statement of Problem

Accurate numerical simulation of large unconventional reservoirs (such as naturally fractured reservoirs, heavy oil reservoirs or underground CO<sub>2</sub> storage reservoirs) on a field scale is time-consuming and computationally expensive. One of the preliminary studies on the coupling of fluid flow processes with rock mechanics is Gutierrez and Lewis (1998) that extend Biot's theory to multi-phase fluid flow in deformable porous media. Based on their formulation, they conclude that the coupling between the geomechanics and the multi-phase flow occurs simultaneously. Thus, fully coupled system equations of deformations, multi-phase flow and heat transfer should be solved simultaneously. However the problem of solving such a non-linear system is computationally expensive and occasionally, a problem may not even converge to a unique solution<sup>1</sup>. For instance, the thermo-hydraulic (neglecting geomechanics) simulation run time of a 3D heterogeneous model with one well pair can exceed two days in simulation time. Therefore conventionally the geomechanical simulation of the reservoir is either neglected or is investigated only in the vicinity of injection well that is subjected to more pressure changes and accordingly more geomechanical changes. The fully coupling approach is therefore not recommended for large-scale problems (with large number of grid-cells) or for full-field reservoirs. The computational load of this technique restricts the application of the method to either very short simulation time-spans or to very small-scale and near-field problems (such as wellbore stability). Under these conditions, analytical methods can be used as approximate techniques instead of numerical simulators, particularly for flat-layered simple shape reservoirs. For stress-sensitive heavy oil reservoirs, where geomechanical responses are taken into account, and at the same time uncertainty quantification, or ranking of realizations<sup>2</sup>, or optimization of well trajectories are desired, the use of analytical proxies are of even greater importance; since the successive numerical simulation of multi-physics processes (either fully coupling or partial coupling) is technically impossible with current computer CPUs (at least in a timely fashion). In thermal recovery techniques, the analytical models assume the heated zone is the same as the zone that hot

<sup>1</sup> However they are unconditionally stable when the simulations is implemented fully implicitly

<sup>2</sup> To assist in selection of a subset of realizations for more precise analysis

water or steam has penetrated through the reservoir, which is generally not the case in reality. This assumption can influence the description of stress and geomechanical responses of the reservoir; the reason is that the stresses induced by thermal effects are different in magnitude and nature than the stresses developed due to pressure and saturation changes. Consideration of this effect in thermal recovery techniques, and devising an analytical method that relates (calculate) the heated zone volume, to the volume of saturated or pressurized zone, and at the same time assesses the geomechanical impacts of each zone separately, is important.

Analytical techniques however are not always the best candidates to simulate the reservoir flow and geomechanical behaviours. Simulation of complex fractured reservoirs with heterogeneous petrophysical and geomechanical properties, with reservoir rocks of non-linear constitutive behavior, and multiphase flow mechanisms, calls for a numerical detailed simulation. This approach is widely more accepted, mainly due to rapid recent progress in computer technology. Fully coupled techniques were presented (Gutierrez and Lewis, 1998) as the most accurate but most expensive simulation approach as well and may face challenging convergence issues. To tackle the convergence issues and to reduce the relatively high computational cost involved in fully coupled (or fully implicit techniques), explicit methods have replaced them for the solution of larger size problems. Different explicit methods of coupling such as sequential one-way or iterative coupling have been used. Even for these methods, their (extremely) high computational costs have prevented their wide-scale application in full-field studies (Tran et al. 2004), unless it is implemented on a very coarse grid-blocks model, which in turn would significantly affect the resolution of the solution. Therefore development of a numerical technique and strategy that is able to capture the geomechanical impacts of the reservoir and at the same time can be applied on a fine-grid full-field scale is worthwhile. Looking at the hydro-geomechanical problem as an explicit problem, that fluid flow problem is solved explicitly from rock deformation problem, allows us to enhance the coupling strategy in terms of computational efficiency by use of numerical fluid flow proxies. This approach is most suitable for the cases where inclusion of geomechanics is important, but at the same time the number of simulation-runs is required for history matching purposes. The approach is still numerical and therefore is able to capture a more robust physics of the reservoir into account. By use of numerical proxies, the

load of coupling is expected to reduce significantly, as the burden on the fluid-flow component of a coupled simulation is significantly removed.

## Thesis Objective

Proxy models to predict the performance of thermal recovery processes are useful tools for preliminary forecasting purposes and sensitivity studies and provide a better insight than simulation models into the physics of thermal and hydrogeomechanical processes. This research, at first place, targets at development of analytical proxies for quick estimate of heated area and rapid geomechanical assessment in thermal recovery techniques of large-scale reservoirs. The other objective of this research is to develop a numerical linear streamline-based proxy for fast fluid flow simulation and ultimately large-scale geomechanical coupling.

This research introduces a new hydro-geomechanical coupling methodology for faster coupled simulations and reduction of computational loads involved in large reservoir systems. Initially, the feasibility of coupling between a newly developed geomechanical code and streamline simulation technique, is investigated, and later the developed coupling scheme applied in the hydromechanical modeling of CO<sub>2</sub> storage. This study also explores different coupling strategies for inclusion of geomechanics into streamline simulation; as well as the feasibility of implementation and the assessment of computational efficiency of each strategy. Incorporation of geomechanics into streamline simulation for hydro-geomechanical simulation of reservoirs is quite novel in the literature. The eventual aim is to develop the capability of making predictive simulations of large scale full-field models.

## Thesis Approach

### **Development of an Analytical Proxy for Large-Scale Thermo Hydro-mechanical Modeling (near and far-field assessment of stress/strain field)**

For development of the analytical proxy for hydro-geomechanical estimate of heavy oil reserves, decomposition of the whole domain into two parts of “heated zone” and “wetted zone” is proposed. An exact analytical model is required that relates the saturation front of injected hot water to temperature front. The frontal velocities are dynamic interfaces for compartmentalization of the domain. Since the intensity and complexity of reservoir geomechanics vary over reservoir domain, one can divide the reservoir into sub-domains and assess different reservoir geomechanical responses separately in each sub-domain. In the

heated zone, the total induced stresses result from both temperature and pressure increase, and in the wetted (saturated) zone beyond the temperature front the total stress change is a function of pressure change only, and accordingly stress and strain induced are due to isotropic unloading. Shear deformation is expected to occur in the near-field zone and more compression or volumetric deformation is expected to happen in the wetted zone. This technique provides a rapid insight into both thermal flow of hot water or steam in the reservoir, as well as the geomechanical processes in each part (near field and far field) of the reservoir. For hot water flooding of large stress sensitive reserves where multiple simulations runs of flow and geomechanics are needed, this approach (analytical domain decomposition) becomes a very practical methodology.

### **Development and Application of a Linear Numerical Streamline-Based Proxy (rapid assessment of fluid flow and geomechanical processes)**

This work takes advantage of streamlines, by using information gleaned from streamline trajectories. Mathematical methods (e.g. singular value decomposition) are frequently used in “reservoir model order reduction” procedures. In this work streamlines are used as an alternative to these classical techniques to decide about which grid blocks’ state variables are mostly effective on each local model. Since the state variables are a complete description of a system, the reservoir can be thoroughly described through state variables and related to the remaining streamlines of the cells. It is shown that local models, which are highly nonlinear in Cartesian or radial coordinates, are linear in streamline-based coordinates. This contributes to have a linear global model with the advantage that analyzing and controlling the behavior of a linear system is much easier than a nonlinear one. The results of simulation on two synthetic field cases will be verified to check the robustness of the method. This technique is well suited to the “ranking” of development scenarios. Ranking of geological and geomechanical models (e.g. MEM properties) is conventionally performed for the purpose of quantifying the uncertainties associated with the space geological and geomechanical static model and their impact on potential development scenarios. The speed of the streamline methods makes them an acceptable and effective way of uncertainty estimation. The proposed proxy model provides an approximate method that is even faster than streamline simulation approach and has less complexity due to its linearity and simpler input variables.



## Coupled Streamline-Based Fluid Flow and Geomechanics (Inclusion of geomechanics in streamline simulation)

Where numerical modeling of the reservoir is essential and hydro-geomechanical modeling of a large heterogeneous reservoir with large number of grid-cells is required, the key idea of this research is exploring and implementation of different methodologies for incorporation of geomechanics into streamline simulation. In order to be able to include geomechanics into fluid flow in a large (e.g. field) scale or improve solution speeds with the inclusion of geomechanics, different approaches can be used.

Brief descriptions are provided below of the techniques adopted in this research to tackle the problem of “scale” and “time” in coupled flow-geomechanics techniques. **Figure 1-1** summarizes all the steps and approaches taken in this research to include geomechanics in the full field scale.

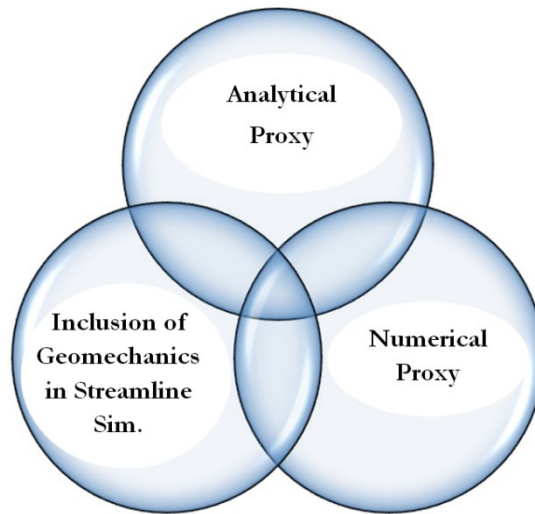


**Figure 1-1- Conceptual diagram explaining the combination and overlapping of the required approaches to include geomechanics in full field scale into conventional and unconventional reservoir simulation workflows**

## Thesis Scope and Methodology

### Development and Implementation of Proxies

For development of the numerical proxy, Matlab programming language was used for both numerical analysis and model order reduction and for scripting purposes. The code has to import the outputted data from fluid flow simulation and streamline trajectories. The numerical proxy is a linearized streamline-based approach and the method’s efficiency and

generality is assessed using synthetic examples of increasing complexity; two synthetic field cases, with synthetic data are selected. The analytical proxy for thermal recovery technique is developed based on some exact method of mass, momentum and heat conservation. Since it is an approximate method, it is benchmarked/validated against a numerical simulation case. The fluid flow and geomechanical simulation of the model were done through a coupled system of FLAC3D and CMG-STARs.

## **Development of a Coupling Interface between FLAC-3D and CMG-STARs**

To validate the analytical proxy with a numerical scheme, FLAC3D was coupled with CMG-STARs for a steamflood scenario by use of Visual Basic Programming Language (plugged in excel macro).

### **Geomechanical Code Development**

The geomechanical code is basically developed based on an existing fully coupled flow-geomechanics code which is a module of open source code simulator Dumux (Flemish et al., 2011) which is based on Distributed and Unified Numerics Environment DUNE (Bastian et al., 2008). The idea was simply to decouple geomechanics code from fully coupled flow-geomechanics code. The discretization scheme utilized the Box-Method (collocated finite volume and finite element method), which is locally mass conservative and can be applied to unstructured grids, for geomechanical simulation. This code is employed for coupling to streamline simulation FORTRAN code for the problem of CO<sub>2</sub> underground storage.

### **Interface and Coupling Tool Development (C++ programming)**

For assessments of streamline simulations coupled to geomechanics, three sets of interfaces need to be developed. The first interface couples the decoupled geomechanical code to streamline code, the second one is the interface which transfers the solution vectors (of primary variables of simulation) from finite volume fluid flow code to finite volume geomechanical code, and the third interface couples the geomechanical software, FLAC 3D (product of Itasca) to streamline simulator (3DSL). The first two interfaces are developed in a Linux environment, and the last one is developed in Windows. The main interface that has to be developed is a C++ based interface which links the decoupled geomechanical code (in Dumux and on Dune Platform) to fluid flow code. This new interface is unlike typical

interfaces in commercial software where “restart files” or “AASCII text files” are used as an exchangeable file for initialization step of next sequential time steps. The new interface exchanges properties between flow and geomechanics code by solution vectors within the frame of the code. Therefore a C++ routine was written in Dumux-Geomechanics to output the vectors for Dumux-Flow, and at the same time a routine was developed to read the solution vectors outputted by Dumux-Geomechanics (porosity and permeability). The first two interfaces were used for the study of streamline-based hydromechanical coupling for a CO<sub>2</sub> storage scenario.

### **Development of Synthetic Large CO<sub>2</sub> Model with Large Number of Grid-Cells**

For hydromechanical modeling, a streamline-based simulation model that is three-dimensional, two-phase, compressible and isothermal was developed with the same model made in the Dumux-Flow module for code comparison reasons. A geomechanical model with proper stress boundary and initialization conditions was also developed.

### **Development of a Geomechanical Model with Relevant Boundary Conditions in Dumux**

The geomechanical model is considered linear and elastic, and the assumption of small strain is accepted. The model uses a linearized discretization scheme. Side-burdens and over-burdens are not considered in the geomechanical model, and they are replaced with proper boundary conditions to account for the load imposed by overburden, and stiffness of side burdens. The model studies the changes in displacement vectors.

### **Development of Streamline and Geomechanical Numerical Models in 3DSL and FLAC**

A few streamline based numerical models were made in 3DSL (streamline simulator) and were initialized properly and were tuned to be compatible with the initial data-file required for developed software. In FLAC-3D the same geomechanical models were built in a consistent way with the streamline-based flow model in terms of geometry, boundary and initial conditions (i.e. pore pressure distribution, datum depth, etc.). In addition to that, some fish functions (scripting language unique to FLAC) were developed to read pressure field from flow simulator on the grid-cell centers and map them to geomechanics model grid

vertices. Also a function was developed within FLAC framework to output volumetric strain field (during solution of geomechanical simulator). Two of the models are: a) Underground CO<sub>2</sub> injection scenario, b) Full-field multi-well compressible water flood black-oil model.

### **Software with GUI Development (QT-based C++ programming)**

Software with advanced Graphical User Interface (GUI) was developed by C++ programming to perform the streamline-based reservoir geomechanics coupling that functions properly with all models designed on FLAC3D and 3DSL platform (data files). All five proposed coupling methodologies to embed geomechanics into streamline simulation workflow are developed and implemented within the software core code (in one of the code classes called RUN). Furthermore, the software performs both the pre-processing and post-processing jobs, and output/input the data in sub-folders related to each forward cycle. The developed tool is explained more in details in Appendix 8-A.

### **Structure of Dissertation**

This dissertation is prepared in the combination of both paper based and monograph formats. Apart from introduction and conclusions chapters, all chapters are papers that were either presented at scientific conferences or are under revision for journal publications.

**Chapter 1** is the introduction chapter that explains objective, approach and methodology of the thesis.

**Chapter 2** provides a quick overview on the background of different physics and numerical techniques addresses in the research.

**Chapter 3** discusses the development of a novel analytical model for thermal recovery techniques. The findings of this chapter in terms of frontal movements are the basis of the next chapter.

**Chapter 4** is the continuation of Chapter 3, but deals with development of an analytical proxy that deploys domain-decomposition mathematical concepts into the thermal and geomechanical physics of thermal recovery applications. The findings of this chapter help rapid prediction of reservoir geomechanical responses in both near and far-field.

**Chapter 5** explains the development and application of a streamline-based numerical proxy. The proxy aims at model order reduction of geomechanics and flow simulation problems of large-scale reservoirs. The objective of this chapter is aligned with the next chapters, which is providing numerical capabilities for fast full-field reservoir-geomechanics coupling.

**Chapter 6** introduces streamline-based reservoir-geomechanics coupling as a novel technique in the world of hydromechanical coupling. This chapter explains development of the methodology, implementation, and its application in underground CO<sub>2</sub> injection and storage.

In **Chapter 7** the same methodology that is discussed in Chapter 6 is extended and is compared in terms of computational efficiency, robustness and accuracy with conventional coupling schemes (sequential coupling, and fully implicit coupling) developed and coded by collocated finite-volume and finite-element schemes.

**Chapter 8** explains the development of different streamline-based reservoir geomechanics coupling strategies for full field reservoir simulations. This chapter further discusses the methodology introduced initially in chapter 5, but introduces new discretization and simulation workflows to embed geomechanics into simulation workflows for large-scale coupling.

In **Chapter 9**, the development and implementation of the methodologies to ensure stable and robust streamline-based hydromechanical coupling is discussed. This chapter also provides the techniques to mitigate material balance error involved in the streamline-based coupling systems.

**Chapter 10** is the conclusion section of the thesis. All conclusions of the individual chapters are summarized in a coherent way. This chapter also discusses the works that can be done in the future to continue the research.

The bundled references and appendices of all the chapters wrap up the dissertation.

## Chapter 2: Literature Survey

### Reservoir Geomechanics

Geomechanics is an important piece of physics for both unconventional and conventional reserves, and is important for dealing with the environmental and technical challenges of recovery from both classes of reservoirs. However in the long history of “conventional” reservoir simulator development, stress changes and rock deformations due to changes in fluid flow properties (e.g. pressure and temperature) during injection or production, are not incorporated. Geomechanics is a quantitative discipline. Like other branches of mechanics, it is involved in measuring and estimating stress and examining how materials respond to that stress. At its basic technical level, reservoir geomechanics in the world of reservoir simulation is simply the inclusion of the so-called stress effects into fluid flow simulations.

The fundamental physics behind geomechanics lies in the concept of effective stress, defined by Terzaghi (1936). Terzaghi’s formulation was extended to three dimensional consolidation problem with Rendulic (1936), and was later modified by Biot where he developed a foundation for coupling of stress and pore pressure in the porous medium for consolidation problem<sup>\*</sup>. Biot’s approach was consistent with two mechanisms which play an essential role in the interaction of porous rock and fluid in place: i) an increase in pore pressure (e.g. injection process from a single well, or water flooding purposes) induces a dilation (particularly for undrained conditions where excess pore pressure cannot be dissipated), and ii) compression of the rock causes an increase in pore pressure. Alternatively the two above-mentioned mechanisms can be interpreted the other way round such that a decrease in pore pressure (e.g. production from a well or field, and reservoir depletion) can cause an increase in effective stress and induces some porous rock shrinkage.

### Thermal Recovery Techniques and Reservoir Geomechanics

Unconventional oil reserves are three times larger than conventional oil reserves, and are mainly located in Western Canada (Alberta, Saskatchewan), Venezuela, Iraq and Saudi Arabia. The main geology of these classes of reserves consists of ultra-heavy oil (e.g. West

---

<sup>\*</sup> Alternative theories have also been developed using the formalism of Mixtures Theory (Crochet, M.J. et al 1966, and Atkin 1976) but in practice they do not offer any advantage over the Biot theory.

Sak field in Alaska), bitumen (Cold Lake, Athabasca, and Lloydminster deposits in Canada,) and oil-shale formations. For instance, Canada has the third largest oil reserves in the world and 97% of these reserves are oil sands type (Upstream Dialogue, 2012); and rich in bitumen. Out of the current estimate of crude oil reserves which is 170 billion barrels (Government of Alberta, 2011) only about one fifth, are close to the surface (e.g. Fort McMurray) that can be mined. However the rest of these reserves are not recoverable by mining, and some other recovery techniques need to be applied. Conventional production mechanisms however cannot be used due to high viscosity of the oil in place, and therefore thermal recovery mechanisms are used for production of heavy oils in these types of reserves. The common thermal techniques are hot–water flood, steam flood, cyclic steam stimulation, steam-assisted gravity drainage (SAGD), and expanding solvent steam assisted gravity drainage.

Performance prediction is essential to provide information for proper execution of any development phase in a thermal recovery process. Three different mathematical models (statistical, numerical, and analytical models) are commonly used to predict steam flood performance. In thermal recovery techniques the main concern is to calculate the volume of heated zone, as this zone determines the amount of recoverable oil.

Consideration of geomechanics into thermal recovery techniques has been investigated extensively, particularly for steam assisted gravity drainage (SAGD) techniques; Chalaturnyk (1996) and Ping Li. The reservoir geomechanical responses have been investigated for both oil sands and sandy-shale formations (sandy and discontinuous layers). If heavy oil reservoirs are classified in terms of permeability; the geomechanical analyses have been done on permeable formations (oil sands), partially permeable (sandy-shales) and impermeable formations (interbed shales and bitumen). Heavy oil reservoirs can also be categorized in terms of bitumen amount. Immense bitumen accumulations can be found in oil sands like in the Canadian fields in Wabasca having a depth of burial from 100 m to 700 m (J.A. Veil, J.J. Quinn, 2008), as well as in tar sands. Both formations consist of non-consolidated to weakly consolidated sediment formations, in which the porosity maximum value ranges to 0.39 whereas the permeability values range approximately to more than 200 mD. All these classes of formations fall in the category of stress-sensitive class of reservoirs, where geomechanical changes play an important role in the recovery mechanisms. The main geomechanical changes occur due to local and global dynamic changes in pore pressure and temperature

fields during injection/production scenarios. The changes in pore pressure cause an isotropic unloading and lead to decrease mostly in the mean principal effective stresses. However the changes in temperature (heating or cooling effect) induce some deviatoric effective stresses that lead to even more changes in volumetric strains (compared to pressure effects) in the reservoir, and also can lead to shear failures in highly stressed zones. The zones that these changes are applied can range from small scales (near field) to large scales (far field and beyond heated zone or cap-rock).

For thermal recovery techniques, in particular SAGD, the effect of petrophysical properties have been shown to be superior to fluid flow properties. In an analytical study by Llaguno et al. (2002) accumulation properties (porosity, thickness, and oil saturation) were reported to have a greater effect on SAGD performance than flow properties (viscosity, API, and reservoir pressure). Also McLennan et al. (2006) stated that the predicted flow performance of SAGD well pairs is sensitive to the spatial distribution of permeability. Petrophysical parameters such as porosity and permeability are one of the primary variables that change due to geomechanical mechanisms. Therefore geomechanics can play a key role in the steam chamber shape, pressure profile and subsequently on the final oil recovery. The dynamic update of porosity and permeability is the main linkage between geomechanics and fluid flow processes. These parameters change mainly due to induction of shear (deviatoric) stresses as well as isotropic unloading during pressure increase, both as a result of volumetric strain changes. Therefore changes in porosity and permeability need to be studied either by analytical models or numerical techniques, as these changes can affect the pressure field significantly. Precise and quick prediction of pore pressure is also of great importance, because the increased built up pore pressure under the cap rock, may guide the cap rock toward failure.

The other impact that geomechanics play in the thermal recovery techniques is estimation of surface heave. Both increase in pressure and temperature during thermal recovery techniques induce some displacement that ultimately lead to disturbance of strain field and redistribution of stress concentration. The displacements (lateral and vertical) are induced both within and around the injection zone, and also far from the injection zone at the cap-rock or ground surface. This effect is more significant for shallow operational depth, where vertical stress can easily push the overburden upward (thermal jacking, Chalaturnyk (1996)).



## Analytical Models for Thermal Recovery Techniques

For many years, attempts have been made to provide analytical models for steamflood production performance prediction. Numerical models require a large amount of data input about the reservoir (geometry and distribution of properties), the in-situ fluids (saturation, pressures, properties, and initial conditions), wells (location, interval opens, skin effect, and well model to be used), and operational variables (rates, pressures and the constraints of each). By contrast, the analytical models generally require the entering of few but critical data.

In all of these models, certain simplifying assumptions need to be made to solve the complex heat and fluid flow equations. In the analytical methods, the reservoir is typically assumed to be homogenous. Since, it is much faster to obtain results from analytical models than from simulation, analytical models are still useful tools for preliminary forecasting purposes and sensitivity studies. In addition, the models provide a better insight than simulation into the physics of the thermal processes (Chandra, 2005).

As mentioned, one of the top key concerns in both numerical and analytical techniques is estimation of the heated area during injection. Several studies have been conducted to develop the theory for the estimation of the radius of the heated zone. This radius is important for computing the volume of recoverable oil, as well as to determine well spacing in steam-flooding and cyclic steam stimulation. There are many different models for thermal recoveries that most of which are applied to continuous steam injection.

The very classical models are Marx and Lagerheim (1959), Willman (1961) and Farouq Ali (1971) that are used extensively for steam-flood performance prediction; and also Boberg-Lantz (1966) to calculate the temperature variation in time; and Jones (1977) for saturation history evaluation. The latter model was used for heavy-oil pressure depleted reservoir. Among these models Lantz Method (1966), Mandl and Volek Method (1969), Farouq Ali (1970), and Myhill and Stegemier (1978), are used and applied widely in the current thermal recovery processes. For the SAGD mechanisms, there have been number of analytical models since three decades ago up until now. Reis (1992) assumed an inverted triangular shape for steam chamber; Vanegas et al. (2008) included the effect of heterogeneity in reservoir parameters in a modified Butler's approach, and Miura and Wang (2012) who proposed an analytical model for estimation of cumulative steam oil ratio (CSOR). One of the analytical models that accounts for mass and heat transfer equations

simultaneously and predicts the initial stage of oil production before steam breakthrough was Nukhaev et al. (2006). Almost all of the major well-known analytical models assume the heated zone is the same as the zone that hot water or steam has penetrated through the reservoir, which is generally not the case in reality. This shortcoming in analytical models can be influential on the final forecast of the oil recovery, particularly for heterogeneous reservoirs. Local heterogeneities were shown to affect the saturation front and hot water breakthrough significantly, but heterogeneities have very slight impacts on temperature breakthrough (Koohmarch Hosseini and Chalaturnyk, 2012). The other shortcoming of these analytical models is that they cannot estimate the approximate location of the heat front (travelled distance by temperature front).

The geomechanical influences of the thermal operations are also neglected in the so-called analytical techniques, which is another shortcoming of the methods. Geomechanics was previously introduced as an important piece of physics in thermal recovery techniques, and therefore understanding the dynamic changes of total and effective stress concentration in different zones of the reservoir (near field and far field) provides a better insight for reservoir management and prediction of ultimate recovery. Thus, development of a new proxy model (analytical equation), which predicts the heated area and stress-disturbed zones during thermal recovery mechanisms, is worthwhile. In simple, layer-cake geometries, a reasonable analytical description of the geomechanics of a field is possible. However for complex geometries with irregular and heterogeneous static geomechanical properties, numerical models are essential to properly characterize the reservoir, and model the mechanical behavior of the rock and account for disturbed stress state.

### **Geomechanical Effects on Reservoir Production Performance**

One of the key expected effects of inclusion of geomechanics into reservoir fluid simulation is mainly the dynamic change of petrophysical properties (porosity and permeability tensor). Geomechanical processes during fluid flow and reservoir life, induce some displacements, and therefore result in volumetric strain redistribution (locally or globally in the field), and accordingly some effective stress disturbance is initiated. All these effects together lead to changes in reservoir geological variables such as porosity and permeability. There are several correlations that relate the stress and strain changes to the petrophysical properties changes. On the other hand these changes in the petrophysical distribution of the reservoir cause a

change in the pore pressure field, which is captured by fluid flow simulator. The successive impact that fluid flow and rock deformation (geomechanics) have on each other can be formulated either analytically or numerically, in the framework of hydromechanical coupling that is explained in the next section. The pore pressure effect in the isothermal processes (non-thermal or cold heavy oil production) such as classical simple problem of water-flooding is not very different than the temperature effect, and changes in the pore pressure can also cause significant changes in the primary static variables of reservoir and also induce some lateral and vertical displacements, and also in some cases cause tensile or shear<sup>†</sup> failure in the critical zones of the reservoir.

There are two approaches in geomechanical assessment of oil and gas reservoirs: 1) coupled 2) uncoupled. The main scope of this research is based on the coupled processes where the mutual influence of fluid flow and displacement vector (strain field) on each other, is taken into account. When the three-dimensional strain field is considered in geomechanical studies, but volumetric strain is changing only due to pressure boundaries, the problem is still considered uncoupled. Uncoupled mechanisms have been used in surface subsidence analysis, or when steady state conditions are assumed, or in the case of a single asymmetric aquifer with fluid withdrawal from a fully penetrating well (Lewis and Schrefler, 1978).

More recently Biot's three-dimensional problem has been used based on the linear stress-strain constitutive equations and has been coupled to a linear form of Darcy's equation. The geomechanical impacts on reservoir simulation, within the framework of thermo-poro-elasticity, were discussed briefly in the previous section. However for simple poroelasticity theorem (isothermal conditions), the geomechanical effects on reservoir performance can be classified into well-known problems of: a) reservoir compaction and compaction drive (global large scale or full-field problem); b) stress effects on porosity and permeability (isotropic and anisotropic); c) reservoir simulation coupled to geomechanics; d) seismic reservoir monitoring and e) casing damage (local small scale). The main issues being addressed here are the changes in porosity and permeability due to fluid injection in underground reservoirs (CO<sub>2</sub> storage problem) or full-field production. In this text whenever geomechanics is mentioned, it denotes the linear poro-elasticity theorem, which is well accepted and sufficient for an accurate simulation of fluid flow in porous medium,

---

<sup>†</sup> Although there are no shear forces associated with the fluid itself, but fluid flow and pore pressure changes can induce some shear failure in the porous rock, when the deviatoric stresses change significantly.

particularly for large-scale geomodels<sup>‡</sup>. Also this research considers the geomechanical effects in the formulations behind the reservoir simulators and addresses the famous problem of “coupling”.

## Reservoir-Geomechanics Coupling

The basic idea behind coupling is taking into account the fact that rocks consist of a solid framework and a pore fluid that cannot be treated independently. In classical reservoir simulators, the changes in volume were limited to the volume changes of fluid in place, mainly due to compressibility. However the accurate simulation of fluid flow in the reservoir requires taking the porous rock deformation and volume changes of the REV (representative volume) into account as well. When pore-pressure changes in the reservoir, the effective stress changes as well based on Terzaghi's theory. This stress<sup>§</sup> is balanced in volume element (REV) by stresses in the solid framework, and partly by hydrostatic pore pressure (or dynamic pressure when injecting or producing) in undrained condition<sup>\*\*</sup>. On the other hand the reservoir simulators should consider the changes in mass fluids in a representative volume derived from two parts: compression/expansion of pore fluid due to pressure changes (compressibility effect), and the change of pore volume itself mainly due to changes in effective stress.

Classically, these sorts of impacts were previously modeled with analytical or simple numerical approaches. However, very often, the geometrical complexity or irregular distribution of mechanical properties makes simple modeling impractical. A more comprehensive numerical approach is therefore required. The evolution of reservoir geomechanics and computer CPUs call for an implementation of geomechanical concepts into reservoir simulation. Analysis of stress and strain redistribution and porosity and permeability variations of oil sand, shale, and sandy-shale requires conducting coupled simulation of geomechanics, fluid flow and thermal simulations. The co-occurrence of all these physics suggests the fully coupling of all the equations system which is computationally the most expensive coupling approach. Methods of hydrogeomechanical coupling can be classified to four main types: 1) fully coupling or monolithic or fully implicit

---

<sup>‡</sup> For small scale and near field problems or for extreme geological features, such as salt diapirs, the concept of associated flow rule and plasticity is conventionally accepted (e.g. wellbore stability, and sand production)

<sup>§</sup> The stress tensor represents the total external stress on a volume element attached to the solid framework

<sup>\*\*</sup> In drained condition, the stress is carried out only by the solid framework

coupling, 2) Iterative coupling, where the flow variables are solved explicitly from geomechanical variables and each solver iterates on each given time-step with the other one, 3) Explicit or One-Way coupling, where flow simulator is run for some time and the outputs are transferred only one way to geomechanics, and geomechanical feedbacks (strain and stress) are not fed back into flow simulator, and 4) Pseudo coupling, which calculates the geomechanical responses by some correlations or empirical models, and porosity and permeability are updated as a function of pressure with a look-up table. In this context, slow deformation of solid phase accompanied by pore pressure changes (due to either one-phase or multiphase) are considered, and therefore inertia forces are negligible. The small strain concept is also accepted. One of the fluid flow simulation techniques that has attracted lots of attentions due to its speed, computational efficiency and wide range of applications is “streamline simulation” that can be used as an alternative (instead of conventional flow simulators) in flow simulations of large heterogeneous reservoirs.

### **Streamline Simulation**

Streamlines are approximate methods for fluid flow in porous medium. In case of an isotropic permeability field, streamlines are orthogonal lines at each point to the isopotential lines, and locally tangent to a defined velocity field, and they represent the direction of fluid flow. The elegance of streamline simulation lies in their power for fast forward flow simulations. They are the most accurate when the flow mechanism behavior is closest to unit mobility ratio (e.g. tracer flow). The efficiency of streamline simulation relies mainly on their power in utilizing larger time-steps with fewer pressure updates, which leads to faster flow simulations. In scenarios where the geomechanical model changes (in MEM or petrophysical properties) and streamlines change and the process requires an iterative approach, streamline simulations scale well and are of significant advantage over finite difference (FD) or finite volume (FV) simulation techniques. The other advantage of streamline simulations is their visualization power (i.e. flow directionality and streamline density from sources to a sink as a flow indicator). Also they mitigate the numerical artifacts (numerical diffusion) due to their dual-grid nature (streamline grid and original Cartesian 3D grid). The beauty of streamline simulation lies in the time-of-flight formulation that helps to decouple the multidimensional transport equation to a series of 1D solution along streamlines. Streamlines represent the best possible grid to model flow in a particular instant

and are decoupled from the underlying Cartesian grids thus representing an optimal transport grid. Particularly for highly heterogeneous porous medium or large domains (i.e. one million cells) streamlines are significantly faster simulator tools compared to conventional flow simulators in terms of CPU load and computational efficiencies. The very first basic commercial streamline simulators were Frontline (for two-dimensional models) and Frontsim (three-dimensional simulator). Thiele et al. published the first 3D streamline results (Thiele et al., 1996). Batycky (1997) and Batycky et al. (1997), was the first who developed a 3D two-phase flow simulator with gravity and changing well conditions. A large literature describes the development and application of streamline simulation to prediction of flow in three-dimensional heterogeneous reservoirs. See the papers of Batycky, Thiele, King and Datta-Gupta (1998) and Crane et al. (2000) for many references to the full range of work on streamlines. The key steps in streamline simulations are explained in **Figure 2-1**. The independent variables (such as pressure and saturation) are mapped from the underlying 3D grid onto the 1D streamlines for initialization purposes at each global time-step when streamlines are updated. The solution obtained from the second grid (1D grid) is then mapped back onto the initial 3D grid to represent phase distribution. Pressure is then solved again and the process continues.

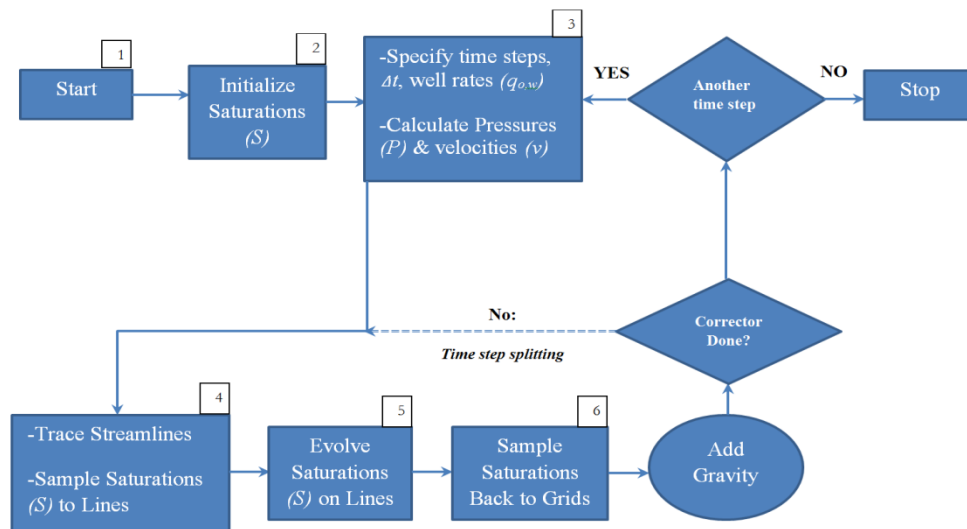


Figure 2-1-Schematic flowchart showing the successive steps of streamline simulation

## CO<sub>2</sub> Sequestration

The storage of CO<sub>2</sub> in geological formations is currently intensively discussed in the world of politics and science as an economical and environmentally sound way to reduce the emissions

of greenhouse gases into the atmosphere. Carbon capture and storage (CCS) technology aims at separating carbon dioxide from the fuel gases of power plants (fossil-fuelled or other CO<sub>2</sub> emitting ones) with subsequent transport to a site where it can be injected for storage into a deep geological formation, such as depleted oil and gas reservoirs, unmineable coal seams, and deep saline aquifers. Suitable formations should be deeper than 800 m, have a thick and extensive seal, have sufficient porosity for large volumes, and be sufficiently permeable to permit injection at high flow rates without requiring overly high pressure.

Reservoir processes during injection and post-injection of CO<sub>2</sub> involve several trapping mechanisms. **Figure 2-2** illustrates different mechanisms related to CO<sub>2</sub> trapping mechanisms. Extensive discussion on physical and chemical mechanisms related to CO<sub>2</sub> storage in sedimentary formations can be found in the works of Gunter et al. (2004), Benson and Cole (2008).

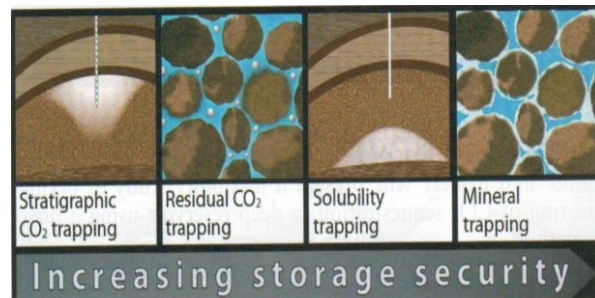


Figure 2-2-Conceptual sketch of sequential physical mechanisms of CO<sub>2</sub> storage -Zhdanov et al. (2013).

The trapping mechanisms can be divided into two main categories: (1) physical trapping (2) chemical gas trapping. Physical trapping encompasses stratigraphic and residual trapping, which are the first two sequences of trapping shown in Figure 2-2. Chemical trapping occurs when CO<sub>2</sub> dissolves in subsurface fluids (solubility) and subsequent reactions with the mineral phases in the reservoir (mineral trapping). The permanence and duration of these trapping mechanisms depends highly on the long-term geological integrity of the target underground reservoir and the seal. Geomechanical processes during CO<sub>2</sub> injection (and potentially in the post-injection period) can play an important role (particularly during stratigraphical CO<sub>2</sub> trapping) on the integrity of the storage formation and bounding seals. Geomechanics is likely of greatest importance during physical trapping stages when CO<sub>2</sub> is being injected into the formation and the fluid flow mechanisms are advection-dominated.

## Geomechanics of Underground CO<sub>2</sub> Injection and Storage

Hydromechanical (HM) processes generally play a significant role during CO<sub>2</sub> injection into deep saline aquifers. These saline aquifers are generally sandstone formations that are initially saturated with saline fluid. Therefore, they can deform either due to variation of external loads (dissolution or precipitation of mineral phases) or changes in pore pressures or temperature in the reservoir. The main topic of this work relates to stress-strain field redistribution and domain deformation due to pore pressure changes both in the near wellbore region and in the far field. Direct and indirect hydro-mechanical coupling mechanisms can explain these sorts of geomechanical changes, as suggested by Rutqvist and Stephansson, (2003). Direct HM coupling refers to both solid-to-fluid coupling and fluid-to-solid coupling. The former refers to the phenomenon where variation in the applied load results in a change in porosity and accordingly in fluid pressure and saturation; and the latter takes place when a change in fluid pressure causes a variation in the volume of the geological media (due to inducement of volumetric strain). Indirect HM coupling however refers to changes in hydraulic or mechanical properties in response to strain changes. According to this definition, the focus of this study is on direct HM coupling.

Even though geomechanics play an important role in CO<sub>2</sub> storage in saline aquifers, the computational burden is much higher using hydro-mechanical coupling than for the standalone hydraulic problem, particularly when the hydrodynamic and mechanics of the process are solved simultaneously (known as monolithic fully coupled HM). Although, there are some coupling strategies available to avoid the full coupling, such as sequential or iterative coupling, these strategies are not still applicable in large domains with multi-million cells due to computational burden. For more detailed discussions on these techniques and discussions over computational efficiencies refer to Mainguy and Longuemare (2002), Settari and Walters (1999), and for frameworks for coupling a flow and geomechanical code and induced geomechanical changes in reservoir properties, refer to Chalaturnyk and Li.

In recent years, a number of coupled fluid flow and geomechanical numerical models have been developed for analysis of various geomechanical issues associated with geological storage of CO<sub>2</sub> (GCS). Examples of the sequentially coupled HM analysis of GCS include FEMH by Bower and Zyvoloski (1997). TOUGH-FLAC by Rutqvist et al., OpenGeoSys by Wang and Kolditz and also Goerke et al. (2011), Eclipse-Visage by Ouellet et al. However



these schemes are not computationally efficient due to large number of coupling variables as well as computational loads, and complexity of multi-physics associated with conventional reservoir simulator. Simplified models have been shown to be sufficient for long term or large-scale processes (i.e. single phase flow coupled geomechanics for fault reactivation analysis in a large domain).

## Chapter 3: A New Analytical Approach To Investigate Heated Area in Thermal Recovery Techniques<sup>††</sup>

### Introduction

Performance prediction is essential to provide information for proper execution of any development phase in a thermal recovery process. Three different mathematical models (statistical, numerical, and analytical models) are commonly used to predict steam flood performance.

For many years, attempts have been made to provide analytical models for steamflood production performance prediction. Numerical models require a large amount of data input about the reservoir (geometry and distribution of properties), its fluids (saturation, pressures, properties, and initial conditions), wells (location, interval opens, skin effect, and well model to be used), and operational variables (rates, pressures and the constraints of each). By contrast, the analytical models generally require the entering of few but critical data.

In all of these models, certain simplifying assumptions need to be made to solve the complex heat and fluid flow equations. In the analytical methods, the reservoir is typically assumed to be homogenous. Since, it is much faster to obtain results from analytical models than from simulation, analytical models are still useful tools for preliminary forecasting purposes and sensitivity studies. In addition, the models provide a better insight than simulation into the physics of the thermal process (Chandra, 2005).

In thermal recovery techniques the main concern is to calculate the volume of heated zone, as this zone determines the amount of recoverable oil. Among these models Marx and Langenheim (1959), Willman (1961), Boberg and Lantz Method (1966), Mandl and Volek Method (1969), Farouq Ali (1970), and Myhill and Stegemier (1978), and Jones (1981) are used and applied widely in thermal recovery processes.

---

<sup>††</sup>This paper was presented at SPE Canadian Unconventional Resources Conference, November 2011, Calgary, SPE-148836

These models assume the heated zone is the same as the zone that hot water or steam has penetrated through the reservoir, which is generally not the case in reality. This study shows that the distance travelled by the hot water saturation front is not the same as the distance travelled by the temperature front. Subsequently, an analytical model is developed to obtain the heated zone radius from the radius of the hot water saturated zone.

## Mathematical Model

To develop the mathematical model, simultaneous heat and fluid flow equations in a porous medium need to be solved and coupled with together. The basic equations, from which the model is developed, are conservation equations (heat, mass, and momentum). Note that the conservation equations need to be written for porous medium. For each conservation equation some reasonable simplifying assumptions are considered.

### Conservation of Heat Equation for Multiphase Flow in Porous Medium

The general partial differential equation obtained based on the conservation of energy that describes the temperature distribution in a convective-conductive two phase flow in a porous medium can be written (Lake, 1989) as:

$$\frac{\partial}{\partial t}(\rho_w \phi s_w E_w + \rho_o \phi (1 - s_w) E_o + \rho_s (1 - \phi) E_s) + \vec{\nabla} \cdot (\rho_w E_w \vec{U}_w + \rho_o E_o \vec{U}_o) = \text{div}(\lambda \cdot \vec{\nabla} T), \quad (3-1)$$

where

$T$  = temperature

$\gamma_{o, w, s}$  = density of oil, water, and reservoir rock

$\lambda$  = thermal conductivity

$E$  = enthalpy of each phase, which can be written as:

$$E = Cp \cdot T, \quad (3-2)$$

where  $Cp$  is specific heat capacity of each phase and  $U_{w,o}$  = Darcy velocity of each phase (oil and water). Darcy velocity can be expressed as below, following the Darcy concept of fluid flow:

$$U_i = -\frac{K \cdot k_{ri}}{\mu_i} \nabla \varphi_i \quad \varphi_i = P_i - \gamma \rho_i g z; \quad (3-3)$$

where  $\gamma = +1$  for ascending flow and  $\gamma = -1$  for descending flow. Based on the above notations, we categorize the problem of coupled heat and fluid flow into three different scenarios where: (1) Heat and hot water flows convectively - this mechanism is accepted in hot water or steamflood process where conduction of heat is neglected; (2) Heat flows conductively and water flows convectively - this mechanism is classically accepted for SAGD operations where the heat transfer mechanisms upward of an advancing front is dominated by conduction (Chandra et. al considered some portion of the heat transfer mechanism to be done by convection); and (3) Heat flow is both convective-conductive and water flow is convective - this occurs in all thermal recoveries where the well spacing is not too large and flow mechanisms should be considered as both convective and conductive, or in cases where heat and fluid flow analysis need to be done in the wellbore vicinity.

Given that thermal recovery is the subject of this study, Equation (1) can be reduced to a different PDE problem. The PDE's later need to be solved when coupled with fluid flow equation to find the radius of heated zone from fluid transport equation. Hereafter we study all three mentioned scenarios for a one-dimensional problem.

### Case 1: Convective Fluid Flow and Convective Heat Flow

In the analysis of large-scale processes, the capillary pressure jump between phases and heat conductivity in the direction of displacement will be neglected (Bedrikovetsky, 1993). Assuming there is only one phase within a porous medium, Equation (3-1) reduces to:

$$[\rho_w C_{pw} \phi + \rho_s C_s (1 - \phi)] \frac{\partial T}{\partial t} + (\rho_w C_{pw} \vec{U}_w) \cdot \vec{\nabla} T = \text{div}(\lambda \vec{\nabla} T), \quad (3-4)$$

where  $\rho$  is the density of displacing fluid (water). The assumption above is correct to a very good extent, as heat is transferred by a convective mechanism with the aid of displacing fluid. The assumption of one phase flow therefore can be made in Equation (3-1) from the injection well up to the oil- water interface. **Figure 3-1** shows an example of temperature distribution in a convection dominated heat transfer mechanism within a porous medium from an injection well (left hand side) to a production well (right hand side). The figure is plotted by Comsol Multiphysics for a two-dimensional one phase model in porous medium.

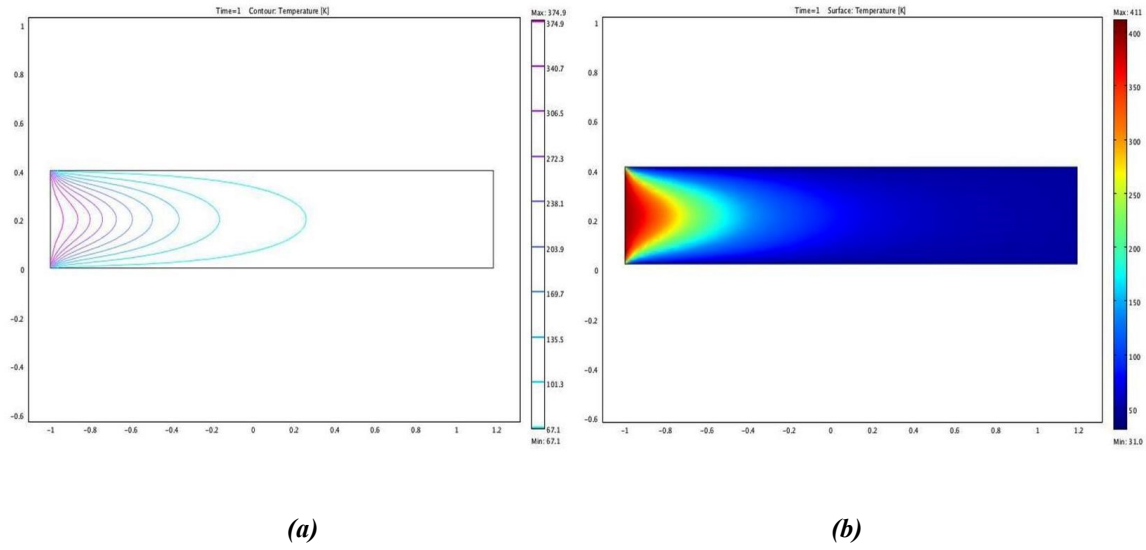


Figure 3-1-Schematic of convective heat flux in porous medium. Picture (a) shows temperature contours at different instances before breakthrough and (b) illustrates the corresponding temperature distribution surface.

$div(\lambda \vec{\nabla} T)$  in Equation (3-4) denotes the conductive term of heat transfer and  $(\rho_w C_{pw} \vec{U} w) \cdot \vec{\nabla} T$  is representative of heat transfer by convection. In the present case where only convection is dominant,  $div(\lambda \vec{\nabla} T)$  can be neglected, and Equation (3-4) for one-dimensional geometry is reduced to:

$$[\rho_w C_{pw} \phi + \rho_s C_s (1 - \phi)] \frac{\partial T}{\partial t} + \frac{1}{A(x)} (\rho_w C_{pw} q_w) \frac{\partial T}{\partial x} = 0, \quad (3-5)$$

where  $q_w$  is the hot water injection flow rate, and  $A(x)$  is the flow cross sectional area.

$$\frac{\partial [\rho_w E_w \phi + \rho_s E_s (1 - \phi)]}{\partial t} = -\frac{1}{A} \frac{\partial}{\partial x} (\rho_w E_w q_w) \quad (3-6)$$

Since Equation (3-5) describes temperature distribution,  $x$  and  $t$  are respectively distance traveled by temperature and temperature travel time. Therefore, temperature advancing front velocity can be expressed as:

$$\frac{\partial x_T}{\partial t} = U_T = -\frac{1}{A} \cdot \frac{\partial (\rho_w E_w q_w)}{\partial [\rho_w E_w \phi + \rho_s E_s (1 - \phi)]} \quad (3-7)$$

As a result Equation (3-7) can be simplified to:

$$U_T = U_f \xi, \quad (3-8)$$

where  $U_f$  is the bulk velocity of water and  $\xi$  is a constant that depends on the reservoir and injected fluid properties,

$$\xi = \frac{(\rho_w E_w \phi)}{[\rho_w E_w \phi + \rho_s E_s (1 - \phi)]} = \frac{\phi}{\phi + \frac{M_s(1-\phi)}{M_w}} \leq 1, \quad (3-9)$$

where  $M_s$  and  $M_w$  are volumetric heat capacity of water and rock and are defined as:

$$M_i = \rho_i E_i \quad (3-10)$$

It must be noted that based on Equation (3-6), the assumption to derive Equation (3-9) is that the temperature travels with only one velocity which is the total bulk hot water velocity ( $U_f$ ). However Equations (3-11) to (3-13) show that that the scenario is still a two-phase flow problem.

Equation (3-7) can be written in a more refined fashion by inserting the individual fractional flow of oil and water ( $F_o, F_w$ ) in order to capture the effect of individual phase velocities by which the bulk temperature of the medium is travelling. The phase velocities should not be mistaken with temperature front velocities ( $U_T$ ). Under the latter assumptions in convective heat flow scenario, the temperature front may or may not fall back from the saturation shock front depending on early or late (after injection) introduction of temperature into the equations. Yet, when temperature is introduced right after injection of water, (which is physically the case in hot water flood or steamflood) temperature fronts moves behind saturation front. Appendix 3-C explains further details and derivation of the equation.

### Physical Interpretation of Equation (3-9)

$U_f$  in Equation (3-8) is the total Darcy velocity of water and does not depend on the distance from the wellbore. As seen in Equation (3-9),  $\xi$  represents a ratio that is always smaller than one.

The physical interpretation of Equation (3-8) therefore is that in a convective one-dimensional problem of hot water injection the water front advances more rapidly than does the temperature front. The reason is that since  $\xi < 1$ , the temperature front velocity is smaller than the water front velocity, such that for each instant after hot water injection, the water front is beyond temperature advancing front. **Figure 3-2** shows the graphical representation of the equation. The temperature profile shown in Figure 3-2 is considered as

a piston like front for simplicity as assumed by Marx and Langenheim (1959). However in the analytical model and numerical results the behavior of temperature profile is different.

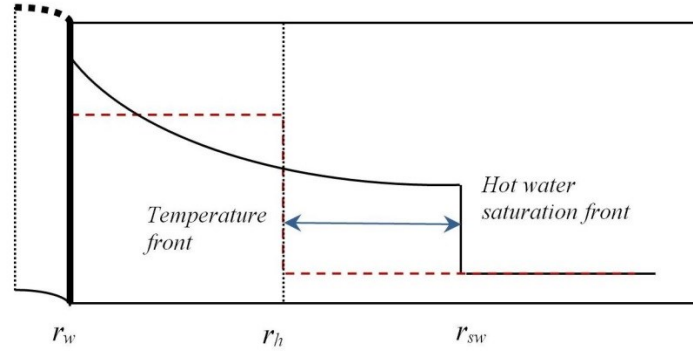


Figure 3-2-Graphical representation of saturation and temperature profile in a radial system when both heat and water flow mechanisms are convective. The red dotted line shows temperature front location and the solid blue line represents the saturation front location.

As Equation (3-9) shows when porosity tends to one ( $\phi \rightarrow 1$ ),  $\xi$  tends to one as well ( $\xi \rightarrow 1$ ) which means that temperature front velocity is equal to water front velocity. As such if hot water is injected in a hollow horizontal pipe the temperature front and water front are expected to be at the same position.

Equation (3-9) implies that in a convective process, when the hot water injection rate is doubled, total velocity will be doubled too (well lateral surface area is constant), and accordingly, the temperature front velocity will also be doubled. As such, by doubling the injection flow rate, the distance between water front and temperature front is also expected to be doubled.

### Displacement Problem in Convective Fluid Flow

The transport equation considered for the present model is Buckley-Leverett, which is simple and suitable for convective fluid flow. The Buckley-Leverett concept of displacement considers the possibility of intermingling between injected hot water and oil. According to Buckley-Leverett transport equation (Buckley and Leverett, 1942), the velocity of water saturation shock can be written as:

$$U_{f_{sw}} = U_f \frac{F(s_f) - F(s_{wi})}{s_f - s_{wi}}. \quad (3-11)$$

This relation, obtained as a result of mass balance equation at the saturation shock wave, is called the “Hugoniot-Rankin” relation, in which:

$U_f$  = total injection velocity of water

$S_f$  = water saturation at the front (value behind the water saturation front).

$S_{wi}$  = initial water saturation of water in reservoir (value beyond saturation front).

$U_{fsw}$  = water saturation front velocity

$F$  = fractional flow function which can be expressed as:

$$F_w(s) = \frac{\lambda_w}{\lambda_o + \lambda_w} = \frac{k_{rw}(s_w)}{(k_{rw}(s_w) + k_{ro}(s_o) \frac{\mu_w}{\mu_o})}. \quad (3-12)$$

According to Equation (3-11), the distance travelled by the water saturation front can be written as:

$$x_f = U_f F'(s_w) t, \quad (3-13)$$

where  $F'(s_w)$  is the derivative of fractional flow function with respect to saturation.

Combining Equation (3-8) with Equation (3-13) leads to:

$$U_T = \frac{x_f}{F'(s_w) t} \xi. \quad (3-14)$$

The position of the water within the saturation front can be found easily from Buckley-Leverett theorem (Equation 3-13) and fractional flow history that is known from relative permeability data. Therefore Equation (3-14) is a simple equation that relates the saturation front to temperature front, and helps to find the distance travelled at each time by temperature front, and accordingly the area heated by hot water at each instant after start of injection.

### The Model Limitations and Assumptions

Since Buckley-Leverett was considered as the flow transport equation, the assumptions behind Buckley-Leverett theorem are the model limitations too. The model is applied for two phase convective flow, capillary pressure between phases is neglected, fluid compressibility is small, there is no concentration and composition exchange during displacement process, and



flow diffusivity is neglected. It is also assumed that there are no lateral heat losses and thermal conduction is ignored. At this early stage of research the model is uncoupled from geomechanics. The formulations are developed for a one-dimensional geometry; however the model can be extended to radial as well, as explained in subsequent sections.

### Inclusion of Gravity into the Mathematical Model

In cases where oil displacement by hot water happens in a steeply inclined reservoir, where the total flow rate is low, or when there is significant difference in densities, gravity plays a more important role in the recovery mechanism. We can use the Buckley-Leverett equation for the gravitational case and couple it with an existing analytical model to find out the distance advanced through the reservoir by the temperature front. The mathematical model similar to Equations (3-13) and (3-14) for a gravitational flow case can be written as:

$$x_f = [F(s_w)(1 \pm \beta k_{ro})]'t \quad (3-15)$$

; where  $\beta$  is the gravity number and  $k_{ro}$  shows oil relative permeability. The same concept in Equation (3-14) can be used to obtain a relation to calculate temperature front velocity and as a result, the front of heated zone:

$$U_T = \frac{x_f}{[F(s_w)(1 \pm \beta k_{ro})]'t} \xi \quad (3-16)$$

The (+) sign in Equation (3-16) is applied for descending flow and (-) is for ascending flow, therefore in a downward flow direction, a larger distance between water saturation front and temperature front is expected. The detailed development procedure of Equations (3-15) and Equation (3-16) is provided in Appendix 3-A.

### Extension of the Model to Radial Geometry

The mathematical model can be extended to radial geometry, which is closer to reality for a hot water flooding process in the reservoir. Buckley-Leverett for radial case can be combined with Equation (3-8) to obtain a relation between the temperature front and the hot water front. Although Equation (3-8) has been developed for a linear one-dimensional problem, it can be considered approximately as correct for a radial case as well. The similar equation to Equation (3-14) for a radial case can be written as:

$$\frac{(r^2(t) - r_w^2) \cdot \xi}{r^2(t) F'(s)} = U_T \quad (3-17)$$

where  $r(t)$  is the radius of transport by hot water, and  $r_w$  is wellbore radius. Equation (3-17) can estimate temperature front velocity  $U_T$ , based on the radius of saturated zone  $r(t)$ . Therefore, at each time radius of heated zone can be calculated as a function of transported radius by hot water front velocity. The detailed development procedure of Equation (3-17) is provided in Appendix 3-B.

## Case 2: Convective Fluid Flow and Conductive Heat Flow

Marx and Langenheim (1959) provided a model to evaluate the steam zone growth with the basic assumption of purely conductive heat flow. Therefore this model is used in the present case. The main assumptions behind the theory were:

- Steam (or hot water) is injected with constant rate
- No heat is transferred ahead of the front
- The pressure drop due to the flow is sufficiently small
- The temperature profile is assumed as an idealized step function
- Heat is transferred only by conduction. Thermal conductivity within permeable formation is infinite

The solution to the following conductive one dimensional heat balance equation was obtained by Carslaw and Jaeger (1959):

$$\frac{\partial T}{\partial t} = \lambda \frac{\partial^2 T}{\partial x^2} ; \quad (3-18)$$

with boundary conditions of

$$\begin{aligned} 0 < x < \infty \\ T(x, 0) &= T_r, \\ T(0, t) &= T_s \\ T(\infty, t) &= T_r \end{aligned} \quad (3-19)$$

where  $\lambda$  is thermal diffusivity. The solution of Equation (3-18) combined with Fourier's first law and a Laplace transformation in a one-dimensional constant thickness geometry is the famous relation of Marx-Langenheim which describes the growth rate of steam or hot water zone and can be written as:

$$\frac{dA}{dt} = \left[ \frac{Ho}{Mh\Delta T} \right] e^{X^2} \operatorname{erfc}(X) \quad (3-20)$$

$$X = \left[ \frac{2D}{Mh\sqrt{\lambda}} \right] t^{1/2},$$

where  $Ho$  is the total heat injection rate,  $D$  is rock thermal conductivity and  $M = \rho_w C_{pw} \phi S_w + \rho_s C_s (1 - \phi) + \rho_o C_{po} \phi S_o$ .

Equation (3-20) shows the solution to the reduced form of Equation (3-1) where the second term of the equation is dropped (pure conductive heat flow mechanism). The solution form of Equation (3-18) suggests a temperature profile decreasing along later direction (x) in an error function form. However a step function temperature is assumed only where volume of heated zone is concerned. The system is a radial flow system, with thermal invasion radius being redefined as the distance from injection well (x) to the midpoint of temperature distribution. The results are also derived from a step temperature idealization. Injected heat can be partly lost conductively to overburden and under-burden.

To calculate the temperature front velocity we can assume that heat is diffused only in the lateral direction (x) and lost only laterally:

$$dA = 2 \pi h dx \quad (3-21)$$

$$\frac{dx}{dt} = \frac{dA}{dt(2\pi h)} = \left[ \frac{Ho}{Mh\Delta T} \right] \frac{e^{X^2} \operatorname{erfc}(X)}{2\pi h}$$

Finally Equation (3-21) can be written as:

$$\frac{dx}{dt} = U_T = U_f \left[ \frac{\rho_w C_w \Delta T}{M \Delta T} \right] \frac{2\pi h r_w}{2\pi h} e^{X^2} \operatorname{erfc}(X), \quad (3-22)$$

where  $U_f$  is bulk water velocity and  $U_T$  is the temperature front velocity. Since  $\rho_w C_w < M$  total volumetric heat capacity,  $r_w < h$ , and  $e^{X^2} \operatorname{erfc}(X) < 1$ , we can conclude that temperature front velocity in this case is also smaller than water front velocity.  $U_f$  in Equation (3-22) can be similarly written in the form of Buckley-Leverett equation. Therefore, Equation (3-22) correlates temperature front to water saturation front in a conductive heat flow.

### Case 3: Convective Fluid Flow and Convective-Conductive Heat Flow

This case is the most realistic case happening in a thermal recovery process as neither conductive nor convective heat flow is neglected. Equation (3-4) can be written in the following form:

$$\begin{cases} C_1 \frac{\partial T}{\partial t} = f(t)T(x, t) + C_2 \frac{\partial T}{\partial x} + \lambda \frac{\partial^2 T}{\partial x^2} \\ T(x, 0) = T_r \\ T(0, t) = T_s \end{cases}, \quad (3-23)$$

where,

$$C_1 = \rho_w C_{pw} \phi + \rho_s C_s (1 - \phi) \quad (3-24)$$

$$C_2 = U_w \rho_w C_{pw} \phi \quad (3-25)$$

The general form of  $U_w$  is assumed as a function of time  $\frac{\partial U_w}{\partial x} = f(t)$ . Therefore, case (3) is solved for a particular case where  $U_w$  is linear with respect to distance  $x$  but nonlinear with respect to time  $t$ . Thermal properties in this case are independent of temperature and position but velocity varies with time and varies linearly with respect to distance from wellbore. Solving the partial differential equation for  $T(x, t)$  is desired in the present case as it enables us to calculate temperature front velocity as follow:

$$U_T = \frac{\partial x}{\partial t} = \frac{\partial T / \partial t}{\partial T / \partial x} \quad (3-26)$$

Note that  $x$ , and  $t$  are distance and time in the Equation (3-23), which is heat balance equation, and they do not represent the distance and time for fluid flow equation. To solve Equation (3-23) we transfer the form of Equation (3-23) to:

$$T(x, t) = e^{(ax+bt)} W(x, t), \quad (3-27)$$

By substituting Equation (3-27) into Equation (3-23), coefficients  $a$ , and  $b$  and a new partial differential equation can be obtained as follows:

$$\begin{aligned} a &= -\frac{C_2}{2} \\ b &= \frac{C_2^2}{4C_1} \end{aligned} \quad (3-28)$$

$$\begin{cases} C_1 \frac{\partial W}{\partial t} = f(t)W(x, t) + \lambda \frac{\partial^2 T}{\partial^2 x} \\ W(x, 0) = T_r e^{-ax} \\ W(0, t) = T_s e^{-bt} \end{cases} \quad (3-29)$$

Equation (3-29) is based on the theory of Eigen Function Expansion and can be transformed to the form of:

$$W(x, t) = \sum_{n=0}^{\infty} A_n(t) \sin \lambda_n x \quad (3-30)$$

$$A_n = A_n(0) \exp[(\int f(t) dt) \lambda_n^2 t] \quad (3-31)$$

$$A_n(0) = \frac{\int_0^x T_r e^{-ax} \sin \lambda_n x dx}{\int_0^x \sin^2 \lambda_n x dx}$$

$$\lambda_n = \frac{n\pi x}{L}; \quad (3-32)$$

where  $L$  is interpreted as well spacing (or radius of drainage zone when only one well exists),  $x$  is the distance temperature travels from an injection well at each time. Therefore, the solution to Equation (3-23) is provided in an integral form, which is very complex for large-scale engineering applications. However it provides a good mechanistic insight into understanding of the simultaneous propagation of temperature and water saturation within the reservoir. The relation between heat front and saturation front is embodied in the coefficients  $a$  and, which include water velocity  $U_w$ .

To obtain a final explicit relationship,  $A_n$  should be inserted into Equation (3-30), and the resulting function should be substituted into Equation (3-23). Finally when  $T(x, t)$  is obtained, it should be replaced into Equation (3-26) to obtain the temperature front velocity.

## Results and Discussions

In order to examine the analytical model results, a simple simulation model is built for hot waterflooding in a long sandpack. In this process, convection is dominant over diffusion/conduction of fluid and heat flows. Therefore the same behavior suggested by the analytical model (Equation (3-9)) is expected to be predicted by the numerical model. Since analytical models are generally developed using simplifying assumptions, it is always a good idea to compare analytical results with real field data, high quality experimental data or reservoir simulation predictions to assess the behavior and precision of the analytical model.

In this study, CMG-STARS is used to simulate a 1-D problem (lab core hot waterflooding) with dominant convective heat and fluid flows. In a simulation run, test long sandpack is flooded with hot water. The objective of the following simulations is mainly to show that numerical simulations at certain conditions are in agreement with the finding of the analytical model that the temperature midpoint front falls back the saturation propagation front. The properties of the sandpack and main simulation parameters are provided in **Table 3-1**. **Figure 3-3** shows temperature and water saturation advancement in the sandpack after 2, 4, 8 and 12 hours. As can be seen from the plot, water front propagated much faster than temperature front. Temperature and water saturation fronts are also compared graphically in **Figure 3-4**. Simulation results indicate that in a process that is dominant by convective heat and fluid flow, water saturation and temperature front are separated. The magnitude of the separation in the fronts is highly dependent on reservoir and fluid properties and operation parameters such as injection rate and pressure. It has to be noted that the discrepancy between the water saturation and temperature fronts decreases when steam is used as the injected fluid (**Figure 3-5**). For steamflood cases, water condensation front is ahead of the temperature front but the discrepancy between temperature and water saturation front is not as marked as hot waterflooding. The focus of this study is hot waterflooding, since the capability of analytical equation to describe steam injection is still under question and needs more investigation.

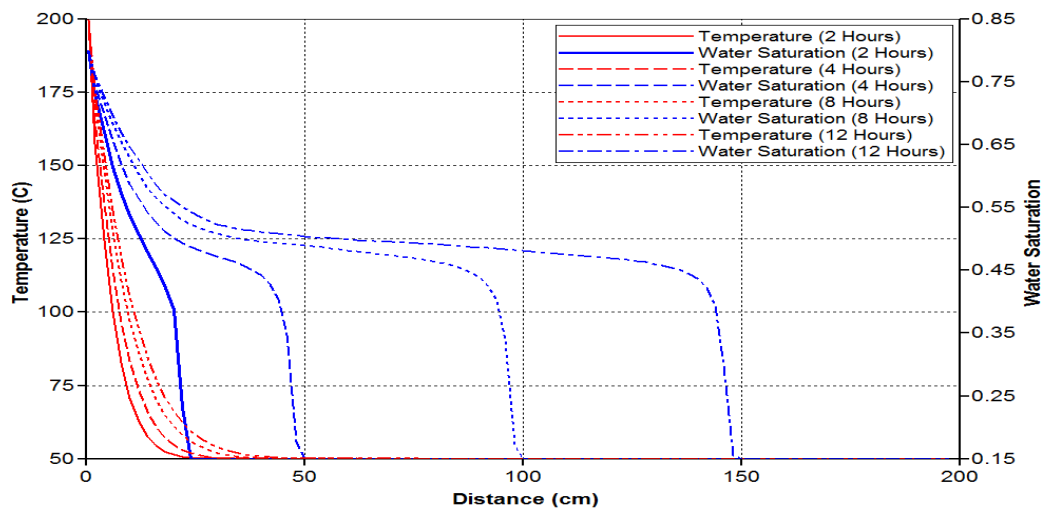


Figure 3-3-Water saturation and temperature front profiles in the hot waterflooding of sandpack. Simulation results show the trend, which is expected from developed analytical models.

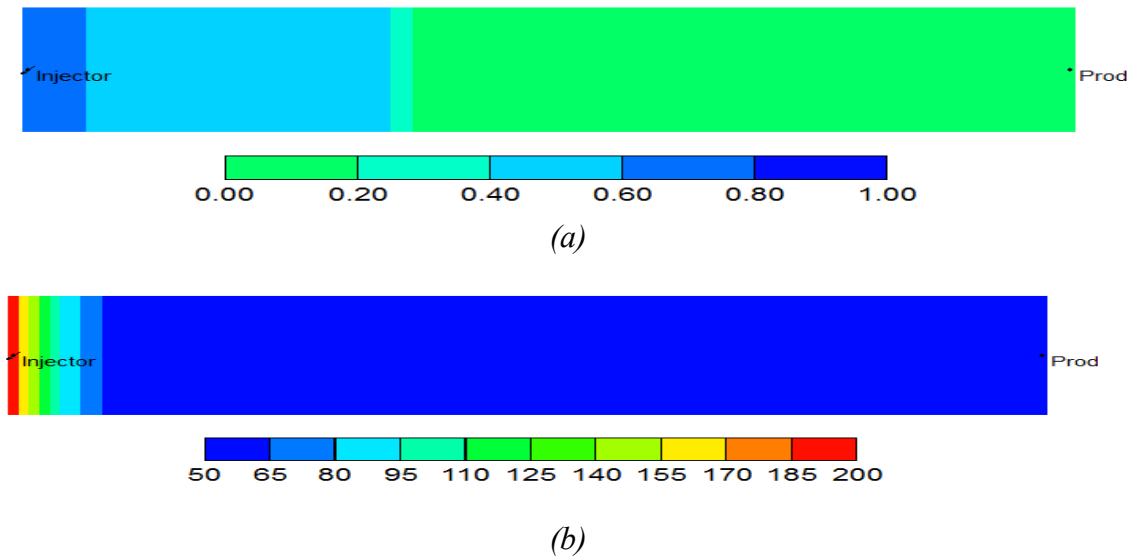


Figure 3-4-Temperature (°C) (b) and water saturation (a) distribution in a 1-D sandpack hot waterflood after 8 hours. The saturation front is ahead of temperature front.

It must be noted that for Case 1(convective flow), the model was simplified to a one-phase flow behind the saturation front. It must be noted that even though the plots are for a multi-phase problem, the temperature front still falls behind the saturation front.

**Table 3-1-Main numerical simulation parameters-Hot water flooding**

Parameter	Value
Reservoir Dimensions	2 m x 4 cm x 4 cm (Nx=100, Ny=1, Nz=1)
Porosity	0.35
Permeability, D	10
Initial Oil Saturation	0.85
Initial Reservoir Pressure, kPa	1000
Initial Reservoir Temperature	50
Injection Point Pressure, kPa	2500
Oil Viscosity at 50 °C, cP	350
Oil Viscosity at 200 °C, cP	3.2
Hot Water Injection Rate cm <sup>3</sup> /s	11.57

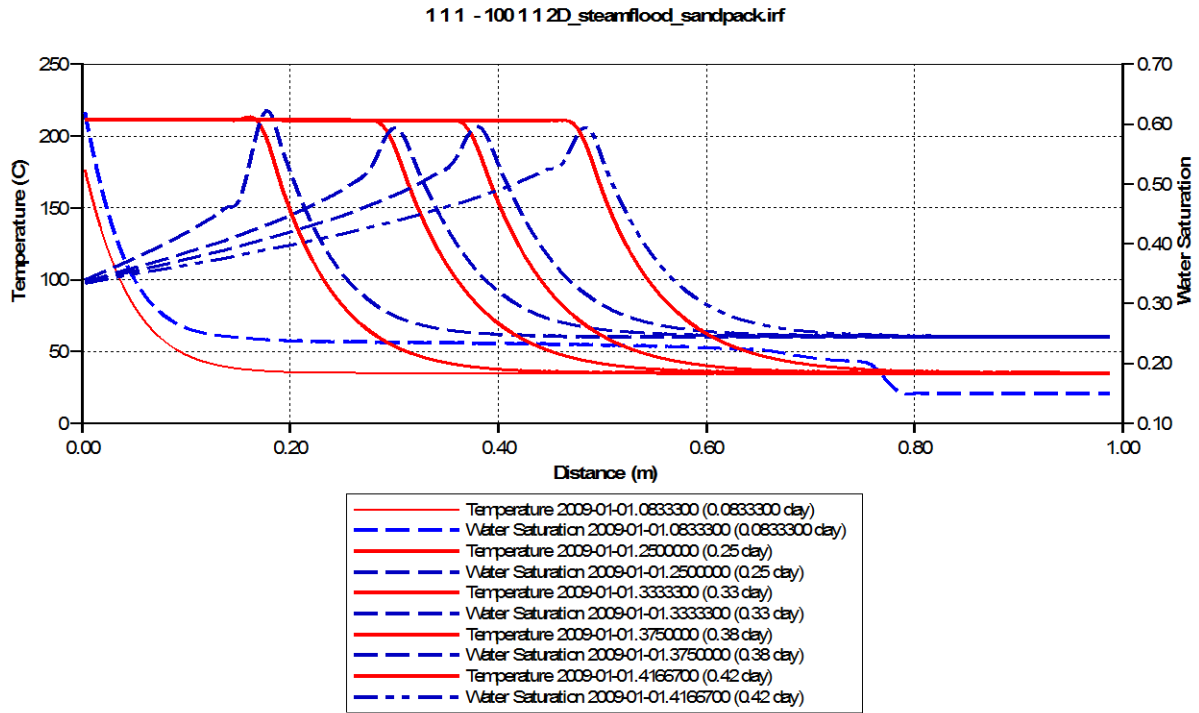


Figure 3-5-Water saturation and temperature profiles in the steamflooding of sandpack. The distance between fronts of temperature and saturation is less compared to the case of hot waterflooding.

## Conclusions

Based on the derived analytical models and analysis it was shown that (in contrary to classical analytical models) in thermal recovery processes, the temperature front and hot water (or steam) front are not at the same position with respect to the injection well as suggested by Equation (3-8), (3-22), and (3-30).

In thermal mechanisms where convection is dominant e.g. hot water flooding, hot water front advances more rapidly than temperature front (Equation 3-8), and as injection rate is increased the distance between these two fronts increases. A numerical simulation of a hot water displacement (core flood) of oil was done and the result of which was in agreement with the developed analytical model.

There were some analytical models used in this chapter such as Marx Langenheim, Buckley-Leverett, and general form of conservation laws that were quite well known, however the other derivations to relate temperature midpoint velocity to saturation front velocity in all three cases were quite novel. Since there is no solution to obtain temperature front velocity



directly from heat flow equation (such as in Buckley-Leverett), development of techniques for all form of heat mechanisms, to obtain temperature front from saturation front was quite useful and important. It was also shown (in Appendix 3-C) that where the displacing mechanism (behind the saturation front) is considered multiphase there can be obtained a balance point between temperature front and saturation front. The findings of this work also showed that where the porosity of the porous medium tends to zero (such as in a conduit) the temperature front and saturation contour are at the same location in each time (based on developed correlating parameter  $\xi$ ).

An analytical relation was found between temperature front and saturation front in three different scenarios. As saturation front position (or radius of saturated zone by hot water) was known from Buckley-Leverett equation, distance of heated zone was estimated.

## Nomenclature

$T$	=	Temperature
$T_s$	=	Steam injection temperature
$T_r$	=	Reservoir initial temperature
$\rho_{o,w,s}$	=	Density of oil, water, and reservoir rock
$k_{ro,rw}$	=	Relative permeability of oil, and water
$\lambda$	=	Thermal conductivity
$E$	=	Enthalpy of each phase
$C_{pw}$	=	Specific heat capacity of water
$C_s$	=	Rock specific heat capacity
$D$	=	Rock conductivity
$U_f$	=	Injection bulk velocity of water
$\Phi$	=	Porosity of porous media
$M$	=	Volumetric heat capacity
$U_T$	=	Temperature front velocity
$U_{f,sw}$	=	Water saturation front velocity
$q_w$	=	Hot water injection rate

---

$S_f$	=	Water saturation behind water saturation front
$S_0$	=	Initial water saturation of water in reservoir
$F$	=	Fractional flow function
$r(t)$	=	Radius of saturated zone by hot water at time $t$
$r_w$	=	Wellbore radius
$Q(t)$	=	Cumulative injected volume into the reservoir at time $t$
$\beta$	=	Gravity number

## **Chapter 4: A Domain Splitting-Based Analytical Model for Rapid Assessment of Hydro-thermo-geomechanical Responses of Large Scale Heavy Oil Reservoirs: A Steamflood Application<sup>##</sup>**

### **Introduction**

Governing equations on conservation of mass, momentum, and heat equations in porous medium, are highly nonlinear, particularly when the independent variables have physical impact on each other (i.e. temperature effect on pressure profile, phase saturations, concentrations and lateral, and vertical local displacements). Certain assumptions on independent variables are required to simplify and linearize the model (Dake, 1998).

On the other hand the co-occurrence of these physics in a highly heterogeneous and geologically distorted reservoir, calls for a numerical fully implicit coupled system for solution of the non-linear problems. However, the solution of such a system is numerically challenging, if nearly impossible, particularly for large heterogeneous reservoirs with multi-million grid-blocks. Other numerical techniques such as IMPES for fluid flow problem coupled to heat flow and geomechanics equations, are not still feasible in large scales with current CPU's, due to forced selection of small time spans for explicit coupling of the physics in order to ensure numerical convergence. Unless the modeling is performed on a small scale (i.e. around wellbore region), the numerical simulations are still challenging.

Domain decomposition techniques combined with variable decoupling is therefore a good approach for full-field modelling, allowing the inclusion of geomechanics into heat and fluid flow processes in thermal recovery techniques. In practice, full-field geomechanical modeling

---

<sup>##</sup> This paper was presented at SPE Heavy Oil Conference, June 2014, Calgary, SPE-170193, as well as submitted to SPE peer reviewed Journal (SPE J).

of reservoirs is essential; to assess the geomechanical responses of the reservoir (surface heave, and stress field), and more accurately estimate reservoir dynamics.

To obtain the numerical solutions for pressures, temperatures, phase saturations, and three elements of displacement vectors (displacement in three principal directions), at each grid-cell in a large field with large number of grid-blocks, a large matrix system needs to be set up; each Jacobian matrix's row, contains six primary variables (in an immiscible non-compositional simulation) multiplied by number of grid-blocks. The solution of the matrix is obviously a challenge in terms of CPU time and convergence, and where multiple simulation runs are needed (i.e. ranking of geological realizations, and optimizations), this approach is technically not practical.

Under these conditions, analytical models, or semi-analytical proxies are better approaches for quick assessment and dynamic prediction of flow and geomechanical responses of reservoir. For performance prediction of the reservoir (given the production and surface heave history of the reservoir), in particular, analytical techniques are widely used.

For treatments of the problem of time and spatial scale, different techniques have been suggested. Variable decoupling, for instance, has been used in fluid flow problems in porous medium. Pressure, was decoupled from phase saturation for solution of mass and momentum equations in two-phase streamline simulations (Batycky, 1997) of reservoir. Decoupling was performed to enhance the computational efficiency by solving each equation explicit from one another, by different discretization schemes, and at different domains (pressure was solved implicitly on model grid-cells, and saturation was solved explicitly along streamline grids), for problem simplicity. Koohmareh Hosseini and Chalaturnyk (2013) used the same technique for inclusion of geomechanics into streamline-based modelling of transport physics.

To circumvent the problem of large scale in reservoir modeling (in addition to the problem of time), domain decomposition techniques have been shown to be efficient both analytically and numerically (Toselli, Widlund, 2005). This work presents an analytical model that uses both variable decoupling and domain decomposition, for rapid assessment of geomechanical responses of the reservoir.

Variable decoupling was adapted in the development of analytical model, to reduce the model non-linearity in fluid flow, and thermal analysis of the reservoir, since simultaneous solution of the multi-physics problems is complex and in some cases is mathematically impossible. Domain decomposition for boundary value problems (BVP) is physically meaningful, if in each non-overlapping sub-domain different coupled physics occur.

### **Motivation for Domain Splitting and Variable Decoupling**

In thermal recovery techniques, where steam or hot water are injected into underground heavy oil reservoirs, the injection pressure is typically more than the reservoir in-situ initial pressure (in both constant injection rate and constant bottom hole pressure). Therefore, pressure builds up around the injection well, and the pressure difference induced in the reservoir, causes a reduction in effective stresses, based on poro-elasticity theorem proposed by Biot (1940), and accordingly material tendency to expand (horizontally and vertically) increases, and as a result the total stress increases, mostly around the wellbore.

Injection of steam (with high qualities  $> 0.95$ ) causes a significant jump in temperature around the wellbore region. Therefore, total stresses around the wellbore increase also due to thermal effects, based on thermo-elasticity concept, and lead to lateral and vertical displacements (thermal jack-up) around the wellbore. Depending on the physics of transport in porous medium (convective or diffusive), which are a function of reservoir type and wellbore injection conditions, the temperature and pressure fronts at each time during injection, are at different distances with respect to injection well. With increasing dominance of convective heat flow, the farther the temperature shock (front) travels, heating a larger area of the reservoir and leading to larger areas undergoing total stress changes.

On the other hand in the analytical model provided in Chapter 3 (Koohmarch Hosseini and Chalaturnyk, 2011), it was shown that the temperature front (where injection temperature reaches to reservoir temperature in far field), lags behind the saturation front. It was also shown that with increased convection-dominated heat flow, the more intense the lag distance became. Therefore beyond the temperature front, the stress changes in reservoir are only a function of pressure changes in the region. It must be noted that the region beyond the temperature front at each instant after start of steam injection, experiences the stress changes induced in near field region. Therefore the geomechanical changes in the domain behind the

temperature front are mainly functions of both temperature and pressure changes, and beyond the temperature front (far field), where the transport process is isothermal, geomechanical changes are “only” functions of pressure. Since different physical processes occur in each domain during and after injection of steam, different characteristic sub-domains can be distinguished. Decoupling of variables, on the other hand, in each sub-domain simplifies the non-linear complex problem into a reduced order model, with fewer variables to be solved in each sub-domain.

### Solution to the Pressure Equation

In the radial form of the diffusivity equation the general form of the solution to the transient flow problem is provided by *Ei* function for an unbounded domain. Pressure profile shape starts at a constant value at the boundary of drainage (i.e. an aquifer or a fault), and decays radially toward the production well. The solution to the radial form of pressure diffusivity equation in a bounded domain is in the form of Bessel’s functions. The radial form of the diffusivity equation is:

$$\frac{1}{r} \frac{\partial}{\partial r} \left( r \frac{\partial P}{\partial r} \right) = \frac{\mu c \phi}{k} \frac{\partial P}{\partial t} . \quad (4-1)$$

The same equation can be written in a uniaxial form in Cartesian coordinates as:

$$\frac{\partial^2 P}{\partial x^2} = \frac{\mu c \phi}{k} \frac{\partial P}{\partial t} . \quad (4-2)$$

In this work the Cartesian one-dimensional form of pressure diffusivity equation is adapted for simplicity in the steady form where the solutions are already available. Similar to the solution of the conductive form of the temperature equation (Butler, 1987), ahead of the steam chamber, the pressure profile can be obtained by (derived by Butler):

$$P = P_r + \left[ \exp \left( - \frac{\mu_w c \phi}{k k_{rw}} V_x \chi \right) \right] (P_s - P_r) , \quad (4-3)$$

where  $\chi$  is the distance beyond the steam front,  $\phi$  is the oil sand medium porosity,  $\mu_w$  is the hot water viscosity,  $c$  is the oil sand compressibility,  $P_s$  is the pressure at the steam chamber interface,  $P_r$  is the initial reservoir pressure, and  $V_x$  is the bulk velocity of steam front.

Conventionally the pressure is assumed as constant in the steam zone and declines beyond the steam front, however given the equation and boundary conditions, the solution to the

problem shows that pressure starts to decline from the injection well toward an infinite boundary. In our work both solutions can be used, but Equation (4-3) is adopted for simplicity. All derivations in this work are based on assumption of one-dimensional flow displacement, where invasion radius of heat and flow is presented by  $x$  (distance from injection well).

### Solution to the Temperature Equation

The temperature equation, where the heat flux mechanism is assumed conductive is as below:

$$\lambda \frac{\partial^2 T}{\partial x^2} = \rho c_p \frac{\partial T}{\partial t} \quad (4-4)$$

where  $\lambda$  is the thermal conductivity of the medium,  $\rho$  is the density of the reservoir (mixture of oil, water, and rock) and  $c_p$  is the specific heat capacity of the reservoir, which contains three phases of oil, hot water, and solid rock.

The solution to the problem in a bounded domain is different than the problem in an infinite domain. Here in our work the solution to the problem (for simplicity) is provided in an unbounded domain, for both the near well bore zone, and far field domain.

Conventionally in some thermal recovery techniques such as SAGD with certain operating parameters numerical simulations, temperature profile seems constant (and equal to injected steam temperature) from the injection well to the steam chamber interface similar to the Butler's model. However in reality, as the solution to the problem suggests, the temperature profile has a declining behavior in both injected steam zone, and beyond the steam front. The focus of this study is steam-flooding where the declining behavior of temperature profile is more visible.

The form of the temperature equation in a convective-conductive scenario is:

$$\lambda \frac{\partial^2 T}{\partial x^2} = \rho C_p \frac{\partial T}{\partial t} + \rho C_p U_w \frac{\partial T}{\partial x} \quad (4-5)$$

; where  $U_w$  is the water bulk velocity. The problem is purely convective if the left hand side term is zero, and is pure conductive if the right hand side of the equation (third term) is zero. The solution to the problem where the transport is purely convective is provided by method of characteristics. The solution of the Partial Differential Equation (PDE) suggests that

temperature remains constant in space and is equal to the steam injection temperature, in the convection zone, and in the conduction zone, the temperature declines in an error function  $erf(x)$  manner. **Figure 4-1** represents the profile of temperature for a convective-conductive case. As shown in Figure 4-1 three different fronts can be defined: the convective front where temperature starts to decline from a plateau (solution provided by method of characteristics or reduced form of Burger's equation), the conductive front that is the inflection point of the rarefaction part of the profile (middle point of the  $erf(x)$  function), and the ultimate temperature front, where temperature is equal to the reservoir temperature.

The convective form of temperature front movement happens when the temperature shock is moving with a considerable bulk velocity (hot water Darcy velocity). Therefore this process happens mainly in the high pressure gradient zones or where there is significant injection rate, and the porous medium is permeable enough to allow for high rate heat and fluid flux. Therefore where the medium is mainly sandstone with high viscosity bitumen in it, the convective flux of heat and fluid is barely possible and the process of steam front movement is more of conductive type. However if preheating wells are turned on, and steam circulated through injection and production wells for a considerable amount of time to reduce the viscosity of in-situ reservoir bitumen, the convective heat flux can be observed after steam injection and eventually the distance that the temperature front (or steam chamber in SAGD scenarios) travels in the porous medium is more than the distance travelled by means of conductive flux.



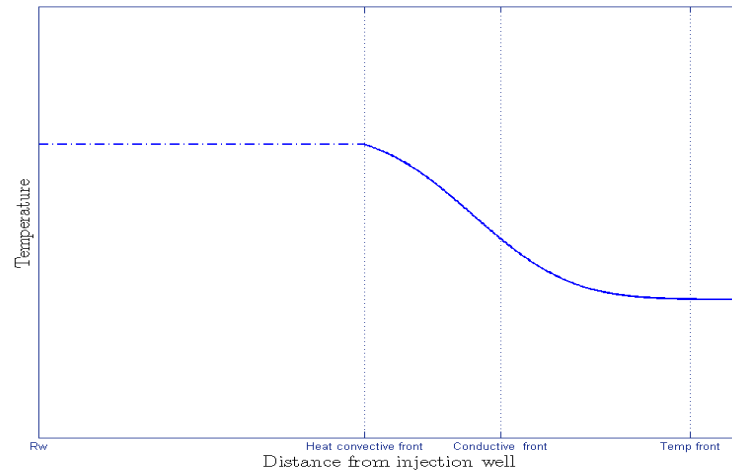


**Figure 4-1-Temperature profile in space where heat flux mechanisms are both convective and conductive**

**Figure 4-2** shows the temperature profile where the process is purely conductive and shows the temperature starts to fall off from the injection well (solution provided by  $erfc(x)$ ).

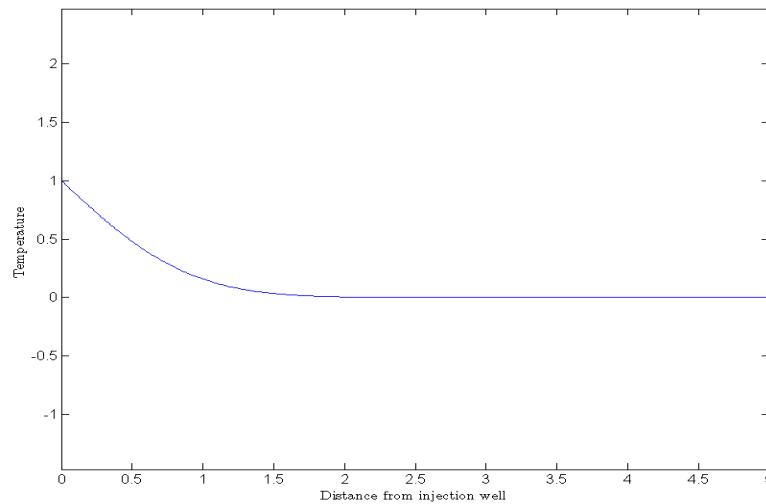


**Figure 4-2-Temperature profile in space where heat flux mechanism is purely conductive**

## Domain Splitting Algorithm

The constitutive equation in continuum mechanics (Hooke's law), that relates strain tensor  $\epsilon_{ij}$  to stress tensor  $\sigma_{ij}$ , where there are both pressure and temperature effects, can be written as below:

$$\varepsilon_{ij} = \frac{1}{E} [(1 + \vartheta)\sigma_{ij} - \vartheta\delta_{ij}\sigma_{kk}] + \alpha_T\delta_{ij}[T - T_r] + \frac{(1-2\vartheta)}{E}\delta_{ij}\Delta P; \quad (4-6)$$

where  $\vartheta, E, \alpha_T$  are representative rock properties and are Poisson's ratio, Young modulus, and linear thermal expansion coefficient, respectively, and  $\delta_{ij}$ , and  $\Delta P$  represent the Kronecker delta and changes in pore pressure, respectively. If one expands the equation in Cartesian coordinates, where only thermal effects are dominant, we have:

$$\varepsilon_{xx} = \frac{1}{E} [(1 + \vartheta)\sigma_{xx} - \vartheta(\sigma_{zz} + \sigma_{xx} + \sigma_{yy})] + \alpha_T[T - T_r] \quad (4-7)$$

The equation can be rearranged to:

$$\varepsilon_{xx} = \frac{1}{E} [\sigma_{xx} - \vartheta(\sigma_{zz} + \sigma_{yy})] + \alpha_T[T - T_r] \quad (4-8)$$

And similarly in y and z direction:

$$\varepsilon_{yy} = \frac{1}{E} [\sigma_{yy} - \vartheta(\sigma_{zz} + \sigma_{xx})] + \alpha_T[T - T_r] \quad (4-9)$$

$$\varepsilon_{zz} = \frac{1}{E} [\sigma_{zz} - \vartheta(\sigma_{xx} + \sigma_{yy})] + \alpha_T[T - T_r] \quad (4-10)$$

As the reservoir can be physically separated into two domains: where geomechanical processes are highly dependent on temperature (near field), and the isothermal domain (where there is only pressure effects in the domain), mathematically the reservoir can be split into two non-overlapping domains with the interface located on temperature front. The governing mathematical concept is similar to domain-decomposition method for PDEs, for non-overlapping domains. **Figure 4-3**, represents a schematic of the main domain (reservoir) and the sub-domains.

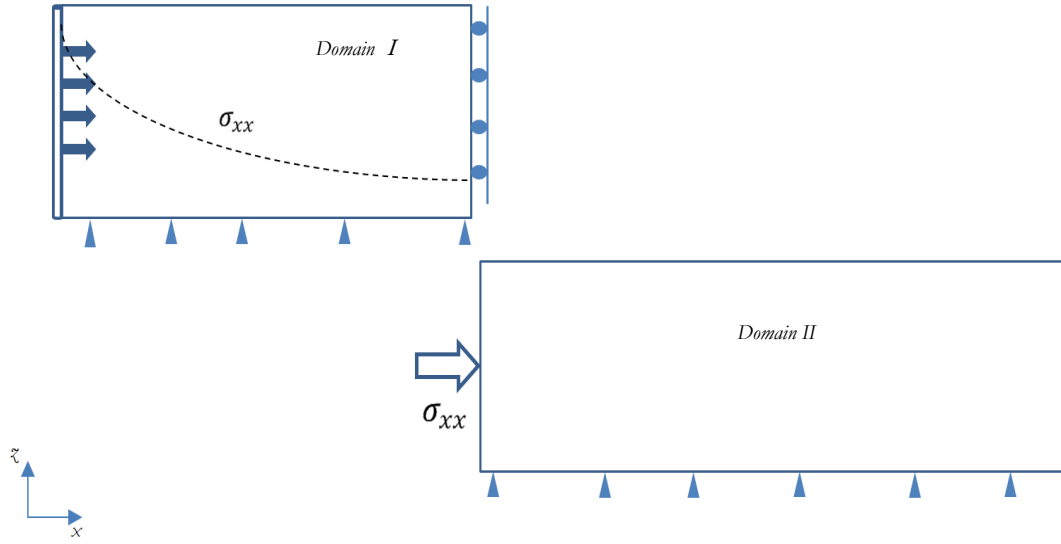


Figure 4-3- Representation of zone 1 and geomechanical boundary conditions

Based on the Schwarz' domain decomposition technique, solution to the problem on the global domain is equivalent to the problem on the two sub-domains, if and only if the geomechanics solution variables (strain or stress) are continuous on the interface. To check on the continuity of stress values on the selected interface (temperature front), we provided a numerically coupled flow-geomechanics model of the same problem with the same geometry. By plotting the stress and strain profiles along x-axis (from injection toward production well), we showed that the curves are continuous and there is not a jump in the solution on the interface. A numerical example of the approach and the profile of solution variables are provided at the end.

Assuming there is no thermal or pressure effects in the zone of study, for a plane strain condition where strain is zero perpendicular to the steam chamber movement ( $\epsilon_{yy} = 0$ ), Equation (4-9) reduces to:

$$\sigma_{yy} = \vartheta(\sigma_{zz} + \sigma_{xx}) \quad (4-11)$$

Substituting Equation (4-11) into Equation (4-8),

$$\epsilon_{xx} = \frac{1}{E} [\sigma_{xx} - \vartheta[\vartheta(\sigma_{zz} + \sigma_{xx}) + \sigma_{zz}]] = \frac{1-\vartheta^2}{E} (\Delta\sigma_{xx} - \frac{\vartheta}{1-\vartheta} \Delta\sigma_{zz}) \quad (4-12)$$

$$\epsilon_{zz} = \frac{1-\vartheta^2}{E} (\Delta\sigma_{zz} - \frac{\vartheta}{1-\vartheta} \Delta\sigma_{xx}) \quad (4-13)$$

Note that all above equations are written for changes in stress and strain values with respect to a reference state (e.g. initial stress and strain condition in the reservoir, prior to injection of any hot fluid). The analysis of geomechanical changes in each domain is different due to different boundary and initial conditions. Therefore two different sets of analyses are provided in each domain.

### Stress Analysis in “Domain I”

To impose the effect of thermal stress changes in the equations, the following boundary conditions are applied and substituted into the original constitutive continuum equations:

$$\varepsilon_{xx} = 0 \quad (4-14)$$

$$\Delta\sigma_{zz} = 0 \quad (4-15)$$

The reason for setting  $\varepsilon_{xx} = 0$  is that Domain I is bound by two set of rollers, as shown in Figure 4-3. Conventionally in geomechanics when a model is cut from a larger underground reservoir, the boundaries on lateral side of the domain are assumed as roller boundaries (no lateral displacement) in order to account for the stiffness of the outer rock regions. When the domain is decomposed in the represented geometry, in order to apply the induced interlocked stresses in Domain I, we apply a no-displacement constant strain condition on the interface between the domains, only when Domain I is concerned. The reason the model is not pinned (no displacement in all three principal directions) is that the pinned boundary induces some shear stress along the cut interface of the sub-domains which is not the case in reality, as such the roller boundary was chosen. Also the symmetry of the domain around the wellbore is another reason to assign the roller boundary condition on the splitting interface. It must be noted that a stress-boundary condition could be applied on the domain interfaces as well, but for stress analysis of Domain II, the magnitude of imposed stress had to be subtracted or added to the stress profile. Therefore, the lateral strain in the entire bulk region of Domain I is zero, however the strain profile does not need to be zero and it changes with distance from injection well, during steam injection. Changes in vertical stress are zero, as the surface of the reservoir is allowed to move freely, and as opposed to  $\Delta\sigma_{xx}$  that builds up in time in Domain I,  $\sigma_{zz}$  remains unchanged during steam injection.

Adapting the two boundary conditions and replacing them in Equation (4-11), total stress in x direction will be obtained as below:

$$\Delta\sigma_{yy} = \vartheta(\Delta\sigma_{zz} + \Delta\sigma_{xx}) = \vartheta\Delta\sigma_{xx} \quad (4-16)$$

$$\varepsilon_{xx} = \frac{1}{E}[\sigma_{xx} - \vartheta(\sigma_{zz} + \sigma_{yy})] + \alpha_T[T - T_r] = \frac{1}{E}[\sigma_{xx} - \vartheta(\vartheta\sigma_{xx})] + \alpha_T[T - T_r], \quad (4-17)$$

and therefore

$$\Delta\sigma_{xx} = \frac{-\alpha_T E \Delta T}{1 - \vartheta^2} \quad (4-18)$$

Replacing the equation for total horizontal stress (Equation (4-18)) into vertical strain equation (Equation (4-13)) yields:

$$\Delta\varepsilon_{zz} = \frac{1}{E}[\Delta\sigma_{zz} - \vartheta(\Delta\sigma_{xx} + \Delta\sigma_{yy})] + \alpha_T[T - T_r] = \frac{1}{E}[-\vartheta(\Delta\sigma_{xx} + \vartheta\Delta\sigma_{xx})] + \alpha_T[T - T_r]. \quad (4-19)$$

Inserting Equation (4-18) in the above equation, and rearranging the equation in terms of temperature changes, will lead to the thermal term of vertical strain increment.

$$\Delta\varepsilon^{Temp}_{zz} = \alpha_T \Delta T \left( \frac{1}{1 - \vartheta} \right) \quad (4-20)$$

Referring back to Equation (4-13), and imposing the effect of thermal strain by superposition in Domain I (with given boundary conditions), will result in:

$$\varepsilon_{zz} = \frac{1 - \vartheta^2}{E} \left( \Delta\sigma_{zz} - \frac{\vartheta}{1 - \vartheta} \Delta\sigma_{xx} \right) + \alpha_T \Delta T \left( \frac{1}{1 - \vartheta} \right). \quad (4-21)$$

By replacing  $\Delta\sigma_{xx}$  with its equivalent in Equation (4-18), and rearranging the equation, total vertical strain changes due to temperature in Domain I will be:

$$\varepsilon_{zz} = \alpha_T \left( \frac{1 + 2\vartheta}{1 - \vartheta} \right) (T - T_r) \quad (4-22)$$

Replacing the solution of uniaxial temperature equation in a pure conductive heat flux in the equation will provide us with the profile of vertical strain from the injection well, up to the boundary interface between the domains (temperature front), as below:

$$T(x, t) = (T_r - T_s) \operatorname{erf} \left( \frac{x}{2 \sqrt{\frac{\lambda}{\rho r c_r} t}} \right) + T_s \quad (4-23)$$

Replacing  $T(x, t) - T_r$  in the equation of vertical strain yields:

$$\varepsilon_{zz} = \alpha_T \left( \frac{1+2\vartheta}{1-\vartheta} \right) \left[ (T_s - T_r) \left[ 1 - \operatorname{erf} \left( \frac{x}{2\sqrt{\frac{\lambda}{\rho_r c_r} t}} \right) \right] \right] = \alpha_T \left( \frac{1+2\vartheta}{1-\vartheta} \right) (T_s - T_r) \operatorname{erfc} \left( \frac{x}{2\sqrt{\frac{\lambda}{\rho_r c_r} t}} \right); \quad (4-24)$$

where the heat flux due to steam injection is convective and conductive, the vertical strain profile can be obtained as below:

$$\varepsilon_{zz} = \alpha_T \left( \frac{1+\vartheta}{1-\vartheta} \right) (T_s - T_r) \operatorname{erfc} \left( \frac{x - u_w t}{2\sqrt{\frac{\lambda}{\rho_r c_r} t}} \right); \quad (4-25)$$

where  $u$  is the displacing phase (hot water) bulk velocity,  $\lambda$  is thermal conductivity of sandstone (reservoir), and  $\rho_r c_r$  is the volumetric heat capacity of reservoir (bulk volume of solid and fluid).

It must be noted that Equation (4-25) and Equation (4-26) are applied only in Domain I, and the process was considered isopotential, where pressure remains constant. In reality, steam injection will result in pressure changes both in space (along  $x$  axis) and in time. However in thermal recovery techniques, pressure is assumed constant behind the steam interface. With constant pressure profile in space, the effect of pressure on vertical and horizontal strains has to be applied by superposition on the bulk volume (of Domain I) scale.

As discussed, in Domain I, in the bulk region,  $\varepsilon_{xx}=0$ , and as  $\varepsilon_{xx}$  is a very small amount in magnitude, it can be omitted from the equation, and after the solution of the problem, it can be replaced back into the equation for obtaining the other root of the equation (an example to support the math behind the infinitesimal variable omission is provided in the appendix). Alternatively the methodology can be supported by singular perturbation theory (Witelski and Bowen, 2009). By re-inserting  $\varepsilon_{xx}$  into the constitutive relation and applying the effect of temperature in the entire bulk volume of Domain I, one can write:

$$\varepsilon_{xx} = \frac{1-\vartheta^2}{E} \left( \Delta\sigma_{xx} - \frac{\vartheta}{1-\vartheta} \Delta\sigma_{zz} \right) + \alpha_T \Delta T \quad (4-26)$$

Knowing  $\Delta\sigma_{zz} = 0$ , and  $\Delta\sigma_{xx} = \frac{-\alpha_T E \Delta T}{1-\nu^2}$  and replace them into the above equation,

$$\varepsilon_{xx} = -\alpha_T (T_s - T_r) \operatorname{erfc} \left( \frac{x}{2 \sqrt{\frac{\lambda}{\rho_r c_r t}}} \right) + \alpha_T \Delta T. \quad (4-27)$$

And as it can be seen from the equation, the horizontal strain tends to change along x axis, but the value is very small, and in the overall bulk region, tends to zero.

### Stress Analysis in “Domain II”

Domain II is decomposed from Domain I, on the temperature interface, therefore temperature remains constant and equal to reservoir temperature in Domain II, and as such the only flow parameter that is influential on stress and strain profiles in Domain II, is pressure.

In order to obtain the stress and strain in the outer domain (far-field), we apply the concept of domain decomposition for non-overlapping domains. The same domain interface that experienced a roller boundary condition on Domain I, now has to experience a constant stress (at each time), or constant strain, along x axis, based on domain decomposition theorem. Physically the concept is meaningful for linear elasticity, since the physical processes in both domains occur simultaneously (time is frozen), and in space they are dependent, and some stress is expected to be interlocked on the domain interface (steam front), at each time. The same stress (that can be translated to strain) has to be applied for geomechanical analysis of Domain II. Therefore the boundary conditions are the same as in the second domain in Figure 4-3.

The stress that is applied on the interface can be named  $\sigma_x^b$ , and can be considered as a body force (stress) that acts horizontally on the second domain bulk volume at each time. The solution for constitutive equations and stress equilibrium equations can be obtained initially with zero body force assumption ( $\sigma_x^b = f = 0$ ), and then replace the body force (boundary conditions) back into the solution of the equation. A mathematical example is provided in the Appendix 4-B for an Ordinary Differential Equation (ODE) equation that shows the concept is mathematically correct.

Since the dominant (if not only) effects in Domain II are pressure changes, the constitutive equations for plane-strain need to be written in terms of pressure changes.

$$\varepsilon_{xx} = \frac{1}{E} \left[ (1 + \nu) \sigma_{xx} - \nu (\sigma_{zz} + \sigma_{xx} + \sigma_{yy}) \right] - \frac{1+2\nu}{E} \Delta P \quad (4-28)$$

The geomechanical condition in Domain II is also a plane strain condition ( $\varepsilon_{yy} = 0$ ), and therefore the horizontal strain formulation can be rearranged as below :

$$\varepsilon_{xx} = \frac{1-\nu^2}{E} \left( \Delta \sigma_{xx} - \frac{\nu}{1-\nu} \Delta \sigma_{zz} \right) - \frac{1+2\nu}{E} \Delta P \quad (4-29)$$

By applying the same conditions as in Domain I, ( $\varepsilon_{xx} = 0, \Delta \sigma_{zz} = 0$ ), the changes in total stresses in Domain II, can be formulated as below :

$$\Delta \sigma_{xx} = \frac{1+2\nu}{1-\nu^2} \Delta P \quad (4-30)$$

Replacing the above equation in plane strain form of equation for  $\varepsilon_{zz}$ , yields:

$$\varepsilon_{zz} = (1 - \nu^2) \left( -\frac{\nu}{1-\nu} \frac{1+2\nu}{E} \frac{\Delta P}{1-\nu^2} \right) = \frac{1}{E} \left( -\frac{\nu}{1-\nu} \right) (1 + 2\nu) \Delta P \quad (4-31)$$

As discussed, the equation for pressure changes can be written in a uniaxial exponential form with assumption of constant pressure equation behind steam zone interface, or in the form of  $E_i$  function for radial geometry with a transient flow, and pressure changes from injection well toward a constant pressure far field (i.e. aquifer). In our formulation, the former case is accepted and is replaced in Equation (4-31) to yield:

$$\varepsilon_{zz} = \frac{1}{E} \left( -\frac{\nu(1+2\nu)}{1-\nu} \right) \left[ \exp \left( -\frac{\mu_w c \phi}{k k_{rw}} V_x \chi \right) \right] (P_s - P_r); \quad (4-32)$$

where  $P_s$  is the steam front pressure and can be approximated as injection pressure. It should be noted that where the injection well constraint is constant injection rate, the form of the equation for pressure changes.

Domain II, can be modelled the same way as “tectonic” modelling in terms of boundary conditions, where a constant strain or stress (at each time) is exerting an increasing force to the lateral sides of the domain, to represent the thrust fault behavior. The other side of the domain, around the production wellbore vicinity, can be modelled with a constant zero lateral displacement (production well). However in early injection time, the production well is



far from the domain interfaces, and as such far field boundary conditions are not influential on the geomechanical analysis. In other words, the effect of boundary conditions on the mechanical solution in Domain II is not as important as in Domain I.

As discussed, the solution of the problem was derived with the assumption of  $\sigma_x = \varepsilon_x = 0$  at initial condition and on the boundaries, however from physical point of view, it is not the case. The impact of lateral straining (by Domain I) on Domain II, and horizontal stress on interface, can be imposed at next step:

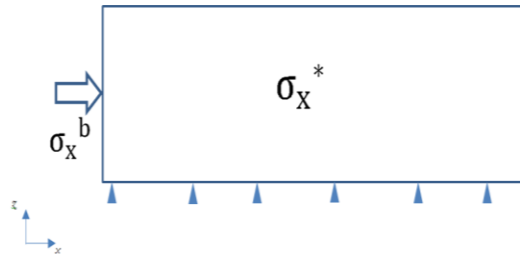


Figure 4-4-Representation of boundary conditions in Domain II

$$\sigma_{xx}^{II} = \sigma_x^b + \sigma_x^*; \quad (4-33)$$

,where,  $\sigma_x^b$  is the horizontal induced stress on interface by Domain I, which was initially assumed to be zero for problem simplification, and  $\sigma_x^*$  is the horizontal stress induced in Domain II due to changes in the pore pressure. Therefore the total stress in Domain II can be written as below:

$$\sigma_{xx}^{II} = \frac{1+2\nu}{1-\nu^2} \Delta P^{II} - \frac{\alpha_T E \Delta T^I}{1-\nu^2}; \quad (4-34)$$

where  $\Delta P^{II}$  shows the pressure changes in Domain II, and  $\Delta T^I$  represents the temperature changes in Domain I. If profile of stress changes in Domain II is needed,  $\Delta T^I$  should be replaced by its values at the domains interface, which is the temperature shock value. It must be noted that even though pressure is assumed constant behind the interface, the bulk volumetric influence of pressure changes in Domain I has to be applied in the calculation of horizontal stresses of both domains.

$$\sigma_{xx}^{II} = \frac{1+2\nu}{1-\nu^2} \Delta P^{II} - \frac{\alpha_T E \Delta T^I}{1-\nu^2} - \frac{1+2\nu}{1-\nu^2} \Delta P^I; \quad (4-35)$$

where

$$\Delta P^{II} = [\exp(-\frac{\mu_w c \phi}{k k_{rw}} V_x \chi)] (P_s - P_r) \quad (4-36)$$

$$\Delta P^I = \frac{P(x=r_w) + P^b}{2} - P_r \cong P_{inj} - P_r \quad (4-37)$$

Equation (4-37) should be applied in the total horizontal stress equation in Domain I as well. And as such the total stress profile remains the same, but the stress magnitudes change. Since the approach we used is uniaxial along the x-axis, and there is no vertical force or momentum exerted from Domain I on Domain II, the equation for vertical strain profile in Domain II does not need to be modified in order to account for strain changes in Domain I. However horizontal strain can be calculated in Domain II, with the same approach as for estimation of horizontal stress, considering the effect of interface strain induced by Domain I.

### Domain Boundary Selection Challenges

As it was discussed before, the key parameter for decision on the selection of the interface location to split the larger reservoir into smaller non-overlapping sub-domains was temperature front location at each time. Temperature front in our approach is obtained from saturation front at each time, based on the suggested relationship developed between these two fronts. But the solution to the temperature equation as well as the discrepancy between saturation front and temperature front was mainly based on the uncoupled heat and fluid flow equation. However the mutual impact of pore pressure and rock solid body was neglected in this approach. In order to obtain the precise location of the temperature front (domain interfaces) at each time after injection of steam, geomechanical responses of reservoir must be taken into account.

The next section shows how the frontal movements will be affected by inclusion of geomechanics into the workflow. Simulation on a synthetic steamflood case suggests that these effects can sometime be significant on the selection of boundary for domain splitting. Therefore prior to applying the developed analytical techniques, one must calculate the location of the temperature front (at the desired time) and mutual flow-geomechanical impacts must be taken into account for frontal movement analysis.

### Effect of Geomechanical Processes on the Frontal Movements

Koohmarch Hosseini and Chalaturnyk (2011) obtained a relationship that relates temperature front from saturation front movement in time and space. They obtained this relationship for three cases of transport mechanisms, where heat and fluid flow are: pure convective, convective-conductive, and pure conductive. They showed the lag between frontal movements is more significant in convective processes, and obtained a dimensionless parameter between two fronts as below:

$$\xi = \frac{(\rho_w E_w \phi)}{(\rho_w E_w \phi + \rho_s E_s (1-\phi))} = \frac{\phi}{\phi + \frac{M_s(1-\phi)}{M_w}}; \quad (4-38)$$

where  $\xi$  is the dimensionless parameter that shows the ratio between travelled distance (from injection point) by temperature front and travelled distance by hot water saturation front,  $M_s$  and  $M_w$  are volumetric heat capacities of solid and hot water, and  $E_w$  and  $E_s$  represent enthalpies of hot water and solid phase respectively. And we have:

$$M_i = \rho_i C_{pi}, \quad (4-39)$$

$$U_{fT} = \xi U_{fw}, \quad (4-40)$$

where  $\rho_i$  represent phase densities,  $C_{pi}$  (J/g °C) shows specific heat capacity of each phase, and  $U_{fT}$ ,  $U_{fw}$  are the temperature contour velocity and hot water bulk velocity. If geomechanics is included in the thermal recovery techniques, the dimensionless parameter changes in time and space. In steam-flood scenario due to increase of pressure and temperature in near field and far field, effective stresses decrease and accordingly volumetric strain increases in the regions of increased pressure and temperature. By increase of volumetric strain, the reservoir rock dilates and in a drained mechanism, porosity increases as a result of rock expansion. It must be noted that material expansion is expected in both elastic constitutive equations (expansion) and plastic (by shear strain or dilation) flow rule. Based on Equation (4-49), changes in porosity (due to geomechanical effects of underground injection into reservoir) will change the dimensionless parameter  $\xi$  and accordingly the distance between saturation front and temperature front will change, at each time after injection, as well. The order of changes in frontal velocities, are mainly a function of pressure and temperature evolution in space and in time. If geomechanics is considered in thermal

recovery processes, porosity values have to be updated due to changes in volumetric strain as proposed by Touhidi-Baghini (1998):

$$\phi = \frac{\phi_0 + \varepsilon_v}{1 + \varepsilon_v} ; \quad (4-41)$$

where  $\phi_0$  is initial reservoir porosity, and  $\varepsilon_v$  is volumetric strain. In continuum mechanics point of view, the overall changes of volumetric strain in a continuum material, where total stress is relatively constant, is related to changes in pressure and temperature as below:

$$\Delta \varepsilon_v = 3\alpha \Delta T + \frac{\Delta P}{K} = 3\alpha_T \Delta T + \frac{3(1-2\nu)}{E} \Delta P \quad (4-42)$$

In the course of hot water injection, volumetric strain increases and therefore porosity increase (in time and space) in a hyperbolic fashion based on Equation (4-41) and so does the dimensionless parameter  $\xi$  that relates the temperature front to hot water saturation front. Therefore, by inclusion of geomechanics, the distance between the saturation front and temperature fronts is expected to increase even more in time and space. **Figure 4-9** shows the changes in  $\xi$  versus porosity changes for a steamflood example.

The other influential parameter on the value of  $\xi$  is the ratio between volumetric heat capacities. Volumetric heat capacity of sandstones changes with time, and as such during injection the ratio between  $M_s/M_w$  is changing as well. Heat capacity of water is relatively constant and does not change with temperature, but specific heat capacity of quartz (major mineral in sandstone reservoirs) increases with time, based on the laboratory work of Vosteen et al (2003) at Aachen University. In our work the specific heat capacity of sandstone was approximated by correlation proposed by Cassis et al (1985).

Therefore, in thermal recovery techniques, to obtain the temperature front at each time (in convective-dominated processes), in thermo-hydro-geomechanical coupled system; modified  $\xi$  has to be multiplied by saturation front travelled distance. Saturation front distance can be easily calculated by obtaining derivative of fractional flow curve versus temperature at shock, which can be calculated from relative permeability data or production data.

$$x_T = U_w f'_{Sw} t \xi^* ; \quad (4-43)$$

where  $f'_{sw}$ , is the Welge tangent to the fractional flow curve,  $U$  is the total velocity,  $x_T$  is travelled distance of temperature front and  $\xi^*$  is the modified so-called dimensionless parameter for scenarios that geomechanics is included in the thermal-flow problem.. It must be noted that saturation frontal velocity changes slightly due to geomechanical changes as well. If changes in displacing phase velocity in space is negligible (based on Buckley-Leverett assumption), the only influential parameters that changes the travelled distance of front is the effect of geomechanics on fractional flow curve and  $f'_{sw}$ . In this work, the geomechanical effects on relative permeability are considered negligible.

Pressure front in a steam-flood scenario is also expected to change, by reservoir geomechanical changes due to changes of effective stress during injection, when the process is transient. Based on poroelastic constitutive equation, reservoir volumetric response can be written as:

$$\frac{-Kk_r}{\mu} \nabla^2 p = \frac{\partial \zeta}{\partial t}; \quad (4-44)$$

where  $\zeta$  is the strain parameter. On the other hand,

$$\frac{Kk_r}{\mu} \nabla^2 p = \frac{1}{M} \frac{\partial p}{\partial t} - \alpha \frac{\partial \varepsilon_v}{\partial t}; \quad (4-45)$$

where  $\alpha$  is the Biot constant, and  $M$  is the storage coefficient (inverse of reservoir bulk porosity multiplied by bulk compressibility). Only in special cases, will pore pressure obey an uncoupled equation. For more details refer to Wang (2000). Volumetric response of the reservoir can be written in terms of drained bulk modulus of elasticity,  $K$  as below:

$$\varepsilon_v = \frac{-1}{K} (\sigma^{total} - \alpha p). \quad (4-46)$$

Assuming the changes in total stress is negligible, by applying chain rule, one can write:

$$\frac{\partial \varepsilon_v}{\partial t} = \frac{\partial \varepsilon_v}{\partial p} \cdot \frac{\partial p}{\partial t} = \frac{\alpha}{K} \frac{\partial p}{\partial t} \quad (4-47)$$

Replacing Equation (4-47) into Equation (4-45), and rearranging Equation (4-47) yields:

$$\frac{Kk_r}{\mu} \nabla^2 p = \left( \frac{1}{M} - \frac{\alpha^2}{K} \right) \frac{\partial p}{\partial t}. \quad (4-48)$$

Comparing the obtained equation for transient processes with uncoupled form of pressure equation shows that the absolute value of term in exponential form of pressure solution  $\frac{\mu_w c \phi}{k k_{rw}}$  is less in coupled form of transient pressure equation. Therefore, with the same assumption adapted from Butler's theory, pressure remains constant behind the steam front, but beyond the steam front, pressure drops more slightly compared to an uncoupled case. As such, the discrepancy between the pressure front and steam front, at each time in a coupled flow-geomechanics system is larger than the pressure front in an uncoupled system. The pressure front in a coupled isothermal system is therefore a function of Biot's coefficient, and for a simple example, the uniaxial pressure profiles for different Biot's coefficients are plotted in **Figure 4-5**, versus distance from steam front during an unsteady state flow (when the pressure front has not reached the radius of drainage or an aquifer with constant head). Must be noted that geomechanical effects on relative permeability curves are neglected again, and in a uniaxial geometry with constant injection rate, the Darcy velocity of displacing phase (hot water) is assumed constant.

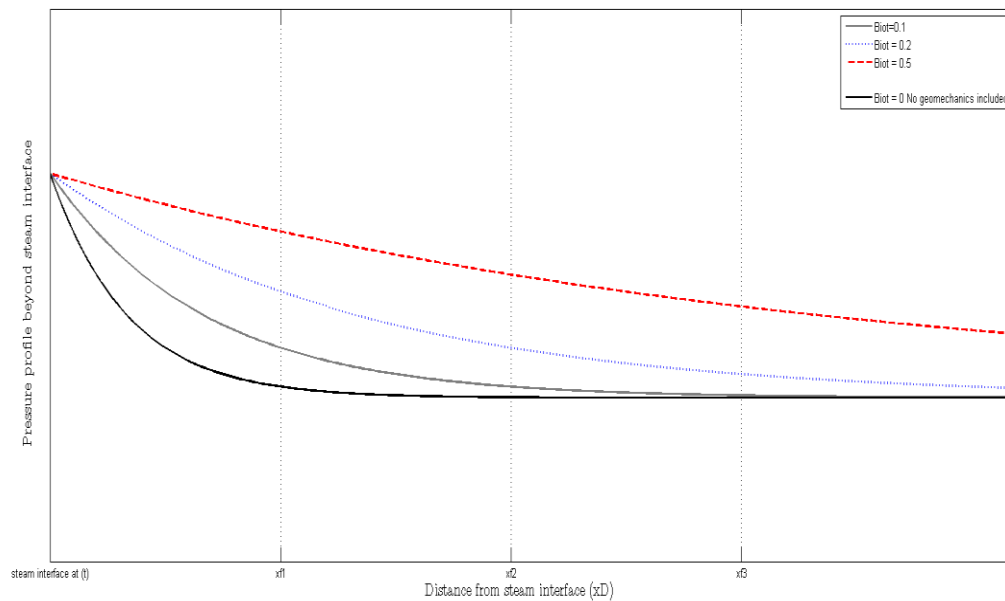


Figure 4-5- Pressure profile changes, beyond steam chamber where geomechanical reservoir volume responses are taken into account.

## Numerical Example

Table 1 represents the hydraulic and numerical properties of a two-dimensional steamflood built in CMG-STARs. The model is made along  $x$ - $z$  plane, and there are 60 cells along  $x$  axis and 20 cells in  $z$  direction.

**Table 4-1-Reservoir fluid and rock properties**

Parameter	Value
<b>Geomechanical properties</b>	
$\theta$	0.25
$E$ , MPa	600
$\alpha_T$ , 1/°C	$10^{-5}$
$\rho_s$ , kg/m <sup>3</sup>	2125
<b>Hydraulic properties</b>	
$\phi_0$	0.3
$k$ , mD	2000
$S_o$ initial	0.75
$\mu_{T=23^\circ\text{C}}$ , cp	5780
$\mu_{T=260^\circ\text{C}}$ , cp	2.5
$P_{\text{injection}}$ , kPa	3400
$T_{\text{initial}}$ , °C	8
$P_{\text{initial}}$ , kPa	625
$c_{pr}$ sandstone, (j/g/°C)	0.7234
$c_{pw}$ water, (j/g/°C)	4.16

**Figure 4-6** shows the pressure and temperature fields after four years of steam injection in the depth of 450 meters from surface.

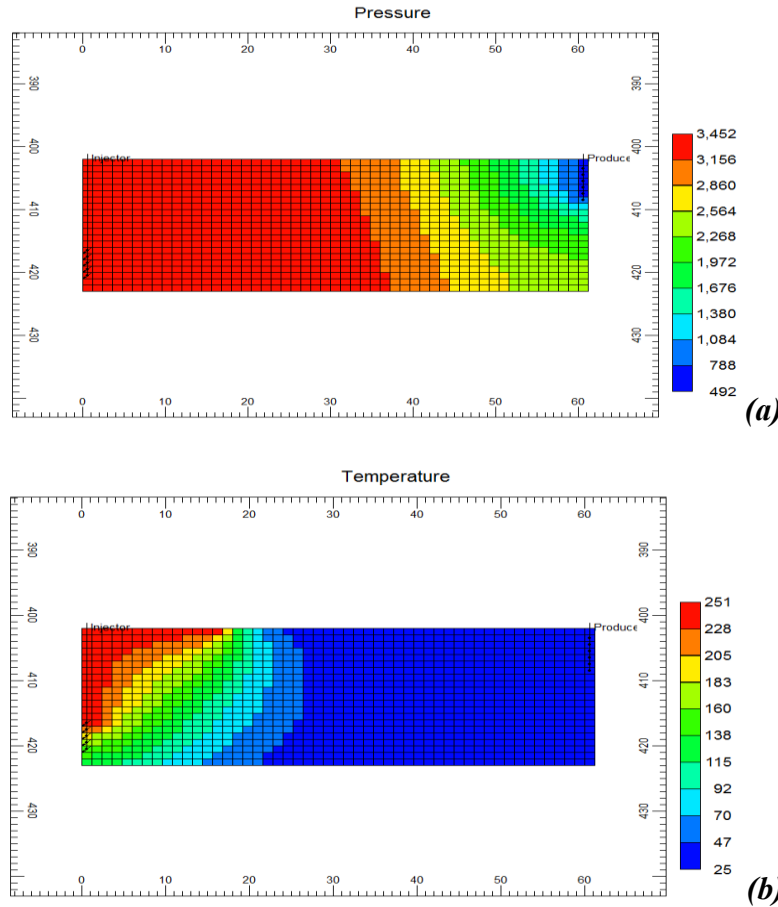


Figure 4-6-Pressure distribution (a) and temperature distribution (b) in a steamflood numerical simulation after 4 years of injection

**Figure 4-7a** illustrates the pressure and temperature changes in the course of injection in the middle of reservoir ( $N_x=28$ ,  $N_z=10$ ). As it can be seen from the diagram, both pressure and temperature increases in time, but the rate of pressure increase curve, decreases in time and the temperature increase rate, increases in time.

**Figure 4-7b** shows the individual components of volumetric strain changes due to temperature and pressure changes in time. The volumetric strain calculations are based on Equation (42). The dotted blue line represents the volumetric strain changes due to thermal effects, the red line shows the pressure effects, and the green line shows the total volumetric strain induced due to ensemble effect of thermal and pressure increase effects in the reservoir. As the curves show, the thermal volumetric strain portion of total elastic volumetric strain is initially less than the portion of volumetric strain induced due to pressure changes. However after almost 1700 days the total strain due to thermal effects exceeds the



total strain due to pressure effects. In SAGD class of operations, however the thermal portion of volumetric strain is more than pressure portion, since the early injection time. The intersection between these two curves shows the time when the temperature front has crossed the mentioned grid-cell number, and the temperature remains constant in time and almost equal to the injection temperature.

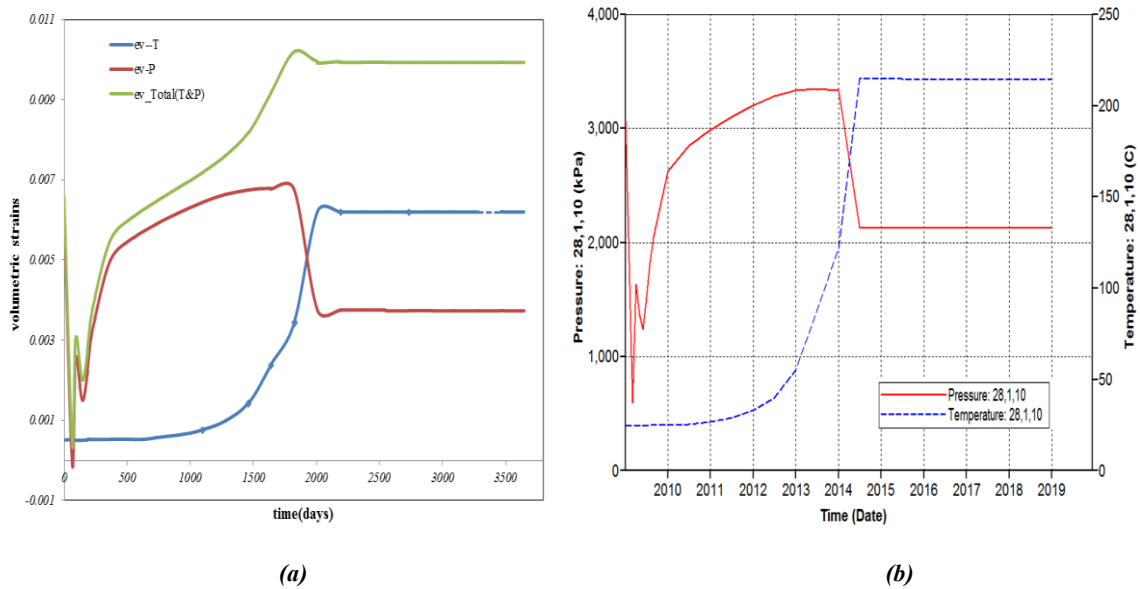


Figure 4-7-Pressure and temperature changes in time (a), and the individual volumetric strain changes due to temperature and pressure changes (b).

**Figure 4-8** shows the porosity changes due to volumetric strain changes based on Tohidi-Baghini proposed equation. The curve is confined only to the range of volumetric strain induced in the steam flood example (represented in Figure 4-6). As it can be seen volumetric strain changes in time, and so does porosity (in a hyperbolic manner versus volumetric strain). The changes in porosity will change the pressure diffusivity equation (as discussed in previous section), as well as the dimensionless parameter that related temperature front to saturation front.

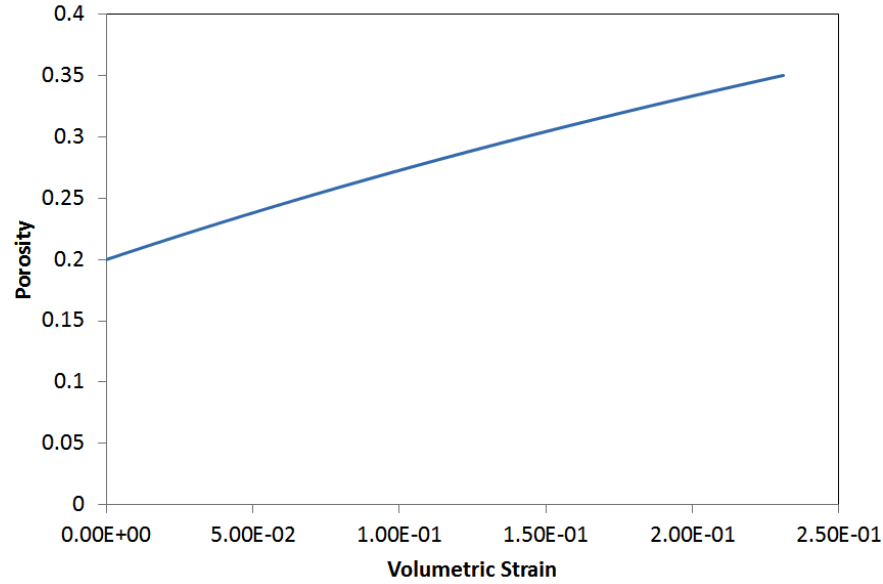


Figure 4-8-Porosity changes due to volumetric strain changes in a steamflood case

The so-called dimensionless parameter, as discussed, is not only a function of porosity but also a function of ratio of phase volumetric heat capacities. Specific heat capacities (and therefore volumetric heat capacities) are temperature dependent. The correlation we used to account for the temperature dependency of specific heat capacity of sandstone was the one offered by Butler (2004) and Cassis et al. (1985):

$$C_p = 0.715 + 1.707 \times 10^{-3}T - 1.908 \times 10^{-6}T^2 \quad (4-49)$$

What matters in the dimensionless parameter, is the specific heat capacity of hot water over specific capacity of solid phase (sandstone). The specific heat capacity of water was (4.12 J/g °C) and independent of temperature, but still their ratio is changing by temperature. Therefore the changes in porosity at one hand and the temperature-dependent volumetric heat capacity on the other hand, alter the discrepancy between fronts.

As shown in **Figure 4-9**, integration of geomechanics into process physics (and increase in volumetric strain and porosity), increases the discrepancy between temperature front and saturation front travelled distances. As such, in uncoupled physics the distance between temperature front and saturation fronts is less than in a coupled system. Figure 4-9 also shows the reverse effect of temperature on the so-called dimensionless parameter  $\xi$ . The

higher the temperature is (due to changes on heat capacity ratio), the lower the discrepancy will be between temperature front and saturation front.

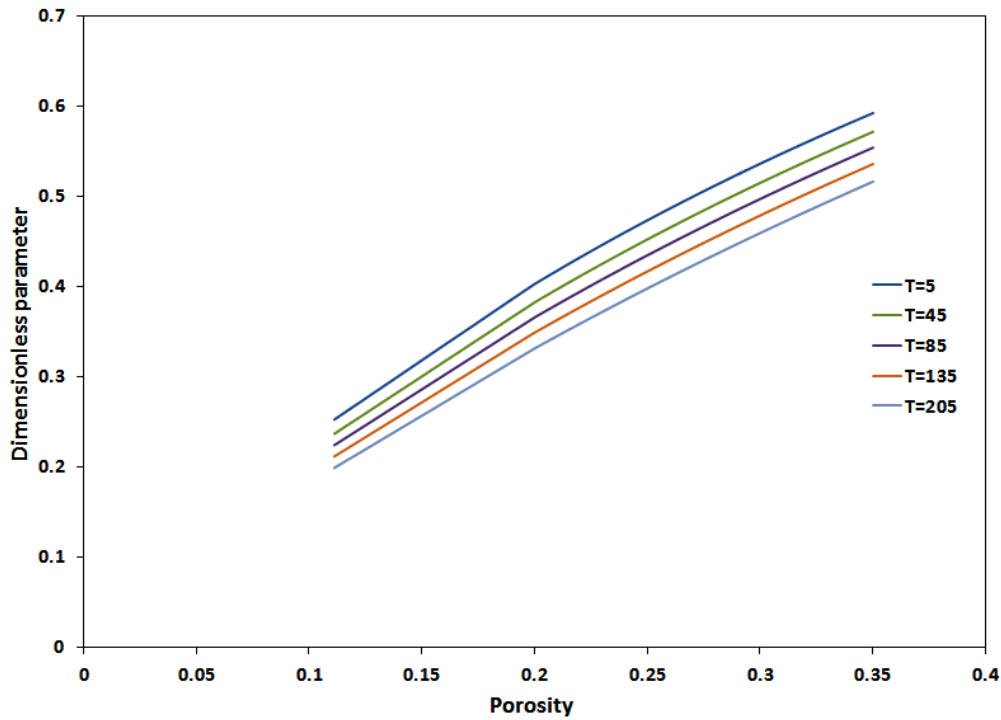
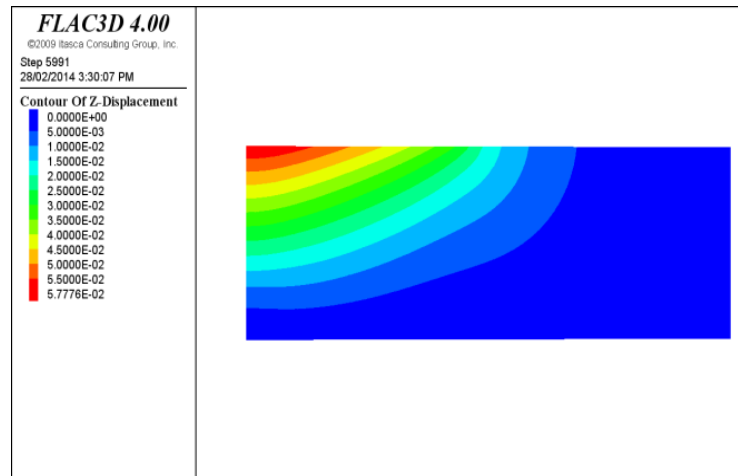


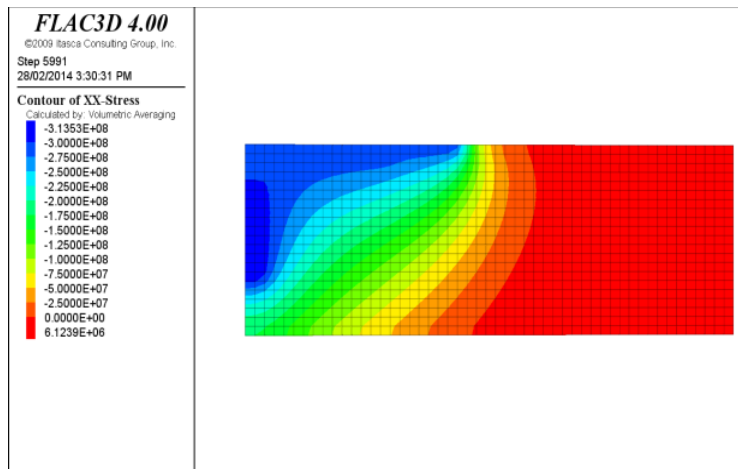
Figure 4-9-Dimensionless parameter  $\xi^*$  (ratio of temperature front distance to saturation front distance) versus porosity at different steam chamber temperatures

### Model Validation and Representation of Problem Continuity

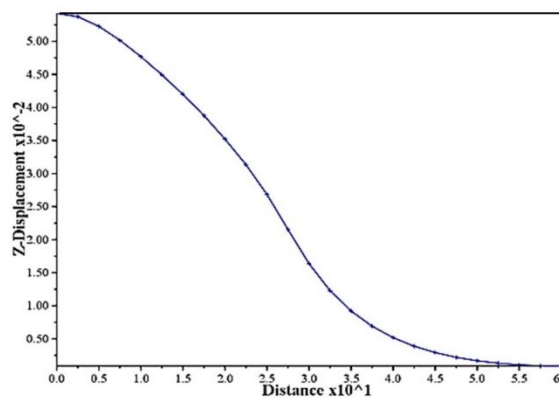
The same steamflood numerical example presented in the paper was coupled sequentially to geomechanics to obtain the stress and strain profiles on the global domain. The thermal fluid flow model was built in CMG-STARS and was coupled with geomechanics on FLAC 3D (product of Itasca) platform. The model parameters are the same as in Table-1 and the geomechanical grid was made identical to the flow problem grid. The geomechanical boundary conditions of the model were free displacement on the top, roller boundary on the right side and zero displacement at the wellbore and zero displacement at the bottom. The results of the coupling scheme after 3 years of steam injection were as below:



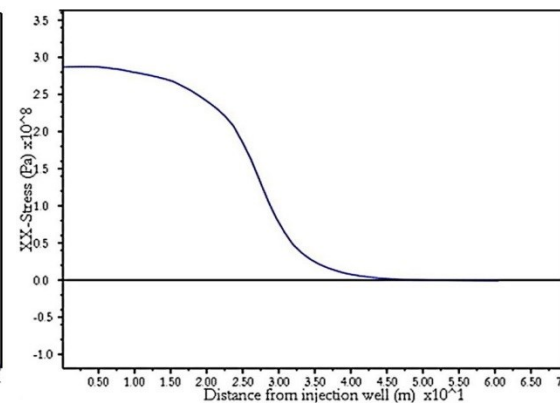
(a)



(b)



(c)



(d)

Figure 4-10- Cross-sectional (x-z plane) representation of vertical displacement contour (a), horizontal stress contour (b), vertical displacement profile (c) and horizontal stress profile (d)

versus distance from injection well, after three years of steam injection. Injection well is located on the left side of the model.

As illustrated in **Figure 4-10**, both geomechanical solution variables (stress and strain) are continuous across the reservoir, including the domain interfaces. As such application of domain decomposition technique is relevant and allowed to be used for our problem, based on Shwarz's theorem. The validity of the solution continuity could be performed by solution of the same analytical model in a unified global model; however we provided the numerical model for most robust analysis. As shown in Figure 4-10 both variables decay from injection well with temperature fall-off, which is in agreement with the analytical model developed here. **Figure 4-11** illustrates that the results of analytical model (vertical displacement profile) at Domain I (25 m from injection well after 3 years) is closely matched with the solution of the numerical coupled CMG-FLAC model at an elevation of 10 m from the bottom of the injection well. It must be noted that the figure shows the global domain (60 m along  $x$  axis), however the analytical model verification was performed only at Domain I for simplicity.

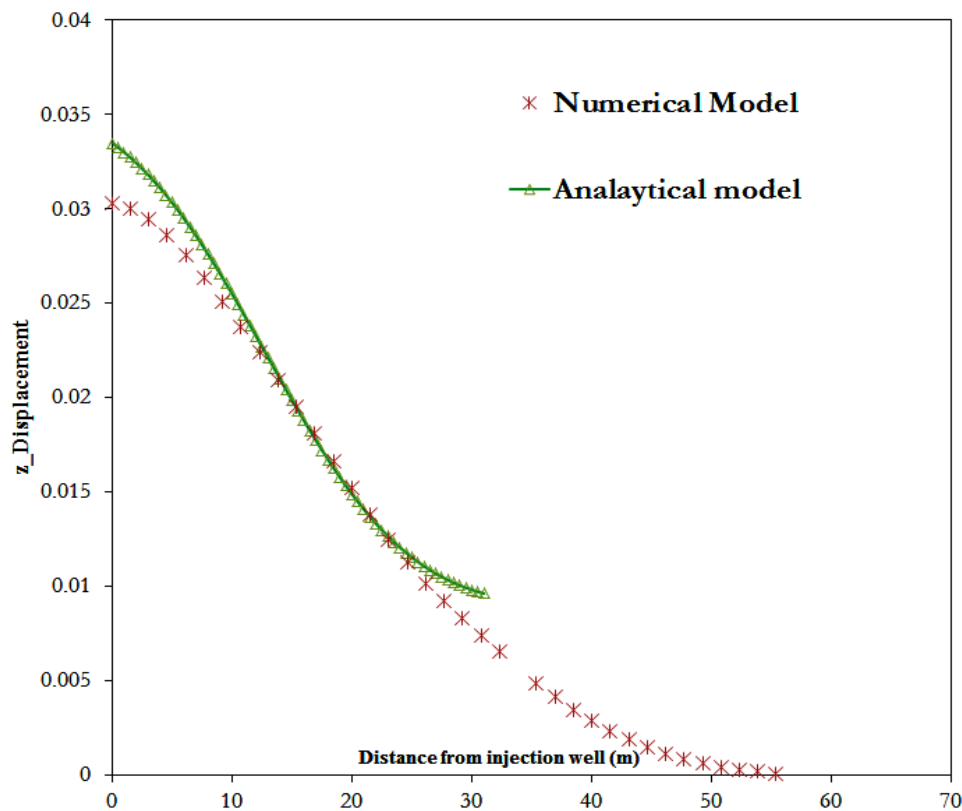


Figure 4-11- Vertical displacement in meters along  $x$  horizontal-axis: validation of the analytical model with coupled numerical model in the middle of the reservoir in Domain I.

## Discussion

The analytical models, presented so far for estimation of geomechanical responses in thermal recovery techniques remain simplified due to the many assumptions required for their solution. Consequently, they are not very powerful tools for performance prediction as their output is independent of operational parameters, and are not reliable tools for highly stress-sensitive class of reservoirs, particularly where failure analysis is concerned.

Jaeger et al (1997) presented an analytical model that reports one displacement value in the entire domain due to overall pressure and temperature changes. However, in the large-scale reservoirs (with a large distance between injection and production wells), different physical processes occur in time and in space, and therefore the analytical proxies have to report stress changes in space. Risnen et al (1982) presented a simplified analytical model, in which they simply replaced pressure equation in Kirsch's equations (1898) for radial wellbore stability stress changes. The original formulations scale well only for wellbore vicinity problems and are not good representatives of full-field reservoir scale, and furthermore the pressure equations they used were a steady state radial form of pressure equation. However, from physical point of view where steam is injected in underground reservoir and the far-field boundary conditions are not necessarily constant pressure head boundaries (i.e. constant production rate producers), there is certainly a transient flow that may never reach to steady state or pseudo-steady state flow. As such, temperature and pressure effects in classical formulations, are not time or space dependent, and only the difference (in dynamic property values), between far-field and borehole wall appeared in equations (Fjær et al., 2008). The analytical model presented in this paper, as opposed to the previous analytical geomechanical proxies, considers the effect of both space and time, and therefore stress and strain fields can be updated in time, and can be calculated everywhere in the reservoir (both at far field and near field regions).

Furthermore, a failure analysis is provided which can predict if for instance in ten years of injection with a suggested maximum operating pressure (MOP), there will be any potential for failure in the reservoir or in the caprock. In thermal recovery techniques, due to high temperature and pressure induced around the injection wells, cap rock integrity is always a challenge. Furthermore, the vast majority of rocks show very small yield stresses (Cristescu, 1989). Increase of significant pressure can cause isotropic unloading in mean

effective stress, whereas the increase in temperature causes a deviatoric stress in the reservoir. The increase in deviatoric stress can lead to shear failure, and potential caprock issues. These behaviors can be different in each location in the reservoir from injection to the production well. To have a better understanding of maximum allowed operating pressure (MOP) and temperature during thermal recovery techniques, one needs to have sufficient information about reservoir stress path and failure criterion. Given the stress and strain profile at each time during steam injection, we can calculate where and when, there is a probability of hazardous shear failure. The failure model adopted here is Drucker-Prager which is one of the simplest viscoelastic constitutive models and requires least information about rock mechanical behavior. The formulations to model failure analysis (failure and stress state at each location, and at each distance from injection well) based on the presented analytical model are provided in the Appendix 4-C.

The main concepts behind the analytical model were: domain decomposition, and temperature and saturation frontal discrepancies. As far as to the knowledge of authors, there has been no analytical model in literature to obtain the temperature shock frontal velocity and location, purely from heat transport equation, such as Buckley-Leverett for saturation forward convective transport equation. We instead obtained the temperature front from saturation front at each time during steam injection. The formulations presented to correlate frontal movements, are based on the assumption of pure convective flow processes; the formulations will be slightly different for the processes that are involved with conduction as well. For further details on the formulations of convective-conductive mechanisms, refer to Koohmarch Hosseini and Chalaturnyk (2011).

As the so-called interface is moving in time, the stress and strain profiles obtained are dynamic and must be updated for each simulation time step. At each time the location of the domain interface can be obtained by the formula presented above, and then applied in each domain separately. It must be noted that the forms of the equations do not change in time, but only the difference in domain sizes is time-dependent.

The key advantages of the technique can be outlined as follow: the solution of the analytical model is space dependent and as opposed to the previous conventional analytical model (for prediction of geomechanical responses of the reservoir in thermal recovery techniques),

pressure and temperature are not inserted into the model as a domain bulk average value, but are space variant. The analytical model also can be applied to time sensitive scenarios (e.g. no-stationary dynamic models), and therefore can be applied in the cases where the well configuration or well rates and pressure change in time, or to the cases where the non-linear displacement process dictates finer resolution of (geomechanical) results in time. The model can also address the problem of caprock integrity in time and space. The same analytical model that was developed here, can be discretized and used in the development of numerical simulation codes in a three-dimensional space, in order to reduce the computational load and increase memory efficiency. The discretization scheme requires decomposition of the geomechanical domain into several sub-domains (based on the presented algorithm) and provide the solution of the problem in each zone differently by applying the proper boundary condition on each domain, due to the neighboring domains, as was discussed in our approach. However numerically, the problem is more complicated, since the solution convergence of the problem is highly sensitive to the choice of the “transmissions condition” as well as “relaxation parameter”. Additional details on numerical domain decomposition techniques can be found in Willien and Shnieder (1996).

The model deficiencies can be outlined as: the profile of stress around the production well must be calculated as well, even though the pressure and temperature changes and accordingly the geomechanical changes are not significant around the production well. Although the pressure and temperature changes along z-axis are negligible (particularly far from injection well), these changes can be still slightly influential on stress analysis. Temperature and pressure changes in our model were considered uni-axial, but geomechanical changes were reported in two-dimensional space (x-z). Therefore the authors recommend developing the same formulations for a radial or cylindrical geometry to overcome this issue. Furthermore, pressure was considered constant behind the domain interfaces (temperature front). This assumption is not irrelevant for processes such as SAGD, but yet due to suggested well-known radial solution of pressure diffusivity equation, pressure is expected to decay from the injection well. The rock constitutive behavior was assumed elastic in our model. Based on the rules of plasticity, the stress changes are only due to elastic portion of total volumetric strain changes; however for more precise failure prediction, extension of the model to plastic flow scenario is suggested for physically more accurate



predictions of displacements. Finally, it must be noted that the separating interface between the domains, can be mathematically anywhere in the reservoir where there is no jump in the solution of geomechanical problem. However our approach used the temperature front as the domain splitter, for problem simplicity and reduction of variables to solve the problem in each domain.

In this work, application of domain decomposition technique in the geomechanical domain, provided us the chance to predict displacement and stresses everywhere in the reservoir, based on the sensitive time-varying temperature and pressure fronts. Application of domain decomposition was in good agreement with the physics of the problem, as in reality at each domain different physical processes happen. The use of domain decomposition must be dynamic as the splitting interface moves in space with time.

## Conclusion

A domain decomposition approach was used to develop an analytical proxy for full-field geomechanical assessment of reservoir. The domain splitting technique was based on temperature front movement. Effect of geomechanics on frontal movements was assessed and it was shown that inclusion of geomechanics into the model simulation causes the discrepancy between temperature front and saturation front to increase. The mathematical model is exact, and a numerical flow-geomechanics model was made to show that the stress and strain field, out of analytical model is in close agreement with the numerical model. The output of proxy model is stress and strain field prediction in near field and far field as well as prediction of an approximate shape of steamed zone. At the end, an analytical based failure analysis was provided to predict shear failure in reservoir during steam injection. A two-dimensional CMG-STARS steamflood model was built for representation of pressure, temperature, and saturation front locations. Temperature and pressure fields obtained from the numerical model, were translated into geomechanical responses (stress, and volumetric strain), and the influence of geomechanics was studied on temperature and saturation front discrepancy.

## Nomenclature

$P_s$	=	Injection pressure
$P_r$	=	Initial reservoir pressure
$V_x$	=	Darcy velocity of steam front

---

$\chi =$	Distance beyond the steam saturation front
$c_p =$	Specific heat capacity of the reservoir
$\mu_{w,o} =$	Water, oil viscosity
$c =$	Oil sand compressibility
$k_{rw} =$	Relative permeability of water
$K =$	Reservoir absolute permeability
$\emptyset =$	Reservoir porosity
$t =$	Time (after steam injection)
$T_s =$	Steam injection temperature
$T_r =$	Initial Reservoir temperature
$\rho =$	Density of the reservoir (mixture of oil, water, and rock)
$U_w =$	Bulk velocity of injected hot water
$\lambda =$	Thermal conductivity of the medium
$\varepsilon_{ij} =$	Strain tensor
$\varepsilon_v =$	Volumetric strain
$\sigma_{ij} =$	Stress tensor
$\vartheta =$	Poisson's ratio
$E =$	Young modulus
$\alpha_T =$	Linear thermal expansion coefficient
$\delta_{ij} =$	Kronecker
$\sigma_x^b =$	Horizontal stress on domain interfaces
$q' =$	Deviatoric stress
$p' =$	Mean effective stress
$M =$	Slope of yield envelope
$C =$	Cohesion factor
$\varphi =$	Rock internal friction angle
$F =$	Yield envelope
$M_{s,w} =$	Volumetric heat capacities of solid, hot water
$U_{fw} =$	Velocity of water (displacing phase) saturation shock
$U_{fT} =$	Temperature front velocity
$f'_{sw} =$	Slope of tangential line on fractional flow function at saturation front
$\alpha =$	Biot's coefficient
$K =$	Reservoir rock bulk modulus (drained)

## Chapter 5: Reservoir-Geomechanics Model Order Reduction by Use of Streamline-Based Domain Decomposition and Linearization<sup>§§</sup>

### Introduction

Solving highly nonlinear unsteady reservoir fluid flow problems several times, rapidly, and iteratively is currently almost intractable, even considering the current state of computer-CPU's. One of the reasons behind this issue is that solving nonlinear equations typically involves a large matrix factorization at every time step of simulation. Analyzing and controlling the behavior of a linear system is much easier than a nonlinear one, since solving the linear form of flow equations requires only one matrix factorization. As such, applying linearization methods in solving complex reservoir fluid flow problem has been proposed recently in several studies. This work, presents a novel linearization method for reservoir models.

Cardoso and Durlofsky (2009) expanded the fluid flow equations around previously simulated (saved) states and corresponding controls. They also showed performing one or more high-fidelity training simulations is necessary in the trajectory piecewise linear method (TPWL). Thus, in an uncertain model (i.e. in history matching process where the simulation of uncertain model needs to be run many times), the method is not particularly useful and the linearized model would likely diverge in the course of history matching. In previous fluid flow linearization methods the coordinate system is not subject to any changes; however in the present paper, we show that the model, which behaves quite nonlinearly in Cartesian or Radial coordinates, behaves linearly in streamline-based coordinates.

In the control design of a fluid flow system, a substantial gain can be obtained using a linearized model. In two-phase flow mode, the number of states (pressure and saturation for incompressible immiscible systems) is twice the number of model grid-blocks. Thus control design, particularly online control implementation, is impractical due to the fact that the

---

<sup>§§</sup> A version of this paper was presented at 9<sup>th</sup> International Geostatistics Congress, Oslo, Norway 11-15 June 2012. This paper has been rigorously peer reviewed and published in the conference proceedings.

computational cost of optimal control design is a power function of system dimension ( $O[n^3]$ ), where  $n$  represents system dimension). Model order reduction is a way to overcome this problem (Gratton, 2004). Projecting the equations onto a set of basis function spanning the flow solution space, is the central idea of previous works, e.g. combination of TPWL with Arnoldi reduced order models (Rewiński, 2003). Nonlinear analogue circuits and micro machined devices are some examples of the application of this method. Also for this application, a truncated balanced realization algorithm has been combined with the TPWL order reduction approach (Vasilyev, 2003). Proper orthogonal decomposition (POD) is another approach in the reduced order model procedure (Cardoso et al., 2010).

In the previous works, nonlinearity effects were neglected as model order reduction was applied to a linearized model. The range of validity of linearized models is restricted to a small perturbation around a steady state. In the present work, instead of using basis functions, state variables of grid-blocks that streamlines pass through are categorized into some groups, and are selected as state variables of the reduced order local models. These state variables are strongly correlated to observation data of each local model. It appears that grid blocks that have no streamlines passing through them, have no effect on our approach on order reduction of the reservoir model.

This paper shows that state variables (water saturation, pressure) of each grid block have a strong correlation with neighboring grid-blocks' values; while the effect of so called correlation is less for more distant grid-blocks. Therefore state variables of any trajectory lines that connect a source to a sink and pass through certain number of grid blocks can be approximated by state variables of neighboring trajectory lines passing through neighboring blocks. In the present work, streamlines play the role of the so-called trajectories. A linear relationship between neighboring streamlines is developed employing least square method.

It must be noted that in this study, the streamline tracings and visualizations are based on the bundle of streamlines that connects each source (injector) to sink (producer) and show the delineation area between each injector/producer well-pair. The decision on localization of the system to sub-systems was also made based on the number of lines that were traced in each grid block between each injector/producer pair. As such traced streamlines are corresponding to the number of lines per each injector/producer.

In this study, we first summarize the governing equations for oil-water flow and develop a scheme to discretize them. Streamline simulation and least square method are then briefly described. In the next step, the development and application of the localization, reduction and linearization method in reservoir flow model is discussed. And finally some synthetic simulation cases are tested to verify the accuracy and efficiency of the proposed method.

### Oil-Water Flow Equations and State Space Model

The reservoir fluid flow equations are obtained by combining mass conservation equations with the Darcy's law, which was shown by Aziz and Settari (1986). In general, these partial differential equations do not have analytical solutions. Consequently, discretization of a reservoir model is commonly performed using well-established techniques of finite element (FE), finite volume (FV), or finite differences (FD). The basic element of the spatial domain in a FD discretization is a grid-block, and the primary variables of the system, here  $p_o$  (oil pressure) and  $S_w$  (water saturation), are defined either at grid-nodes or at grid centers. By using FD technique, the PDE equations were approximated by Markovinovic (2009) for the grid block  $ijk$  as below:

$$V_{ijk} W_{ijk} \frac{dx_{ijk}}{dt} = T_{ijk} \begin{bmatrix} x_{i,j,k-1} \\ x_{i,j-1,k} \\ x_{i-1,j,k} \\ x_{i,j,k} \\ x_{i+1,j,k} \\ x_{i,j+1,k} \\ x_{i,j,k+1} \end{bmatrix} + G_{ijk} \begin{bmatrix} D_{i,j,k-1} \\ D_{i,j-1,k} \\ D_{i-1,j,k} \\ D_{i,j,k} \\ D_{i+1,j,k} \\ D_{i,j+1,k} \\ D_{i,j,k+1} \end{bmatrix} + V_{ijk} \tilde{q}_{ijk}; \quad (5-1)$$

where

$$x_{ijk} = \begin{bmatrix} p_{ijk} \\ S_{ijk} \end{bmatrix}. \quad (5-2)$$

Stacking the above equations for all the grid-blocks  $ijk$  on top of each other yields a time-continuous (*generalized*) *state-space* formulation (Markovinovic, 2009):

$$VW \frac{dx}{dt} = Tx + Gd + V\tilde{q}; \quad (5-3)$$

where the state vector  $\mathbf{x}$  consists of pressures and water saturations of each grid block,  $V$  is a diagonal matrix with entries that are functions of grid-block volume and fluid densities,  $W$  is a block diagonal matrix with entries being functions of compressibility, porosity and water saturation,  $T$  and  $G$  are sparse block matrices accommodating block-interface transmissibilities for oil and water,  $d$  is the depth-vector, and  $\tilde{q}$  denotes the well flow-rates.

$T$  matrix transmits the vector of previous time step state variables into the next one. The properties of the transmission (mapping) matrix (sparse block) enable us to split the large-scale state space model into the smaller ones that are independent from each other. It can be shown that the state variables of each grid block do not have necessarily a correlation with the state variables of all grid blocks, since there are some grid blocks that have zero coefficients in calculation of state variables of certain grid blocks. This fact is used in the development of the proposed method and shows that the state variables (i.e. pressure, saturation) along each streamline could be obtained by just knowing the value of the state variables of the adjacent streamline and the relation between these two lines. The relationship is explained in the following sections.

### Streamline Simulation

Streamline simulation is a reservoir simulation technique by which the reservoir is split into series of one-dimensional trajectories, and the transport equations are solved along the trajectories. Each trajectory is called a streamline, and is computed by drawing the tangential line to the velocity vector, or orthogonal to pressure contours at each location. In streamline class of simulations, transport problem (convective saturation equation) is solved along these lines and moved forward along streamlines, rather than underlying 3D grids. Under these conditions the time-steps are much larger compared to those in conventional finite difference simulators. Therefore streamline simulation is a fast technique (faster than finite difference simulator) to model large heterogeneous reservoirs with water injection as a mechanism for reservoir pressure maintenance. Very early studies on streamline technology can be found in Thiele et al. (1996), Datta-Gupta et al. (1995). More about streamline simulation can be found in Batycky et al. (1997), Thiele (2001), Theil et al. (1997), Datta-Gupta (2000). The technique is suited mainly for optimization techniques that require a number of forward simulations in sequence. The number of time steps is only a function of well events and also

the changes in physics of fluid transport, and is independent of reservoir heterogeneity, reservoir geometrical properties and grid block size and orientation (Thiele, 2001).

Due to its versatility, streamline simulation has been used in a number of applications, for example screening and ranking geostatistical models, rapid assessment of production strategies, and upgridding and upscaling. Other advantages of streamline simulators are reduction in grid-orientation effects and quantitative flow visualization (Thiele, 2001). The last mentioned attribute of streamlines is what we mainly seek in this study, which is development of a proxy, as the trajectories carry some fluid flow and petrophysical information along themselves.

### Least Square Model Fitting

Least square method is one of basic methods of identification. Since this method is one of the main bases of this study, the least square model fitting is summarized in this section. The model relates an observed variable  $y_t$  (the regressand), to  $p$  explanatory variables (the regressor)  $u_{1t}$  to  $u_{pt}$ , and all are either known in advance, or observed. The model deals with only one unknown coefficient per explanatory variable. Thus, if the regressor vector has  $p$  elements, coefficients are collected into  $p$ -vectors (Norton, 1986):

$$u_t = [u_{1t} \quad u_{2t} \quad \dots \quad u_{pt}]^T. \quad (5-4)$$

$$\theta = [\theta_1 \quad \theta_2 \quad \dots \quad \theta_p]^T. \quad (5-5)$$

Then the model is:

$$y_t = f(u_t, \theta) + e_t \quad (5-6)$$

$$t = 1, 2, 3, \dots, N;$$

where  $e_t$  accounts for observation and modeling error. The main objective of the method is finding the value  $\hat{\theta}$  (function of  $\theta$ ) which minimizes  $S$  defined as follow:

$$S = \sum_{t=1}^N e_t^2 = \sum_{t=1}^N (y_t - f(u_t, \theta))^2. \quad (5-7)$$

In linear cases,  $f(.,.)$  is linear in the unknown coefficients

$$y_t = u_t^T \theta + e_t \quad t = 1, 2, 3, \dots, N. \quad (5-8)$$

To make the algebra tidy,  $N$  – vectors  $Y$  and  $e$  are defined as a collection of all samples  $y_1$  to  $y_N$  and  $e_1$  to  $e_N$  respectively. The matrix  $U$  (with dimension of  $N \times P$ ) is a collection of all the  $u_i$  vectors.

$$Y = U\theta + e; \quad (5-9)$$

and

$$S = e^T e. \quad (5-10)$$

The value  $\hat{\theta}$  which minimizes  $S$  can be calculated as below:

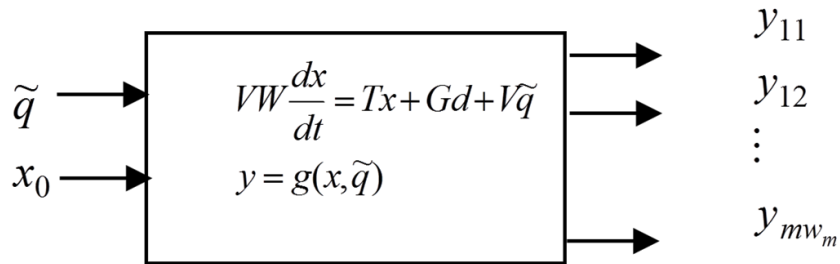
$$\hat{\theta} = [U^T U]^{-1} U^T Y. \quad (5-11)$$

To check that  $\hat{\theta}$  gives a minimum value of  $S$  (not a maximum or saddle point), any small change ( $\delta\theta$ ) about  $\theta$  must increase  $S$ . If  $U^T U$  is positive-definite, then  $\delta\theta^T U^T U \delta\theta$  cannot be zero for any real non-zero  $\delta\theta$  and also the existence of the inverse of  $U^T U$  is guaranteed.

## Development of the Method for Linearization and Reduction of Reservoir Model

### Streamline-based Assisted Localization and Reservoir Model-reduction

A typical commercial reservoir simulator provides some dynamic outputs such as water-cut, production rate, etc. for a given reservoir and well condition as inputs. The schematic of a flow simulator is shown as below:



$y_{ij}$  is the  $j^{th}$  output of  $i^{th}$  well, and  $m$  is the number of wells

Figure 5-1-Schematic description of flow simulator and definition of sub-systems



If the vector of outputs is decomposed into  $m$  vectors  $z_i = (i = 1, \dots, m)$ ,  $z_i$  being the output of the  $i^{th}$  well, then the system can be decomposed into  $m$  sub-systems. Each sub-system has its own region of influence, in a way that the region has the largest possible influence on the outputs of a certain well (Arroyo-Negrete et al., 2006). If the region of influence for each sub-system is defined, the model obtained from each sub-system does not have the complexity of the original system since there is a large group of state variables that have no effect on the outputs of a given sub-system. Therefore, each sub-system has a limited number of state variables and a simple state space model. There are certain ways to identify the regions of influence of each sub-system (Emanuel et al., 1998). The use of streamline trajectories to identify these regions has proved to be useful in the past, especially in history matching problem which deals with large scale system. Emanuel et al. (1998) used streamlines to identify the grid-blocks that affect the production response in a specific well. In this paper, the information gleaned from streamline trajectories is used to identify the effective grid-blocks for a specific sub-system, then it is possible to restrict the model of subsystem to these grid blocks. In fact, the large scale reservoir model is localized into a number of subsystems that is equal to the number of wells. Any model will have a limited range of validity which may be restricted by the experimental conditions. A model is called "local model", when it has a range of validity that is smaller than the desired range of validity. Moreover, "operating regime" is a region in which local model is valid (Johansen et al., 1995). In this paper, local models are the models of each sub-system and the operating regime of each model is defined using streamline trajectories. Therefore, many state variables which have no influence on the observations are truncated from the proposed model, decomposing into the significantly small local models.

Construction of the proposed reservoir model has three main steps: (1) Decomposition of output vector of the reservoir model into a number of output vectors equal to the number of wells. Each new output vector belongs to a certain well and contains the outputs of the well. (2) Identification of the effective grid-blocks of each sub-system using streamline trajectories. (3) Third, a local model structure must be developed for each operating regime. It is necessary to mention that if the local structures are linear in parameters, the global model will be linear in those parameters. Therefore, the parameters can be identified by standard system identification tools. In the next section, the local linear models will be developed using least square method.

### Local Linear Model Structure Development

In the introduction section, the differences between a linear and non-linear system were mentioned in terms of behavior control, and it was recommended to use a linear system. Also the levels of correlation between some certain grid-blocks (connected by a streamline trajectory) with the neighboring and farther grid-blocks were discussed. This section explains how to develop a linear relation between each pair of adjacent streamline trajectories. We show here that a non-linear model can be transformed to a linear one using streamline-based coordinates. To verify this approach, the simulation results of a synthetic case are introduced in the next section.

A simulation of the full flow model must first be performed and the state variables of the system (saturation and pressure of all grid-blocks in two-phase flow) should be saved. The streamlines' configuration and distribution must be calculated in the next step using a streamline tracing algorithm, or any other streamline simulation commercial tools (3DSL<sup>\*\*\*</sup> was used for the present work).

By eliminating some grid blocks that streamlines of a certain well do not pass through, fewer grid blocks remain that control the most significant state variables of the systems. Since the state variables represent a very good description of a system, the state variables related to the remaining cells can describe well the desired operating regime of the reservoir. After eliminating excessive state variables, streamlines are sorted based on the proximity to each other. A value from 1 to  $N$  ( $N$  is the number of remaining streamlines, after elimination) is assigned to each streamline.

Having  $N$  regular lines, and knowing that they have a linear relationship, we need to figure out this relationship. Least square is a good approach to obtain the so-called relationship, due to its linearity and having sample data in several time steps. The next part explains how to obtain the linear relationship.

### Implementation of Least Square in Model Construction

First, some definitions are necessary to explain the method:

$S(i, j)$  = index of  $j^{th}$  cell of  $i^{th}$  streamline.

$Ns(i)$  = the number of cells that the  $i^{th}$  streamline pass through

---

<sup>\*\*\*</sup> Streamline simulator tool plugged in StudioSL, product of StreamSim.

$Xp_i(t)$ =pressure of the cell with index  $i$ ,  $t$  is index of time.

$Xs_i(t)$ =saturation of the cell with index  $i$ ,  $t$  is index of time.

The regressand vector of  $i^{th}$  streamline is the state variables of grid-blocks that  $(i + 1)^{th}$  streamline pass through. Similarly, the regressor vector of  $i^{th}$  streamline is the state variables of grid-blocks that the  $i^{th}$  streamline path through.

$$\begin{aligned} y_i(t) &= [Xp_{s(i+1,1)}(t) \quad Xp_{s(i+1,2)}(t) \quad \dots \quad Xp_{s(i+1,Ns(i+1))}(t) \\ &\quad \dots \quad Xs_{s(i+1,1)}(t) \quad Xs_{s(i+1,2)}(t) \quad \dots \quad Xp_{s(i+1,Ns(i+1))}(t)]^T. \\ u_i(t) &= [Xp_{s(i,1)}(t) \quad Xp_{s(i,2)}(t) \quad \dots \quad Xp_{s(i,Ns(i))}(t) \\ &\quad Xs_{s(i,1)}(t) \quad Xs_{s(i,2)}(t) \quad \dots \quad Xp_{s(i,Ns(i))}(t)]. \\ y_i(t) &= \theta_i u_i(t). \end{aligned} \quad (5-12)$$

The problem is converted to a simple linear regression equation. Knowing the  $n$  sample times of the vectors at  $(t_1, t_2, \dots, t_n)$ , one of the best approaches to solve the problem and obtain the optimum value for  $\theta$  in the regression equation is least square method.  $\theta_i$  for each streamline is obtained by least square method as follow:

$$Y_i = \begin{bmatrix} y_i^T(1) \\ y_i^T(2) \\ \vdots \\ y_i^T(n) \end{bmatrix}_{n \times Ns(i+1)}, U_i = \begin{bmatrix} u_i^T(1) \\ u_i^T(2) \\ \vdots \\ u_i^T(n) \end{bmatrix}_{n \times Ns(i)}, Y_i = U_i \theta_i. \quad (5-13)$$

$$\hat{\theta}_i = (U_i^T U_i)^{-1} U_i^T Y_i. \quad (5-14)$$

Consequently, if the value of state variables of grid-blocks through which the first streamline is passing, are known during the time steps (the elements of  $u_1(t)$  are known), the values of all state variables of all streamlines can be calculated. The linear local models can be simply replaced by simulator, thus the proposed method is computationally very robust. The remaining issue is that elements of  $u_i(\cdot)$  are not completely independent of one another as they are the values of state variables of grid-blocks through which a certain streamline passes. Singular value decomposition (SVD) is embedded in the workflow to overcome this problem. The next section explains briefly the coupling approach of SVD with the proposed method.

### Singular Value Decomposition Assisted in Model Construction

Matrix  $U_i$  can be transformed into the following form by singular value decomposition (Maciejowski, 1989):

$$U_i = WSV^T. \quad (5-15)$$

with  $W^T W = W W^T = I_{Ns(i)}$ ,  $V^T V = V V^T = I_n$ , and  $S$  being  $Ns(i) \times n$  with singular values of  $U_i$  distributed diagonally. Singular values of  $U_i$  are positive square roots of Eigen values of  $U_i U_i^T$ . The columns of  $V$  are orthonormalized eigenvectors of  $U_i^T U_i$  and the columns of  $W$  are orthonormalized eigenvectors of  $U_i U_i^T$ . The rank of  $U_i$  equals the number of nonzero singular values. If the rank of  $U_i$  is  $r$ , the first  $r$  columns of  $W$  are orthonormal basis of the range space of  $U_i$ . Singular values of stable system indicate the respective state energy of the system (Cardoso, 2010). Therefore, reduced order can be directly determined by examining the system singular values. If  $s_1, \dots, s_n$  are singular values of  $U_i$  in decreasing order, singular values with small amount can be removed. The ratio of remaining energy to total energy is calculated as follows:

$$\frac{\sum_{i=1}^l s_i^2}{\sum_{i=1}^n s_i^2}. \quad (5-16)$$

Transfer matrix  $\varphi$  will contain only first  $l$  columns of  $W$ . Then we have:

$$U'_i = \varphi_i^T U_i. \quad (5-17)$$

$$\hat{\theta}_i' = (U_i'^T U_i')^{-1} U_i'^T Y_i. \quad (5-18)$$

Using SVD helped to overcome two main issues: (1) singularity of inverse problem in calculating  $\hat{\theta}_i$  is solved by transforming the space into the space which is spanned by vectors related to largest singular values, and (2) the computational load is significantly reduced due to dimension reduction of  $U_i$  to  $U'_i$ .

### Wave Advanced Model Construction

By defining a new state vector,  $X(k)$ , which has state variables of gird-blocks that the  $k^{th}$  streamline pass through them for each operating regime, Wave Advanced Model (WAM) is constructed as below:

$$X(k + 1) = A(k)X(k). \quad (5-19)$$

$A(k)$  can be defined as:

$$A(k) = \theta_k, \quad X(k + 1) = y_k, \quad X(k) = u_k. \quad (5-20)$$

It can be seen that the number of cells that each streamline passes through varies the size of state vector. The linearity of local models along streamlines leads to linear global model along streamlines as well. This approach can be used in controller design or other field of reservoir engineering such as history matching problem.

It must be noted that since the state variables are a complete description of a system, reduced state variables can thoroughly describe dynamics of a reservoir. Moreover, the value of outputs can be obtained by an intelligent proxy (e.g. fuzzy systems), where the inputs are reduced state variables and the outputs derive from the reservoir model.

The proposed model has some important advantages:

- The model scans the space instead of the time, making the model quite efficient in terms of computational time. This is mainly because the large state vector of a reservoir model is decomposed into a number of state vectors, and at each step only state variables of this new state vector is updated. The localization procedure is very simple and can be done by categorizing the outputs by their own wells.
- According to the one dimensionality and linearity of the state vectors in Equation (5-19), all linear state estimators and controllers can be used in the proposed approach. For instance, the classical Kalman filter can also be used by slight changes in its formulation because of the size variation of state vectors.
- In addition to state vector decomposition, the state variables are reduced by the aid of streamline trajectories. Therefore, the error due to the reduction of the model is negligible.

## **Inclusion of Geomechanics in the Proxy Development Workflow**

Similar to fluid flow localization technique, geomechanics can be performed in the sub-domains that encompass the delineation region between each well-pair (source-sink pair).

The state variables of the system in geomechanical simulation are displacement in three directions ( $u_x, u_y, u_z$ ). Since by knowing the three displacements one can have a complete description of the system, as volumetric strains and the entire entities of stress tensor can be calculated by just knowing the displacement vectors. By considering the constitutive rock behavior as linear (elastic), the total ultimate response of the reservoir displacement field can be obtained by summing all the sub-domain linear systems calculated on each drainage/delineation regions. Furthermore, Canonical component analysis between volumetric strain field and pressure gradient (velocity) field showed that higher streamline densities (number of streamlines per each grid-cell) indicates regions of higher pressure gradient as well as larger volumetric strain changes. Therefore, where inclusion of geomechanics targets permeability changes and its impact on ultimate production rate changes, geomechanics can be performed only in the regions that streamlines pass through them (or number of streamline per grid cell is more than a certain number), and the rest of the model be neglected for hydromechanical coupling.

However, as opposed to fluid flow mechanisms, geomechanical responses of the reservoir (displacement vectors) cannot be predicted by the wave-advanced model. The reason is that geomechanical solution vectors cannot be solved along streamlines. The two equations below show that displacements have to be calculated on three principal directions (basis vectors along principal stress directions), and cannot be solved along a trajectory. The alternative form of the equilibrium equation can be written as below:

$$\sum_{j=1}^3 \frac{\partial}{\partial x_j} \left\{ G \left( \frac{\partial u_i}{\partial x_j} + \frac{\partial u_j}{\partial x_i} \right) \right\} = \frac{\partial (\alpha p - \lambda \epsilon_v)}{\partial x_i}; \quad (5-21)$$

where  $x_j$  shows the three directions of  $x$ ,  $y$ , and  $z$  (principal coordinates), and  $u_i$  shows the main three displacements in three directions,  $p$  represents the pore pressure, and  $\epsilon_v$  is a scalar value that shows the volumetric strain.  $\lambda$  is the Lamé's constant that is related to mechanical properties.

Alternatively the above equation can be rearranged and written as:

$$G \nabla^2 u_i + (G + \lambda) \frac{\partial \epsilon_v}{\partial x_i} = \alpha \frac{\partial p}{\partial x_i} \quad (5-22)$$

Furthermore to calculate the state vector of the geomechanics system, one has to solve the entire system by FEM or FD. Therefore there is not any potential gained value in terms of computational load reduction.

$$Ku = f; \quad (5-23)$$

where  $K$  shows the stiffness matrix ( rock property) ,  $u$  represent the displacement vector at each point, and  $f$  shows the residual matrix.

Inclusion of geomechanics on the linearized localized model enhances the computational efficiency, as the solution of the system on sub-domains is easier and faster. Furthermore, cutting the global domain to a smaller size where only streamlines pass through reduces the size of the matrices in the above equation, and as such the computational load increases significantly. Therefore geomechanics can be applied on each sub-domain separately and the coupling (one-way or two way) with fluid flow solution vectors (state variables) has to be performed right after “localization” stage, and the input for the mechanical simulation of next step is taken from the output (pressure and saturation) of the fluid flow streamline-based proxy.

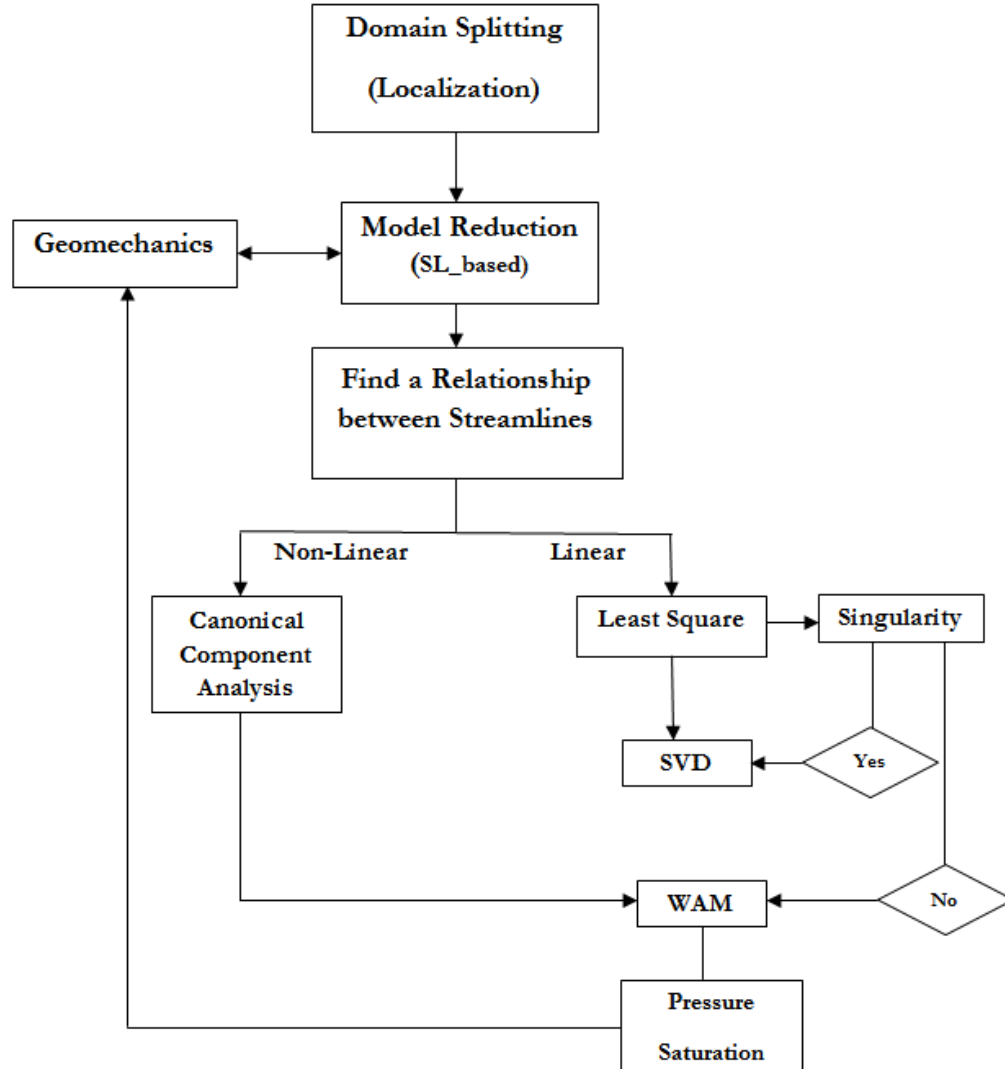


Figure 5-2-Workflow and steps for SL-based model order reduction of reservoir-geomechanics of large scale reservoirs

### Model Limitations and Powers

In order to apply Equation (5-14) and Equation (5-18) to the neighboring streamlines, the configuration of streamlines require staying unchanged during simulation. The model needs to be trained by inputting the state variables of the system for the first couple of time steps (i.e. ten initial time steps:  $t_0$ - $t_{10}$ ), in order to obtain the matrix  $\hat{\theta}_i$  or  $\hat{\theta}_i'$  for all streamlines. As such the proxy is best suited to the incompressible fluid flow problems or for linear displacement scenarios where the configuration of streamlines (and accordingly the grid blocks they pass through) does not change periodically during simulation run time.



Once the model is well trained and is reliable to use, the developed proxy has the predictive power to estimate the pressure and saturation of all streamlines in the subsequent time steps (i.e.  $t > t_{11}$ ). As such the only input for the proxy are the state variables (pressure and saturation) of grid blocks along only streamline No.1.

For large models the streamline transport step represents 40% to 80 % of the total CPU run time (Batycky et al., 2011). Obviously since the developed proxy needs to solve the saturation transport equation along only one streamline, the developed proxy is significantly faster than the streamline (or conventional FD ) simulator, particularly for large refined models.

It must also be noted that the pressure fields at the beginning of each global time step need to be calculated prior to streamline tracing step. As such for the proxy to start with the state variables along streamline No.1, the solution of the pressure field for the entire domain is an essential and inevitable step. Therefore, predicting pressure field in the domain (along all streamlines) is not a potential added value for the proxy, however the pressure matching results are shown for the numerical examples to represent the robustness of the linearized proxy.

## Numerical Example

**Case I:** This example is one of FrontSim<sup>†††</sup> sample streamline-based models (sample07). It is the two-dimensional reservoir that is discretized by  $25 \times 25$  square-shaped grids of 20m length. The model contains two pairs of injection-production wells. **Figure 5-3** illustrates the streamline configuration of the system. It can be seen that the model can be categorized into two groups: (1) the production well P1 and the injection well I1, (2) the production well P2 and the injection well I2. Each group contains 144 streamlines within the drainage area. Starting from the farthest (from the center of the model) right streamline to scan the entire streamlines of group (1) and obtain the linear relationship between the trajectory lines. For instance, after obtaining a relationship between state variables of second and first streamlines (by least square method), the state variables of second streamline can be obtained by knowing the state variables of the first streamline. The procedure is repeated for every two consecutive streamlines, until the entire first half of the reservoir (group 1) is scanned

---

<sup>†††</sup> FrontSim is the trademark name for Schlumberger's streamline simulator, which was one of the very first commercial streamline simulators. It is a three-dimensional, three-phase fluid flow simulator based on a state-of-the-art streamline concept.

(illustrated in Figure 5-3). All of the tasks are done for the second region. After obtaining the linear relationships between all of consecutive adjacent streamlines, the obtained model needs to be tested. The testing is done by estimating the state variables of all streamlines by knowing just the values of the farthest right and the farthest left ones (from the model center) and the relationship that was obtained in the previous step. In **Figure 5-4**, **Figure 5-5**, **Figure 5-6** the value of the pressure of the proposed method and simulator are compared in three different time steps. The comparisons show that the estimated values are well matched to the simulation data. For instance where the saturations equal to 0.25 the estimated model has exactly the same value.

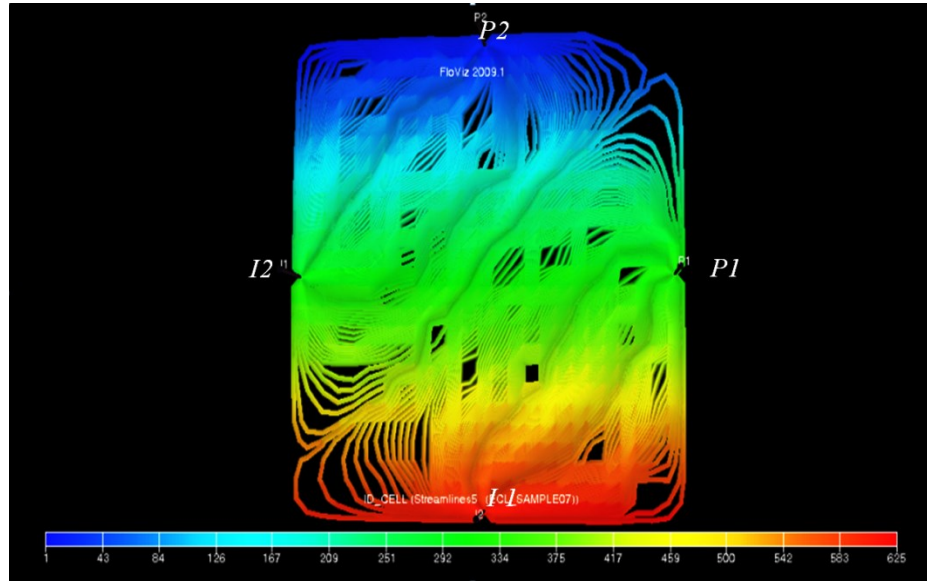


Figure 5-3-Streamline configuration of the two-dimensional model (case I). Illustration of two drainage areas (operating regimes), represented by I2-P2 and I1-P1.

In order to compare quality of proposed method, root mean square (RMS) error is used as the criterion, which is defined as:

$$\sqrt{\frac{1}{n} \sum_{j=1}^n (\hat{X}_j - X_j)^2}, \quad (5-24)$$

where  $n$  is the number of reduced cells (in the present case it equals to 548, whereas the original domain contains 625 grid cells),  $\hat{X}_j$  represents the estimation of state variables in  $j^{th}$  cell and  $X_j$  shows the value of state variables obtained by simulator in  $j^{th}$  cell.

**Table 5-1**, summarizes the RMS values of state variables in several time steps. The results

verify the accuracy of the method about the linear relations between two consecutive streamlines.

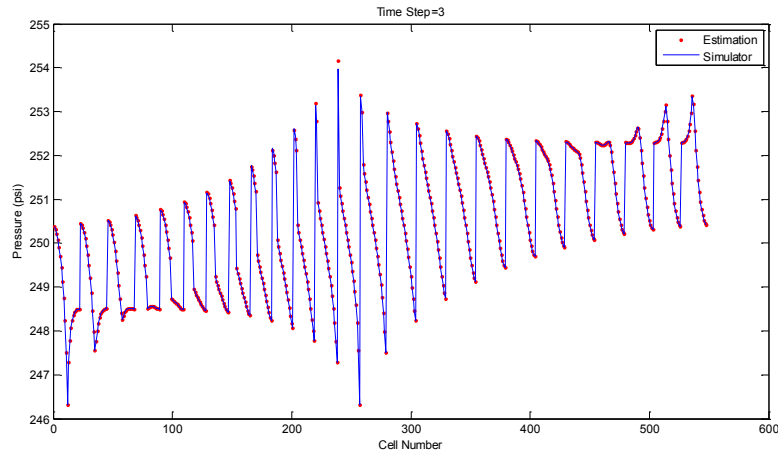


Figure 5-4-Comparison between estimated pressure of reduced cells by proposed model and values of streamline simulator, Time step=3.

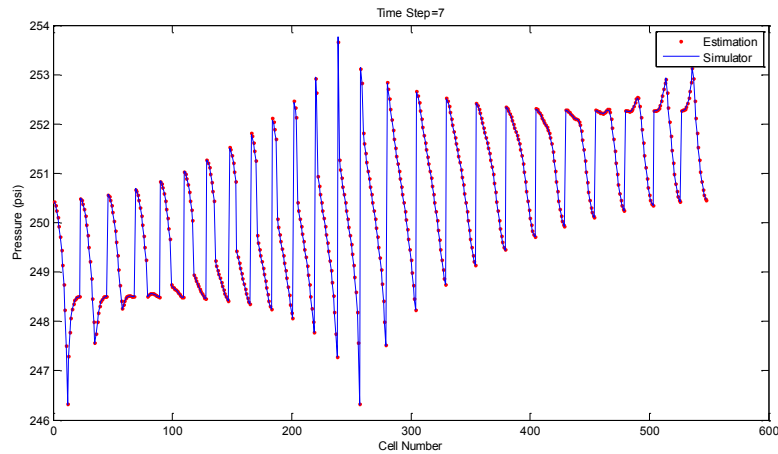


Figure 5-5-Comparison between estimated pressure of reduced cells by proposed model and values of streamline simulator, Time step=7.

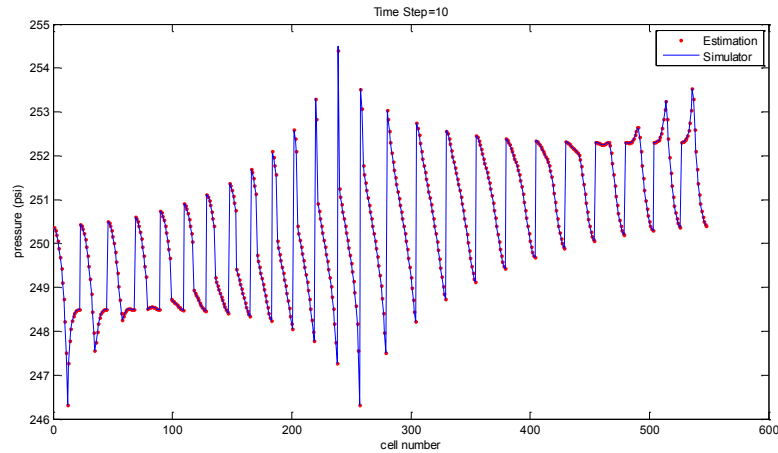


Figure 5-6-Comparison between estimated pressure of reduced cells by proposed model and values of streamline simulator, Time step=10.

**Table 5-1-RMS of state variables of the proposed method**

Time-step:	1	2	3	4	5	6	7	8	9	10
<b>RMS of Pressure</b>	$5 \times 10^{-10}$	$2 \times 10^{-10}$	$3 \times 10^{-10}$	$2 \times 10^{-10}$	$7 \times 10^{-10}$	$2 \times 10^{-10}$	$2 \times 10^{-10}$	$5 \times 10^{-10}$	$5 \times 10^{-10}$	$5 \times 10^{-10}$
<b>RMS of Saturation</b>	$4 \times 10^{-30}$	$1 \times 10^{-30}$	$4 \times 10^{-30}$	$1 \times 10^{-30}$	$4 \times 10^{-30}$	0	0	0	$1 \times 10^{-30}$	$1 \times 10^{-30}$

**Case II:** The geo-model and the configuration of streamlines are illustrated in **Figure 5-7**. The reservoir model can be categorized into four bundles of streamlines. Then the coefficients of linear state space local model, WAM, are computed by least square method assisted SVD for each group. **Table 5-2** shows the root normal mean square NRMS of state variables related to some samples of streamlines. The results show that the proposed model functions fairly robustly. Comparison between two models' pressure and saturation of a random cell are shown as an example in **Figure 5-8**.

**Table 5-2- NRMS of state variables related to streamlines**

Number of Streamline	2	10	19	25	31	36
NRMS	0.002	0.002	0.013	0.014	0.018	0.002

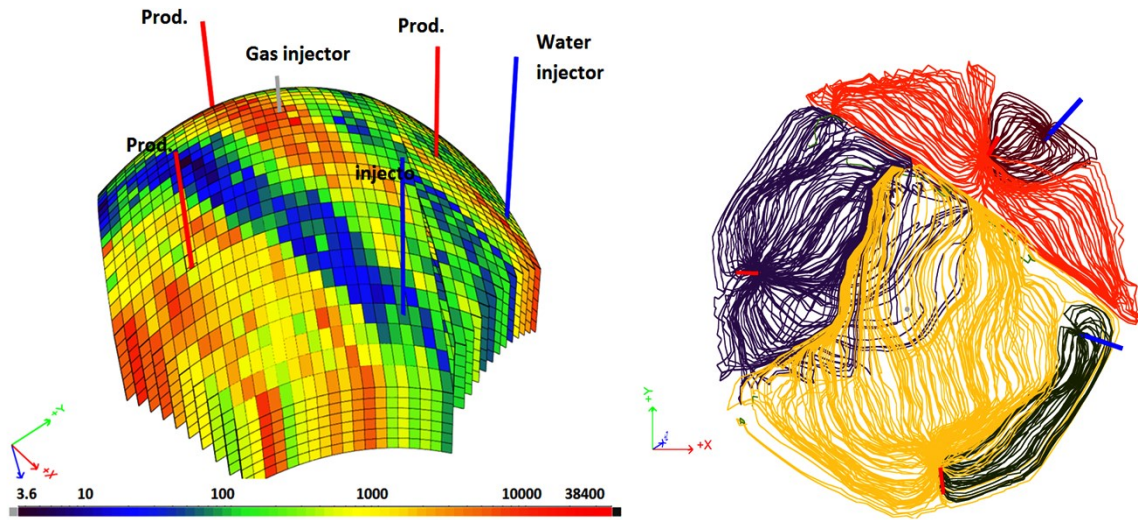
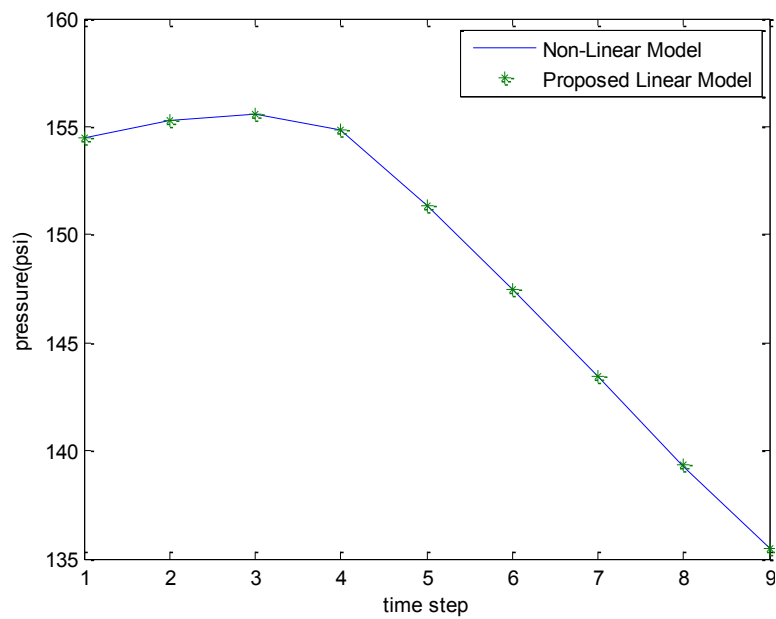
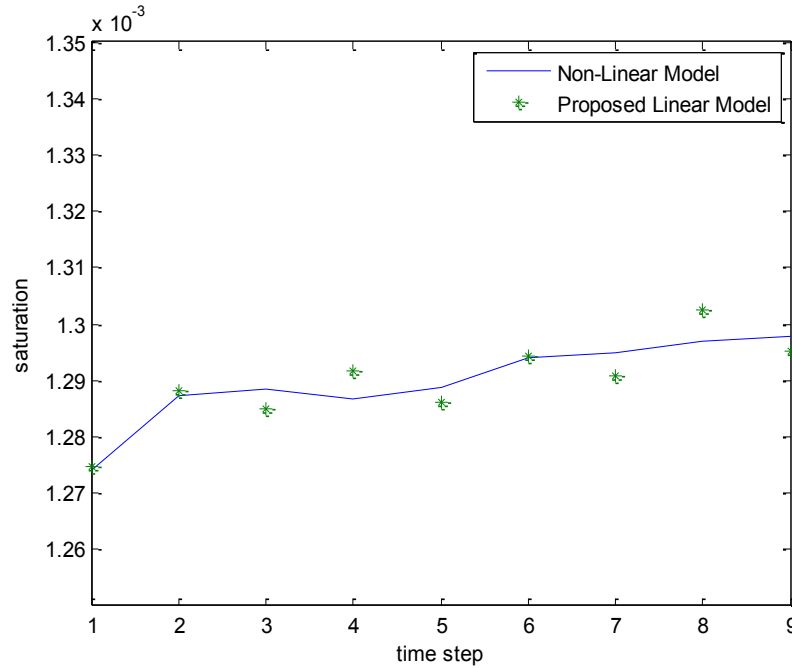


Figure 5-7-Model II: Permeability distribution mapped on 3D geo-model (left). Streamline distributions colored based on well-pair drainage areas (right). Each drainage area shows a single domain (operating regime).



(a)



(b)

Figure 5-8 -Matching results between simulation data and proposed linearized method's results for first grid of second streamline: pressure history (top-*a*) and saturation history (bottom-*b*).

## Discussion

### Selection of Streamline-based Geomechanics Coupling Sub-Domains

As discussed above, streamlines are tangential lines to the velocity field and as such show flow movement path from a source to a sink. Consequently, regions with a higher concentration of streamlines highlights areas with increased influence of pressure gradient and viscous forces (i.e. flow activity) than regions with less number of streamlines or with no streamline passing through them.

The global domain can be decomposed to  $z$  number of sub-domains (**Figure 5-9**), where  $z$  can show either the number of wells or well-pair bundles. However the remaining challenge is a criterion for selection of the subdomains to conduct the hydromechanical coupling.



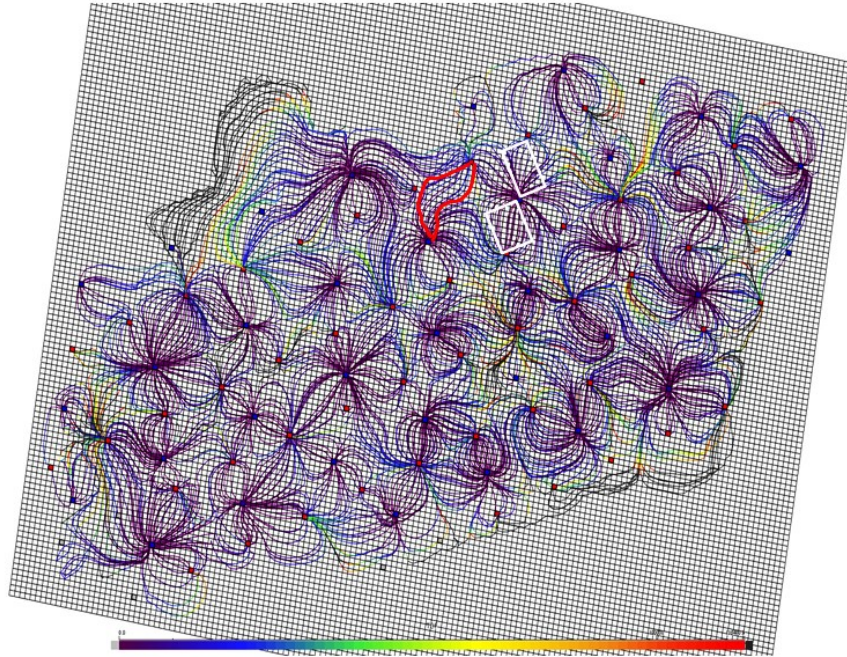


Figure 5-9- Representation of system decomposition into subdomains – model localization. The sub-domains in this research are selected as the flow regions between the well pairs and/or the zones with higher density of streamlines per area/volume (**Figure 5-10**) . The reason is not only because more number of streamlines show more flow activity but also the regions with more gradient of pressure exhibit more geomechanical responses.

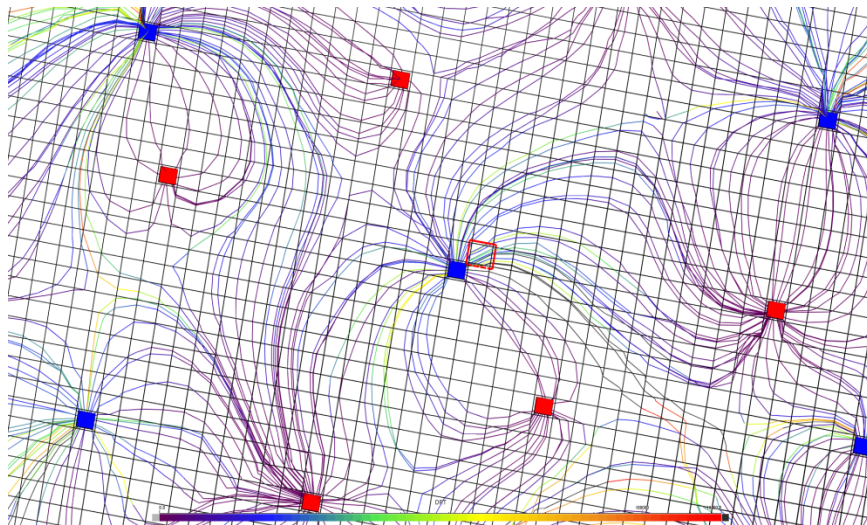


Figure 5-10- Representation of number of streamline per grid-cell as an index for selection of geomechanical coupling domain localization.

Based on a study (Rothenburg and Obah, 1995) the zones with higher gradient of pressure in the reservoir, are the zones that are prone more to “shear” type of stress than isotropic stress changes. **Figure 5-11** is a synthetic representation of pressure versus distance in the reservoir. In the regions where the pressure influences are more of the pressure changes with respect to a reference pressure and the pressure gradients are less steep (across the streamline or orthogonal to streamlines) the pressure changes contribute more to isotropic stress and strain responses. However the zones with steeper pressure gradient ( $\frac{\partial P}{\partial \tau}$ , along the streamlines) indicated a greater potential for increase in shear stress changes and accordingly lead to more shear strains.

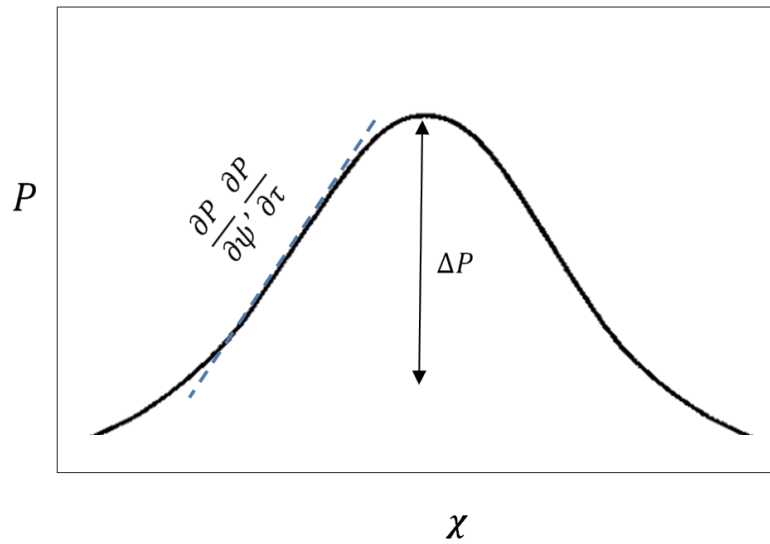


Figure 5-11-Pressure versus distance, representation of impact of pressure difference and pressure gradient and individual influence on the stress tensor components.

In the elastic coupled flow-geomechanics processes, the only impact that geomechanics has on the fluid flow problem are the changes in the absolute permeability and porosity. On the other hand shear stress plays a more important role compared to isotropic stress changes in terms of permeability updates (Chalaturnyk, 1996). **Figure 5-12** (Chalaturnyk, 1996) shows that with constant volumetric strain, the permeability changes are larger due to shear stress effects than isotropic principal stress changes. For one certain value of volumetric strain in Figure 5-12, if the induced strain is purely due to isotropic responses the permeability changes are less than the case where the volumetric strain induced is under the conditions of shear distortion in the reservoir. This effect can physically be interpreted that the increase



in shear dilation reduces the sheared porous rock tortuosity, and accordingly lead to increase in absolute permeability. As such the higher the streamline density and the more pressure gradients are in one zone of reservoir, the more shear stresses are induced, and more shear stresses can mean to interpret more geomechanical (absolute permeability) responses.

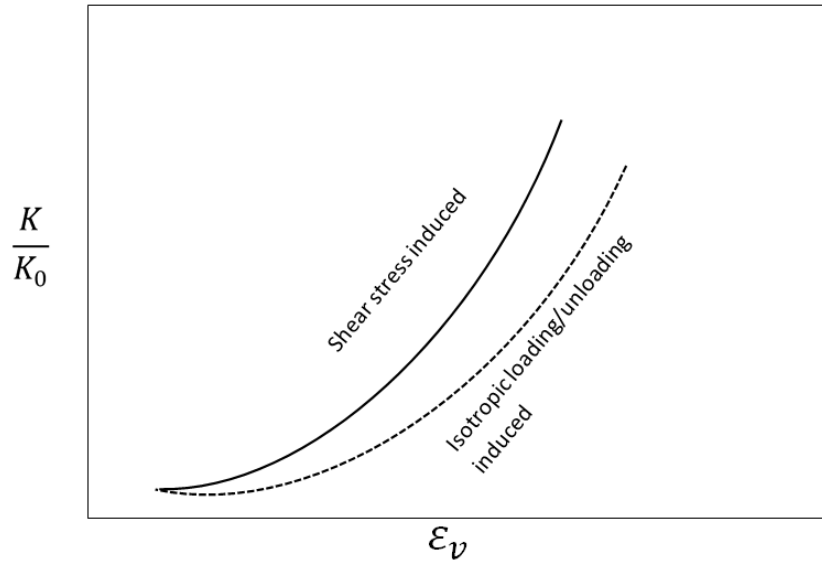


Figure 5-12- Comparison of permeability changes due to changes in shear stress versus changes in principal stresses (after Chalaturnyk, 1996).

## Conclusion

A new reduced-order linear localized model (streamline-based proxy) was presented for a highly nonlinear multi-phase flow in underground formations. The proposed model took advantage of streamlines by using information gleaned from streamline trajectories.

In this work localization method was used to split and categorize the output (state variables) vector of reservoir model. Streamlines were used as an alternative to mathematical techniques to identify the effective region of each local model. A novel linearization method in reservoir modeling was presented based on the density of number of streamlines per grid cell. It was shown that the model, which is highly nonlinear in Cartesian or Radial coordinates, is linear in streamline-based coordinates, due to the linearity of local models along streamlines. The results of simulation on a synthetic case verified the accuracy of the method. The method can be a very useful technique where the simulation model must be run many times (i.e. optimization problems) or where the dimensions of the model are large or the original model has a high uncertainty (i.e. history matching problem). The method had significant

computational cost reduction compared to current reservoir simulators, and can be used as a proxy model for optimization techniques.

## Nomenclature

$u_{x,y,z}$	=	Displacements in $x$ , $y$ , and $z$ directions
$x$	=	State variables of each grid block (pressure and saturation)
$S(i,j)$	=	Index of $j^{th}$ cell of $i^{th}$ streamline
$Ns(i)$	=	The number of cells that the $i^{th}$ streamline pass through
$Xp_{s(i+1,1)}$	=	Pressure at streamline +1 , and cell $i$
$XS_{s(i+1,1)}$	=	Saturation at streamline +1 , and cell $i$
$Y_i$	=	Output state variables vector of streamline ( $i + 1$ )
$U_i$	=	Output state variables vector of streamline ( $i$ )
$\varepsilon_v$	=	Volumetric strain
$G$	=	Shear modulus of rock
$\lambda$	=	Lame's constant
$K$	=	Stiffness matrix

## Chapter 6: Inclusion of Geomechanics in Streamline Simulation for Hydromechanical Modeling of Underground CO<sub>2</sub> Storage<sup>##</sup>

### Introduction

The storage of CO<sub>2</sub> in geological formations is currently intensively discussed as an economical and environmentally sound way to reduce the emissions of greenhouse gases into the atmosphere. Carbon Capture and Storage (CCS) technology aims at separating carbon dioxide from the fuel gases of power plants (fossil-fuelled or other CO<sub>2</sub> emitting ones) with subsequent transport to a site where it can be injected for storage into a deep geological formation, such as depleted oil and gas reservoirs, unminable coal seams, and deep saline aquifers (Bachu et al., 2009; Bickle, 2009). Suitable formations should be deeper than 800 m, have a thick and extensive seal, have sufficient porosity for large volumes, and be sufficiently permeable to permit injection at high flow rates without requiring overly high pressure (Benson et al., 2008). **Figure 6-1** shows a schematic of a suitable target formation and also the primary migration of CO<sub>2</sub>.

Sequestration capacity estimates for saline aquifers and coal beds are highly uncertain, although in the past several years, there has been some progress in developing standard methods for capacity estimation and improving regional estimates (Bachu et al., 2007).

---

<sup>##</sup>A paper format of this chapter was presented at ARMA-47<sup>th</sup> U.S. Rock Mechanics-Geomechanics Symposium, June 2013 San Francisco, US, paper ID No. 631. This paper has been selected based on a technical and critical review of the paper by three technical editors of the conference and published in the conference proceeding.

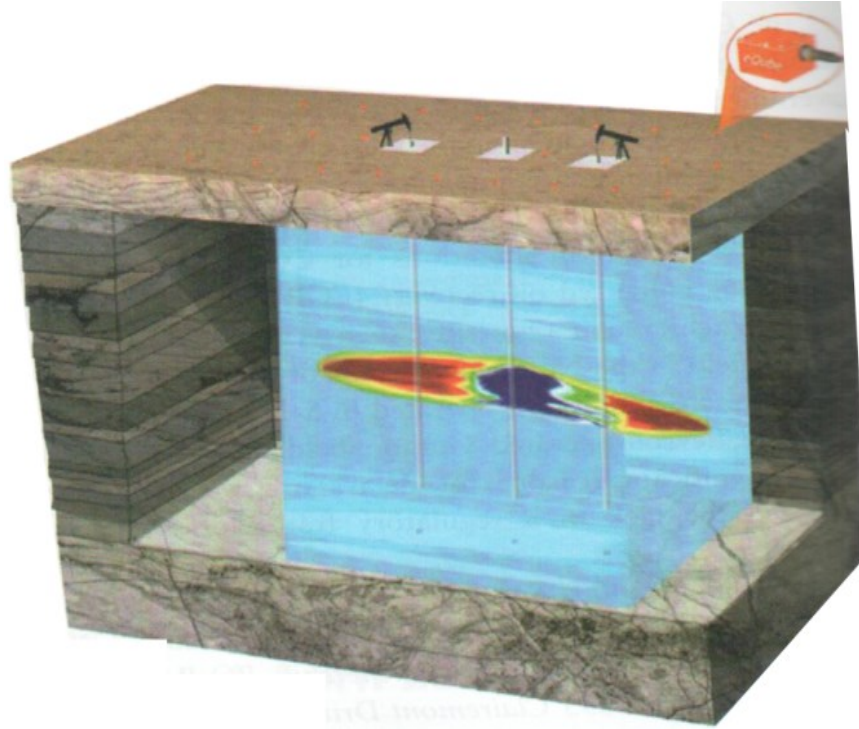


Figure 6-1-Schematic of a reservoir target and CO<sub>2</sub> plume migration in a host geological formation (Zhdanov et al., 2013)

Reservoir processes during injection and post-injection of CO<sub>2</sub> involve several trapping mechanisms. **Figure 6-2** illustrates different mechanisms related to CO<sub>2</sub> trapping mechanisms. Extensive discussion on physical and chemical mechanisms related to CO<sub>2</sub> storage in sedimentary formations can be found in the works of Gunter et al. (2004), Benson and Cole (2008).

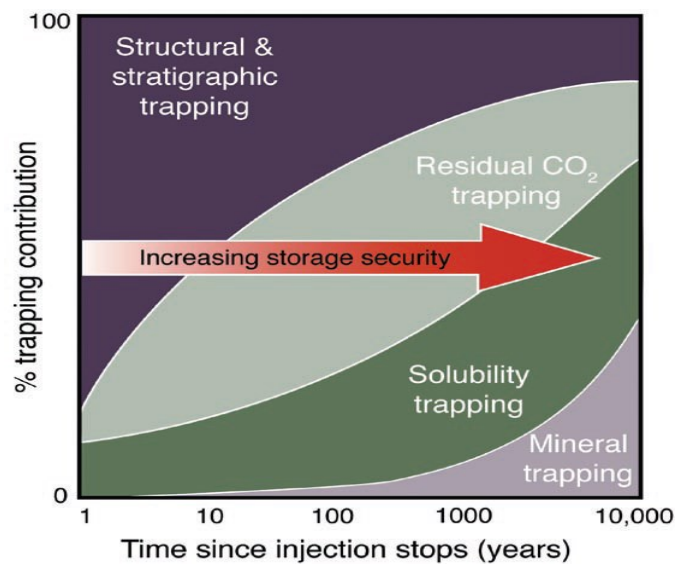


Figure 6-2- Conceptual sketch of sequential physical mechanisms of CO<sub>2</sub> storage

The trapping mechanisms can be divided into two main categories (Rutqvist, 2012): (1) physical trapping (2) chemical gas trapping. Physical trapping contains stratigraphic and residual trapping, which are the first two sequences of trapping shown in Figure 6-2. Chemical trapping occurs when CO<sub>2</sub> dissolves in subsurface fluids (solubility) and subsequent reactions with the mineral phases in the reservoir (mineral trapping). The permanence and duration of these trapping mechanisms depends highly on the long-term geological integrity of the target underground reservoir and the seal. Geomechanical processes during CO<sub>2</sub> injection (and potentially in the post-injection period) can play an important role (particularly during stratigraphical CO<sub>2</sub> trapping) on the integrity of the storage formation and bounding seals. Geomechanics is likely of greatest importance during physical trapping stages when CO<sub>2</sub> is being injected into the formation and the fluid flow mechanisms are convective-dominated.

Hydromechanical (HM) processes generally play a significant role during CO<sub>2</sub> injection into deep saline aquifers. The target formations are generically fractured sandstones that are initially almost saturated with saline fluid. Therefore, they can deform either due to variation of external loads (dissolution or precipitation of mineral phases) or changes in pore pressures or temperature in the reservoir. The main topic of this work relates to stress-strain field redistribution and domain deformation due to pore pressure changes both in near wellbore region and far field. Direct and indirect hydromechanical coupling mechanisms can explain these sorts of geomechanical changes, as suggested by Rutqvist and Stephansson (2007). Direct HM coupling refers to both solid-to-fluid coupling and fluid-to-solid coupling. The former refers to the phenomenon where variation in the applied load results in a change in porosity and accordingly in fluid pressure and saturation; and the latter takes place when a change in fluid pressure causes a variation in the volume of the geological media (due to inducement of volumetric strain). Indirect HM coupling however refers to changes in hydraulic or mechanical properties in response to strain changes. According to this definition, the focus of this study is on direct HM coupling.

Even though geomechanics play an important role in CO<sub>2</sub> storage in saline aquifers, the computational burden is much higher using hydromechanical coupling than for the hydraulic problem alone (Tran et al., 2004), particularly when the hydrodynamic and mechanics of the process are solved simultaneously (known as fully coupled HM). Although, there are some

coupling strategies available to avoid the full coupling, such as sequential or iterative coupling, these strategies are not still applicable in large domains with multi-million cells due to computational burden. For more detailed discussions on these techniques and discussions over computational efficiencies refer to Mainguy and Longuemare (2009), Settari and Walters (1999), and for frameworks for coupling a flow and geomechanical code and induced geomechanical changes in reservoir properties, refer to Chalaturnyk (1996) and Li (2004).

In recent years, a number of coupled fluid flow and geomechanical numerical models have been developed for analysis of various geomechanical issues associated with geological storage of CO<sub>2</sub> (GCS). Examples of the sequentially coupled HM analysis of GCS include FEMH by Bower and Zyvoloski (1997), TOUGH-FLAC by Rutqvist et al., (2011), OpenGeoSys by Wang and Kolditz (2011) and also Goerke et al. (2011), and ECLIPSE-VISAGE by Ouellet et al. (2011). However these schemes are not computationally efficient due to large number of coupling variables as well as computational loads, and complexity of multi-physics associated with conventional reservoir simulator. Simplified models have been shown to be sufficient for long term or large-scale processes (i.e. single phase flow coupled geomechanics for fault reactivation analysis in a large domain).

This paper introduces a new HM coupling strategy for faster coupled simulations and reduction of computational loads for large underground reservoirs. This paper first studies the feasibility of coupling between a newly developed geomechanical code and streamline simulation, and later applies the developed scheme in the hydromechanical modeling of CO<sub>2</sub> storage in a large synthetic underground model.

### **Streamline Simulation**

Streamlines are approximate methods for fluid flow in porous medium. In case of an isotropic permeability field, streamlines are orthogonal lines at each point to iso-potential lines, and locally tangent to a defined velocity field, and they represent the direction of fluid flow. The elegance of streamline simulation lies in their power for fast forward flow simulation. They are the most accurate when the flow mechanism behavior is closest to unit mobility ratio (e.g. tracer flow). The efficiency of streamline simulation relies mainly on their power in utilizing larger time-steps with fewer pressure updates, which leads to faster flow simulations. In scenarios where the geomechanical model changes (in MEM or petrophysical

properties) and streamlines change and the process requires an iterative approach, streamline simulations scale well and are of significant advantage over finite difference (FD) or finite volume (FV) simulation techniques. The other advantage of streamline simulations is their visualization power (i.e. flow directionality and streamline density from sources to a sink as a flow indicator). Also they mitigate the numerical artifacts (numerical diffusion) due to their dual-grid nature (streamline grid and original Cartesian 3D grid). The elegance of streamline simulation lies in the time-of-flight formulation that helps to decouple the multidimensional transport equation to a series of 1D solution along streamlines. Particularly for highly heterogeneous porous medium or large domains (i.e. one million cells) streamlines are significantly faster simulator tools compared to conventional flow simulators in terms of CPU load and computational efficiencies. Batycky (1997) and Batycky et al. (1997), was the first who developed a 3D two phase flow simulator for field scale scenarios such as heterogeneity, rearranging well conditions, and gravity (Batycky, 1997). A large literature describes the development and application of streamline simulation to prediction of flow in three-dimensional heterogeneous reservoirs. See the papers of Batycky, Thiele, King and Datta-Gupta (1998) and Crane et al. (2000) for many references to the full range of work on streamlines.

Streamlines also have been used as proxies for reservoir model order reductions. For more details please refer to the work of Kovcek and Wang (2005) and Jesmani, Koohmarch Hosseini, and Chalaturnyk (2012).

Streamline simulation technology and its application in underground CO<sub>2</sub> storage has also been extensively discussed by Blunt, Ran Qi (2009).

## **Model Geometry and Boundary Conditions**

For model geometry selection as well as petrophysical modeling, standard concepts that have been suggested for suitable formations as target reservoirs for CO<sub>2</sub> storage have been used (Benson and Cole, 2008).

Most geomechanical analyses of CO<sub>2</sub> storage consider the reservoir seals as impermeable at the top of the formation to be able to trap CO<sub>2</sub> in saline underground aquifers such as Sleipner (Korobol and Kaddour, 1995). The sealed formation scenario has also been considered for scenarios related to oilfields such as Weyburn, Canada (Chalaturnyk, 2007;

White, 2009). In a similar fashion, the model shown in **Figure 6-3** considers no-flow boundaries at the top and bottom (i.e., Neumann boundary conditions). The lateral boundaries however are considered to be aquifers with varying heads based on the depth from the ground surface. Both aquifers on the right and left have the same conditions (i.e., Dirichlet boundary condition) The geomechanical (deformation) boundaries were considered as roller boundary on the lateral sides and the bottom side of the reservoir was considered as no-displacement boundary condition where displacement in all three directions is set to zero. And the overburden was replaced with a constant vertical stress at the top of the injection formation. The injection well was in the middle of the model and the injection depth was chosen to be larger than 1000 m. This injection depth is important and necessary in order to have sufficiently high pressures at these depths. At these depths (>800 m) CO<sub>2</sub> is supercritical and its density is high enough to allow efficient pore filling and also no significant buoyancy difference is observed compared with in situ fluids (Benson et al., 2008).



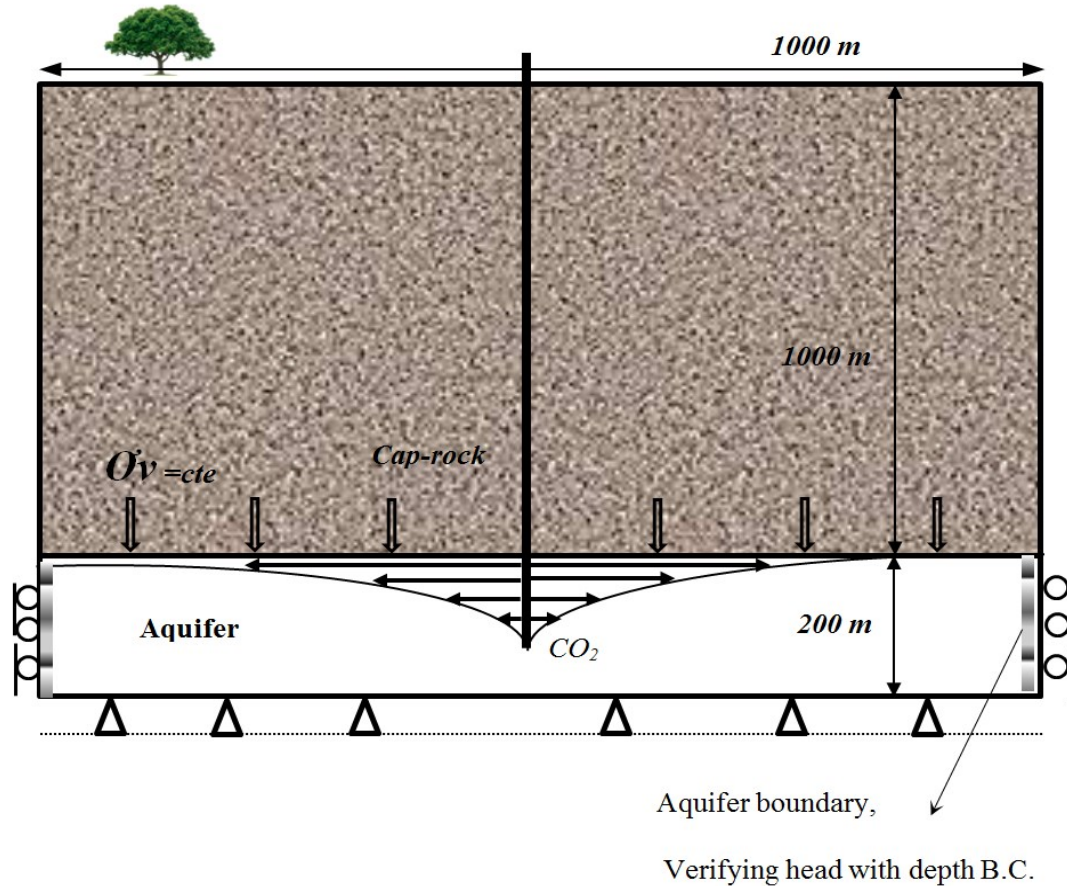


Figure 6-3-Schematic description of the model geometry and flow and geomechanical boundary conditions.

### Fluid Flow Mechanism

The aquifer was considered to be initially fully saturated with saline water. The injection phase was  $\text{CO}_2$ . The fluid system was therefore two phase (brine-  $\text{CO}_2$ ) system with no component exchange. The process was assumed to be isothermal; therefore no thermal strain inducement is expected due to cooling of the formation. Density was assumed to change with compressibility and pore pressures in the domain. The fluid flow mechanism was performed by two approaches: Box method (incorporates both finite element and finite volume) and streamline method. For calculation of capillary pressure and saturation, Van Genuchten functions were selected, which were, developed on the basis of a bundle of capillary tubes model (Van Genuchten, 1980).

Under conditions where the fluid phases are immiscible, the pressure needed to inject  $\text{CO}_2$ , the rate at which the leading edge of the  $\text{CO}_2$  plume moves and the fraction of the pore

space filled with CO<sub>2</sub> are all governed by multiphase flow relationships as suggested by Bear (1972).

## Geomechanics

Poroelasticity concepts proposed by Biot (1940) are usually adopted to resolve the (geo) mechanical problem. In this initial phase of the research exploring the inclusion of geomechanics in streamline simulation, the theory of poroelasticity has been adopted. Therefore the geomechanical code was developed based on the assumption of existence of isotropic linear elastic material. The code is based on a linearized approach for momentum balance equation with the final form of the momentum balance equation for calculation of linear elastic deformations during CO<sub>2</sub> injection into saline aquifers as:

$$\text{div}(\Delta\bar{\sigma}' + \Delta P_{eff} \cdot \bar{I}) + \phi S_n(\rho_n - \rho_w)g = 0, \quad (6-1)$$

where  $S_n$  is the non-wetting phase (CO<sub>2</sub>) saturation,  $\Delta\bar{\sigma}'$  shows the changes in effective stress with respect to initial/previous time-step state,  $\Delta P_{eff}$  shows the pore pressure between two different states, and  $\rho_n$  represents the non-wetting phase density. The assumption behind the formulation is that  $S_w$  is initially equal to one, which is the case for all CO<sub>2</sub> injection scenarios, constant solid density and small changes in porosity. As shown in Eqn-1, when gravity ( $g$ ) is considered in the calculations, not only saturation and pressure from flow simulation has to be fed into geomechanical simulator, but also porosity (from previous cycle for sequential coupling) as well as phase densities needs to be inputted to the geomechanical simulator.

There are several issues to be addressed when geomechanics is coupled (directly or indirectly) to flow simulation, for GCS mechanism such as fault reactivation, limits on injection pressure, micro seismicity and injection induced strains, ground surface displacement, or caprock integrity. The geomechanical focus of this study is on induced strain and stress field redistribution which result in changes in petro-physical properties, and consequently on fluid underground migration.

## Discretization Scheme

The fully coupled flow-geomechanics code is a module of open source code simulator Dumux (Flemisch et al., 2011) that is based on Distributed and Unified Numeric

Environment DUNE (Bastian et al., 2008). For this work a (decoupled) geomechanical code was developed based on the already developed fully coupled scheme, but explicit from fluid flow module. The discretization scheme used was the Box-Method (collocated finite volume and finite element method) for decoupled geomechanical simulation. In the decoupled scheme, the fluid flow numerical scheme was fully implicit, where both pressure and saturation equations (as primary variables for two phase isothermal flow system) are solved at the same time with the same Jacobean matrix. The time discretization is Euler time-integration and the spatial discretization is based on vertex-centered control-volume finite-element method (also called box method, (Huber & Helmig, 2000)). More on Box method and detailed discretization scheme utilized in development of fully coupling, sequential coupling scheme that are worked with in this paper, as well as short explanation on streamline simulation discretization are provided in the next sections.

### Box Method

Box method is a control-volume finite-element method (CVFEM). The advantage of the FE method is that unstructured grids can be used for simulation, and the advantage of FV method is that it is locally mass conservative. As such the computational domain is discretized by a dual mesh, as illustrated in **Figure 6-4**. One mesh handles the finite volume scheme (shown as dashed blue line in the middle of the larger square), and the other mesh is used for FE. Each FE mesh contains four sub-control volumes from four neighboring boxes (FV meshes).

### Fully Coupled Scheme

In this type of coupling the variables of flow and geomechanics are solved simultaneously through a system of equations with displacements (geomechanical primary variables) and pore pressure and saturation (as primary flow variables). The technique is also called implicit coupling as a single discretization scheme is used (Settari et al., 2004). In fully coupled scheme the geomechanical equations are solved by finite element technique while the fluid flow equations are solved by the Box method. Therefore the primary variables of fluid flow equations (pressure  $P_w$ , saturation  $S_n$ ) are solved on the box centers (finite volume mesh) and the flow gradients properties (i.e., fluxes) are solved on integration points (represented by IP in **Figure 6-5**). The geomechanical equations and momentum balanced equations on the other hand, are solved on FEM points (vertices), using standard Galerkin finite element

technique. The gradient properties of primary variables (solid displacement in three directions) are solved on Gaussians points, and therefore effective porosity and permeability are also calculated on these points. As such a mapping algorithm is needed to map the calculated displacements on the Gauss points back onto FEM points to be able to be coupled fully with fluid flow. The mapping is based on a sub-control volume face area average; therefore a loop over all sub-control volumes is needed to obtain an averaged value on the FE points (vertices). It must be mentioned that use of box method for both mass and momentum balance equation has been tried but lead to instability and oscillation in pressure. More about the discretization scheme can be found in the literature (Darcis et al., 2012).

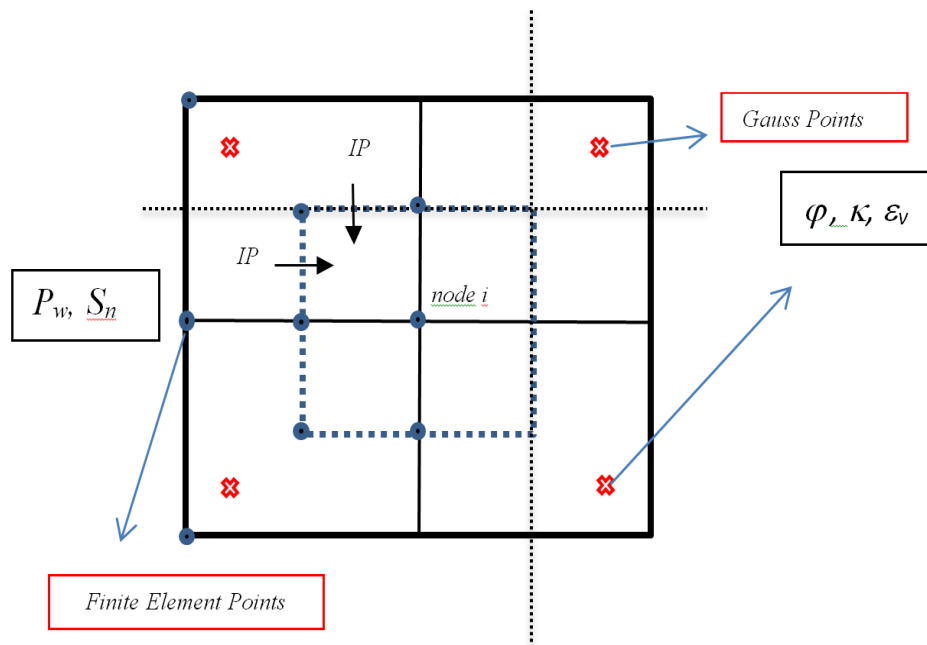


Figure 6-4-Schematic of spatial discretization (Fully Coupled Scheme)

### Sequential Coupling Scheme

In the decoupled scheme, both fluid flow and geomechanical equations are solved by the Box method. Therefore flow gradients (fluxes) are solved on integration points as well as gradient geomechanics terms (i.e. strain, stress). It has been shown that effective dynamic porosity and permeability are functions of volumetric strain (Tohidi-Baghini, 1998); as such these values are also obtained on integration points in the decoupled scheme, and therefore need to be mapped back onto grid vertices (box centers) by a mapping technique. The mapping technique adopted here was similar to the fully coupled scheme where the properties were multiplied by the surface area of sub-control volumes edges, and averaged to the box centers.

Decoupled fluid flow equations are solved by fully implicit approach assuming a two phase (saline water and supercritical CO<sub>2</sub>) isothermal system.

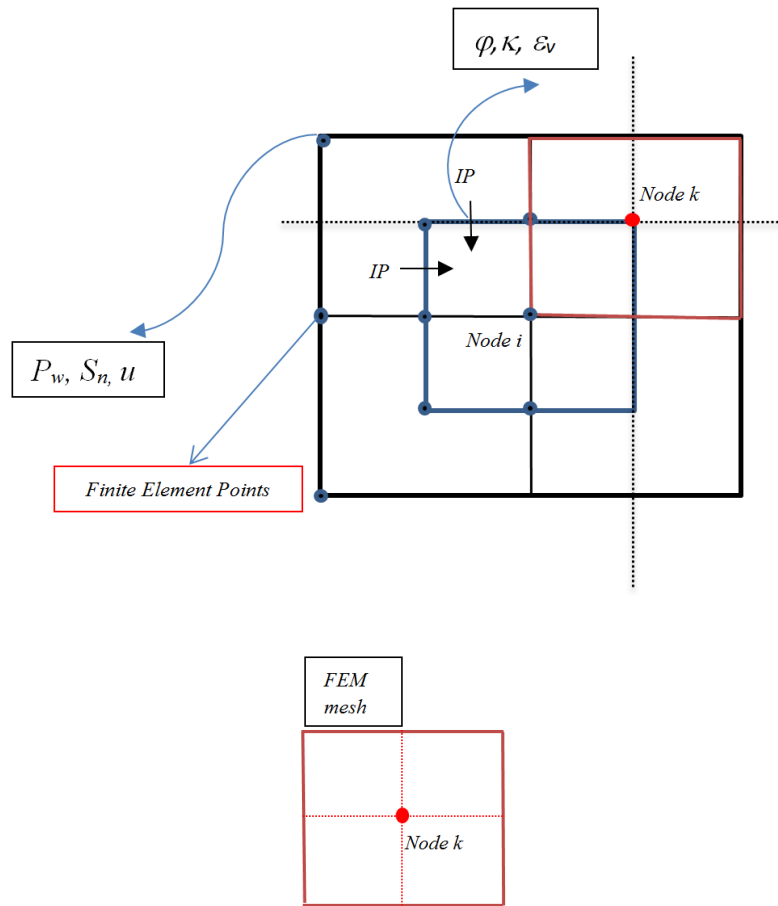


Figure 6-5-Schematic of spatial discretization (Decoupled Flow and Geomechanics)

### Streamline Simulation Discretization Scheme

Unit mobility displacement with constant boundary conditions over all time steps are the most suitable scenarios for one-dimensional mapping of analytical solutions along streamlines, otherwise the numerical solutions are better approaches for solving transport equations along streamlines as they accommodate easily non-uniform initial condition and is totally general (unlike analytical solutions). The numerical approach for solving saturation equation along streamlines was first proposed by Bommer and Schecter (1979).

Streamline numerical solutions are an IMPES type reservoir simulation where pressures are solved implicitly, but explicitly from saturation equation (transport equation). Therefore the main idea behind the discretization technique in streamline simulation is at first place the

decoupling of the pressure equation from the saturation equation, and more importantly decoupling of saturation equations along streamlines from each other. Although the pressure field is solved in the same way as in conventional FD reservoir simulators, the discretization technique and the grid dimensionality for solving saturation/conservation equations is different. For solving the transport equation, a three-dimensional heterogeneous domain is decomposed into a series of 1D grid (along streamlines). Therefore streamline simulations deal with a dual-grid system. The discretization technique (for time and space) for 1D grid uses a standard explicit scheme and single-point upstream weighting for solving one-dimensional problem along streamline as the equation below represents (Blunt & Rubin, 1992):

$$S_{j,i}^{n+1} = S_{j,i}^n - \frac{\Delta t_{sl}^{n+1}}{\Delta \tau_{sl,i}} (f_{j,i}^n - f_{j,i-1}^n) ; \quad (6-2)$$

where  $S_{j,i}^{n+1}$  shows the saturation along streamline at time step (n+1),  $\Delta t_{sl}^{n+1}$  shows the time step size used to solve saturation equation (convective time step),  $f_{j,i}^n$  shows fractional flow function at each node along streamline, and  $\tau$  is the time of flight (TOF) which is the time taken for a neutral tracer particle to move a distance  $x$  along a streamline starting from a source (i.e. injector).

Prior to this step, streamlines need to be traced based on instantaneous velocity field obtained from pressure distribution in last step:

$$\vec{v}_\alpha = \frac{\bar{K} K_{r\alpha}}{\mu} (\text{grad}P - \rho_\alpha g). \quad (6-3)$$

The independent variables (such as pressure and saturation) are mapped from the underlying 3D grid onto the 1D streamline for initialization purposes at each global time-step when streamlines are updated. In 3DSL, the solutions to the numerical problems are provided either by the Adoptive Multigrid Method known as AMG or Algebraic Multigrid Methods for Systems known as SAMG, both developed in Fraunhofer SCAI (Scientific Computing Institute) a German research center (Stüben et al., 2001). The solution obtained from the second grid (1D grid) is then mapped back onto the initial 3D grid to represent phase distribution. And then pressure is solved again and the process continues. Since streamline models are based on IMPES (Implicit in Pressure and Explicit in Saturation) scheme, and

therefore, a time-varying velocity field can be modeled by a series of successive stationary velocity fields (Gupta and King). For unsteady state flow, streamlines configuration changing in time, generating transverse flux to the origin of flow.

## Hydromechanical Coupling

Injection of CO<sub>2</sub> can result in high-pressure buildup, leading to low effective stresses (ultimately fracture pressure) and potentially large deformations, and consequently redistribution of stress-strain field. Changes in stress-strain field in the domain can lead to changes in petrophysical properties of the aquifer (i.e. porosity and absolute permeability), surface displacement and aquifer deformation. These types of interactions between fluid flow and rock mechanics are known as hydromechanical coupling. Classical reservoir simulators do not consider this interaction; therefore a proper strategy is needed to include the geomechanical impacts of fluid flow on reservoir simulation process. Ideally the flow problem needs to be solved at the same time in one set of equations known as fully hydromechanical coupling. The basis of this system formulation is Biot's poroelastic problem (Biot, 1940). However this approach is computationally expensive and therefore cannot be applied to large domains with large number of grids. In many coupling strategies, porosity and permeability are updated (simultaneously or at each time step) due to change in volumetric strain as follow:

$$\phi = \frac{\phi_0 + \varepsilon_v}{1 + \varepsilon_v}; \quad (6-4)$$

proposed (based on poroelasticity assumption) by Touhidi-Baghini (1998):

$$k = k_0 \exp \left[ 22.2 \left( \frac{\phi}{\phi_0} - 1 \right) \right]; \quad (6-5)$$

proposed by Rutqvist and Tsang (2002). In both equations  $\varepsilon_v$  is the volumetric strain at each time step,  $\phi_0$  and  $k_0$  are the initial porosity and permeability before inclusion of geomechanics respectively.

## Coupling Strategy

The basic concept behind inclusion of geomechanics in streamline simulation lies in the streamline time stepping. Streamline time stepping is different than conventional flow simulation time steps. There is a global time step that is simply the pressure updates due to

changes in flow regime. There is another time steps, which is technically the user provided time steps and is mainly defined based on the existing production history. The other time step is the convective time step that is used for solution of saturation transport equation along streamline grids (time of flight-based coordinate). The size of this time step depends on the Courant-Fredrich-Levy (CFL) condition, which is a formulation of a corrector step that leads to a mechanism to ensure numerical stability, to solve one-dimensional saturation transport equation along streamlines. To perform all coupling strategies on a solid platform two set of interface were developed. **Figure 6-6** provides a schematic illustration of the coupling strategy and how the parameters are exchanged between each simulator at each time step.

With the same strategy as conventional coupling sequential strategies, streamline simulation can be coupled to geomechanics, with the structure illustrated below:

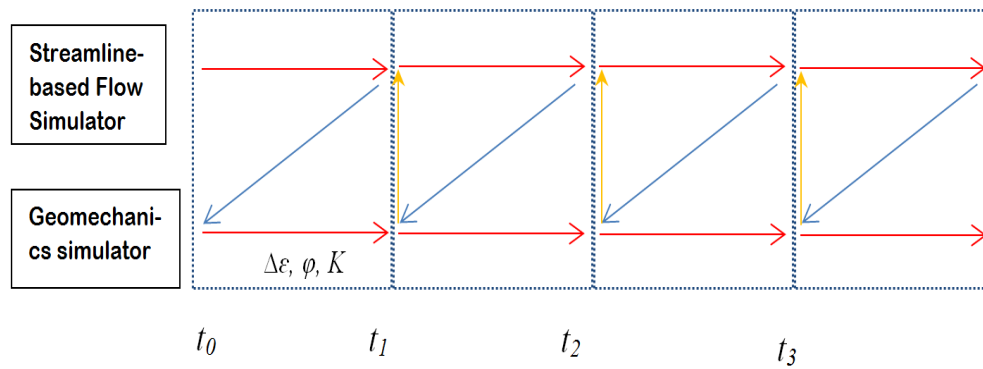


Figure 6-6-Schematic of coupling strategy for sequential Streamline Based Flow - Geomechanical simulator.

The red line in the figure illustrates the forward flow and geomechanical simulations and the time interval of each cycle. The diagonal blue lines show the step during coupling at each cycle where fluid flow simulator outputs (pressure, saturation, phase density difference) are fed into geomechanical simulator. And the yellow lines show the step (and timing) where geomechanical outputs being inputted into flow simulator; each blue block represents a cycle of fluid flow-geomechanics coupling from  $t_i$  to  $t_{i+1}$ .

Time steps are kept constant in this stage of the research, however the time steps can be adoptive based on convective time steps of streamline simulation, before each pressure



updated. Even with constant fixed time steps streamlines (for large domains) are faster techniques in hydromechanical coupling strategies compared to conventional coupling techniques.

### **Geomechanical Influence on Selection of Time-Steps**

Changing streamlines also requires the ability to solve transport problems with generalized initial conditions along each streamline (suggested by Batycky et al., 1997). Changing porosity and permeability means a pseudo-change of boundary conditions and general initial conditions (at each time-step), and therefore streamlines require to be updated as the global pressure of the domain is updated. Therefore treating the geomechanical influences as an explicit factor, which changes porosity and permeability (due to inducing of volumetric strain in the reservoir with high pressure gradients) in the course of simulation, requires that streamlines be updated in the course of coupling. The frequency of pressure updates, and hence streamlines spatial configuration update, dictates the time-step sizes of coupling. Because the main and most important factor common in fluid flow and geomechanical simulation is the pore pressure and pressure gradient all over the domain. It should be noted that if the streamline simulation was performed at the coupled hydromechanical simulation, where significant heterogeneity is induced by geomechanics, the streamline simulator performs faster.

Geomechanical effects are not only limited to the petrophysical properties (such as porosity and permeability, MEM properties, etc.) but can also cause changes in the relative permeability curves and change the end point mobility ratio, which is a source of nonlinearity in flow problem. As such the flow simulator is expected to function slower as it needs to smaller time-steps and larger number of pressure updates, and therefore results in a slower hydromechanical coupling simulation. This part however is not the main focus of this study, yet can be an influential factor in all flow-geomechanical coupling schemes including streamline-based one, particularly where rigorous capillary flow exists. A preliminary study was done by Ojagbohunmi and Chalaturnyk (2012) for a conventional flow simulator, IMEX (CMG) coupled to FLAC geomechanical simulator. For these types of geomechanical influences on streamline simulation, the forward transport equation (saturation) must be solved numerically. For this study however time-step size is kept constant.

## Results and Discussions

To investigate the migration of CO<sub>2</sub> in saline aquifers, fluid flow simulations were performed with both finite volume based flow simulator and streamline based simulator. Two geometries were proposed: a two-dimensional (a cross-sectional view along the aquifer, as shown in Figure 6-3) and a three-dimensional model.

The injection process was considered to be immiscible, yet compressible (densities of brine and CO<sub>2</sub> both changes with pressure, and were taken from a look-up table based on existing correlations). Reservoir hydraulic properties are provided in **Table 6-1**. For comparison of computational efficiency sensitivity on number of grid cells, the simulations were performed on two different grid refinement levels. Viscosity was kept constant for the formation brine and injected CO<sub>2</sub> for streamline simulation.

**Table 6-1-Reservoir hydraulic parameters**

Input Parameter	Unit	Values
Porosity $\phi$	%	0.2
Permeability $K$	mD	100
Initial Gas saturation $S_n$	%	0.05
Injection Water Saturation $S_w$	%	0.3
Van Genuchten $\alpha$	Pa <sup>-1</sup>	0.0037
Van Genuchten $n$	-	4
Temperature $T$	K <sup>0</sup>	315
CO <sub>2</sub> viscosity $\mu_n$	cP	0.06
Brine viscosity $\mu_w$	cP	0.5
Brine density $\rho_w$	kg/m <sup>3</sup>	1024
CO <sub>2</sub> density $\rho_n$	kg/m <sup>3</sup>	850

**Table 6-2-Reservoir mechanical parameters**

Input Parameter	Unit	Values
Rock density $\rho_s$	kg/m <sup>3</sup>	2500
Young's modulus $E$	Pa	5.e9
Shear Modulus $G$	Pa	2.e9
Constitutive model	-	Linear elastic
Poisson's ratio	-	0.25

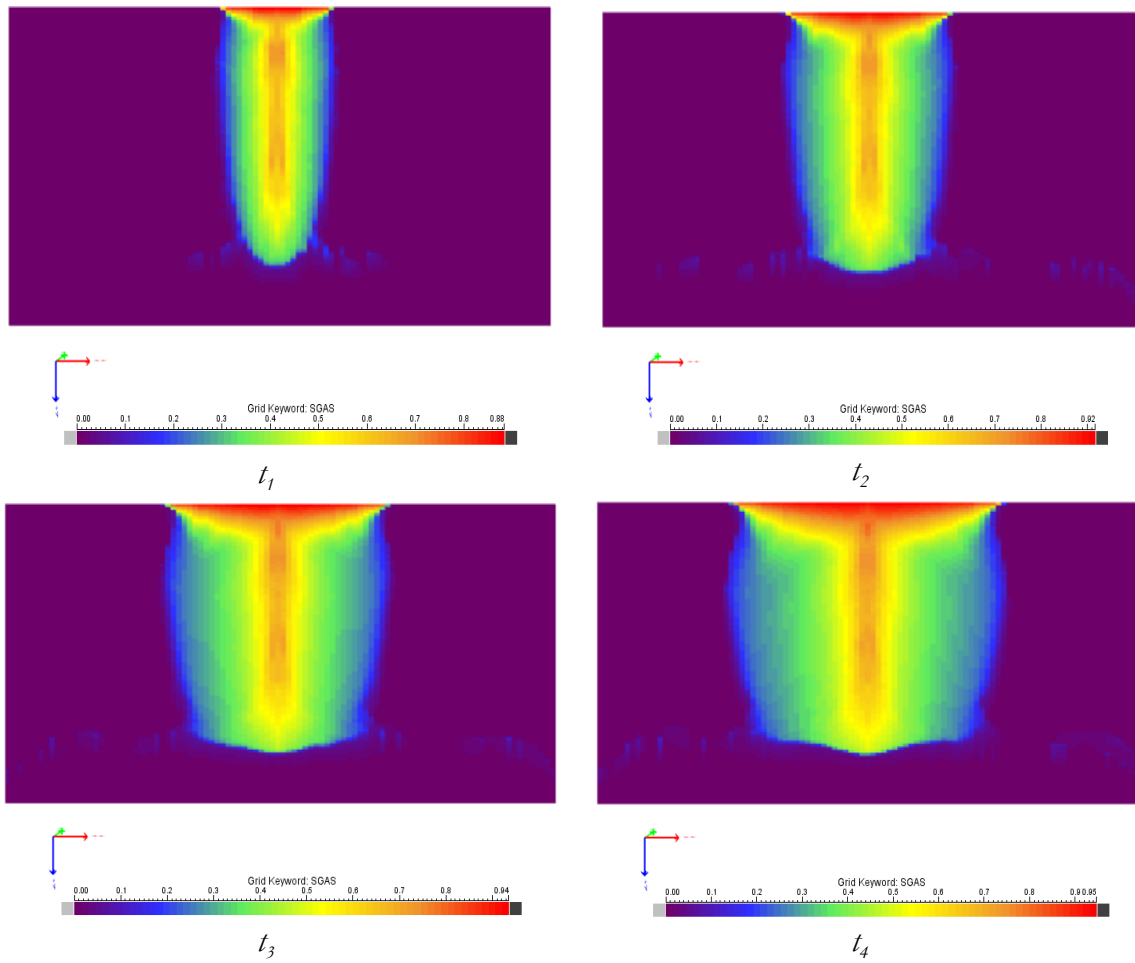
### Two-Dimensional Model

To understand the mechanism of fluid flow using streamline simulation technique, a two-dimensional model was initially considered for simulation, which provides a better visualization for monitoring of CO<sub>2</sub> plume in the course of injection. Furthermore as our

flow simulation is streamline-based, for visualization reasons (streamline paths, and flow directionality from sink to source in the model) the geometry was considered as a two-dimensional one. (Visualization of streamlines in a 3D domain can sometime be misleading, as streamlines seem to be intersecting each other.)

### High Resolution Model

The simulation results for a homogenous domain are presented in **Figure 6-7** and **Figure 6-8**. The injection rate was considered as 0.8 kg/s (with injected phase density of 800 kg/m<sup>3</sup>) to be able to capture the convective migration of CO<sub>2</sub> plume and ensuring the flow mechanism scales well with streamline simulation which is the fastest technique for convective flow processes. The number of cells are Nx=100, Nz=100, and the domain is 2000 m in x direction and 200m in z direction.



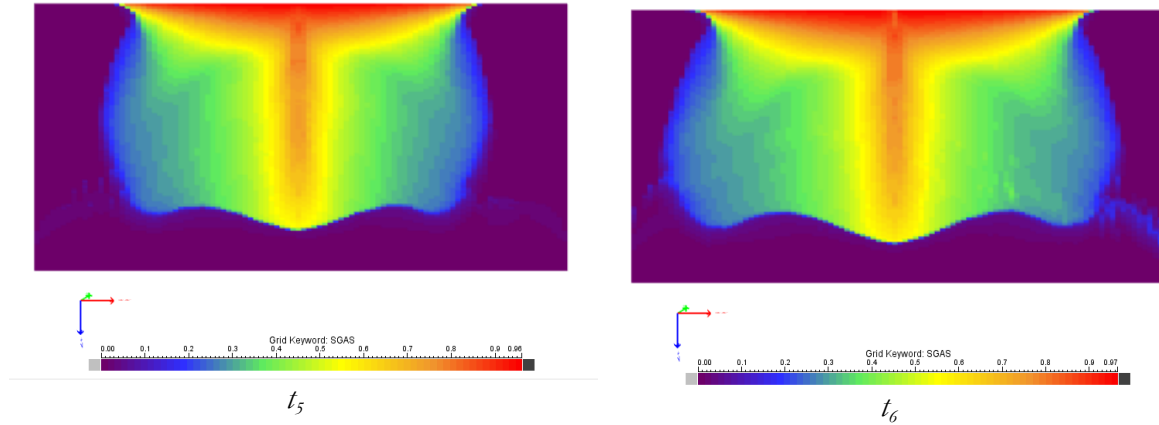


Figure 6-7-Cross-sectional CO<sub>2</sub> saturation map (CO<sub>2</sub> plume evolution) in different time steps of simulation:  $t_1=100$  days,  $t_2=200$  days,  $t_3=300$  days,  $t_4=400$  days,  $t_5=700$  days  $t_6=800$  days.

The streamline paths and configuration for the last two time steps ( $t_5$ ,  $t_6$ ) are represented in the following figure:

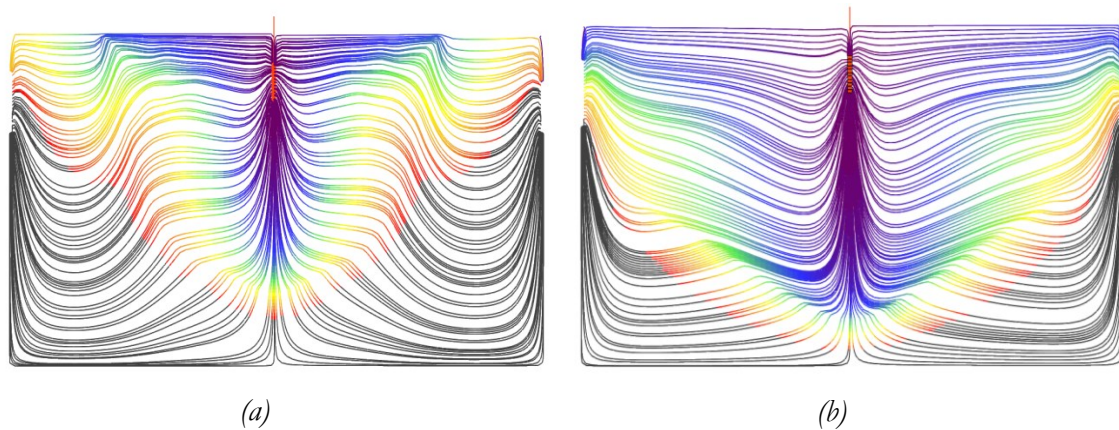


Figure 6-8-Streamline configuration represented after 500 days (a) and 900 days (b) of injection; time of flight as a streamline property is also mapped along streamlines which is the colorful region around the wellbore.

As it can be seen from the picture, the only sink and source in the system are the injection well, and two mirror aquifers (boundaries with constant head). Therefore streamlines trajectory and drainage area are separated into two parts between these pairs: 1) injection well-right aquifer and injection well-left aquifer. Streamlines not only show the flow directionality between each two source-sink term, but also show the density of flow (i.e., around the injection well more streamlines exist which means the flow activity and pressure gradients are higher in those zones) and therefore can provide even visually a quick understanding of the regions that undergo more geotechnical changes and are affected more by effective stress and thus more volumetric strain is expected to evolve in the regions with

large density of streamlines. Also the signature of plume can be roughly seen visually from the streamlines paths.

### Low Resolution Model

Assuming the same injection scenario with the same fluid and reservoir rock properties, the number of cells in each was lowered 10 times.

**Figure 6-9** illustrates the results obtained from this analysis.

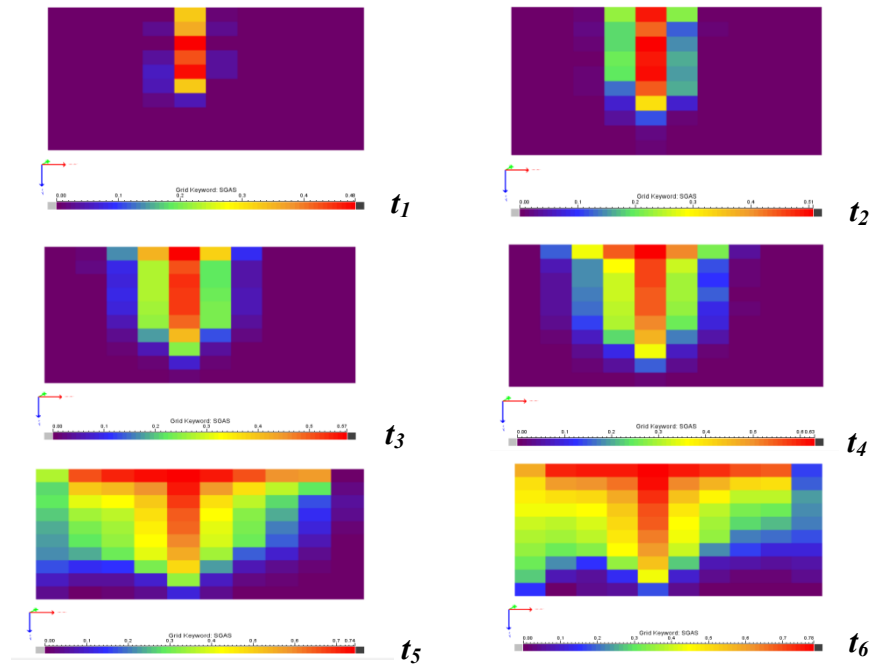


Figure 6-9-Evolution of CO<sub>2</sub> plume in the aquifer for the same model as before with coarse grids.  $t_1=100$ ,  $t_2=200$ ,  $t_3=300$ ,  $t_4=400$ ,  $t_5=700$ ,  $t_6=800$  days.

As shown in Figure 6-9 , the low resolution model provides results which might not be reliable in long term. However they are still informative as an approximate assessment of the migration process (i.e. when the CO<sub>2</sub> arrival time will be, and what will be the pressure value after 3 years of injection in the domain). In terms of computational efficiencies, the computational load required to carry out either of simulations is not significantly different, compared to the expected difference between two levels of resolutions performed by conventional reservoir simulators. A rule of thumb (about the number of grid-blocks in the domain and its impact on CPU time) is that CPU time is expected to increase to the power of two, if the number of grid blocks is doubled. As it is presented in the **Figure 6-10** , it is not

the case for streamline simulation as in streamline simulation the huge computational load is mitigated by decomposition of SL grids from underlying grids.

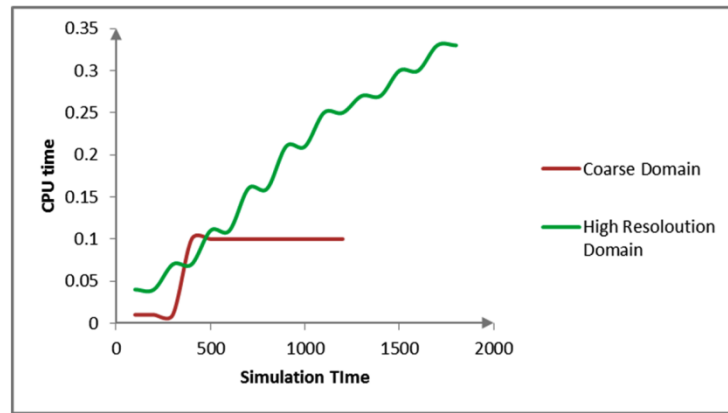


Figure 6-10-Impact of grid refinement on computational load for standalone streamline simulation (decoupled from geomechanics).

### Three-Dimensional Model

For exact hydro-mechanical study of the model a three-dimensional geometry was considered. The geometry was kept the same but the model was extended in  $y$  direction with the same length as in  $x$  direction. The result of long-term simulation of the three-dimensional model is represented in the next pictures. **Figure 6-11** and **Figure 6-12**, respectively, represent the top view from a three model ( $N_y=20$ ,  $N_x=20$ ,  $N_z=50$ ) and the  $\text{CO}_2$  saturation map and corresponding streamlines bundle after 900 days of injection. The streamline patterns are homogenous and symmetric around the injection well from the top views since porosity and permeability are assigned as equal and constant in the course of simulation, however they are categorized into four groups based on their drainage area and the boundaries they are travelling to. Each streamline belonging to a particular region (source-sink) is shown by a different color.

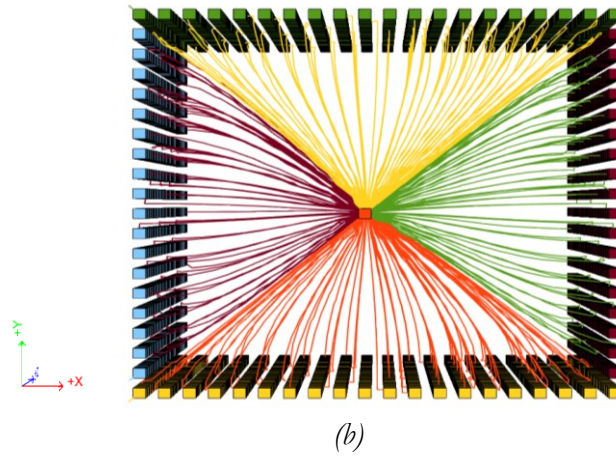
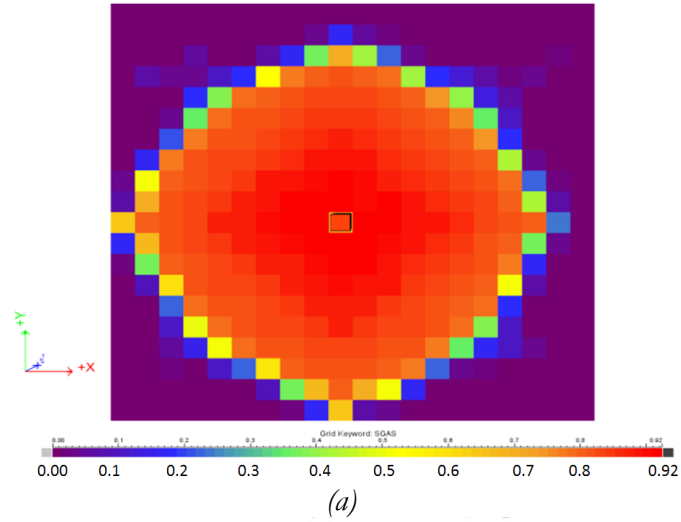
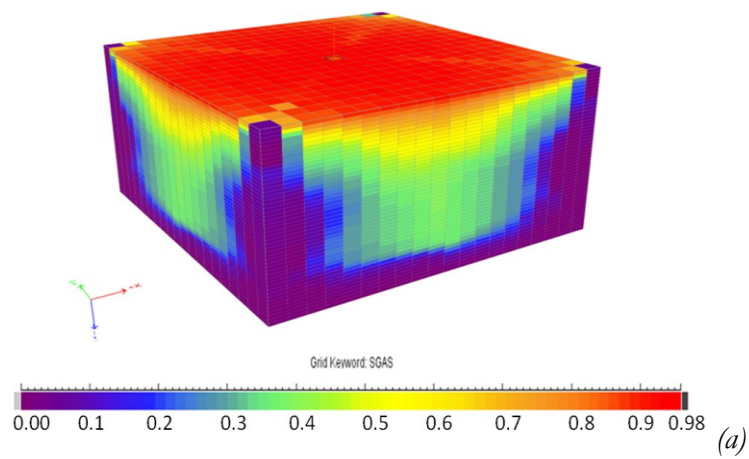
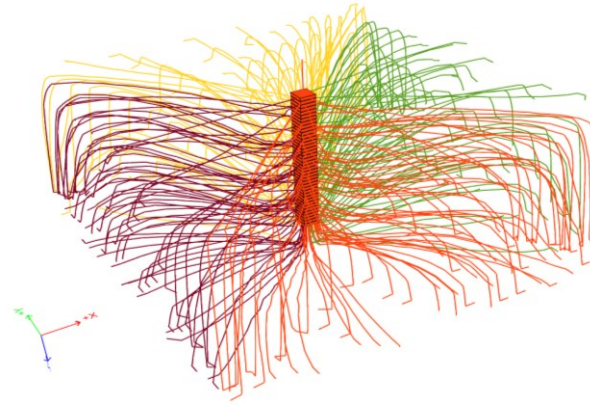


Figure 6-11- Representation of model top view: (a) shows signature of CO<sub>2</sub> after 900 days, and (b) shows the corresponding streamlines configuration for the same time of injection.





(b)

Figure 6-12-Lateral view of 3D-model representing (a) CO<sub>2</sub> saturation map, and (b) shows corresponding streamline configuration after 1500 days of injection. Injection well is located in the middle of the domain.

With the same coupling strategy explained before streamline-based flow simulation for the same physics and model was coupled to a decoupled purely geomechanical code. A graphical user interface was developed which was able to couple both tools at different cycle time intervals as well as adoptive time-stepping which is suggested by streamline simulation (based on CFL condition and auto-time-stepping technique) at each cycle (Model geometries can also be adjusted in the interface GUI). However the coupling for our study was based on a constant time step interval for each cycle. The cycle forwarding time interval was considered as 100 days for all cycles. The reason for this selection comes back to the long term nature of CO<sub>2</sub> injection in underground formations, that can be on the order of decades, as well as the power of streamline simulation in capturing large time step and providing reasonably accurate results specially for convective and linear (or close to linear) flow mechanisms. However 100 days is relatively small time interval for sequential hydro-mechanical coupling of such physics which is computationally expensive and can cause huge material balance errors which might stop the flow simulator to even initiate next cycle simulation.

For comparison of all coupling strategies, the target model was kept the same as previous three-dimensional example except the number of gridlocks in  $z$  direction was reduced to  $N_z=10$ . The sequential coupled flow simulation was performed much faster than a fully coupled simulation of the same physics, and as expected in the high gradient pressure zone due to changes in effective stress, strain (volumetric) field was disturbed and two primary geomechanical parameters changed; porosity and permeability. Keeping the injection parameters and boundary conditions the same, changes in petrophysical parameters will



cause some changes in dynamical parameters such as phase pressures and saturations. **Figure 6-13** illustrates how these variables change using the streamline-based hydromechanical coupling scheme.

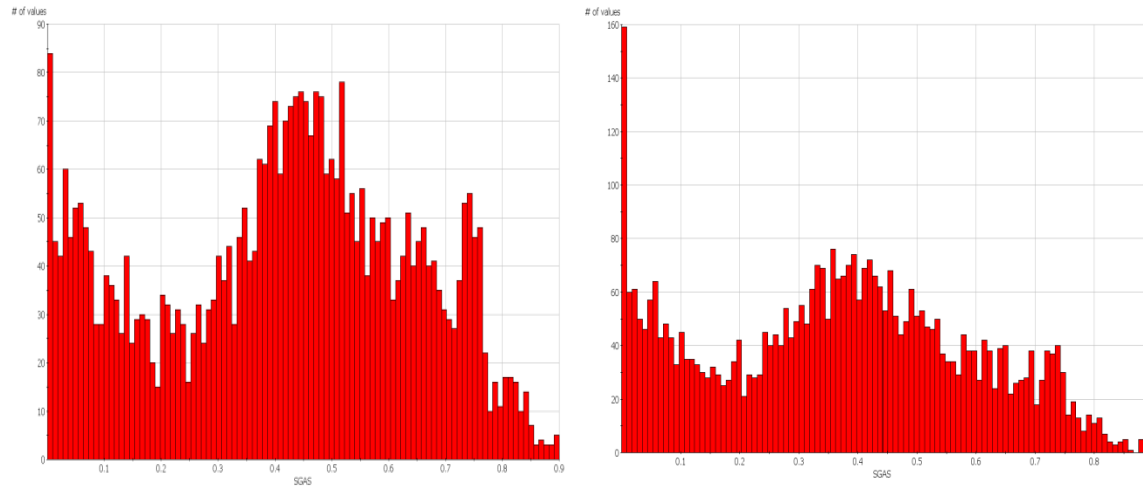


Figure 6-13-Histogram of CO<sub>2</sub> saturation after 500 days of injection in the streamline-based hydromechanically coupled scheme (left) and in the standalone streamline simulation (right).

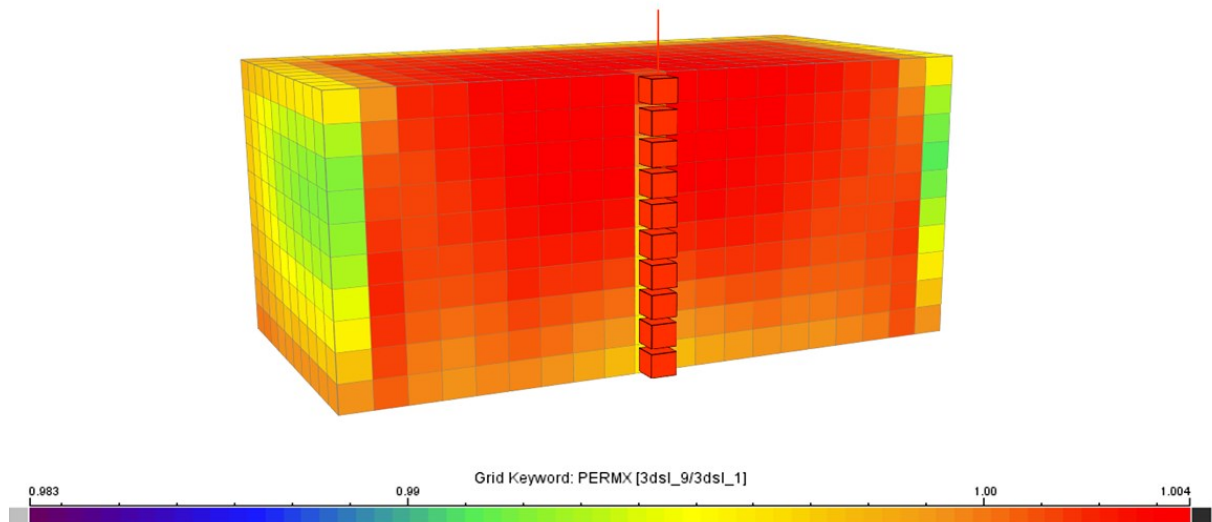


Figure 6-14-Permeability difference ratio-map between cycle 9 (900 days after injection) and cycle 1 (100 days of injection).

The maximum permeability difference after 900 days of injection is about 9-10 mD at some cells from different layers and depths. **Figure 6-14**, **Figure 6-15**, and **Figure 6-16** illustrate the changes in porosity and permeability. The scatter plots of petrophysical properties at two different injection times were plotted against each other.

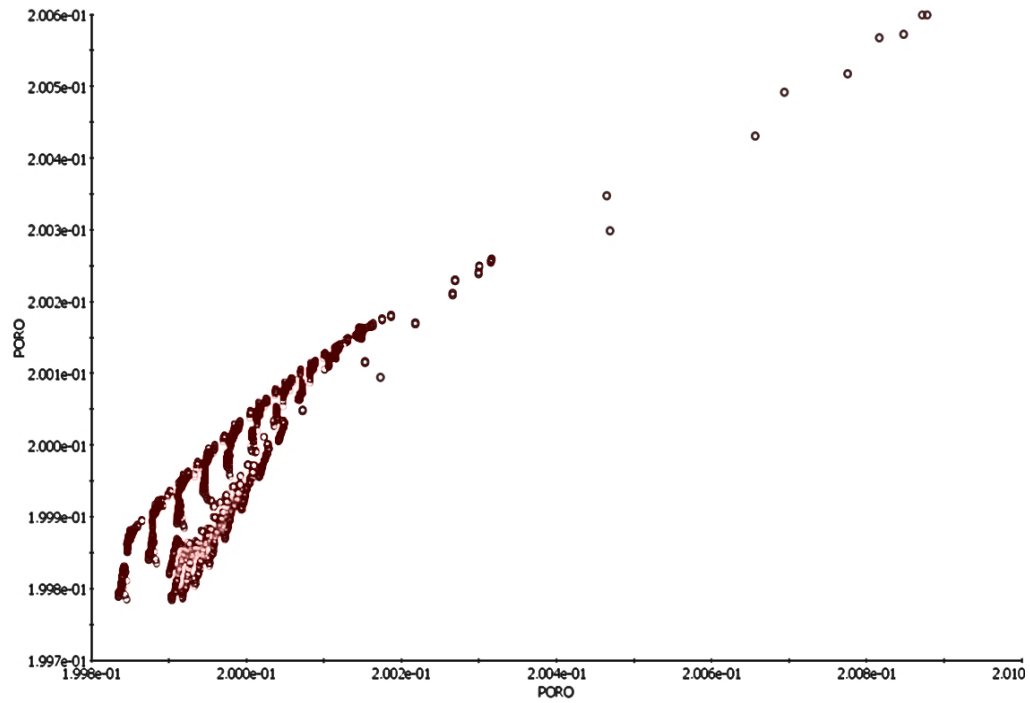


Figure 6-15- Scatter-gram between porosity (in all cells) in cycle 1(100 days) vs. porosity values at cycle 9 (900 days).

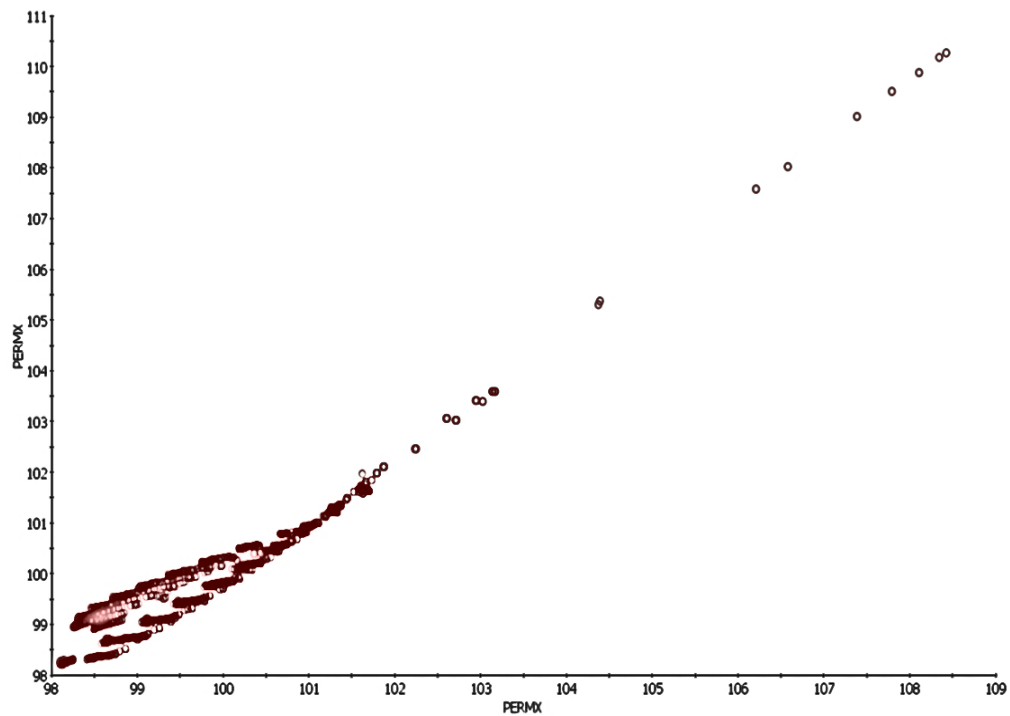


Figure 6-16-Scatter-gram between permeability (in all cells) in cycle 1 (100 days) vs. permeability values at cycle 9(900 days).

Even though the plots show the changes have not be very significant, it shows there is severe hysteresis in the update of porosity and permeability especially at small values of the two properties (right left corner of the two diagrams).

**Figure 6-17** and **Figure 6-18** show how displacements in the  $x$  and  $z$  direction changes after 400 days of injection. Both values are reported in meter. Due to the poroelastic formulation and the chosen formation properties, the displacements are small. Changes in displacements are associated with changes in volumetric strain and accordingly to porosity and permeability as reservoir geomechanically influenced parameters.

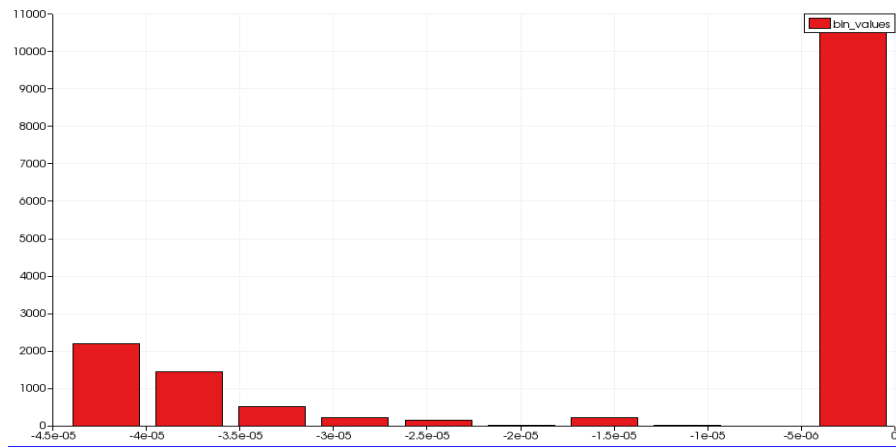


Figure 6-17-Histogram of vertical displacement  $u_{zz}$ -divided by cell length in  $z$  direction- after 4 cycles (400 days) of  $\text{CO}_2$  injection.

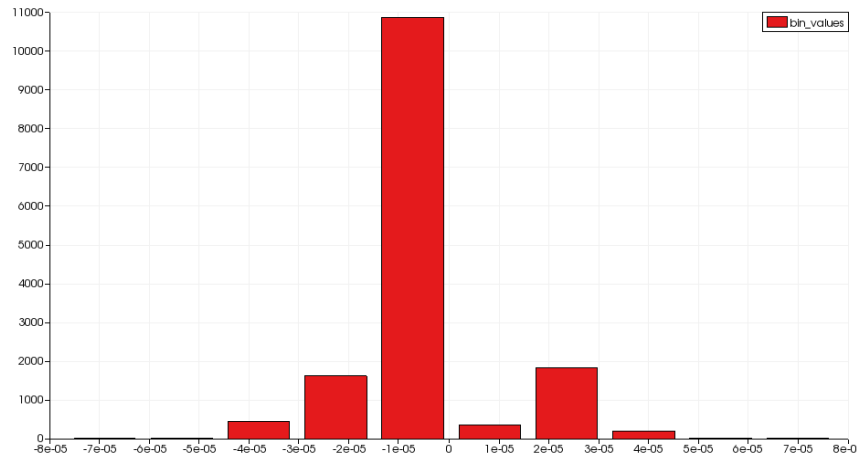


Figure 6-18-Histogram of lateral displacement  $u_{xx}$  in  $x$  direction-divided by cell length in  $x$ - after 4 cycles (400 days) of  $\text{CO}_2$  injection.

## Discussions

Comparison between fully coupled and sequential coupled simulations is reasonable provided the simulators engine (grid or multi-grid solvers) as well as the core code and programming language behind the tools are the compatible. On this basis, a decoupled geomechanical code (from fluid flow code) based on the same fully coupled code which was developed on the same platform (DUNE), with the same programming language (C++), and the same discretization scheme (Box method), and the same simulation grid manager was developed. Comparison of a computational load and third party simulator with different simulation technique is also reasonable as long as the simulations are both performed with the same CPU and the solvers use the same technique for system solving. The solver that streamline code is based on can be either AMG or SAMG, and Dumux is also able to switch (to be compiled with) to Algebraic MultiGrid (AMG). However for problem simplicity the library embedded in our approach was SuperLU (Li, 2005) as system solver in Dumux; still the computational load to carry on the simulations are significantly different (in streamline-based geomechanical coupling than finite volume based flow-geomechanical coupling) that switching to even a faster solver (i.e. SAMG) does not change the comparison scenario significantly.

Inclusion of the CFL (Courant–Friedrichs–Lewy) condition and assignment of proper CFL values and criteria, in both simulators (streamline based and FV-FEM based) is another important key parameter which might change the simulation computational load as well as resolutions of the results. Auto time stepping also might be taken into account if FV-FEM technique is compared versus streamline based geomechanical coupling, as fixed time steps can sometimes be bottle-neck in forward flow and geomechanical simulations.

All approximate methods in reservoir simulation are associated with some disadvantages in capturing full physics of simulation or in model accuracy. (e.g., proxy methods, IMPES scheme, streamline simulations, convex optimization techniques, model order reduction approaches, upscaling, etc.). All these class of techniques have been offered to the world of reservoir simulation to enhance simulation CPU inefficiencies, but on the other hand they result in a reduced model accuracy, depending on the physics of the problem (compositional, diffusion, capillary, multi-phase or single phase, gravity, etc.), model size and simulation time. The main disadvantages associated with streamline-based hydromechanical coupling, are the disadvantages in the streamline simulation, as they are approximate

methods. For highly nonlinear systems such as compositional miscible flood simulations, gravity dominant systems, systems with rigorous capillary pressure effects, etc., streamline-based hydromechanical techniques are not expected to provide accurate results. It is expected that increasing model non-linearity would reduce the CPU efficiencies achieved by inclusion of geomechanics in streamline simulation. Furthermore, since streamline simulation deals with a dual-grid system (Cartesian grids to solve pressure and streamline grid to solve saturation equation), the mapping in the streamline workflow between these two grids is associated with some material balance error. However the technique is not associated with numerical solution divergence during iterative simulation, in contrary to traditional coupling techniques. When porosity is updated often in traditional coupling schemes, the solution diverges, (forward simulation will be interrupted) and a convergence criterion must be defined for the simulation.

For the dynamic hydro-geomechanical problems, where both fluid flow and geomechanics problems are considered dynamic, the solid material velocity term in Darcy equation becomes important, which leads to a time derivative compressibility term (bulk volume for each node) and the fluid flow formulation needs to be extended to a two-phase flow system with deformable porous medium, and a displacement velocity term is required to be added to saturation transport equation. This technique is mainly important where some wave is induced in the medium, or the problem is studied around the wellbore vicinity with high-pressure gradient, (e.g. sand production). Our problem, however, is considered dynamic in fluid flow and quasi-static in geomechanics, and therefore this term is neglected in our formulation, considering that the problem is for a large field (not necessarily around the wellbore vicinity). Furthermore a quick comparison between solid displacement velocity and fluid velocity (pressure gradient) for a time step showed that these two are different by orders of magnitude and therefore assumption of zero solid velocity is physically meaningful and would not affect our solution.

## Conclusions

Simulation of underground CO<sub>2</sub> injection in saline aquifers was studied. Geomechanics was introduced as an important piece of physics that is influential in the storage mechanism. Different existing strategies of coupling were introduced. Above that, a novel hydro-mechanical strategy was introduced. Initially we investigated the feasibility of the approach

and if the coupling is doable. For that purpose, a geomechanical code was developed (based on an existing research open source code) and was linked to a FORTRAN based tool for streamline simulation. This approach was implemented on the CO<sub>2</sub> storage scenario, as it was well suited to the nature of streamline simulation and dimensionality and large size of aquifers. Streamline simulation was coupled to an elastic geomechanical code and was shown to be computationally robust and efficient especially for larger reservoirs. The approach was also compared to the fully coupled technique, which is generally expected to provide more precise numerical solutions but can come with severe computational burdens, particularly for large domains with large number of grid blocks. Streamlines are most suited when the process of fluid flow is convective, which is the most relevant to the primary trapping mechanism that is occurring during injection process of CO<sub>2</sub>. Geomechanics also is best fitted to this trapping mechanism, therefore linking of these two pieces of physics at the time span of several years was found to be relevant.

Initial assessment of fully coupling technique for scenario of CO<sub>2</sub> injection is completed; however the current challenges in all the coupling strategies discussed in this paper, are how the three coupling strategies explained will result in approximately the same fluid flow and stress redistribution results for different model geometries and complexities of physics. Conventionally most of techniques in simulation of fluid flow and reservoir geomechanics that are computationally faster are usually involved with some approximations and loss of precision. Therefore further investigations are required to find a criterion for reconciliation between precision of results and model CPU efficiency where geomechanics is coupled to fluid flow (particularly in sequential coupling techniques). Ongoing research is on exploring different coupling strategies with different time steps and improved model efficiencies toward inclusion of geomechanics in-streamline simulation. A reservoir property index is recommended to be proposed to devise the extent, distance from injection well, and time span that inclusion of geomechanics in streamline simulation for physics of CO<sub>2</sub> storage would be relevant.

## Acknowledgement

The authors would like to gratefully acknowledge the helpful contribution of Holger Calss (Professor at University of Stuttgart) and Bernd Flemisch. We also thank Rod Batycky for

providing the 3DSL research code and academic license for StudioSL. The authors also acknowledge the financial support provided by the Helmholtz Alberta Initiative.

## Nomenclature

$\Delta \bar{\sigma}' =$	Changes in effective stress
$\Delta P_{eff} =$	Pore pressure changes between two states
$\rho_{n,w} =$	Non-wetting phase, water density
$S_{n,w} =$	Non-wetting phase, water saturation
$\bar{I} =$	Identity matrix
$\emptyset =$	Porosity
$\bar{K} =$	Permeability tensor
$\emptyset_0 =$	Initial porosity
$k_0 =$	Initial permeability
$\Delta \tau_{sl,i} =$	Time of flight along streamline ( $i$ )
$\Delta t_{sl}^{n+1} =$	Convective time step size
$f_{j,i}^n =$	Fractional flow function at cell ( $i, j$ ) along streamline at time step ( $n$ )
$K_{r\alpha} =$	Phase relative permeability
$\vec{v}_\alpha =$	Velocity of phase $\alpha$
$\mu_{n,w} =$	Viscosity of non-wetting phase, water
$T =$	Temperature
$\alpha, n =$	Van Genuchten parameters
$E =$	Young modulus

## Chapter 7: Streamline-Based Coupled Geomechanics and Reservoir Simulation for Hydromechanical Modelling of CO<sub>2</sub> Storage in Saline Aquifers\*

### Introduction

The injection of CO<sub>2</sub> into deep geological formations with environmental purposes and storing the greenhouse gas for long time-periods may have complex geomechanical impacts. These impacts can sometime be significant and may lead to environmental hazards, fault reactivation and seismic events and safety issues such as caprock sealing, wellbore integrity, and determination of maximum injection pressure. These mechanical impacts are mainly due to pore pressure buildup around the injection well that causes redistribution in the effective stress field (Terzaghi, 1936) and a subsequent change in the volumetric strain (Biot, 1940) that can be observed in the form of detectable vertical displacement on the ground surface. The change in the volumetric strain and the pore volume (porosity) in the reservoir will mutually change the pore pressure field as well as the transport of saturation in the porous medium. Therefore for thorough analysis and modeling of CO<sub>2</sub> injection the hydro-mechanical simulation (coupling) is essential.

However inclusion of geomechanics is involved with large computational load particularly for large reservoirs where continuous monitoring of geomechanical changes is required. To tackle this problem, streamline simulation (Batycky, 1997) were suggested to be used in the simulation of coupled system. Streamline simulation is an IMPES based dual grid approach that solves pressure field explicit from saturation. Pressure equation is solved on the Cartesian grid and the saturation equation is solved along the streamlines (by use of time-of-flight property). The approach is significantly faster than conventional simulation techniques, particularly for incompressible immiscible systems. Previously a new reservoir-geomechanics coupling scheme was introduced in the work of Koohmarch Hosseini and Chalaturnyk

---

\* A version of this paper was presented at SPE Heavy Oil Conference, in Calgary, Canada June 2013, SPE-165409, and published in the proceeding of the conference.



(2013) that allowed full-field large-scale hydro-mechanical coupling of reservoirs. The novel technique was applied and tested in the scenario of CO<sub>2</sub> injection in saline aquifers. In this work the same scheme is compared with the other two coupling approaches that were developed by Box method (collocated FV-FEM) discretization technique: 1) sequentially coupled and 2) fully implicit coupling.

It must be noted that the detailed physics and modeling of CO<sub>2</sub> storage is of the second order of priority in this work. The main focus of this study is comparison of different developed coupling strategies in terms of CPU efficiency and accuracy from reservoir-geomechanics modeling point of view. That is why injection of CO<sub>2</sub> was considered as an immiscible and the component exchange between CO<sub>2</sub> and saline and rock phase (chemical trapping) was neglected. However the injection process was still considered compressible and the model dimensions and operating parameters were tried to be close to reality.

Koohmarch Hosseini and Chalaturnyk (2013) showed that the novel developed coupling scheme was suited mostly to the problems with convection-dominated displacement processes, large scale heterogeneous reservoirs, and slightly compressible immiscible scenarios that require a very long forward simulation time (more than 10 years). These physical attributes are very close to the physics of underground CO<sub>2</sub> storage (particularly in the physical trapping phase), therefore underground CO<sub>2</sub> injection was selected as the method of choice for testing of the new developed coupling methodology with the other two developed techniques.

The main focus of this study is the numerical comparison of different following strategies: SL-based, sequentially coupled Box method, fully coupled Box method. The latter two schemes get use of the novel discretization scheme but in terms of CPU load are pretty much similar to conventional coupling schemes. Furthermore the philosophy of the coupling and the approach that flow simulator communicates with mechanical simulator is well addressed in literature (Settari and Mourits, 1998).

The results of this study are quite important in terms of fast full-field reservoir simulation where geomechanics can play an important role (e.g. caprock integrity, CO<sub>2</sub> leakage). Also these studies provide a very good foundation for future industrial decision on whether to include geomechanics into the modeling workflows as well as selection of the proper hydro-

mechanical coupling scheme with respect to the available resources (computer CPUs and time).

In this work, first the simulation results of the injection process (stress field, strain redistribution and ground surface deformation with respect to evolution of time) are presented and an analysis and interpretation are performed on the role of geomechanics in the early injection phase. The subsequent sections are mainly about the CPU added values that streamline-based reservoir geomechanics coupling offers over conventional coupling schemes (sequential coupling scheme and fully coupled scheme) and the extent that the results are reliable and comparable with the reference model output (fully coupled scheme). The studies showed that the new coupling scheme is very robust in terms of added computational efficiency, and the simulation results are in close agreement with the FV-FEM sequential coupling scheme.

### **Simulation Results of Box-Method (collocated FV-FE) Based Hydromechanical Coupling**

**Figure 7-1** and **Figure 7-2** illustrate the distribution of lateral and vertical deformations on the model cross-sectional view on  $x$ - $z$  plane after 400 days of sequential coupling between C++ packages (box method) of fluid-flow and geomechanics. These figures show that displacements are mostly induced around the injection well. The distribution and magnitude of displacements are symmetric and centered mostly on the injection zone. However the displacements peak values are somewhere away from the injection well in the reservoir, but not adjacent to the injection point. The negative sign in the values of displacements are only the sign conventions defined based on the location of the injection well. Negative displacement means a solid particle movement toward left ( $-x$  direction), with respect to its initial location.

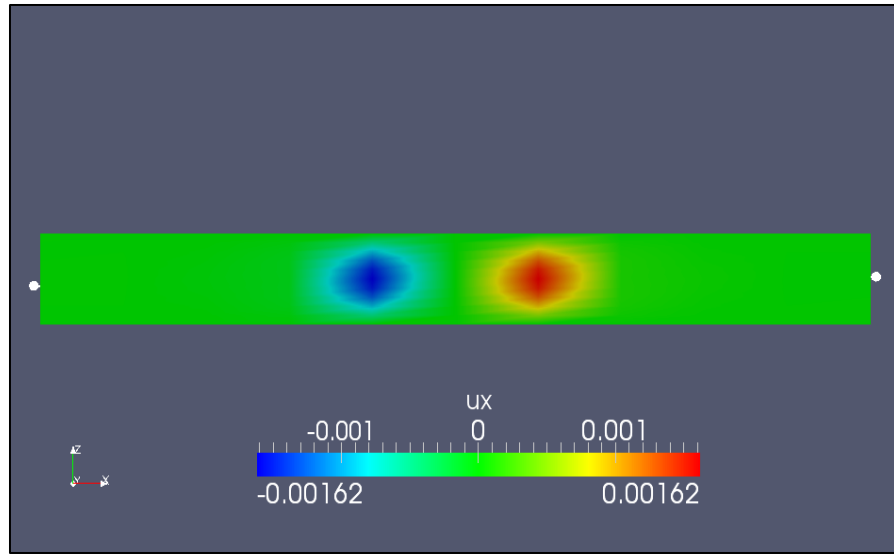


Figure 7-1-Distribution of lateral displacement ( $u_x$  in meters) on x-z plane cross-section after 400 days of coupled simulation, from bottom to top of the reservoir.

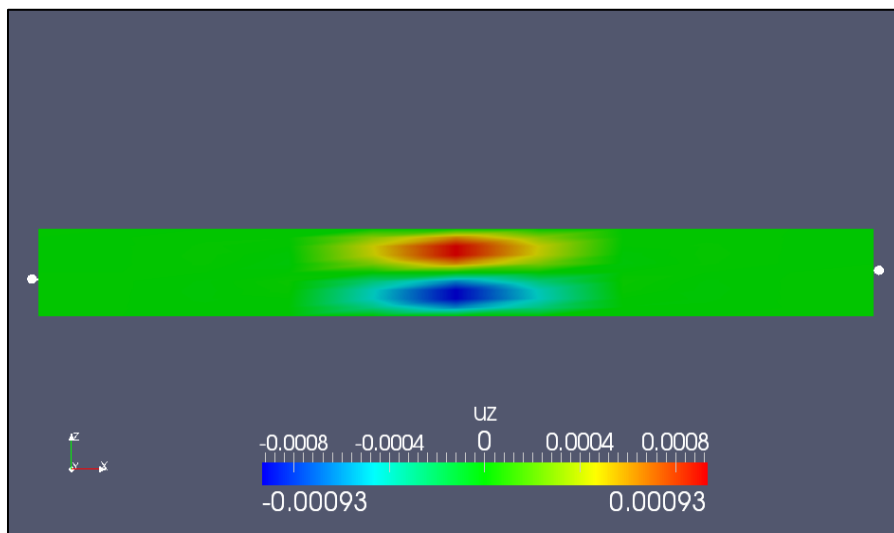


Figure 7-2-Distribution of vertical displacement ( $u_z$  in meters) on x-z plane cross-section after 400 days of coupled simulation, from bottom to top of the reservoir.

**Figure 7-3** explains the same concept as in Figure 7-1, and shows the profile of lateral displacements on the top cross sectional-view on  $x$ - $y$  plane. The two pictures in Figure 7-3 show that the displacement values are larger close to the injection well than in a higher elevation and closer to caprock, due to reservoir rock stiffness. The right hand side plot shows the lateral displacements in the middle of the reservoir and on  $x$ - $y$  cross sectional view, while the left hand side shows the displacement values on the top of the reservoir (5 meter below the caprock). The same results are expected for vertical displacements as they

are related to one another by linear Hooke's law formulations. Due to homogeneity in the reservoir MEM properties, as well as the model symmetry, the lateral displacements in  $x$  and  $y$  directions are identical.

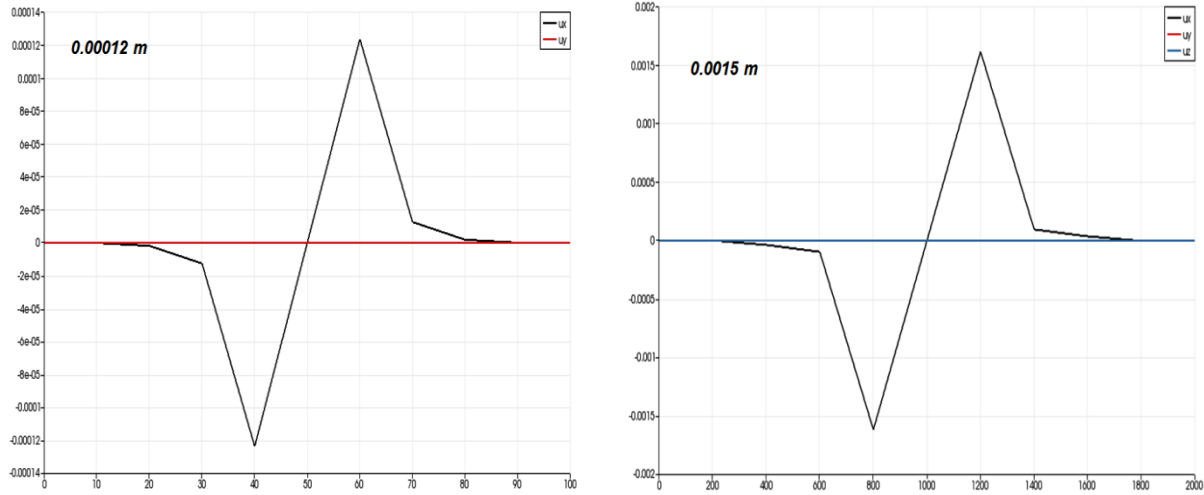


Figure 7-3-Lateral displacements ( in meter) on top of the reservoir (left) and in the middle of the reservoir (right) on x-y plane, orthogonal to z-axis at t=400 days.

**Figure 7-4, Figure 7-5, and Figure 7-6** show the effective stress distribution on the same plane discussed so far (x-y plane orthogonal to  $z$ -axis and in the middle of the reservoir). As it can be seen more redistribution in stress values are centered on the injection well. As pore pressure builds up the effective stress (both lateral and vertical stresses) goes down in the vicinity of the injection zone. However this reduction in magnitude of stress is compensated elsewhere in the reservoir to honor the momentum balance equation (for total stresses) and conservation of energy. Therefore effective stresses increase elsewhere in the reservoir as the injection extends far into the domain, however the concentration of stress is not as much as around the reservoir as the stresses are shed out to a larger area.

Figure 7-5 represents the 3D-contour pictures of stresses that provide a better understanding of the stress redistribution due to injection and pressure increase. Figure 7-6 shows the vertical effective stress changes due to injection. Obviously a decrease in the effective stress is expected, however the rapid decrease is not only due to injection but also arching effect. Since all the formulations are based on linear elastic stress equations, ideally equal total stress is expected only when the injection/depletion zone reaches out far into the reservoir (particularly for a 2D-case), however our model is limited to a certain height in  $z$ -direction,

and therefore some arching of the overburden prohibits the maintenance of the full vertical stress, and the true solution is different than constant top-vertical stress. The arching effect also affects the lateral effective and total stress distribution. Although the constitutive model here is elastic, but generally neglecting of arching effect might lead to shear failure, where a plastic yield envelope is defined for the geomechanical analysis.

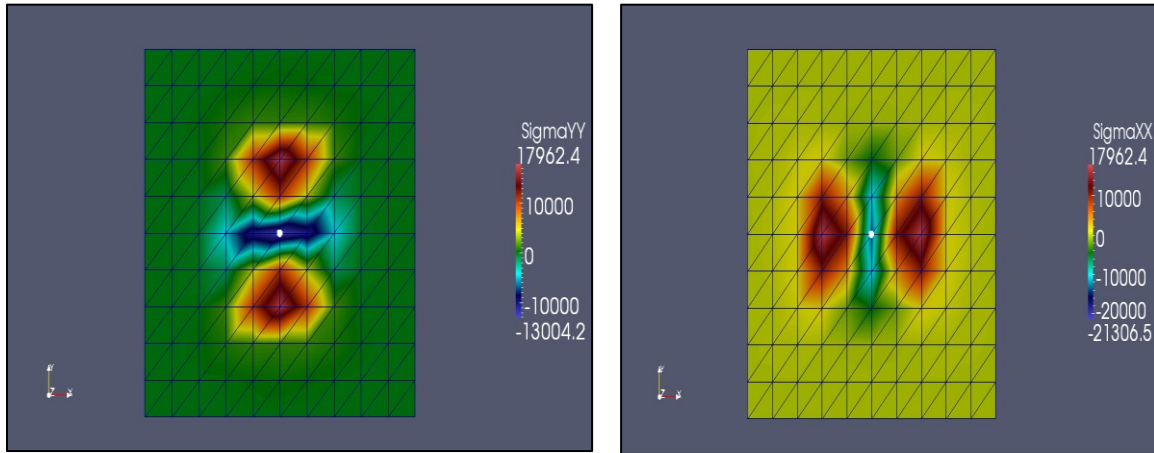


Figure 7-4- Lateral effective stress ( $S_{xx}$ : left ;  $S_{yy}$ : right) on x-y plane in middle model cross-section at  $t=500$  days.



Figure 7-5-Contour plot of effective lateral stress in x-direction ( $S_{xx}$ ) on right and  $S_{yy}$  on left both on x-y plane in the middle of the reservoir at  $t=500$  days.

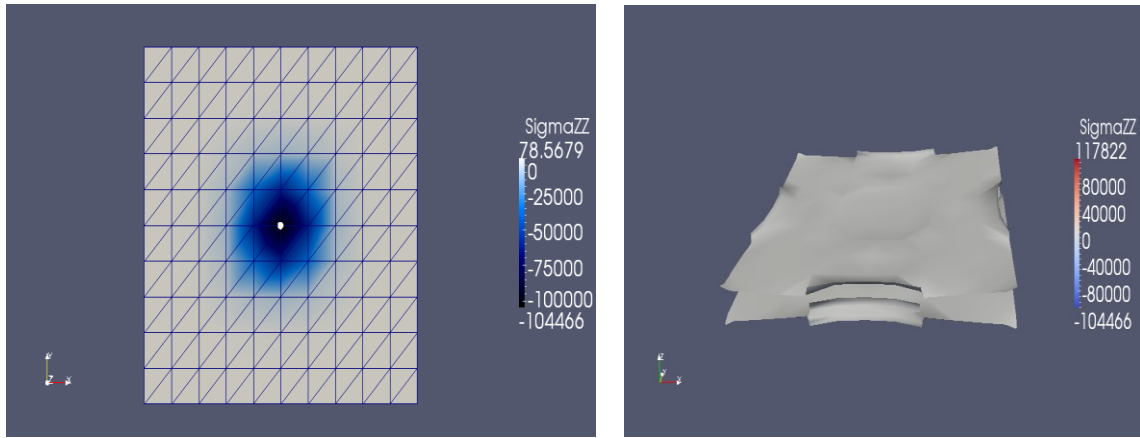


Figure 7-6-Contour plot of effective vertical stress ( $S_{zz}$ ), on right and its distribution on left, both displayed on x-y plane in the middle of the reservoir at  $t=500$  days.

## Numerical Analysis

Numerical analysis and CPU efficiency analysis of all classes of coupled reservoir-geomechanics simulations are of paramount importance for each coupling strategy. The main reason is that inclusion of geomechanics into classical reservoir simulations in all forms (fully coupling, iterative coupling, sequential one way/two way coupling, pseudo coupling) is a bottle neck in coupled scenarios. As discussed, a full coupling, is likely the most precise approach in common/classical coupling strategies since the primary geomechanical variables (changes in vertical and lateral displacements) are solved simultaneously along with other primary variables corresponding to other reservoir physics (fluid flow, thermal, geochemical, etc.) such as saturation and pressure for physics of underground fluid flow. Therefore, a single set of coupled governing equations that capture both the mechanical and the fluid flow behaviors, is implemented numerically. However the fully coupling approach cannot be used for models with large DOFs or with large dimensions, or when long forward simulations are required, since the assembly of the Jacobean matrix and the solution of the arising stiffness matrix is computationally quite demanding with current CPUs and linear or parallel algebraic solvers. Therefore, sequential coupling techniques are preferred generally for scenarios where far field studies are required (such as  $\text{CO}_2$  sequestration). Still, sequential coupling techniques are also associated with large computational costs, particularly for large number of DOFs, and where large number of coupling cycles (forward intervals) is needed to model full reservoir life.

The streamline based reservoir-geomechanics coupling was developed in previous sections of this paper to remove the major bottleneck in the coupled analysis. Next figures discuss the CPU efficiency improvement, when the so-called SL-Based coupled approach was employed. To do so, the computational cost associated with streamline simulation and geomechanical simulation of the same model discussed before, was studied. Computer CPU load was considered as the primary factor under investigation, as it is a computer sensitive run-time parameter.

The target model has exactly the same physics as the three dimensional model studied in SL-based hydromechanical coupling section, except the model dimensions changed to a lower resolution model to allow us to perform the comparative study versus finite volume-based coupling scheme, as FV-based coupling were computationally intensive to be run for a couple of cycles for large models. The new model dimensions are as below, and the length of each coupling cycle was kept the same as before (100 days).

**Table 7-1-Model dimensions**

$L_x$	$L_y$	$L_z$
2000 m	2000 m	2000 m
$N_x$	$N_y$	$N_z$
10	10	10

**Figure 7-7** shows the CPU run time for each coupling interval (100 day time span). The left hand side cones show the CPU load of streamline based fluid flow part of coupling, and right hand side represent the same thing related to the geomechanical part of coupling process. The small tags above each column show the number of each coupling cycle. The columns are adjusted in the order of time, and therefore from left to right each column shows the forward 100 days of coupled simulation.

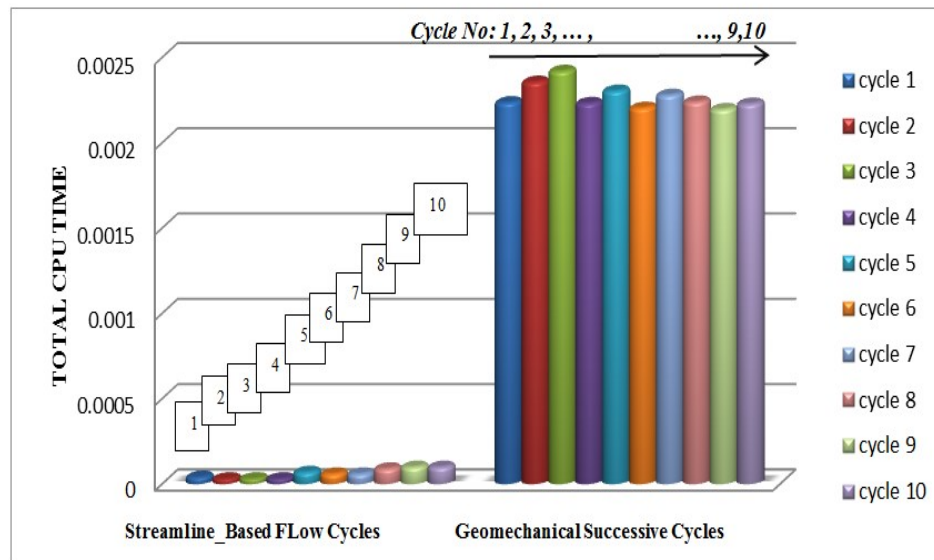


Figure 7-7-SL-Based reservoir-geomechanics scaling behaviour for a homogenous reservoir. Left hand side columns illustrate CPU time associated with streamline simulation for each cycle, and right hand side columns represent the same thing for geomechanics forward coupling cycles.

As Figure 7-7 shows, there is no uniform trend in the computational cost as the coupled simulation moves forward. However, at each point in the coupled analysis, regardless of the number of the coupling cycle, the CPU time related to streamline simulation is much smaller than the CPU run time in geomechanical part. In other words, up until this part we know that not only inclusion of geomechanics in streamline-based hydromechanical coupling was feasible, but also the CPU load induced by introduction of the new piece of physics (instead of FV/FD flow simulation) was much smaller, compared to geomechanics run time.

### Comparison of the Coupling Strategies (Streamline-based vs. Box Method: FV-FEM)

To study robustness of the new coupling technique, streamline simulation-based hydromechanical coupling was compared versus classical finite-volume based hydromechanical coupling. The same model with the same dynamic attributes in terms of fluid flow in porous medium was developed. The discretization scheme was explained before (FV/FEA -box method). The geomechanical model in both physics (initial and boundary condition, rock mechanical parameters, etc.) and discretization scheme were kept the same as in streamline-based coupling. The forward coupling cycles were also the same (100 days).



Both coupling strategies were implemented in the same environment (Linux), and the same computer CPU was used to have a fair comparative study.

**Figure 7-8** shows the same plot as in Figure 7-7, but for finite-volume based fluid flow simulation. As the picture shows, in this coupling strategy the CPU time in the fluid flow simulation is even higher than geomechanical CPU time usage for each cycle. Comparison of Figure 7-8 versus Figure 7-7 clearly shows that the new streamline-based hydromechanical coupling is computationally more efficient and robust compared to classical sequential coupling techniques. It must be mentioned that conventionally the geomechanical part of coupling, is expected to be computationally more crucial, however here the geomechanical part, uses a smaller CPU load in the course of coupling process. The main reason is the linearized momentum formulation described, as well as discretization scheme. But still looking at only fluid flow part, is sufficient to judge on the power and efficiency of new technique, since the geomechanical engine in both coupling strategies were the same. The difference in CPU time shows orders of magnitude difference for a model with 1000 cells.

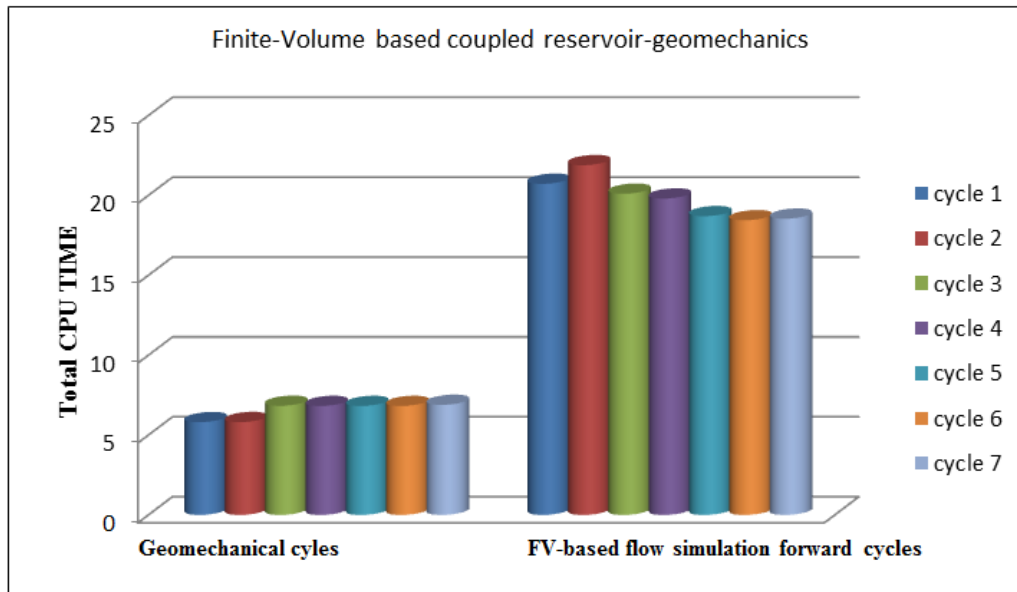


Figure 7-8-Finite volume-based reservoir-geomechanics scaling behaviour for a homogenous reservoir. Left hand side columns illustrate CPU time associated with geomechanics forward cycles, and right hand side columns represent the same thing during forward finite-volume-based fluid flow simulation.

A total (ensemble flow and geomechanics) cumulative computational cost analysis in the course of coupling is also needed to ensure about the strength and robustness of the technique. **Figure 7-9** and **Figure 7-10** show the CPU time diagram versus simulation time for both the case of streamline-based hydromechanical coupling and finite-volume-based coupling.

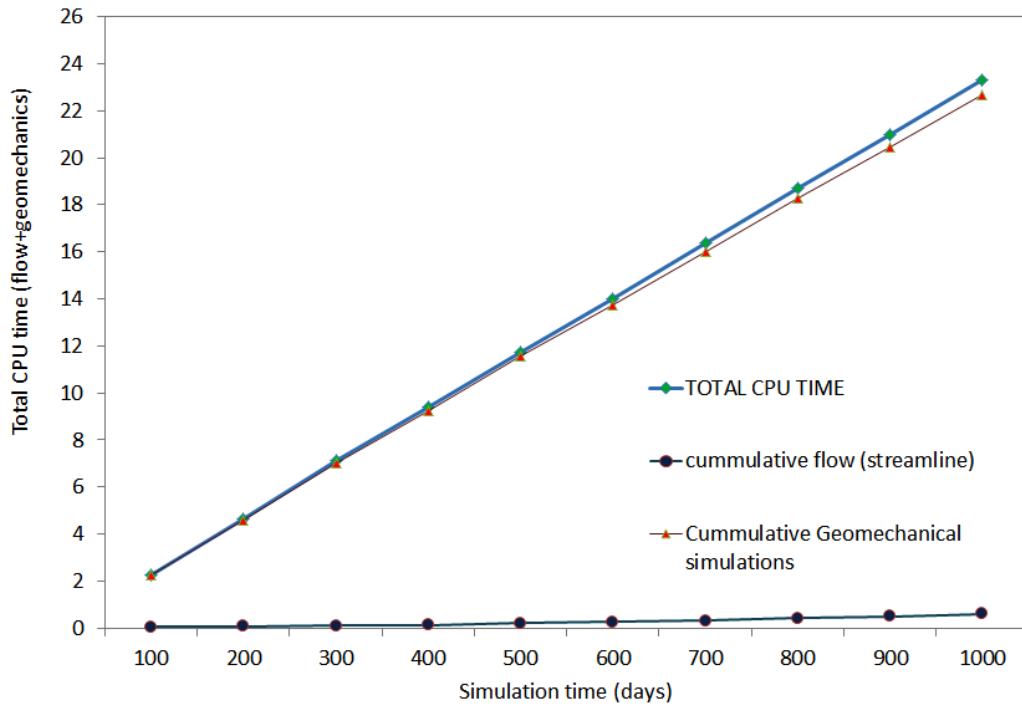


Figure 7-9-Cumulative computational cost scaling behaviour (streamline-based hydromechanical coupling).

Figure 7-9 shows the cumulative CPU load in the course of coupling (0-1000 days). The lower curve shows the computational behavior of streamline simulation part of coupling, and has the lower CPU cost compared to the other curves. The middle curve shows the cumulative geomechanical computational load and the curve above represent the sum (fluid flow and geomechanics) cumulative CPU load, which is the actual CPU load of coupling. As it is seen the computational load of streamline simulation portion of the coupling is negligible compared to the total cumulative CPU load.

Figure 7-10 studies the same behavior of each component of coupling (geomechanics and fluid flow), and compares the CPU load for the finite-volume hydromechanical coupling (as an example of conventional classical coupling techniques) to the streamline-based hydromechanical coupling.

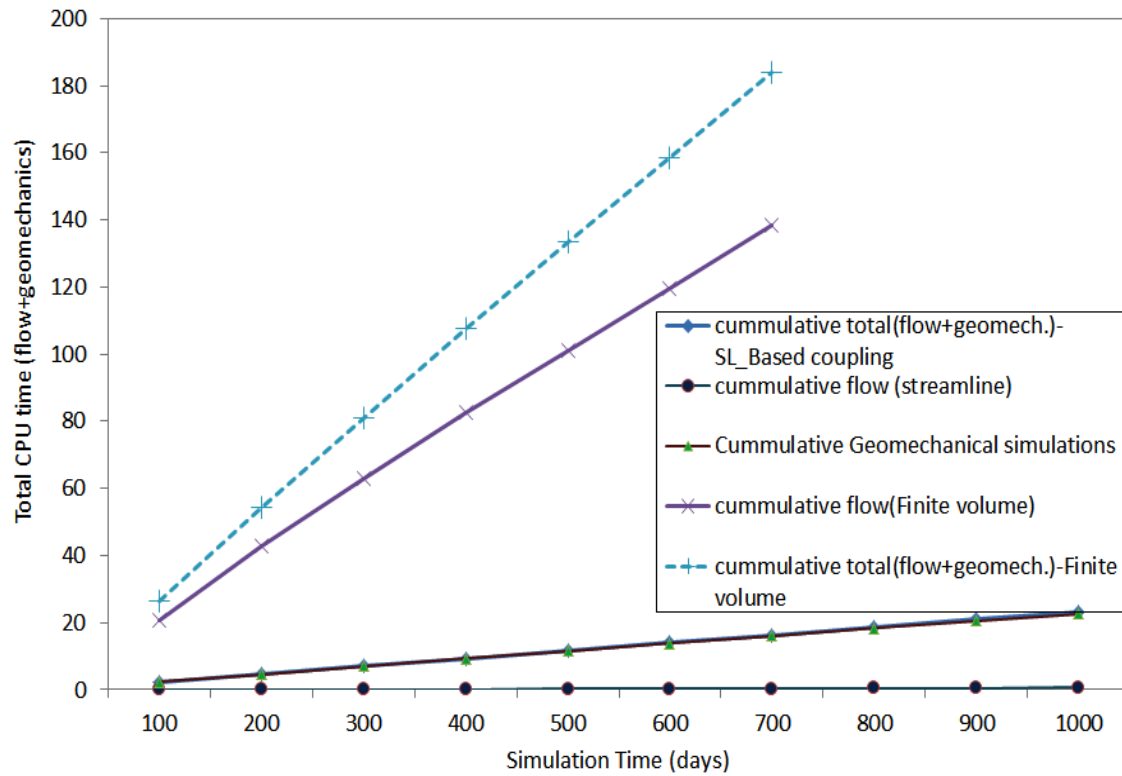


Figure 7-10- Cumulative computational run-time scaling behaviour: streamline-based hydromechanical coupling vs. finite-volume based hydromechanical coupling.

The three lower curves are the same curves related to the streamline-based hydromechanical coupling (Figure 7-9), and the two top curves show the cumulative computational cost in the course of coupling for finite-volume-based fluid flow portion of coupling (solid line), and the total cumulative -sum of geomechanical and fluid flow- computational cost (CPU run time). The dashed line represents a large difference in terms of CPU load compared to the total CPU load associated with the introduced coupling technique (streamline simulation based). As noticed, for simplicity reasons, the comparison study was done for only seven cycles (700 days) due to huge computational loads of finite-volume based coupling approach.

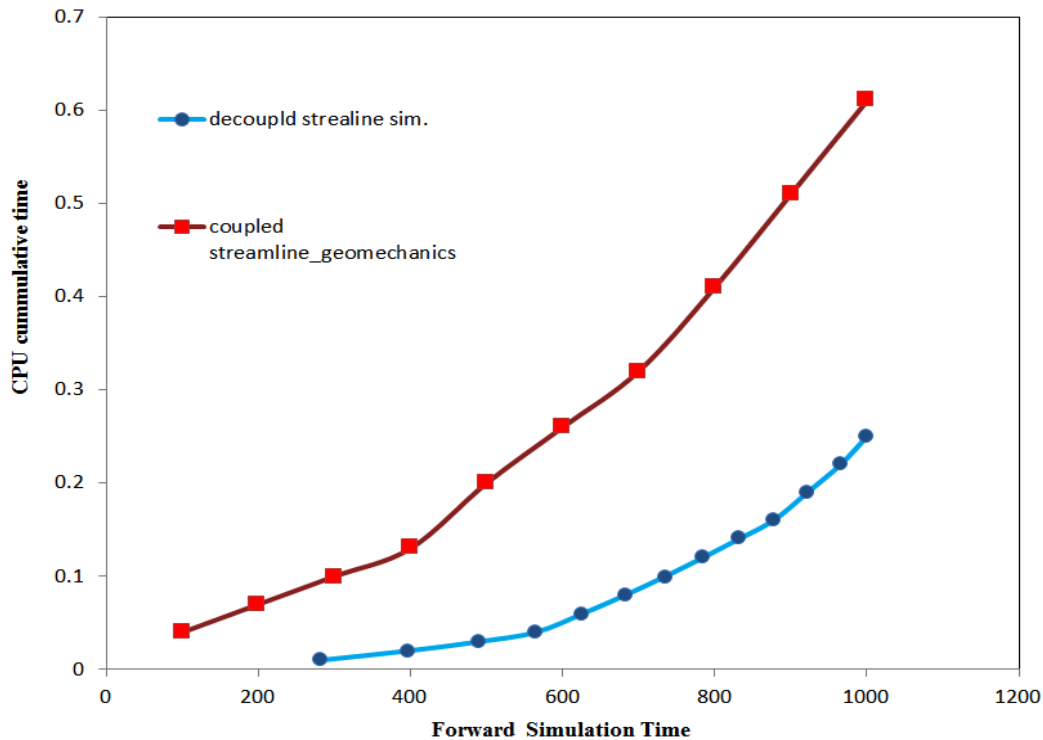


Figure 7-11-CPU load behavior of streamline simulation in the course of forward simulation.

**Figure 7-11** shows the trend of cumulative computational load of streamline simulation. The red top curve shows the trend for the coupled fluid flow-geomechanics scenario, and the lower curve illustrates the same trend for the case of stand-alone streamline simulation during the same time span of simulation. As it is observed, streamline simulation carries out lower computational cost when it is not coupled to geomechanics. The reason is mainly due to auto-time stepping and convergence reasons, since streamline simulation has to re-calculate the pressure field and trace streamlines and solve forward 1-D transfer equation, at the end of each cycle. These processes along with limited time step size (100 days) slows down the forward flow simulation and prohibits the full power demonstration of streamline simulations. However still the coupling approach is significantly faster than conventional coupling techniques.

**Figure 7-12** and **Figure 7-13** show the behavior of finite-volume based components of coupled scheme, during each cycle. Previously the behavior of the simulators discussed over the full span of simulation (100 days), however in each interval there are sub-time steps that all together form the end-cycle CPU load. Figure 7-12 shows the behavior of computational load of geomechanical portion of coupled scheme for five different cycles.

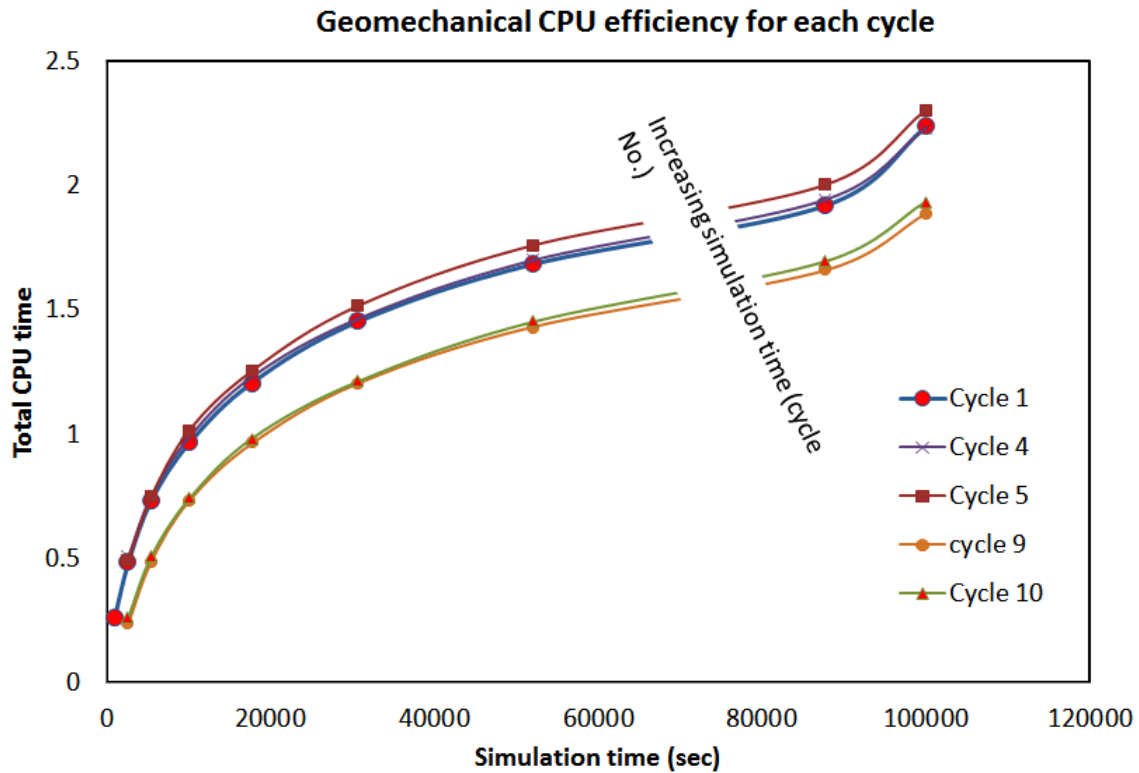


Figure 7-12-Geomechanical simulation CPU run-time for each sub-interval of coupled simulation. The numbers are reduced by  $1/100^{\text{th}}$ .

As it is seen, the numerical time steps increase in the course of each simulation cycle, and therefore the CPU time does not increase prohibitively. And as the cycles move forward (cycle 9 and 10), and we reach to the end of coupling, less CPU time is observed due to problem convergence and matrix solution stabilization. Therefore at the last two cycles, identical Newton iterative time steps in both cycles were reported. The time steps in geomechanical simulation are not real time steps, but are pseudo time steps.

Figure 7-13 shows the same diagram for fluid flow part of coupling for two cycles. Number of time steps as well as CPU run-times is larger than geomechanical part. As it can be seen from the curve, the end time for each cycle is 8640000 seconds which is equivalent to 100 days (sequential coupling time intervals). The time in numerical solution of fluid flow is the real time. The same as in geomechanical part, as the number of sequential cycles increases, and we approach toward the end of simulation the time-step sizes stabilize, and slightly lower CPU loads are reported.

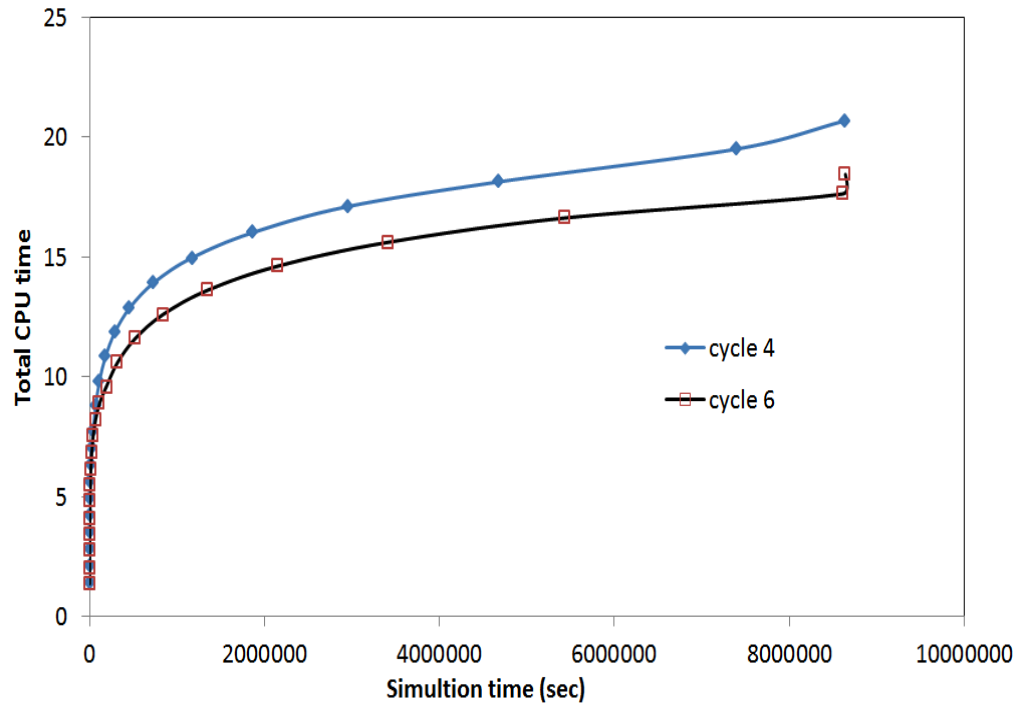


Figure 7-13- FV-based fluid flow CPU run-time for each sub-interval of coupled simulation.

**Figure 7-14** and **Figure 7-15** illustrate an approximate investigation over the accuracy of the introduced coupling scheme. The updated porosity outputted from the fourth cycle of SL-based hydromechanical coupling (after 400 days) was compared to the one reported out of finite-volume coupling technique. A slice of the model orthogonal to  $\hat{x}$ -plane (along  $x$ - $y$  plane) was chosen to illustrate the distribution of porosity. The left hand side picture shows updated porosity distribution after four cycles of finite-volume-based simulation, and the right hand side picture shows the same property at the same time reported from SL-based hydromechanical coupling.

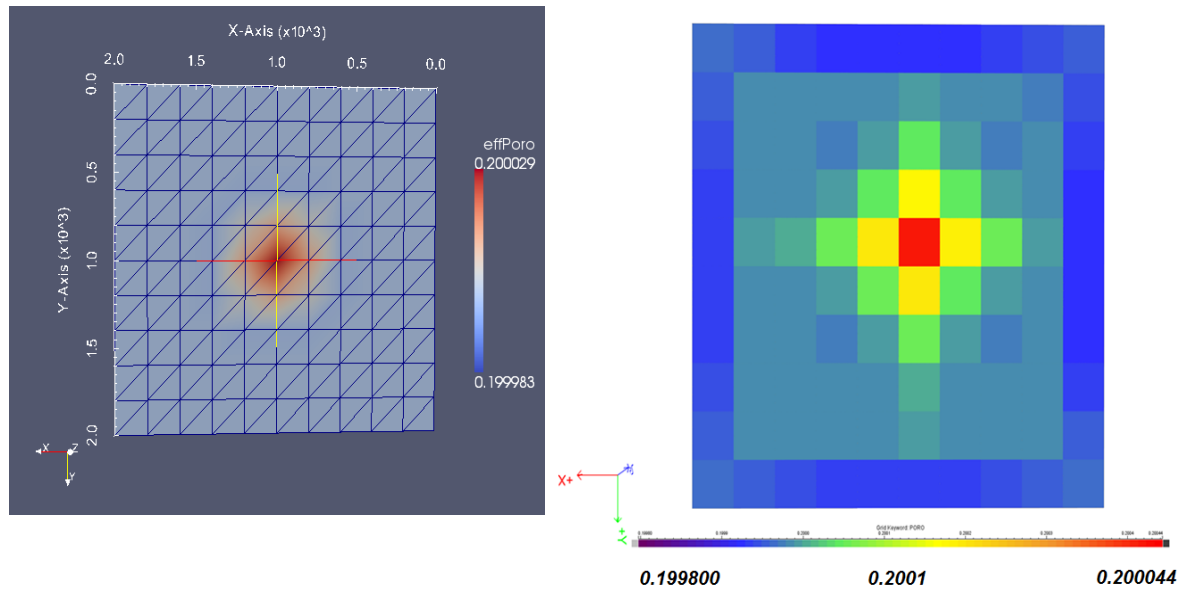


Figure 7-14-Porosity distribution after 400 days of coupled simulation-LHS picture (finite-volume coupled simulation), RHS (SL-based coupled simulation), on x-y plane in the center of the model.

As Figure 7-15 shows, porosity builds up in the middle of the section as the injection well is located there, and the region around the injection well experiences the compressional load due to injection and pressure build up, and therefore increase in volumetric strain is expected. The porosity updates, in two pictures looks approximately the same. The porosity ranges from 0.199800 to 0.200044 in the SL-based case, and in the left picture it ranges from 0.199983 to 0.200029, which are very close; and porosity is at its maximum value in the center of the model and decreases toward the model boundaries to its initial value. The volumetric strain profile along the  $x$ -axis, on the same model section is compared in the two scenarios in the next diagram.

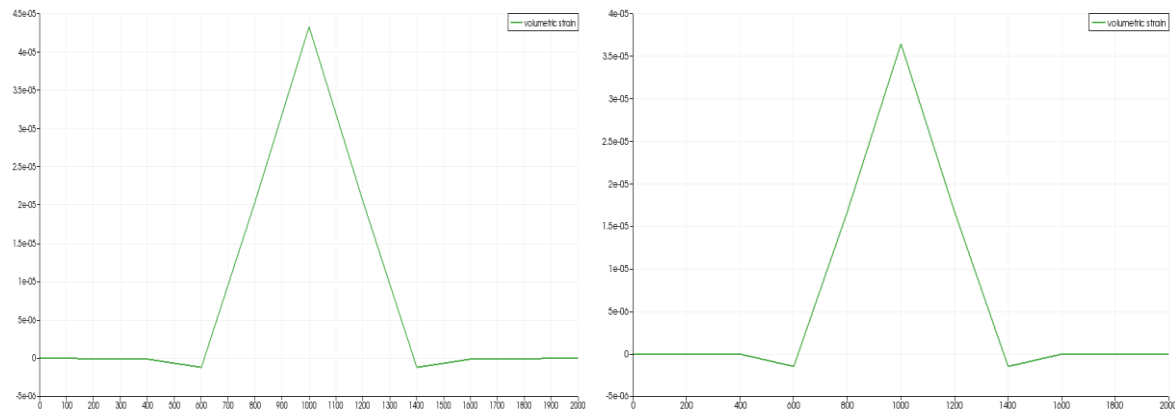




Figure 7-15-Volumetric strain profile along x-axis on the middle z-plane cross section after 400 days. LHS represents the FV-based and RHS represents the SL-based coupled system.

As the volumetric strain profile shows, there is a rapid increase in volumetric strain due to pressure build up and reduction of effective stress in that zone. The increase in volumetric strain leads to increase in porosity and permeability in the region. The volumetric strain peak values after fourth cycle of simulation are not identical but are relatively close. However in larger scales the difference in results might be a bit larger, due to different numerical schemes and material balance errors in each coupling scheme. Furthermore the more fluid flow complexities are in our model; the more different results are expected. Increase in flow non-linearity or inclusion of compositional physics into the problem affects both the final results and numerical efficiency.

## Discussion

A fair comparison between streamline-based hydromechanical coupling and classical conventional sequential hydromechanical coupling is not achieved, unless the computer CPU on which each computational scheme is performed is identical, as well as the system environment (e.g. Linux, Windows), grid managers and numerical solvers. On this basis, the decoupled stand-alone geomechanical code (based on the same fully coupled code) was developed on the DUNE platform, and was used as the geomechanical core, for both hydromechanical coupling, with C++ as the programming language and SuperLU as the solver in both hydromechanical scenarios. The grid manager on the geomechanical side was kept the same as well. On the fluid flow side, the solver used was SuperLU for simplicity. However, Dumux (where fluid flow was performed on) is able to switch the numerical solver to Adaptive MultiGrid (AMG). Streamline simulation can be carried out either by AMG or SAMG. Our system environment in both cases was Linux. However, the computational load that the new coupling strategy represented, was smaller in orders of magnitude compared to conventional/classical hydromechanical couplings, therefore the effect of system environment or even grid solver will be out casted in large scales.

The authors expect that the new coupling technique provides even larger computational benefits and more efficient hydromechanical coupling, for larger models with larger number of grid-cells. Also for models with high heterogeneity in petrophysical properties (e.g. porosity and permeability), SL-Based hydromechanical coupling is expected to be even more

robust compared to conventional coupling approaches. Future sensitivity analysis on these two is required.

Auto time stepping is also important for a fair comparison of FV-FEM technique versus streamline based geomechanical coupling, as fixed time steps can sometimes be bottle-neck in forward flow and geomechanical simulations. In both of our coupling strategies we considered adoptive time stepping. Most of the techniques in simulation of fluid flow and reservoir geomechanics that are computationally more efficient are involved with loss of accuracy. Therefore, further investigations are required to find a criterion for reconciliation between precision of results and model CPU efficiency where geomechanics is coupled to fluid flow (particularly in sequential coupling techniques). Ongoing research is on exploring different coupling strategies with different time steps and improved model efficiencies toward inclusion of geomechanics in-streamline simulation.

Conventionally, pressure is the only parameter taken from the fluid flow simulator, and being fed into the geomechanical simulator. The linearized geomechanical technique used here, however takes saturation from fluid flow calculations into account as well. Saturation is used when the fluid flow mechanism is considered as multiphase flow (to calculate the average pressure to define effective stress in geomechanical computations), and where gravity is turned on in the hydromechanical coupling. Porosity is not conventionally considered in linear geomechanical calculations either, and usually stress analysis of an elastic material with a geomechanical tool is independent of porosity (or permeability) of the medium. The effect of porosity is mainly reflected in the fluid flow simulation, and a different porosity field leads to a different pressure field and consequently a different stress field. In the technique we used, however, porosity is a parameter, which is transferred to both fluid flow and geomechanics cores, at the end of each cycle. It must be mentioned that for geomechanical simulation of the medium where the material behavior is considered as plastic and is characterized with a certain yield function (e.g. Cam-Clay for sandstones), porosity is a decisive parameter in calculations. One may assess the effect of plasticity on the presented coupling technique in terms of accuracy and CPU efficiency.

## Summary and Conclusions

Geomechanics was introduced as an important piece of physics that is influential in the storage mechanism of CO<sub>2</sub> in saline aquifers. Different existing strategies of coupling were

introduced. Above that, a novel hydro-mechanical strategy was introduced. At first place we investigated the feasibility of the approach and if the coupling is doable. For that purpose, a geomechanical code was developed (based on an existing research open source code) and was linked to a FORTRAN based tool for streamline simulation. Then, the working system was implemented on the CO<sub>2</sub> storage scenario as it was fitting well to the nature of streamline simulation and dimensionality and large size of aquifers. Streamline simulation was coupled to an elastic geomechanical code and was shown to be computationally robust and efficient especially for larger reservoirs. The approach was also compared to the fully coupled technique, which is generally expected to provide more precise numerical solutions but can come with severe computational burdens, particularly for large domains with large number of grid blocks. Streamlines are most suited when the process of fluid flow is convective, which is the most relevant to the primary trapping mechanism that is occurring during injection process of CO<sub>2</sub>. Geomechanics also is best fitted to this trapping mechanism, therefore linking of these two pieces of physics at the time span of several years found to be relevant.

The three coupling strategies explained in the paper will not result in exactly the same results, but are approximately close in terms of fluid flow and stress redistribution results for different model geometries and complexities of physics. Depending on the desired simulation time-span as well as domain of interest (study) to be simulated, one needs to select the proper coupling strategy.

Streamline-based hydromechanical coupling showed to be faster (in orders of magnitude) compared to the hydromechanical coupling technique we used for comparison for a model with 1000 grid-cells. The conventional reference approach for comparative study was a finite volume-finite element based hydromechanical technique. An approximate comparative study was performed to check on the accuracy of the presented coupling technique. The comparisons showed the results are exact to a good acceptable extent. To generalize the results with respect to performance one should, of course, pursue a systematic investigation of different conventional coupling schemes in comparison with the streamline-based approach as proposed here. In either case, this paper showed that it is worth doing it.

## **Acknowledgement**

The authors would like gratefully acknowledge the contribution of Melanie Darcis, and Holger Class, members of department of Hydromechanics and Hydrosystem Modeling at University of Stuttgart, Germany. We also would like to thank Rod Batycky for providing the 3DSL research code and the academic license of studioSL software.

## Chapter 8: Streamline-based Reservoir Geomechanics Coupling Strategies for Full Field Simulations

### Introduction

In simulation of large stress sensitive reservoirs, geomechanics physics processes play a great role in efficient economic recovery. Geomechanics play a role in both environmental concerns (e.g. reservoir subsidence due to extreme production) and accurate prediction of dynamic responses of reservoir (production rates). Therefore reservoir geomechanical responses are important information that needs to be taken into account for reservoir management and proper production optimization during reservoir life cycle.

Injection into underground reservoirs or continuous hydrocarbon production from oil fields changes pore pressure in the reservoir. Pressure depletion (due to production) depending on the reservoir and caprock stiffness, may lead to significant changes in earth stresses and accordingly to crucial subsidence (e.g. Ekofisk field in Norway) or to caprock failure when pressure builds up (e.g. CO<sub>2</sub> storage in saline aquifers). Injection and production processes and the consequent pressure changes in the reservoir change the effective stress in the reservoir (based on Biot's theory) and the changes in effective stress lead to pore volume expansion or contraction and accordingly porosity and permeability changes. The changes in porosity lead to changes in dynamic responses of the reservoir in the course of injection or production. For both types of challenges (environmental or hydrocarbon recovery impacts) geomechanics need to be taken into account and must be integrated on a full field scale to fully capture the impact of drainage regions and pressure zones on each other. However integration of geomechanics into workflows for future decision-making and reservoir management purposes has been quite challenging, mainly because its inclusion has not been computationally practical at the field scale. Particularly for large reservoirs with large number of active cells the computational load of inclusion of geomechanics is even more of a bottleneck.

The mathematical concept to capture the mutual impacts of fluid flow (pore pressure) and solid rock frame on each other is called coupling. The basic idea behind coupling is to

numerically account for the fact that rocks consist of a solid framework and a pore fluid, which cannot be treated independently. The numerical techniques to perform the coupling processes in literature are classified into four types: 1) full coupling (monolithic or fully implicit coupling), which is computationally the most expensive approach as three more set of equations have to be solved in one matrix system along with fluid flow equations, and convergence is not always guaranteed; 2) Iterative coupling, where the flow variables are solved explicitly from geomechanical variables and each solver iterates on each given coupling time-step with the other one until desired convergence is achieved (Settari and Walters (2001), Mainguyand and Longuemare (2002)); 3) Explicit or One-Way coupling, where flow simulator is run for some time and the outputs are transferred only one way to geomechanics, and geomechanical feedbacks (strain and stress) are not fed back into flow simulator (Samier and Gennaro , 2007); and 4) Pseudo-coupling, which calculates the geomechanical responses by some correlations or empirical models, and porosity and permeability are updated as a function of pressure with a look-up table. All the above mentioned coupling strategies result in increased computational load when they are applied on large scale reservoirs; therefore their implementation has either to be limited to small scale or to be carried out over a very small time window of simulation.

Where inclusion of geomechanics is important in ultimate forecast of production rates of large fields with multi-million cells or where some workflows that require iterative coupled flow-geomechanics simulation such as full field well level history matching, ranking multiple realizations, and optimization are concerned, current computers' CPU are not able to carry over the computational load. Even recent advances in desktop hardware and advent of multicore CPUs or running the models on clusters of CPUs (parallel computation) have not made a significant breakthrough to sequential simulation of mechanical problems in large finely gridded models that need to go under iterative workflows.

Here, we introduce the incorporation of geomechanical process physics into a streamline simulation framework for full field simulations of reservoir-geomechanical influences on reservoir productivity. This work is in continuation of previous recent works by Koohmarch Hosseini and Chalaturnyk (Koohmarch et al., 2013) in which a comparative study on computational load and numerical precision of coupled streamline-geomechanics versus sequential conventional coupling scheme (on Box method) in a CO<sub>2</sub> injection scenario was

performed. All coupling workflows are based on assumption of elastic rock constitutive model. Linear poroelasticity theorem is well accepted and sufficient for an accurate simulation of fluid flow in porous medium, particularly for large-scale geo-models.

The main purpose of this work is introduction and development of different simulation workflows and strategies for streamline-based reservoir geomechanics coupling. All simulation methods were tested on several numerical cases and the potential added value; advantage and disadvantage of each coupling technique were discussed in detail. Also we discuss the numerical capabilities that are unique to streamline-based coupling schemes and workflows.

All simulation techniques were developed on a C++ based platform (QT programming language) with workflows that adopted the use of 3DSL (StreamSim, 2014) for successive forward pressure solutions and FLAC3D (Itasca, 2014) for solution of mechanical displacement vectors (volumetric strain field) in each coupling time step.

The key factor that differentiates streamlines class of simulations from conventional reservoir simulators is the streamline-based time steps. The numerical difficulties encountered by conventional methods for highly nonlinear multiphase displacements have still remained a serious problem in many field-scale compositional studies. The usual workaround is to use an implicit or adaptive-implicit formulation, but for large problems, these solutions can become prohibitively expensive in terms of CPU time and memory.

To answer the question of what is the proper choice of stable time steps for streamline simulation-geomechanics coupling, it is important to determine the frequency of the pressure solutions when geomechanics is included in the streamline simulation's framework. The frequency of pressure solutions becomes important for having converged and stable solutions in both flow and geomechanics. In finite difference (FD) simulations, finer models not only cause smaller time steps due to smaller grid blocks but usually face problems because of increased heterogeneity as finer models tend to have wider permeability and porosity distributions.

## Overview: Streamline Simulation and Time Stepping Methods

Streamline simulations solve the saturation forward equation on the 1D streamlines (Lagrangian flow-based grids) explicitly from pressure equation that is being solved on the underlying 3D grids (static Eulerian grids). The solution steps for incompressible problems with no capillary pressure effects are as follows: (1) the pressure equation is solved for fully implicit in the same way as finite difference (FD) methods; (2) the velocity field is then calculated and streamlines are traced based on the velocity field; (3) the mass balance equation for phase saturations (convective equation) are then mapped along 1D streamlines using a property called “time of flight”; and (4) ultimately the calculated 1D convective solver outputs are mapped back onto the underlying 3D grids. For more mathematical details of streamline simulation, see Batycky et al (1997) and Datta-Gupta and King (2005).

The streamline class of simulations for incompressible fluid displacement problems exhibits much faster simulation times than conventional finite difference simulators (10 to 100 times faster than FD methods (Batycky et al., 1997) due to the reduced number of pressure solves required and larger time steps allowed). The usual workarounds in conventional FD or finite volume (FV) simulation techniques such as fully implicit or adaptive-implicit methods become prohibitively expensive in terms of CPU load for large problems with non-linear flow characteristics. Also in FD’s finely gridded models (with large number of cells), not only smaller grid blocks cause very small time steps (the Courant-Friedrich-Levy *or* CFL condition) but also increased heterogeneity causes additional increase in CPU time since finer models tend to have wider permeability and porosity distributions, and the sparse matrix system converges very slowly when the Jacobian terms are not similar (due to heterogeneity). Streamline simulations (in frequency of streamline updates) scale independently of the size and heterogeneity contrast of the 3D model.

The key factor that differentiates streamline class of simulations from conventional reservoir simulators is the streamline-based time steps. Time stepping in streamline simulation is very different than conventional flow simulators. Conventional FD and FV simulators have one single time step deployed for solution of both pressure and saturation equations. In streamline simulation, however, there are two different time steps: (1) one for update of pressures (global time step) and (2) a second time step for solution of saturation convective equation along streamlines (convective time step). If gravity or capillary physics also come



into play, there are additional time steps, which are the operator splitting time steps. For every pressure time step, there is an equivalent saturation time step. However, saturation time steps may be smaller than the estimated pressure update time step, as saturation transport equation is limited due to stability purposes. If the system is incompressible then there is no time step size in the pressure equation, and accordingly there is no limit on the pressure time step. If the system is compressible, both saturation and pressure are moved forward during the saturation time step, meaning that at the end of the saturation time step, pressure and the saturation are the same time step level.

## **Coupling Strategies**

In order to embed geomechanics into a streamline simulation workflow and perform coupling at a large (e.g. field) scale or a less CPU intensive manner, different approaches can be used. A brief description of the five coupling techniques developed and implemented in order to assess the problem of “scale” and “time” in coupled flow-geomechanics techniques is provided below. Appendix 8-A explains the software that is developed to link the physics of streamline simulation to geomechanics by implementing all the following strategies. The key difference between streamline-based reservoir geomechanics coupling and conventional coupling schemes lies with the streamline time stepping where pressure updates are different than saturation time steps and the coupling scheme can be performed either on saturation time steps or pressure time steps or both.

### **Approach 1: One Way Coupling**

One way coupling, or loose coupling, is the simplest coupling technique where fluid flow effects on the geomechanical solution are taken into account, but the impact of geomechanical responses of the reservoir (e.g. rock deformation) on fluid flow are neglected. The flow simulator is run only once and the outputs (pressure and saturation) are fed into geomechanical simulator at user defined time steps, and the geomechanical simulator runs sequentially based on the input data received from the flow simulator. For cases with notable geomechanical impacts on reservoir, such as 8.5 meters of subsidence in Ekofisk, one way streamline-based coupling is a good approach for quick assessment of potential geomechanical risks of the reservoir, but for cases with small displacements where 1-5 centimeters vertical displacements are important, one way coupling is not the accurate

technique to use. Comparison of displacement history of simulation test case 2 through one way coupling with the other coupling strategies supports this statement.

One way coupling in a streamline-geomechanics workflow does not differ from conventional finite-difference simulators, except that the coupling time step can occur on either the pressure global time steps or on the saturation convective time steps (**Figure 8-1**). Use of this streamline-based reservoir geomechanics coupling technique is particularly suited to the applications that are mechanically highly non-linear and need to run the geomechanical problem many times successively, since the flow simulation part is quite fast even for reservoirs with large number of grid blocks, and hence the dynamic solution variables can be calculated rapidly and fed into geomechanics problem frequently. In terms of computational speed, one way streamline based flow-geomechanics coupling is obviously much faster than conventional one way coupling techniques. The reason is that the flow simulator for both approaches runs only once (not sequentially or iteratively), and the computational load involved with the sequential solution of the mechanical problem is identical in both class of simulations, and a significantly faster forward flow simulation (SLs) result in faster one way coupled system. Consequently, for large heterogeneous reservoirs where only geomechanical impacts of the reservoir are important and fluid flow displacement problem is assumed incompressible or linear (e.g. single phase tracer flow with fixed well rates), this approach is the most suitable one, and has accordingly significant CPU efficiency gain compared to conventional FD simulators. The more linear the flow problem is the larger the global time step sizes are allowed to be, and therefore even more CPU efficiency gain is achieved. This approach was constructed and implemented on two numerical cases (see numerical example section). It must be noted that the coupling time steps can be larger (constant time step size) if the mechanical problem is linear elastic, and the final mechanical solution of the problem is a function of final pore pressure field only. The coupling time steps can also be adaptive for compressible cases where the time step sizes are determined by convective time steps.

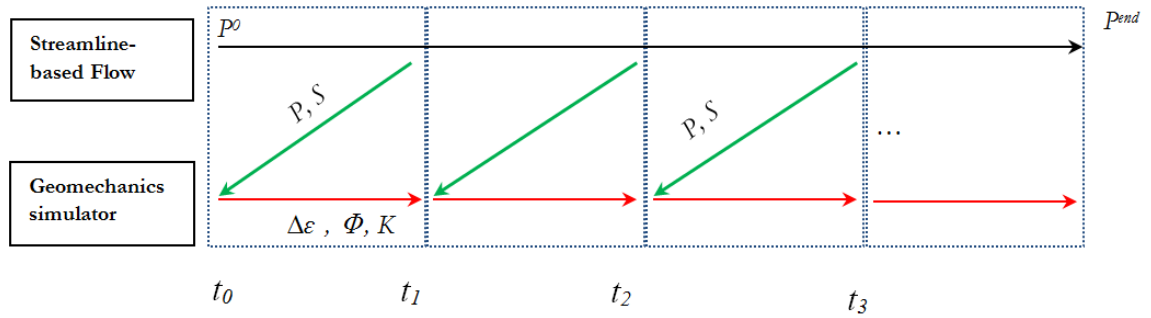


Figure 8-1-Schematic of coupling strategy for one-way streamline-based hydromechanical coupling with constant user-forced time steps. (P = pressure, S = saturation, t = time,  $\Delta\epsilon$  = volume change).

As opposed to conventional finite difference reservoir flow-geomechanics sequential coupling (either one way or two way sequential coupling), where both flow simulation variables (pressure and saturation) have to be solved simultaneously and then be transferred to the mechanical run cycle\*, streamline-based reservoir geomechanics coupling mechanism functions differently in terms of time and in domain size (grid-cells). In one way sequential coupling, on flow simulation side, pressure is solved explicit from saturation equation, on the reservoir 3D grids. Then, saturation is solved explicitly along the streamlines and thus allows for larger coupling time steps compared to FD simulators for both compressible and incompressible problems (as CFL condition is based on larger TOF grids).

## Approach 2: Sequential Coupling (IMPESG)

At first glance the technique may appear to be identical as the conventional sequential one-way coupling techniques; however it is not. As opposed to the conventional reservoir flow-geomechanics sequential coupling where all dynamic solution variables (pressure, saturation, etc.) are solved at one time level and then are transferred to the geomechanics problem on a certain interval, IMPESG coupling is performed only on 3D global pressure updates that are different and larger than saturation 1D time steps. The other difference between our coupling scheme and conventional schemes is that in FD or FV coupled systems, geomechanics is coupled to flow problem (pressure) in a certain time interval (which might be ten or hundred times larger than numerical pressure updates in fully implicit or IMPES

\* The time span for coupling of the two physics is called a (coupling) cycle. Cycles are shown by blue dashed squares in the figures.

scheme) but in the presented streamline-based coupling strategy, coupling time steps are exactly the same as frequency of pressure field solutions when streamline patterns are recalculated. The only input variable that mechanical problem requires for stress field solution is “pressure” to update effective stresses in the reservoir. Since global pressure time steps are different than saturation convective time steps (frequency of pressure field updates is not bound to frequency of saturation updates and grid block sizes) the coupling time steps between fluid flow and mechanical problem can be much larger than FD or FV simulators. The more incompressible and linear the displacement problem is and the higher the level of geological heterogeneity of the reservoir is, the larger the coupling time step can be which obtaining an identical result to the conventional coupling techniques. **Figure 8-2** illustrates an overview of this coupling strategy.

Figure 8-2 shows that on path **1** pressure is solved on global time step in a fully implicit approach on 3D grids, and updated from  $P^{(n)}$  (pressure at time level  $n$ ) to  $P^{(n+1)}$ , then in the next step saturation is moving forward along streamlines with smaller time steps than pressure updated time step on 1D grids, and pressure is fed into geomechanics on path **2**. Due to induced volumetric strain induced on path **3**, porosity and permeability are updated and are input in the next step to the next coupled streamline-geomechanics cycle. On path **4** a correction step for material balance errors might be needed (depending on the time step size and nature of mechanical problem) that will be discussed in detail in the next sections.

To have an understanding of how streamline simulation can be used in lieu of conventional flow simulation techniques, (e.g. finite volume or finite difference) one needs to compare the coupling strength, speed and efficiency of classical coupling techniques with the new methodology. To do so we implemented a sequential coupling scheme between finite volume geomechanics code and finite-volume fluid flow code (Box method) and compared the results with the coupled streamline-based flow with the same geomechanical code, on the same coupling- cycle interval, and showed that the novel technique is computationally faster and more memory efficient than Box method coupled system. The comparative study was implemented on an incompressible underground CO<sub>2</sub> storage scenario (Koohmarch et al., 2013).

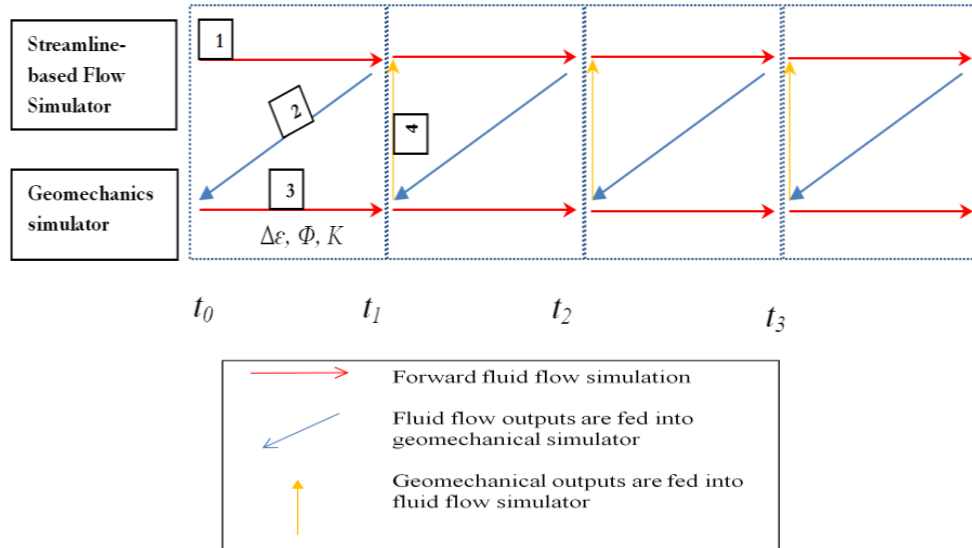


Figure 8-2-Schematic of coupling strategy for sequential streamline-based hydromechanical coupling with constant user constrained time steps ( $\square$  signifies paths followed during the time stepping).

### Approach 3: Staggered Coupling

This technique signifies the importance of material balance and convergence. Since streamline simulation is an IMPES based approach, the saturations are solved explicitly after the pressure field is calculated. As discussed for isothermal elastic problems, the only input that geomechanics get from fluid flow simulator in all coupling strategies is “pressure” and not saturation. However for physically reasonable and robust flow simulation (e.g. high resolution production profiles) and to ensure the convergence in solution, the saturation profile needs to be obtained based on the physically corrected and simultaneously updated petrophysical properties mapped along streamlines. Therefore this technique attempts to ignore the saturations (of all grid-cells) at the first step (path  $\square 1$  in **Figure 8-3**), and then transfer the calculated pressure field to geomechanical simulator and then the updated porosity and permeability (after geomechanical simulation was done on path  $\square 3$ ) are fed back into beginning of time step for streamline simulation (on path  $\square 4$ ), and then mapped along streamlines, and this time both pressure and saturations are solved at the same step but yet at different time steps. The reason porosity and permeability are given back to the beginning of time step to resolve the flow problem is not only having a converged value of porosity and permeability through iterative approach but is also due to material balance error reduction, and accurate solution of pressure wave equation. In the solution of diffusivity



the schematic of the coupling strategy looks like classical two way sequential coupling, as shown in Figure 8-3, the solution strategy is quite different. Apart from skipping the saturation equation, the other speed up factor and advantage of this coupling technique over the conventional two-way coupling technique is that forward flow simulations are faster than conventional FD or FV flow simulations. For incompressible problems, the forward simulations are much faster in comparison to FD schemes on an equal coupling time step. For reservoirs with coarse meshes, the technique can be utilized without skipping the convective saturation solution in each inner-cycle, and the numerical results showed that the convergence in volumetric strain and pressure (porosity and permeability) in each cycle is usually achieved within the solution of two successive inner cycles.

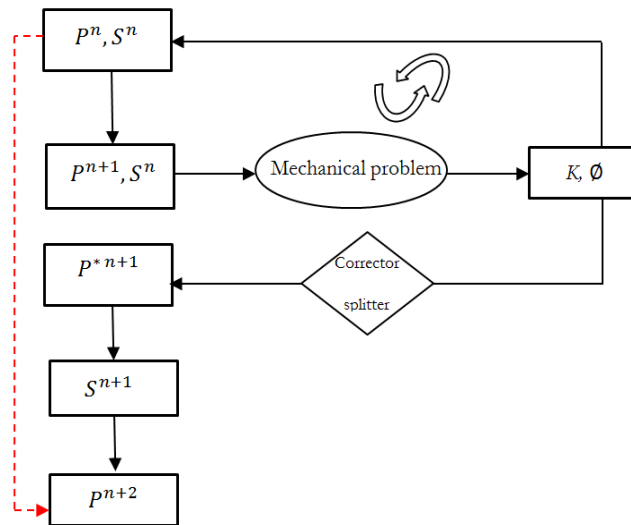


Figure 8-4- Numerical time steps evolution for semi-fully coupling of streamline simulation-geomechanics.

As geomechanics is embedded within the flow chart of streamline simulation and saturations are solved after pressure recalculation in a different stage, we alternatively entitled the technique as semi-fully coupling of streamlines with geomechanics. However, as shown in Figure 8-4, the solution of the mechanical problem (three displacement vectors) can be performed on the same Jacobian assembly along with pressure equation (in a fully implicit fashion) for more robust results, and then trace streamlines based on the converged velocity field and solve the saturation equation with updated and physically more realistic time of flights. For this situation, however, three more primary solution variables are added into the mapping matrix (two horizontal and one vertical displacement vectors), which make the

computational load of solving the non-linear system quite expensive. When dynamic flow parameters are stress-sensitive (e.g. density, pressure, relative permeability), a rigorous convergence criterion is needed and the solution may not converge easily. It must be noted that streamline class of simulations are an IMPES scheme by nature and one variable (pressure) is solved decoupled from the other (saturation), and also the corrector steps on 3D grids are performed separately and explicitly from (and after) explicit solution of saturation. Inclusion of geomechanics into streamline simulation has to abide by streamline workflow, and has to be done either explicitly or semi-fully implicitly. As such there is not such a technique as fully coupled or monolithic streamline-based reservoir geomechanics.

By use of this technique the saturation results are expected to be more exact and the material balance errors are also expected to be mitigated. Development of a mapping technique and pressure corrector step can be quite helpful and in some cases essential in reduction of the material balance error involved with this approach. The technique was developed on the same QT C++ based platform and two numerical examples were solved by use of this technique.

#### **Approach 4: Full Flight Streamline-Geomechanics Coupling**

**Figure 8-5** shows Approach 4, a potential coupling strategy for streamline-based hydromechanical coupling. The scheme allows the flow simulator to run from the beginning of the simulation rather than the current interactive time step. Since geomechanical processes within the reservoir can increase petrophysical property heterogeneity (i.e., through induced volume changes from stress changes), streamlines are therefore expected to remain unchanged for a longer time-step, and therefore long time-steps are allowed for streamline simulator and streamline simulation (only) can be run from time zero to the current time-step to improve the value of the pressure update to be given to the geomechanical simulator in the subsequent step.

If dynamic properties of the reservoir model are not updated at the end of each cycle and the beginning of the next cycle, the flow simulator will generally encounter a material balance error, since a new porosity (pore volume) is provided in the middle of the simulation but the pressure field remains unchanged. Significant errors will be encountered for problems of increasing compressibility and problems involving larger time steps. Figure 8-5 schematically



illustrates the overall procedure of the technique. The reason that permeability and porosity are fed into the initial coupling cycle is to reduce the material balance error, so each time a cycle run is over, the next coupling cycles act as an independent forward simulation from previous cycles with new initial conditions and boundary conditions. However, to account for dynamic changes of porosity and permeability in the course of the hydromechanical simulation time steps, an averaged value of porosity and permeability over all coupling cycles must be calculated and fed into the flow simulator (on yellow off-diagonal line). Therefore porosity at the end of explicit mechanical run of cycle  $n$  is:

$$\phi_n^* = \frac{\sum(\phi_0 + \phi_1 + \phi_2 + \dots + \phi_n)}{n+1} \quad (8-2)$$

$$K_n^* = \frac{\sum(k_0 + k_1 + k_2 + \dots + k_n)}{n+1}, \quad (8-3)$$

where  $\phi_n^*$  and  $K_n^*$  are porosity and permeability values that are fed into the flow simulator at the end of each cycle (yellow line), and  $n$  shows the number of the last cycle where streamlines and geomechanics have been coupled.

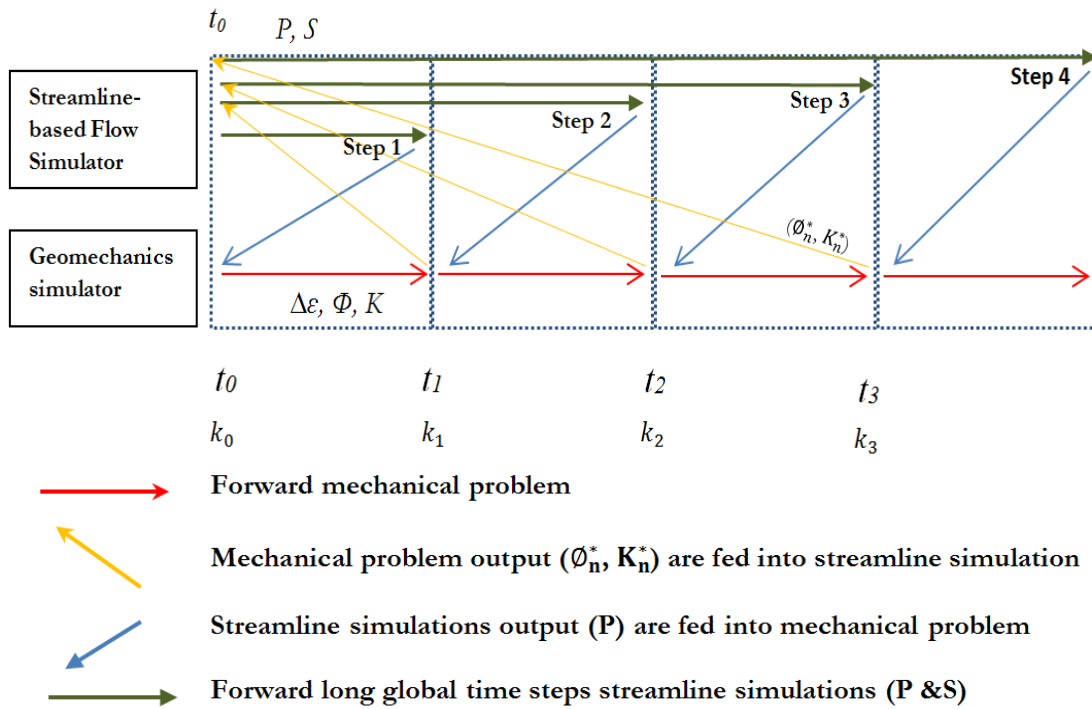


Figure 8-5-Schematic of full flight coupling scheme for sequential streamline-based

hydromechanical coupling; at the end of each cycle fluid flow start time is from day 0.

Since after each cycle-end, a long forward streamline simulation is performed with a long jump on geomechanics from cycle  $^{0\text{th}}$  to cycle  $^{(n)}$ , we called this strategy “full flight coupling”. This coupling strategy has been also implemented on a QT platform with C++ programming language, and has been tested on two numerical cases and compared with the other approaches discussed above.

### Approach 5: Adaptive Global Timestep Coupling

All coupling techniques described above are based on a constant forced time step set by the user. However coupling can be performed on the longer and adaptive time steps. In incompressible problems coupling can be performed on very large time steps, and if the stability condition developed in next section is honored, the velocity field remain unchanged and therefore the long step can remain constant as well. But if the condition (on the velocity vectors between two successive time steps) is not satisfied, we reduce the time steps to three fourth or half of the original time steps, and continue the simulation with new suggested stability-based time steps.

For compressible displacement problems however the time steps are auto time-steps for both pressure and saturation evolutions, and are dictated either by saturation equation based on the CFL condition on the TOF grids or by compressibility of the system (fluid volume changes at previous time level), and the pressure and saturation on previous streamline-based time steps.

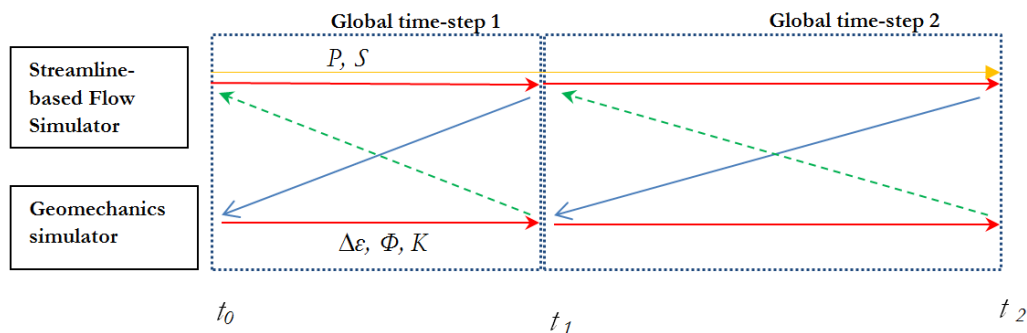


Figure 8-6-Schematic of adaptive long time step coupling scheme for streamline-based geomechanical coupling- example on staggered technique.

The coupling time step should not necessarily obey the pressure update time steps. The pressure time steps could be on the automated time step (for compressible cases), but the user can fix the coupling time step. Results of Approach 5 were not included in the simulation results and comparative studies on the run time with the other approaches.

## Results and Discussion

Numerical simulations of coupling approaches 1, 2, 3 and 4 were performed on two test cases:

**Case 1:** A multi-well compressible back oil model with four injection wells and five production wells. The in situ fluid phases are compressible oil and gas and slightly compressible water. The model is a black-oil (live-oil) compressible model, and the driving mechanism of production is by waterflooding. The model dimensions are  $5\text{ km}$  in lateral directions and  $120\text{ m}$  in vertical direction with  $10000$  active grid cells. The number of cells in Cartesian coordinates are  $N_x=100$ ,  $N_y=100$ ,  $N_z=1$ . The initial geological model of the reservoir (before inclusion of geomechanics) is highly heterogeneous. Average permeability of the reservoir is  $91.8\text{ mD}$  (minimum =  $0.3720$ , maximum =  $2808$ , variance =  $35400$ ) and porosity was considered constant and equal to  $0.2$ . The injection wells 1, 2, 3, 4 are operating at water injection rates of  $1600$ ,  $1000$ ,  $3000$ , and  $1600\text{ stb/day}$  respectively. The control rates for production wells 1, 2, 3, 4, and 5 are SGRAT (surface gas production rate) =  $3000\text{ Mscf/day}$ , SORAT (surface oil production rate) =  $1200\text{ stb/day}$ , SGRAT =  $900\text{ Mscf/day}$ , SORAT =  $800\text{ stb/day}$  and SGRAT =  $500\text{ Mscf/day}$  respectively. **Table 8-1** below summarizes the input data for the model:

**Table 8-1- Reservoir fluid and rock properties of Case 1**

Parameter	value
<b>Geomechanical properties</b>	
$\vartheta$	0.2
$E$ , MPa	500
<b>Overburden</b> ( $\sigma_v'$ ), MPa	-4.5
$\rho_s$ , kg/m <sup>3</sup>	2500
<b>Hydraulic properties</b>	
$\phi_0$	0.2
$k$ (average), mD	91.8

$P_o$ initial (bottom of the reservoir), MPa	5.2
$\rho_{o,g,w}$ (kg/m <sup>3</sup> ) standard	721, 1.12, 1010
$\mu_{oil}$ cP	0.89-1.2
$\mu_{gas}$ cP	0.0125-0.0195
$\mu_{water}$ cP at P=24.8 MPa	0.2998
$P_{injection}$ , MPa	27.6
$c_w$ water, kPa <sup>-1</sup> at P=24.8 MPa	1.45e-7
$c_o$ oil, kPa <sup>-1</sup>	1.00e-5
$R_s$ (Mscf/stb)	0.006-1.81
$B_g$ (Rbbl/Mscf)	0.41-2.95
$B_o$ (Rbbl/stb)	1.012-1.155

**Case 2:** CO<sub>2</sub> injection into a saline aquifer that is originally saturated with brine with one single well located in the middle of the reservoir, with constant head boundary conditions. The model is three-dimensional and the problem is incompressible. The model dimensions are  $2\text{ km}$  in each lateral direction and  $200\text{ m}$  in vertical direction. The initial geology of the model (before inclusion of geomechanics) is assumed homogenous in order to observe the impact of inclusion of geomechanics on static model distribution. **Table 8-2** summarizes the input data for case 2:

**Table 8-2- Reservoir fluid and rock properties of Case 2**

Parameter	value
<b>Geomechanical properties</b>	
$\theta$	0.25
$E$ , MPa	1000
<b>Overburden</b> ( $\sigma_v'$ ) MPa	-7.74
$\rho_s$ , kg/m <sup>3</sup>	2188.5
<b>Hydraulic properties</b>	
$\phi_0$	0.2
$k$ , mD	100
$P_o$ initial (bottom of the model), MPa	8.5
$\rho_{gas}$ (kg/m <sup>3</sup> ) standard	850
$\rho_{water}$ (kg/m <sup>3</sup> ) standard	1100
$\mu_{gas}$ cP	0.06
$\mu_{water}$	1

### Case 1– Simulation Results

Inclusion of geomechanics into streamline simulation workflow on model case 1 leads to significant changes in petrophysical distribution and dynamic responses of the reservoir. As discussed below, these results help to demonstrate the significance of “full-field “ inclusion of geomechanics where the mutual impacts of source-sink regions are taken into account for prediction of hydromechanical responses of reservoir in a conventional water flood scenario.

**Figure 8-7** illustrates how streamlines (dominant flow directionality) as well as time of flights along streamline will change in a streamline-based geomechanics coupled system within 700 days of production (with coupling time step of 100 days). Since the well or boundary conditions did not change throughout the simulation the changes in streamlines pattern (pressure gradient field) is primarily due to the impact of geomechanical processes.

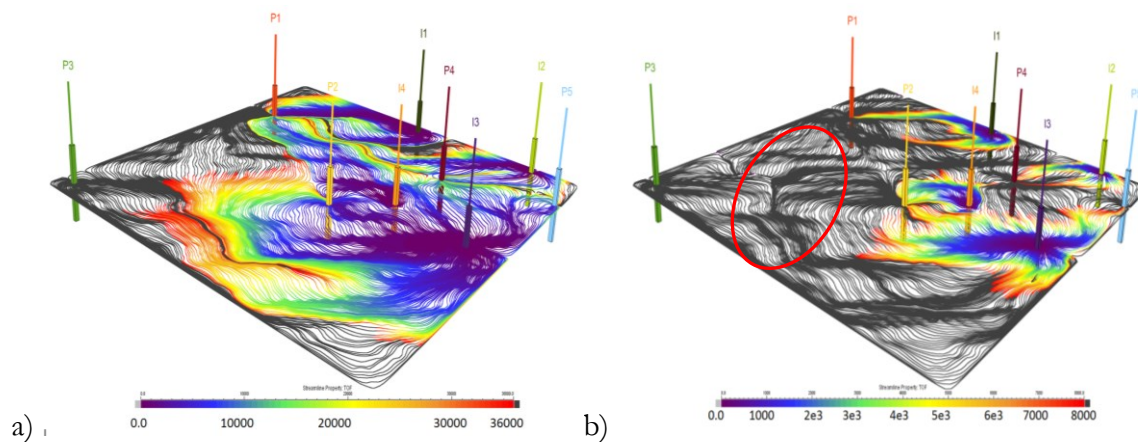


Figure 8-7- Comparison of streamline configurations along with mapped time of flights on streamlines at two different cycles: a) cycle 2 and b) cycle 9. While the well conditions have remained intact geomechanics have changed the streamline configurations within 700 days of production (see red ellipse in 7b). Production and injection wells are shown with “P” and “I” respectively.

**Figure 8-8** and **Figure 8-9** illustrate the difference between a coupled and uncoupled system in terms of streamline configurations, TOF distribution, well allocation factors and field production data. FPMs show the percentage of the flow at reservoir conditions along a connection. They determine how much of an individual well’s production is due to various

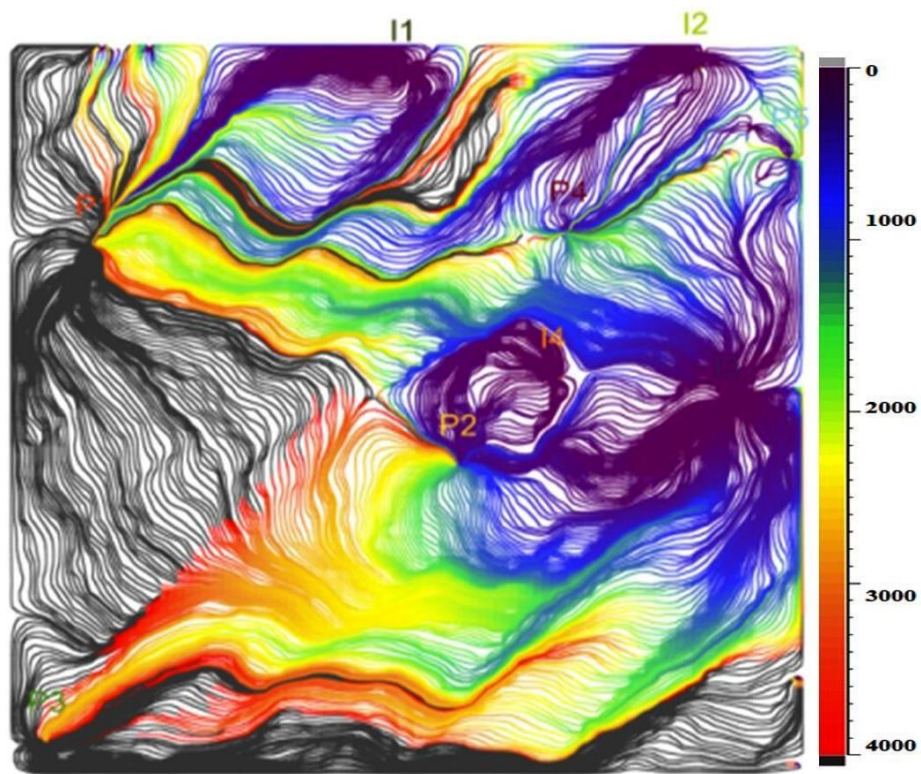
injectors and conversely, how much support an individual injector is giving to various producers.

As illustrated in Figure 8-9 consideration of geomechanical effects into the workflow on a multi-wells full-field case study can be quite important in terms of ultimate reservoir production data. In all cases the cumulative productions out of coupled streamline-geomechanics model have been less than SL-standalone case. The reason is mainly because in the course of production the overall reservoir pressure has dropped down and accordingly the effective stress in the reservoir (particularly in high permeability regions) has increased, which leads to decrease in porosity and permeability values (contraction).

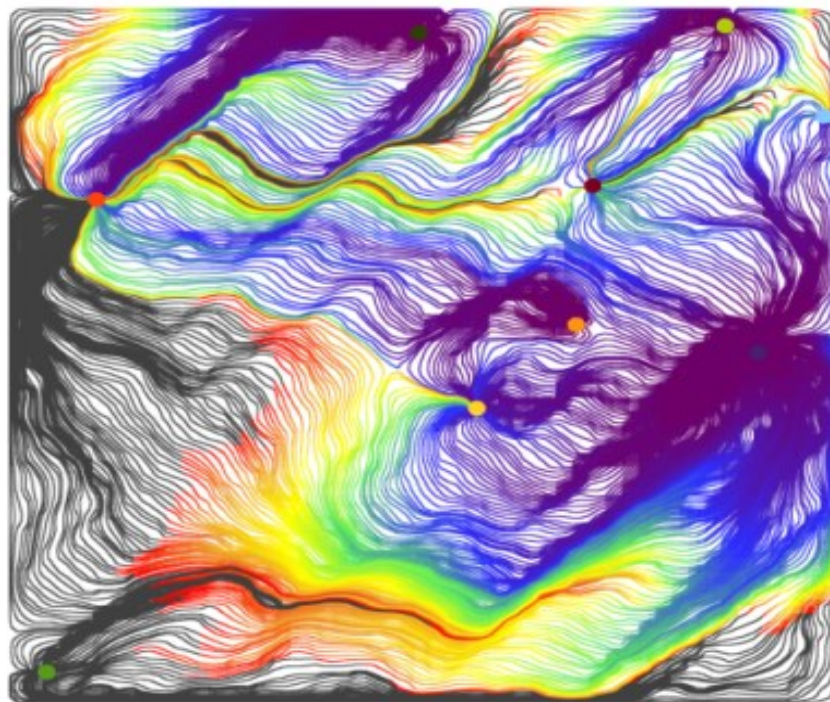
**Figure 8-10** shows the petrophysical changes (permeability difference map after 1600 days of production) in the reservoir due to inclusion of geomechanics physics into streamline simulation workflow. Permeability changes have been mainly the same all over the reservoir except in the zones with initially high permeability values and higher flow activities, where the change in permeability has reached to *1000 mD*.

On a single cycle coupling time step (100 days) Approach 3 and Approach 2 showed slightly different responses in terms of production data. **Figure 8-11** shows the oil production rate at cycle 5, and compares the results of Approach 2 with Approach 3, at five inner cycles. Approach 2 shows slightly lower oil production (yellow line) between day 400 and day 500 after production, than the inner cycle 1 (green line). Inner cycle 1 also reports a different production rate than the other inner cycle, but after inner cycle 2 the coupled problem converges to a unique solution (inner cycles 3, 4, 5). This emphasizes the use of staggered technique for physically more robust solution of very stress sensitive problems, and also shows that only two inner cycles in each global cycle are required for the problem to converge.





(a) Coupled



(b) Uncoupled

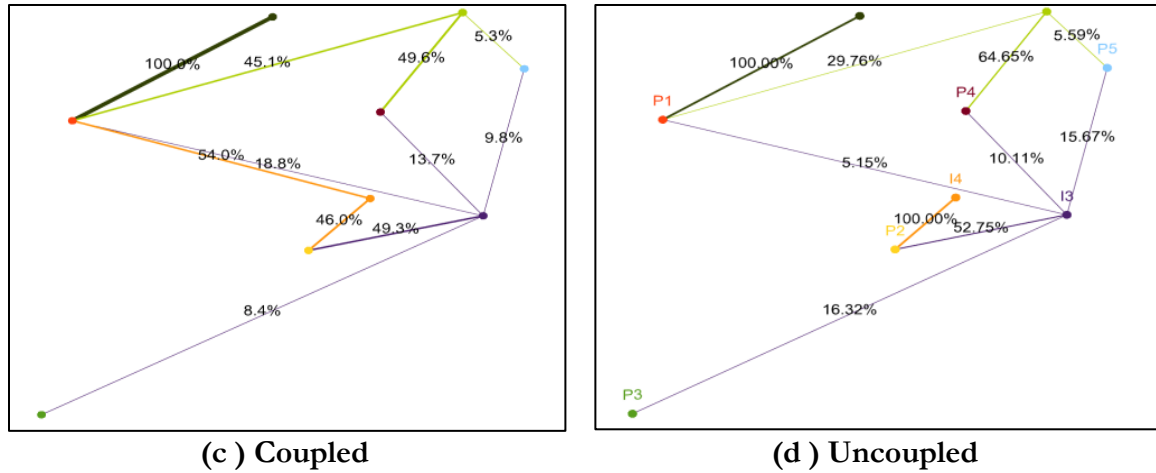


Figure 8-8- Comparison of streamline configurations: a) coupled and b) uncoupled (colors represent TOF – blue is low from 0 days and red is high TOF values up to 4000 days) and well allocation factor maps: c) coupled and d) uncoupled after 4000 days.

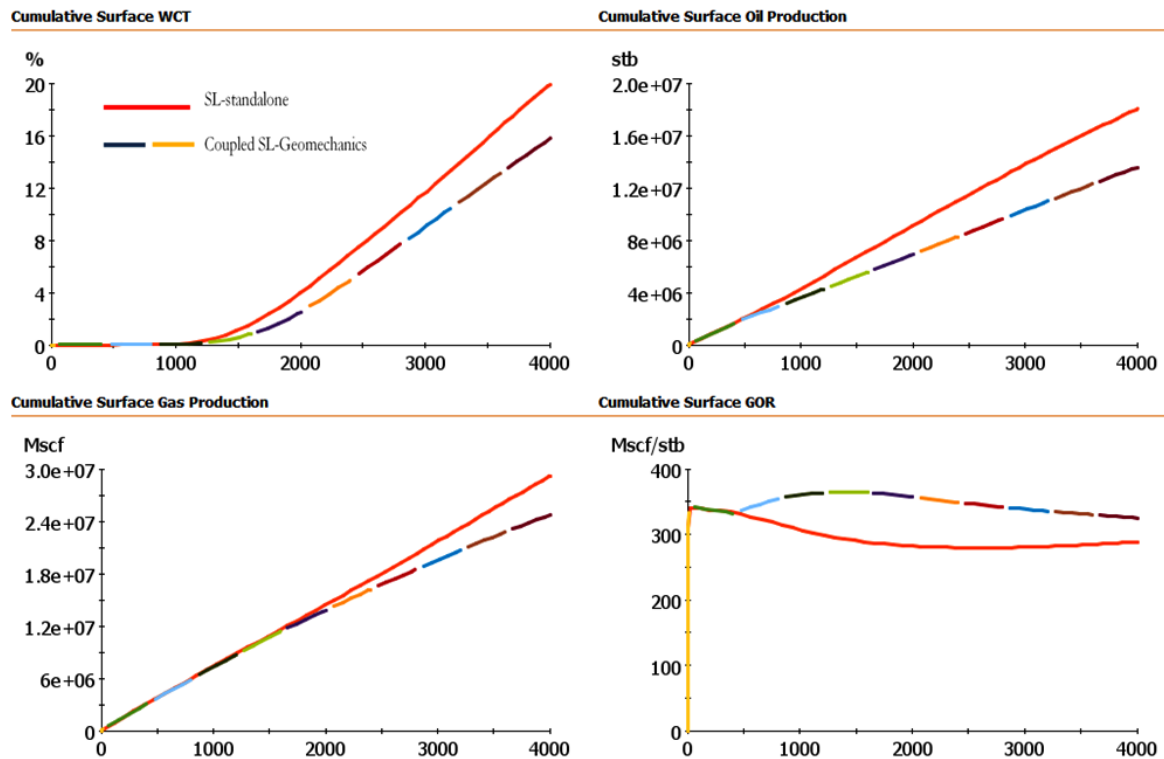


Figure 8-9- Impact of inclusion of geomechanics (through Approach 2) into streamline simulation on cumulative production data within 4000 days of production (x axis represents time in days).



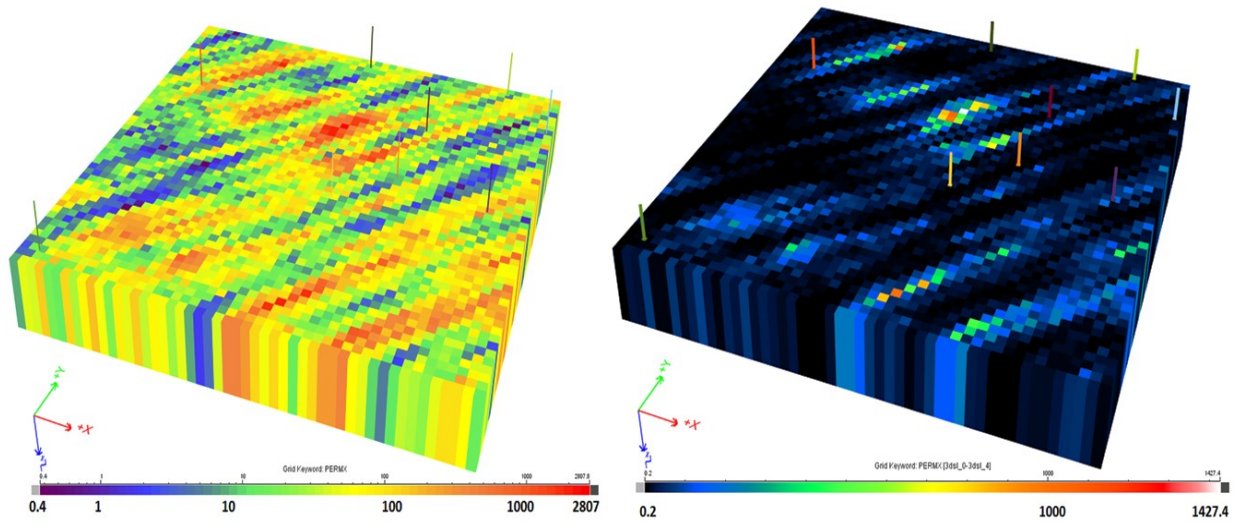


Figure 8-10- Initial permeability distribution of the reservoir and well configuration (left), and updated permeability difference map ( $K[\text{cycle}_0] - K[\text{cycle}_9]$ ) due to reservoir geomechanical effects (right).

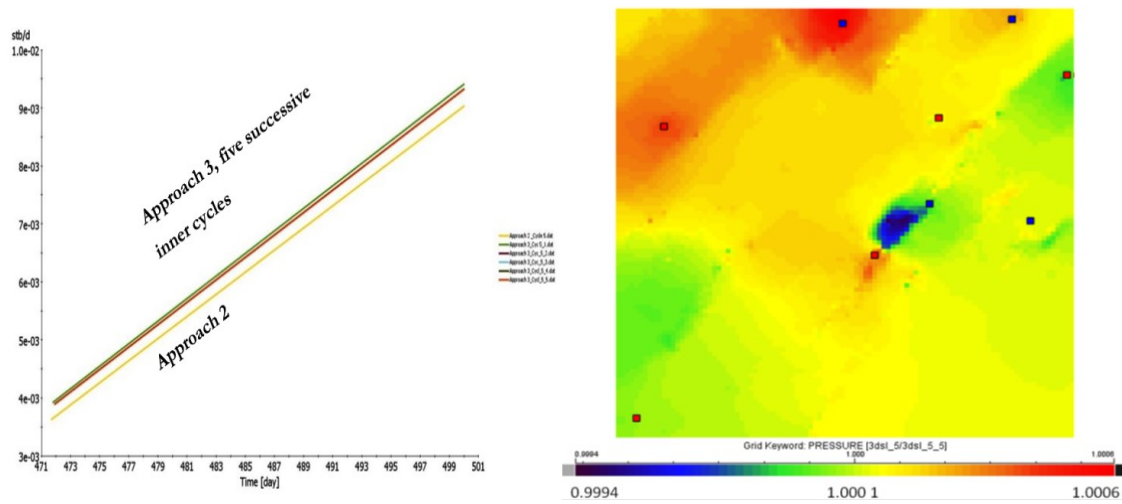


Figure 8-11-Left picture compares field oil rate by use of Approach 2 versus Approach 3 and right picture shows the top view of pressure field ratio of Approach 2 over Approach 3, at cycle 5 (400-500 days).

On the large scale and long injection production time, however there was not a noticeable difference between Approach 2 and Approach 3 in terms of production data. The problem of convergence was experienced for smaller coupling time steps in Approach 3 (staggered) than in Approach 2.

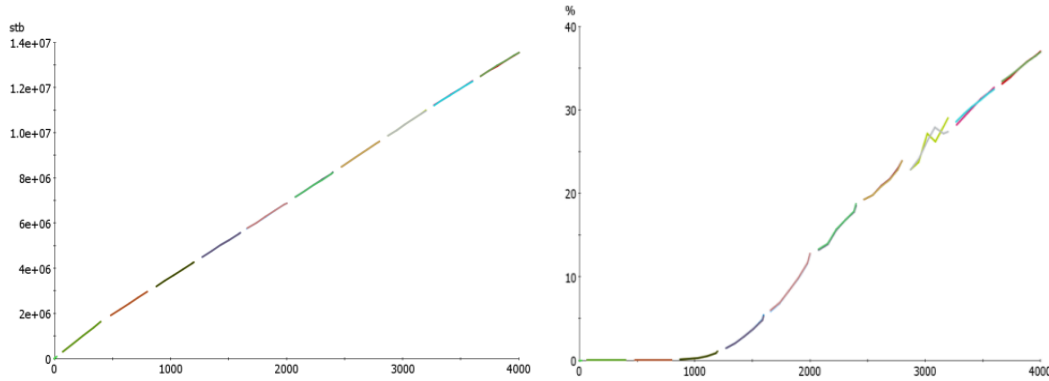


Figure 8-12-Comparison of production data in coupled system from Approach 2 vs. Approach 3. Left figure shows cumulative field oil production and right figure shows field water cut rate.

It must also be noted that even though Approach 3 can allow the user to undertake longer coupling time step (expecting faster coupled simulation run time) compared to Approach 2, the comparison on the total CPU run time over 1000 days of production shows that Approach 2 (2832 milliseconds) is ultimately faster than Approach 3 (3202 milliseconds). Therefore depending on the problem size and problem compressibility one has to perform a comparison between Approach 2 and 3 on the run time and convergence before undertaking the simulation on the longer simulation time steps on the models with larger number of cells.

**Figure 8-13** shows that there was no significant difference between Approach 3 (staggered system) and semi-fully coupling approach in terms of dynamic responses of reservoir after 1000 days. Simulation results also showed that geomechanically updated porosity and permeability fields were almost identical by use of either of approaches.

**Figure 8-14** illustrates that the cumulative responses of the reservoir are very similar as well. Cumulative oil production rates were almost identical and Gas-Oil-Ratio cumulative curves are slightly different. The comparisons are performed on a 100 days coupling time step with 3 numbers of inner cycles/iteration in each cycle.

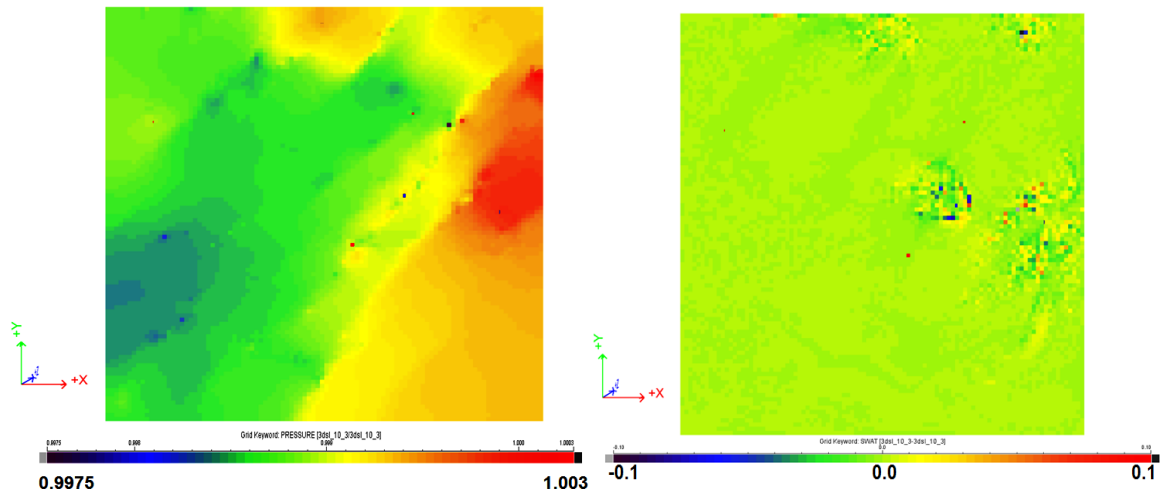


Figure 8-13- Left figure shows pressure ratio and right figure shows saturation field ratio of Semi-fully coupled approach over Staggered approach (3).

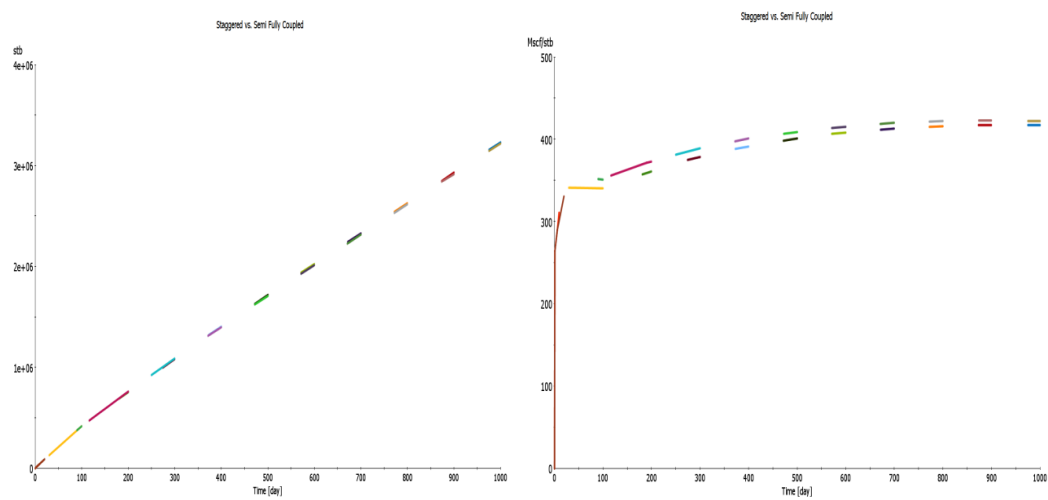


Figure 8-14- Comparison of production data between Staggered Approach (3) vs. semi-fully coupled Approach. Left picture shows cumulative surface oil production and right picture shows cumulative surface gas-oil-ratio.

As such semi-fully coupling approach can be used in lieu of staggered coupling approach for large systems, and ultimately with higher CPU efficiency, identical reservoir dynamic responses are expected. **Figure 8-15** shows that use of semi-fully coupled system on the same model, reduces the total CPU run time by 65 %. It must be noted as the geomechanical run time remains almost the same in both approaches, the more the number of inner cycles are (i.e. 5 than 3) the less the CPU efficiency gain is expected by use of semi-fully coupling system. Therefore, the number of inner cycles is suggested not to exceed two or three.

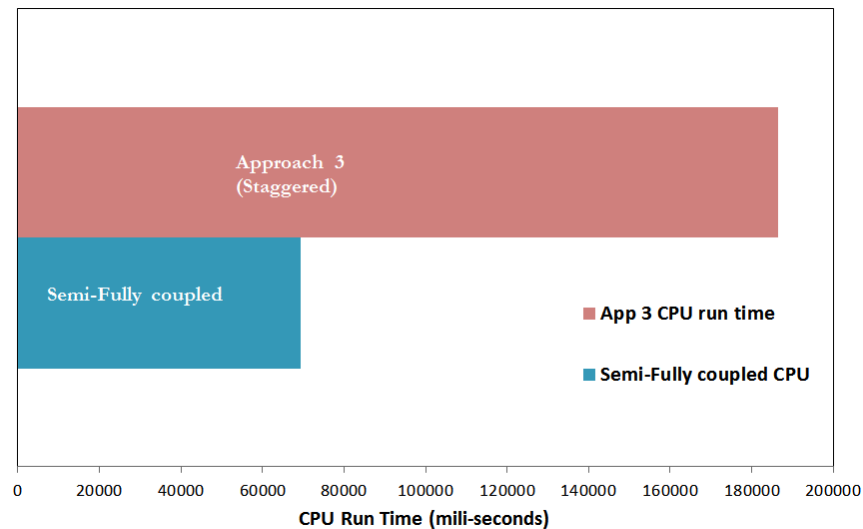


Figure 8-15- Comparison of total CPU run time of Staggered Approach (3) vs semi-fully coupled approach in model 1 within 1000 days of coupled simulation run with 10 cycles and 3 inner-cycles.

**Figure 8-16** illustrates how the convergence (on field oil production rate and water cut rate) occurs through full flight cycles of Approach 4. As it can be seen each cycle is longer in time-length compared to the previous cycle and reports slightly different production rate due to geomechanical updates.

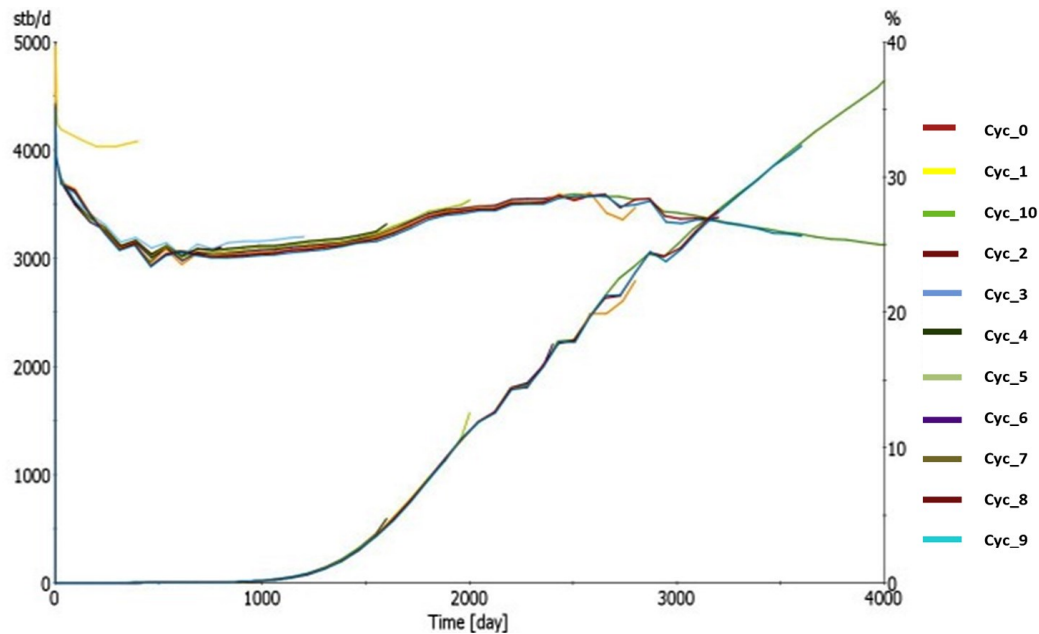


Figure 8-16- Convergence of field oil production and water cut rates by use of Approach 4 at 10 full flight cycles over 4000 days of coupled simulation. Each single cycle is illustrated by different color.

### Case 2 – Simulation Results

Case 2 is a problem of  $\text{CO}_2$  injection into a saline reservoir under the assumption of an incompressible fluid. The numerical simulations were performed for an injection time of 2000 days. All different coupling strategies were tested on the case 2. **Figure 8-17** illustrates the geomechanical responses of reservoir using Approach 1 (one way coupling). As shown in Figure 8-17, through constant injection of  $\text{CO}_2$  in underground reservoir with stress sensitive rocks pore pressure builds up (mainly around injection well in early time and propagates to far field in the course of injection) and therefore effective stress reduces and displacements increase in all three directions. As a result total stresses increases in horizontal directions, however the stress change and distribution in each direction is different (Poisson ratio's effect), leading to development of deviatoric stress components that are potential for inducement of shear failure at high injection rates. The negative sign for stress values means that the stress regime in the reservoir (and around injection point) is compressive. The stress and displacements on the 3D model show only the reservoir portion of our geomechanical model. The model boundary conditions were roller boundaries at the side burdens and constant vertical stress at the top of the reservoir (over burden) and zero displacements at

the bottom. The base case model number of cells is 20x20x10 in x, y, and z directions respectively.

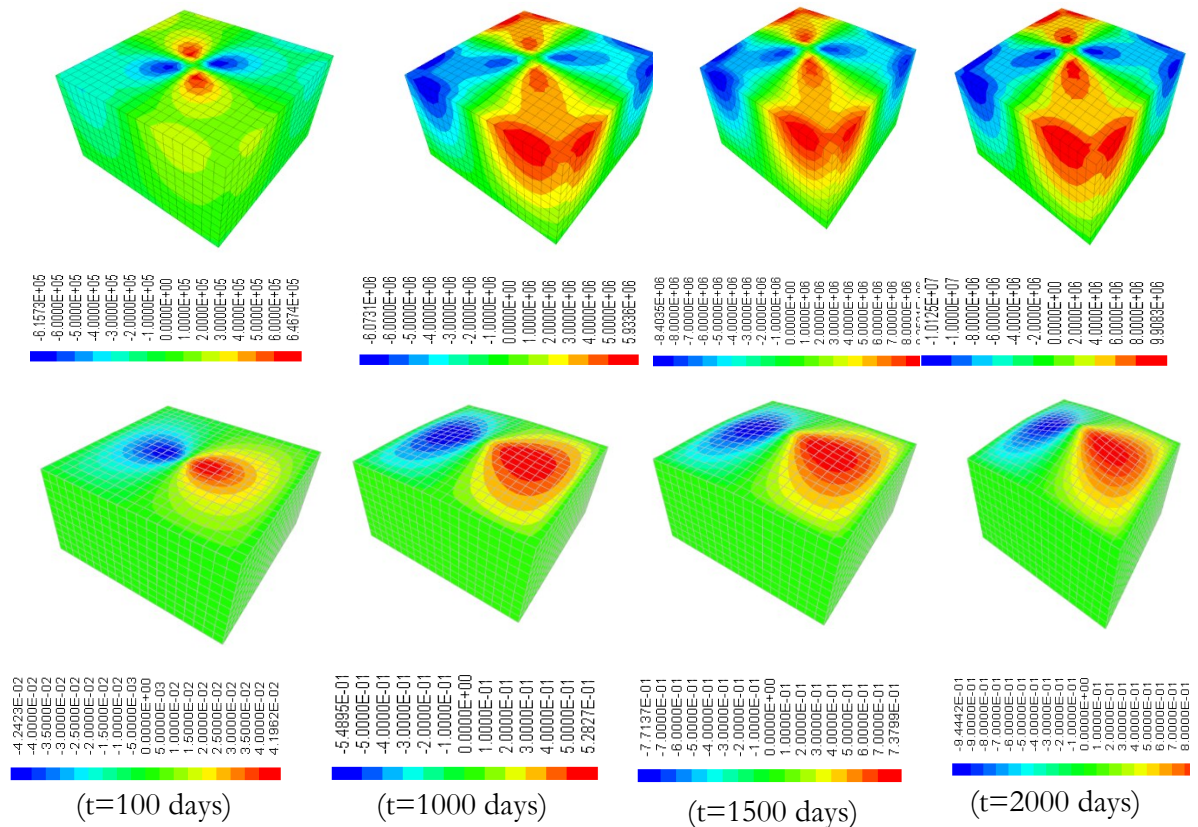


Figure 8-17- Illustration of off-diagonal stress tensor component  $\sigma_{xy}$  (top) and horizontal displacement along x axis (bottom) at four different time steps. Results are obtained through Approach 1 at SL-geomechanics coupling time step of 100 days.

These results show that for one-way simulation results, reservoir rock deformations are significant in response to pressure and therefore coupling strategies can play a role in the ultimate flow regime and mechanical responses of the reservoir.

The stress paths at top, middle and bottom of the reservoir were plotted for three different coupling strategies: Approach 2, Approach 3 and one way coupling, all at the coupling time steps of 100 days. The comparisons showed that the stress paths calculated at the end of day 2000 day (after injection) is very similar from Approach 2 and Approach 3, but Approach 4 shows slightly different stress path. Also the stress paths of Approach 3, and 4 were compared at two different coupling time steps (100 versus 200 days); the stress paths were almost identical through both approaches and on time step sizes. The vertical displacements in the middle of the reservoir from day 0 to the end of 2000<sup>th</sup> day were plotted, and the

maximum value reported in one way coupling system was *48 cm* (**Figure 8-18**) and *66 cm* through Approaches 2, 3, and 4. These findings signify the use of coupling in simulation workflow where reservoir rocks are stress sensitive and reservoir main drive mechanism is by convection.

**Figure 8-19** compares the dynamic responses of the reservoir where the coupling approaches 2 and 3 were used. The comparison shows that the average reservoir pressure and gas injection rate in the reservoir (with constant bottom hole pressure) calculated by Approach 2 do not differ significantly with Approach 3. Also for incompressible systems the increase of time step size from 100 days to 400 days do not affect the final simulation results. This was not the case however for the compressible problem described in case 1.

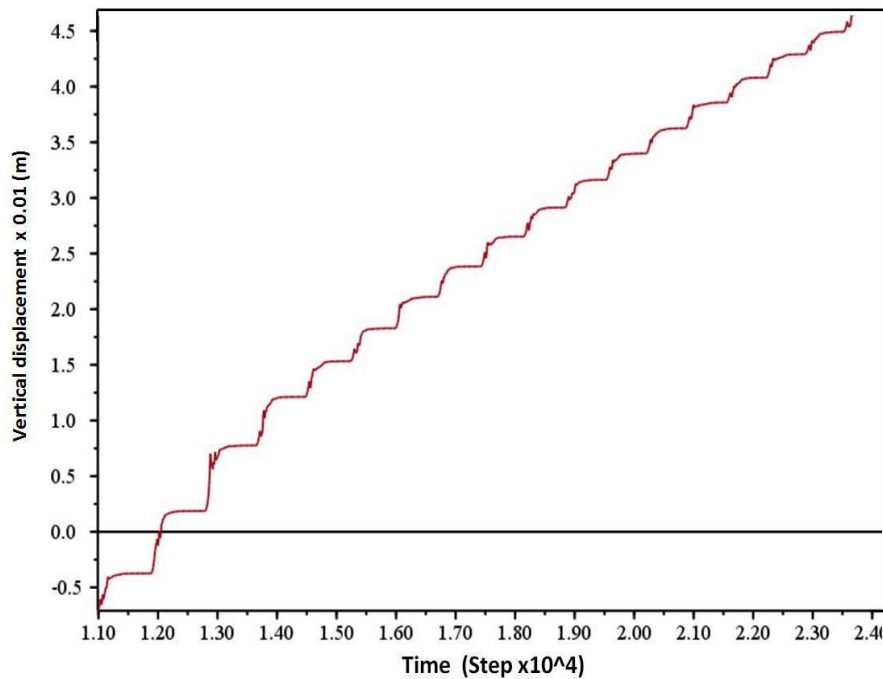


Figure 8-18-Vertical displacement history in the middle of the reservoir out of one way coupling. Vertical axis shows vertical displacement in meter and horizontal axis shows mechanical problem time steps (from day 0 to 2000).



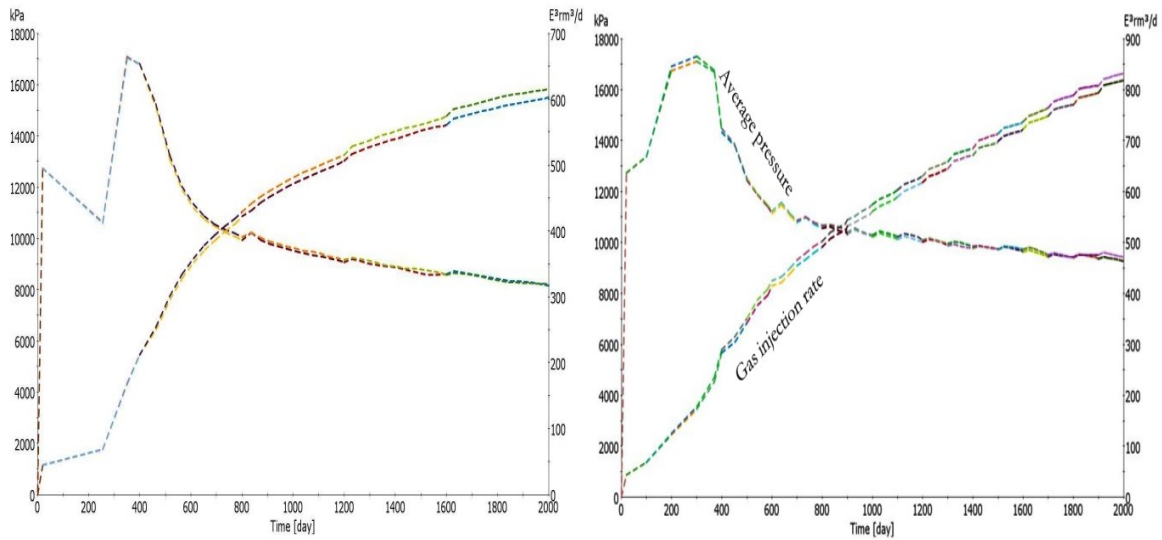


Figure 8-19- Comparison of two different Approaches (2 and 3) at a coupling time step of 400 days (left) and 100 days (right). Representation of average reservoir pressure and reservoir gas injection rate.

### Computational Efficiency

The CPU load analyses were performed on an Intel core™ i7 chip running at 2.7 GHZ, with 16 GB of RAM, and both mechanical and streamline calculations were performed on a single thread. **Figure 8-20** shows the CPU time (computational load) for each coupling strategy and shows how the CPU time will change in each individual cycle of each strategy in the course of coupling.



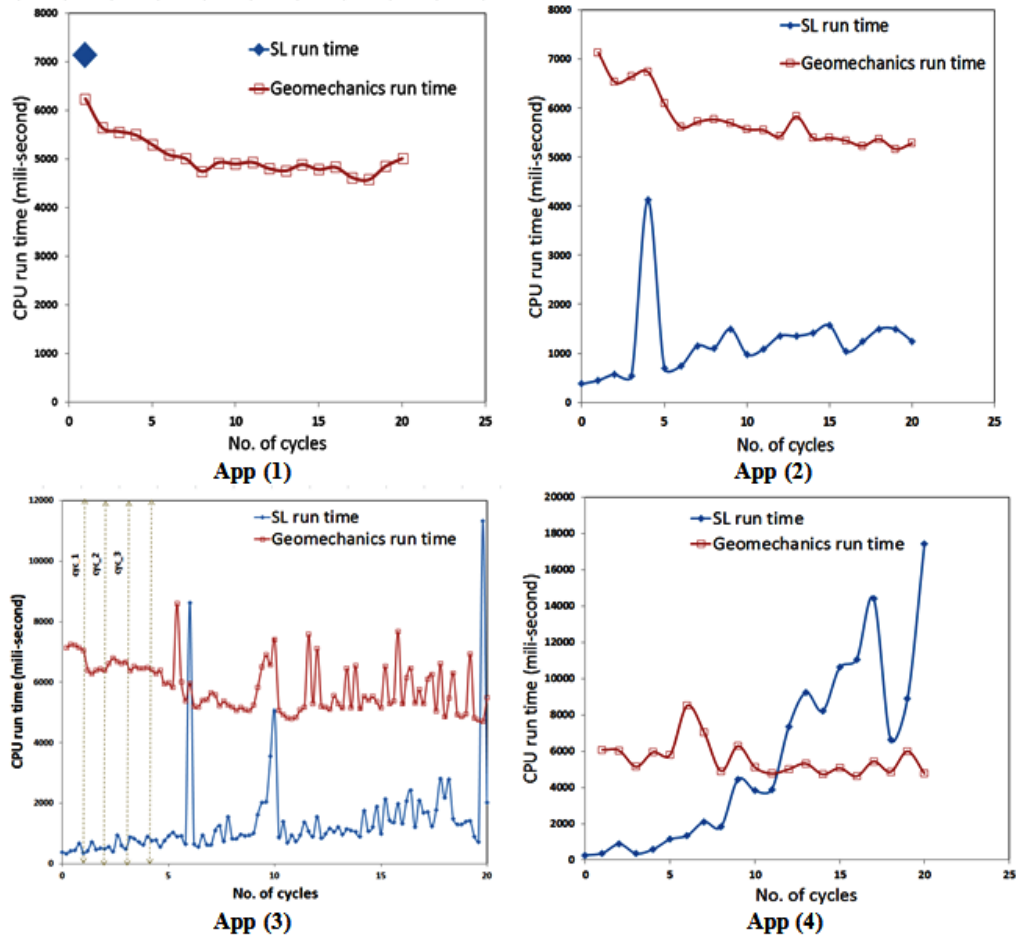


Figure 8-20- Individual cyclic CPU run time of streamline versus geomechanics for different coupling strategies.

And **Figure 8-21** shows the total CPU run time of four different coupling strategies on incompressible model with  $20 \times 20 \times 10$  number of grid cells.

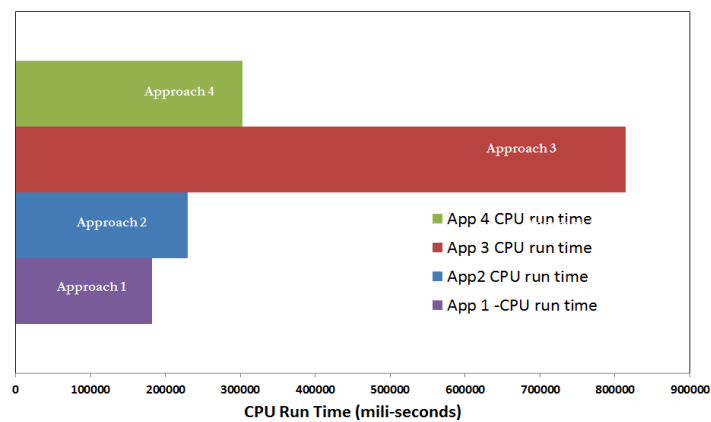


Figure 8-21- Comparison of computational load involved in each coupling strategy on the 3D model with 2000 active cells on 20 cycles with coupling time step of 100 days. Each cycle of Approach 3 includes 5 inner cycles.

As shown in Figure 8-21, Approach 3 (staggered approach) carries the largest computation load compared to the other approaches. However it must be noted that the computational load reduces significantly if number of inner cycles are reduced (from 5 in the present analysis to 2) and if staggered approach is carried on the semi-fully coupled system that was discussed (resolving only pressure field in each inner cycle).

**Figure 8-22** and **Figure 8-23** show the computational loads efficiency gained through use of semi-fully coupled approach over staggered technique. As shown in Figure 8-23 the total computational load for a model with 2000 gridblocks ( 5 inner cycles and 20 cycles) is almost 25% less than the staggered technique. However by reducing the number of inner cycles (i.e to 2) the CPU efficiency gain can increased significantly as successive geomechanical runs are avoided.

Figure 8-22 shows that streamline-based simulations (forward cycles and inner cycles) in the semi-fully coupled are significantly faster (involved with less CPU time) than Approach 3 (staggered system).

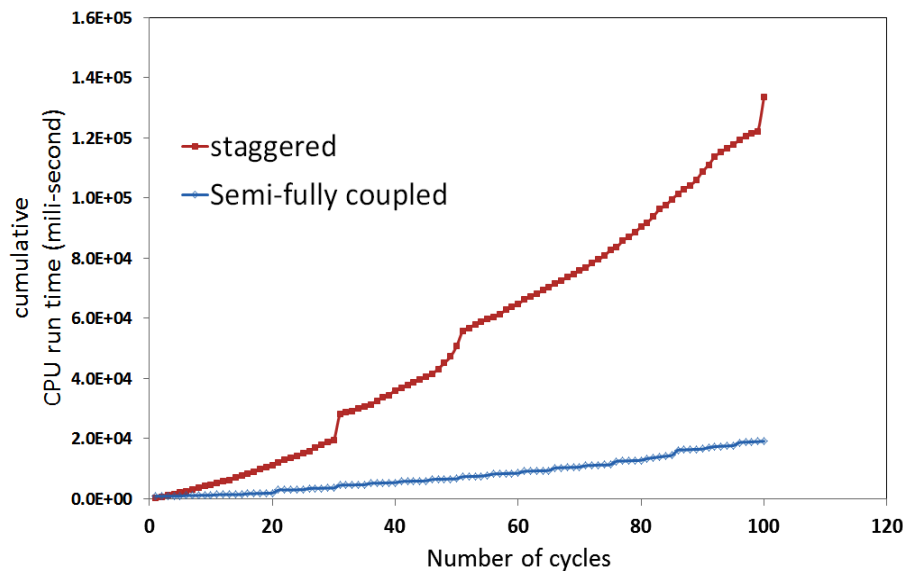


Figure 8-22-Comparison of streamline simulation CPU run-time in Approach 3 (staggered) vs. Semi-fully coupled approach, with 20 cycles and 5 inner cycles (model size 20x20x10).

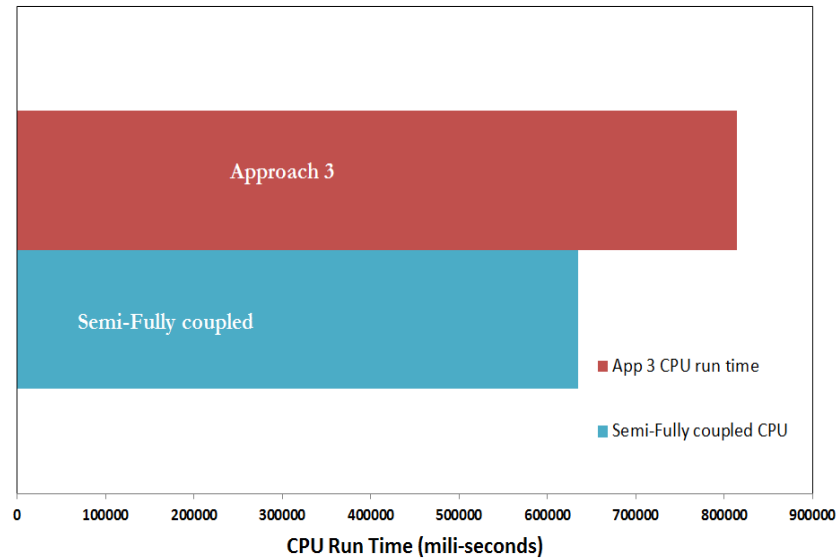


Figure 8-23-Comparison of computational load of Approach 3 (staggered) with Semi-fully coupled, on the 3D model with 2000 active cells on 20 cycles and 5 inner-cycles with coupling time step of 100 days.

**Figure 8-24** illustrates the scaling behavior of coupling Approach 2 at a coupling time step of 100 days. The findings of this figure are very important in terms of full-field inclusion of geomechanics. Streamline-based reservoir geomechanics simulation exhibits a near linear scaling in run times as a function of active cells. The linear scaling behavior means the computational load for larger number of grid cells (e.g. multimillion cells) can be extrapolated from CPU run time of the coarse model with small number of cells. The other important conclusion derived from the results shown in Figure 8-24 is that the computational load is much less than the computational load of FD simulators that increase in a polynomial behavior with increasing number of active cells like  $N^{2 \rightarrow 3}$  where  $N$  is the number of active grid blocks. Scaling behavior of uncoupled standalone finite difference flow simulations from SPE 71596 (Gorell, S. and Bassett, R., 2001) was shown to be quadratic as a function of active grid cells. By inclusion of mechanical problem and adding three more set of equations (three displacements vectors) into the problem, the scaling behavior of FD coupling technique will be even more crucial in term of CPU run time as a function of active cells. However, Figure 8-24 shows that by increasing the number of grid cells from 2000 cells (base case) to 256000 and 512000 grid cells, the CPU time increases proportional to the number of grid blocks by use of Approach 2.

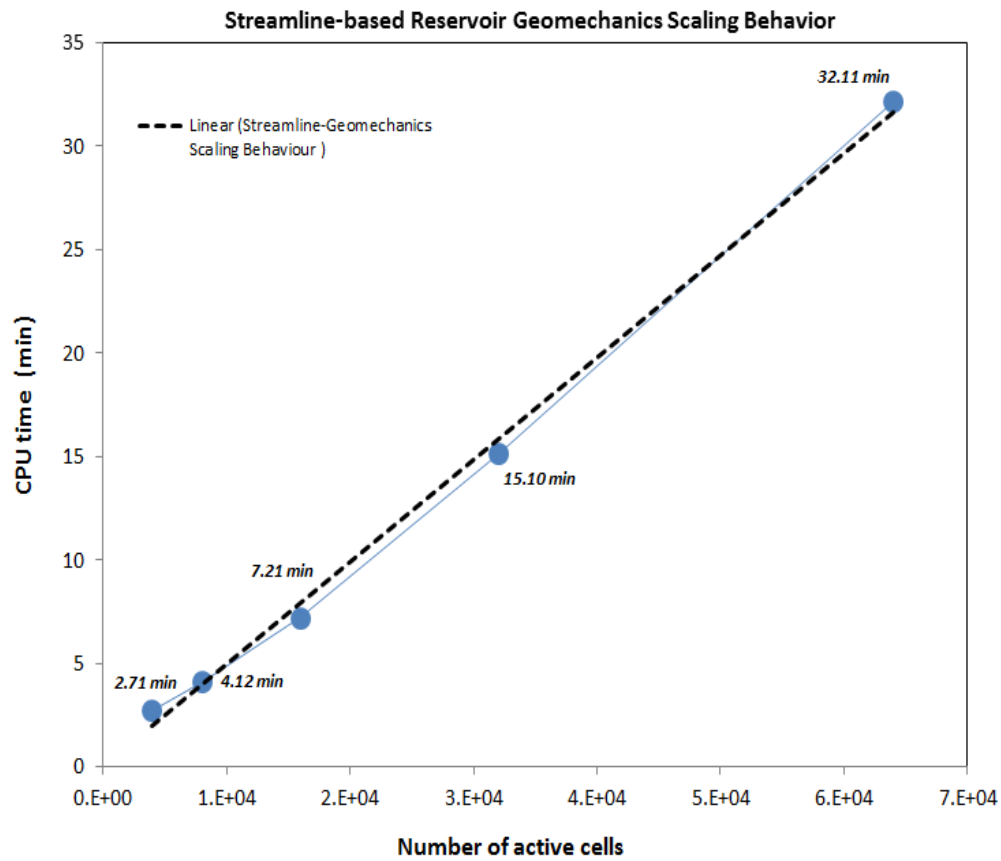


Figure 8-24-Example of linear scaling of coupled streamline-geomechanics run time (Approach 2,  $\Delta T=100$  days) versus number of active grid-blocks for an incompressible  $\text{CO}_2$  injection scenario.

## Conclusions

Inclusion of geomechanics in streamline simulation workflow was shown to be effective in performing large-scale hydromechanical simulation of reservoirs within long simulation time windows. Several different coupling strategies were proposed and designed and advantage of each coupling strategy, its potential added value versus conventional coupling schemes and its application in petroleum engineering were discussed. All the proposed coupling approaches were developed on a QT platform (C++ based programming language) to sequentially or semi-fully implicitly couple 3DSL (streamline simulation tool) to FLAC3D (geomechanical tool). The developed schemes were tested and performed on two numerical cases of compressible and incompressible scenarios.

The simulation results on a full-field case showed that inclusion of geomechanics into fluid flow physics processes changes the flow directionality (streamline configuration) and

consequently may lead to a significant change in final cumulative produced oil (six million barrels of oil within 4000 days of production in the presented simulation case).

In order to mitigate the material balance and enhancement of problem convergence, development of corrector steps within the streamline-geomechanics coupling framework for updating of pressure field at each coupling strategy is recommended.

Approach 3 (staggered semi-fully coupling scheme) exhibited the largest CPU run time compared to the other approaches, but resulted always in the converged solution. In both compressible and incompressible test cases, Approach 3 showed a converged solution after second inner cycle; therefore to avoid large CPU run time, increasing number of inner cycles (more than two or three) is not suggested. Approach 3 (with five inner cycles) and Approach 2 showed approximately close simulation results within 4000 days of coupled simulation, at a small coupling time step size of 100 days. All the coupling strategies showed almost the same reservoir stress path and displacement profile in time in the middle of the reservoir, but Approach 1 (one way coupling) exhibited slightly different stress path, but significant displacement profile. The latter conclusion signifies the use of coupled hydromechanical systems for prediction of dynamic and mechanical responses of the reservoir.

The scaling behavior of streamline-based reservoir geomechanics (strategy1) CPU run time as a function of active grid blocks is close to linear. Therefore streamline-based geomechanics coupling is the method of choice for prediction of hydromechanical responses of large heterogeneous reservoirs with large number of cells (more than 250,000).

## **Acknowledgement**

The authors would like to gratefully acknowledge Rod Batycky for his sustained support and helpful discussions and providing the academic license of StudioSL and 3DSL research code. This research was conducted with the acknowledged financial support of the Helmholtz Alberta Initiative and support from the Foundation CMG Research Chair in Reservoir Geomechanics.

## Chapter 9: On Stability and Material Balance of Full-Field Streamline-Based Reservoir Geomechanics Couplings

### Introduction

For prediction of ultimate reservoir production and dynamic field responses, inclusion of geomechanics is an important step in the simulation framework, which has classically been missed in most simulation studies. For stress-sensitive reservoirs geomechanics plays even a greater role in changing the reservoir pressure field as well as dynamic update of reservoir petrophysical properties (porosity and permeability). Geometrical complexity or irregular distribution of mechanical properties of large reservoirs makes a call for numerical simulation of the reservoir. The numerical inclusion of geomechanics in dynamic modeling of reservoir is called coupling. The mathematical expression describing the mutual impacts of stress (geomechanical effects) and pore pressure (fluid flow effects) on each other and its implementation in numerical simulators core code is called “reservoir-geomechanics coupling”. It must be noted that geomechanics can be included into modeling workflow through “uncoupled” system as well, but where inclusion of geomechanics has a significant impact on fluid flow production rate, coupling is essential. However the detailed high precision simulation of these effects requires a huge CPU load, and is not possible by conventional coupling schemes. In the recent work a new coupling workflow was introduced as streamline-based reservoir geomechanics coupling which takes advantages of streamline time stepping (Koohmarch Hosseini and Chalaturnyk, 2014). In the previous work we introduced five different SL-based coupling strategies and discussed the limitations and powers of each approach. However the selection of the proper time step size as well as problem convergence was not studied previously. This work is the continuation of the previous work on SL-based reservoir-geomechanics class of coupling. In this work the emphasis is put on the fact that even though SL-based coupling gained lots of CPU efficiency compared to the previous techniques, the coupling time step cannot be infinitely long, and is limited to the physics of the problem.

To account for influence of geomechanics into reservoir simulations, rock compressibility (and accordingly total compressibility) of the system used to be adjusted in the transient form of pressure diffusivity equation. This approach was the most simplistic one to account for geomechanical changes, as it neglects the impact of fluid flow on geomechanics (in both explicit and fully implicit approaches). This technique, however, may involve convergence issues, particularly where the reservoir rock is significantly compressible. Settari and Mourits (1998) deployed a compressibility corrector for linear elastic mechanical problem to enhance the solution convergence. Mainguy and Longuemare (2002) used a pore volume (porosity) corrector (in between mechanical and flow problems communication) to improve the stability and convergence of the coupled system.

As opposed to previous classical techniques, in this study the correctors that we developed and used were applied on the pressure field in both sequentially and semi-fully coupled SL<sub>2</sub>-based coupling strategies. The use of the correctors is highly dependent on the physics of the problem (drained vs. undrained and compressible fluid vs. incompressible). The mathematical formulations obtained are exact and are developed based on the fundamental geomechanical equations in porous medium.

Material balance analysis is quite essential in the coupled system simulation for two main reasons. The first reason is to account for accurate and correct physics. If some mass is (synthetically and mathematically) lost and the conservation of mass and momentum rules are not well honored during the simulation, the proper and accurate results (close to reservoir dynamic history) cannot be expected. Reservoir simulators therefore should consider the changes in mass fluids in a representative volume derived from two parts: 1) contraction or expansion of pore fluid due to pressure changes (compressibility effect), and 2) the change of pore volume itself mainly due to changes in effective stress. The second reason is that an improper and incomplete material balance analysis or ignoring of that, will lead to problem solution divergence in both fully implicit and sequentially coupled reservoir-geomechanics simulation. An obvious outcome of material balance negligence can often be seen in the crash of coupled flow-geomechanics forward simulations during sequential coupled system, as the flow simulator at the end of each time step has to deal with a new pore volume at each REV but the pressure is re-started from the previous time step

(reservoir dynamic state). Different types of material balance errors in the coupled streamline-geomechanics system are explained in the subsequent sections.

For various coupling SL-based reservoir geomechanics strategies discussed in the previous chapters, a mathematical stability analysis (based on CFL criterion and streamline global pressure updates) was performed in this work. In addition, progressive increase of coupling time steps for various coupling strategies (for a constant SL simulation global time step) provide a guideline for selection of proper time step for each individual compressible and incompressible system to ensure problem stability.

A fully coupled (monolithic or fully implicit) flow-mechanical problem is unconditionally stable. However a sequential coupling scheme does not succeed unless a proper stability criterion is developed and applied within the framework of explicit coupling. In the previous work it was demonstrated that streamline-based reservoir geomechanics coupling cannot be performed on a fully implicitly approach (due to explicit/IMPES nature of SL simulation), but can be performed on a semi-fully coupled framework. Therefore stability analysis is an important component of the coupling strategies, in order to ensure the simulation results are both convergent and reliable.

The simulation results demonstrated in this work showed that for SL-based reservoir geomechanics class of couplings, the stability of both drained and undrained splits is dependent on the (coupling) time evolution. The mathematical analysis and simulation results also showed that an incompressible problem is more stable than compressible and undrained mechanical problem is also more stable than drained one. Even though the selection of coupling time steps are limited by the stability criterion, the SL-based reservoir geomechanics are still fast, robust and are the method of choice for hydromechanical modeling of large heterogenous reservoirs with large number of grid-cells.

The simulation results in this work for linear poroelasticity showed that the developed mathematical formulation and guideline for stability of the coupled system have robust stability and convergence properties.



## Stability and Convergence Study

Changes in porosity and permeability due to inclusion of geomechanics into streamline simulation lead to the changes in the velocity fields and therefore streamlines need to be recalculated. Changes in velocity field, during pressure global time steps is a challenge in streamline standalone simulations, as the assumption of treating total fluid velocity as constant on the global time steps is not physically accurate. Even if the porosity and permeability do not change between two sequences of pressure updates, solution of the saturation equation along streamlines leads to a change in relative permeability values (e.g. in Corey functions) and accordingly, changes in velocity field. However, large pressure time steps can still be chosen depending on the magnitude of change in velocity field and on the linearity of the displacement problem. Particularly for cases with incompressible and slightly compressible fluids these changes are considered negligible.

The stability of an IMPES 1D Buckley-Leverett equation is governed by the CFL condition:

$$\lambda = \frac{u}{\emptyset} \frac{\Delta t}{\Delta x} f'_w. \quad (9-1)$$

The CFL criterion states that a necessary condition for an explicit FD scheme to solve a hyperbolic PDE to be stable is that, for each mesh point, the domain of dependence of the discretization (i.e. FD) approximation contains the domain of dependence of the PDE (Piero and Sherwin, 2005).

Spivak and Coats (1970), suggested the same formulation in 3D where distances and velocities are replaced with cell volumes and influx rate of each cell as below:

$$\lambda = \frac{\Delta t}{PV} \sum_{all\ cell\ faces} [Max(f'_{sw})(\vec{u}_f \cdot \vec{n}_f)]; \quad (9-2)$$

where  $Max(f'_{sw})$  shows the maximum slope of the tangent to the fractional flow curve, and contributes in the formulation of the fastest wave speed, which is the wave speed that plays a key role in the stability solution. In the 1D equation,  $\emptyset$  represents porosity,  $\Delta x$  shows cell length, and in the 3D equation  $PV$  shows cell volume,  $u_f$  shows velocity and  $n_f$  represents cell face area, and in both equations  $\Delta t$  and  $u$  represent simulation time step and velocity respectively.

In both cases the limit of stability is  $\lambda = 1$ . Beyond this limit, the solution for the convective solution will be unstable, which will lead to oscillation in the solution results of production rates or water cut profiles as well as non-monotonic contours of saturation that cut across with streamlines (Osako et al., 2004).

By inclusion of geomechanics into streamline simulation, porosity and permeability fields change in the reservoir (particularly in the zones with high pressure gradients), leading to a more significant velocity field changes. Therefore a limit on the pressure time step is needed to ensure a convergent solution. To ensure numerically stable streamline-based geomechanics coupling results, we adopt the same approach as King and Gupta (2005) to deploy a corrector step when there are transport mechanisms transverse to the streamlines. Instead we introduce the geomechanical effects into the formulation. Modified CFL condition is required to account for the inclusion of geomechanics and assessment of choice of time step selection for pressure updates. It must be noted that the stability is performed on the saturation transport equation, as the pressure equation is solved implicitly and therefore is unconditionally stable.

For a two-phase incompressible water flood problem, where porous medium is considered as deformable and geomechanics plays a role in fluid flow displacement problem, Darcy's law is expressed as fluid velocity relative to the moving solid (Geresevanov, 1934, cited by Biot) as below:

$$\phi(\vec{u} - \vec{v}_s) = \frac{-k}{\mu} \nabla p; \quad (9-3)$$

where  $\vec{u}$  shows the fluid bulk velocity and  $\vec{v}_s$  shows the solid bulk velocity, and are the intrinsic (interstitial) velocity. It must be noted that a fluid particle moves along streamlines with interstitial velocity (not Darcy's velocity).

To account for unsteady state effects of geomechanics, the initial fluid and solid velocities  $(\vec{u}_0, \vec{v}_{s0})$  are distinguished from instantaneous fluid velocity field  $(\vec{u}, \vec{v}_s)$  during the long global time steps (pressure updates). Therefore the numerical instability criterion can be developed as below:

$$\phi \frac{\partial S_w}{\partial t} + \vec{u} \cdot \nabla F_w = 0 \quad (9-4)$$

Streamline simulations are a dual-grid system of simulation, and therefore we have two set of system coordinates:  $(\tau, \psi, \chi)$  where time-of-flight is defined and saturation transport problem gets solved, and a normal Cartesian coordinate system  $(x, y, z)$  where pressure diffusivity equation is solved decoupled from saturation equations. Time of flight (TOF) along a streamline is defined as:

$$\tau = \int \frac{\phi}{\vec{u}_0} d\xi \quad (9-5)$$

The key roles that geomechanics plays in fluid flow processes is mainly update of porosity and permeability during production or injection from a representative volume, as well as the changes in the Darcy velocity due to solid velocity changes. And in most extreme cases geomechanics can also be a source of transverse flux due to the induced changes of end-point relative permeability curves and fractional flow functions.

For simplicity, it is assumed that the changes in porosity are linearly related to pressure changes and therefore the equivalent effective porosity in forward coupled transport equation with presence of geomechanics can be written as  $\frac{\phi + \phi_0}{2}$ . Also, the bulk velocity term multiplied by the fractional flow function is the modified velocity accounting for solid bulk velocity as well. Therefore, where source and sink terms are dropped Equations (9-4) and (9-5) are required to be modified to account for geomechanical influences. Definition of time of flight changes as below:

$$\tau = \int \frac{\phi + \phi_0}{2(\vec{u}_0 - \vec{v}_{so})} d\xi, \quad (9-6)$$

and accordingly:

$$\nabla \tau \cdot (\vec{u}_0 - \vec{v}_{so}) = \frac{\phi + \phi_0}{2}, \quad (9-7)$$

and forward saturation equation changes as below:

$$\frac{\phi + \phi_0}{2} \frac{\partial S_w}{\partial t} + (\vec{u} - \vec{v}_s) \cdot \nabla F_w = 0; \quad (9-8)$$

where  $\vec{u}$  and  $\vec{v}_s$  are Darcy velocity (not interstitial velocity), and represent bulk fluid velocity of fluid and solid respectively. The second term in above equation can be rearranged in terms of initial velocity and the corrector velocity:

$$(\vec{u} - \vec{v}_s) \cdot \nabla F_w = (\vec{u}_0 - \vec{v}_{s0}) \cdot \nabla F_w + (\vec{u} - \vec{u}_0 - \vec{v}_s + \vec{v}_{s0}) \cdot \nabla F_w. \quad (9-9)$$

Combining Equation (9-8) and (9-9) applying the chain rule on the first term of the above equation in 1D, we will have:

$$(\vec{u}_0 - \vec{v}_{s0}) \cdot \nabla F_w = (\vec{u}_0 - \vec{v}_{s0}) \cdot \frac{\partial F_w}{\partial x} = (\vec{u}_0 - \vec{v}_{s0}) \cdot \frac{\partial \tau}{\partial x} \cdot \frac{\partial F_w}{\partial \tau} \quad (9-10)$$

Based on Equation (9-7) the latter term can be written as:

$$(\vec{u}_0 - \vec{v}_{s0}) \cdot \nabla F_w = \frac{\phi + \phi_0}{2} \frac{\partial F_w}{\partial \tau}. \quad (9-11)$$

Now we can apply an operator splitting approach on Equation (9-8) and decompose the time evolution to two parts of “convective time step” where saturation equations are solved along the geomechanically modified time of flights (TOF) and the “corrector time steps” where saturations are corrected due to geomechanical induced transverse flux on grid-blocks level:

$$\frac{\phi^{n+1} + \phi_0^n}{2} \frac{\partial S_w}{\partial t} + \frac{\phi^{n+1} + \phi_0^n}{2} \frac{\partial F_w}{\partial \tau} + (\vec{u} - \vec{u}_0 - \vec{v}_s + \vec{v}_{s0}) \cdot \nabla F_w = 0 \quad (9-12)$$

One can split the above equation in terms of two time-steps discussed:

$$\frac{\partial S_w}{\partial t_1} + \frac{\partial F_w}{\partial \tau} = 0 \quad (9-13)$$

*predictor time step*

$$\frac{\phi^{n+1} + \phi_0^n}{2} \frac{\partial S_w}{\partial t_2} + (\vec{u} - \vec{u}_0 - \vec{v}_s + \vec{v}_{s0}) \cdot \nabla F_w = 0 \quad (9-14)$$

*geomechanical corrector step*

The solution of the predictor part of the equation generally leads to stable results; however on grid-level the problem needs further stability analysis. For stability analysis of the corrector step of coupled streamline-based reservoir-geomechanics problem, and understanding the proper size of allowed coupling time steps, a CFL is constructed based on

Equation (9-15) as below. As it can be seen from Equation (9-15) pore volumes and velocity terms are different than conventional finite difference CFL formulations:

$$\gamma = \frac{\Delta t}{\frac{\phi^{n+1} + \phi_0}{2}} \left( \sum [(\vec{u} - \vec{u}_0) \cdot \vec{n}_f - (\vec{v}_s - \vec{v}_{s0}) \cdot \vec{n}_f] \cdot \text{Max}(f'_{sw}) \right). \quad (9-15)$$

In 1D the stability parameter formulation changes to:

$$\gamma = \frac{1}{\frac{\phi^{n+1} + \phi_0}{2}} [(\vec{u} - \vec{u}_0) - (\vec{v}_s - \vec{v}_{s0})] \frac{\Delta t}{\Delta x} f'_{sw}. \quad (9-16)$$

The limit of stability on  $\gamma$  is one; beyond this value the transport solution on corrector step of streamline-based hydromechanical problem is unstable, leading to oscillatory production results. Equation (9-14) shows that for undrained scenarios the stability parameter is time-dependent unlike to findings of Kim et al. (2010) for undrained split coupling stability parameter, where the stability parameter (for conventional sequential coupling problems) was time-independent.

Taking the solid bulk velocity out of Equation (9-15), and approximating it on 1D scale:

$$\frac{-(\vec{v}_s - \vec{v}_{s0}) \cdot \vec{n}_f}{PV} \cong \frac{-(\vec{v}_s - \vec{v}_{s0})}{\Delta x} = -\nabla \vec{v}_s \quad (9-17)$$

On the other hand,

$$\nabla \cdot \vec{v}_s = \frac{1}{V_b} \frac{\partial V_b}{\partial t} = \frac{\partial \epsilon_v}{\partial t}; \quad (9-18)$$

where  $V_b$  is the bulk volume and  $\partial \epsilon_v$  is the instantaneous changes in volumetric strain of the bulk volume due to geomechanical effects during global pressure time steps.

Defining  $\gamma^*$  as the parameter that reflects the changes during pressure update leading to the stability/instability of the solution, one can write:

$$\gamma^* = f \left( \frac{K^{n+1}}{\phi^{n+1}}, \nabla \cdot \vec{v}_s \right), \quad (9-19)$$

since,  $\vec{u}$  is proportional to  $K$  (absolute permeability of porous medium). Equation (9-15) shows that the factors that lead to instability on the grid-block level during forward coupled streamline-based flow-geomechanics simulations are the changes in Darcy velocities, the

changes in pore volumes (interchangeably porosity) , and the changes in solid bulk velocities. Therefore  $\gamma^*$  can be reformulated as below:

$$\gamma^* = \frac{K - K_0}{\frac{\phi + \phi_0}{2}} - \Delta \varepsilon_v ; \quad (9-20)$$

where  $K$ ,  $\phi$  are the cycle-end permeability and porosity and  $K_0$  and  $\phi_0$  represent initial permeability and porosity. Adopting the correlation for update of absolute permeability suggested by Rutqvist and Tsang (2002), and correlation for update of porosity proposed by Touhidi-Baghini (1998):

$$\phi = \frac{\phi_0 + \Delta \varepsilon_v}{1 + \Delta \varepsilon_v} \quad (9-21)$$

$$K = K_0 \exp \left( 22.2 \left( \frac{\phi}{\phi_0} - 1 \right) \right), \quad (9-22)$$

and replacing the above mentioned equations in Equation (9-20) leads to:

$$\gamma^* = \frac{2K_0 [\exp(22.2 \left( \frac{\phi}{\phi_0} - 1 \right)) - 1]}{\phi_0 \left( \frac{\phi}{\phi_0} + 1 \right)} - \Delta \varepsilon_v \quad (9-23)$$

By rearranging Equation (9-21) in term of  $\varepsilon_v$ , and defining  $n^* = \frac{\phi}{\phi_0}$  as the ratio of updated porosity to initial porosity and replace in the equation (9-23), we have:

$$\gamma^* = \frac{[\exp(22.2(n^* - 1)) - 1] - \frac{(n^* - 1)}{\left(\frac{1}{\phi_0} - n^*\right)}}{(n^* + 1)} \quad (9-24)$$

Since the term  $\frac{K_0}{\phi_0}$  is constant, it was omitted from the final form of formulation. Therefore  $\gamma^*$  is an instability parameter in coupled streamline-geomechanics problems which is only a function of  $t$  (time -from time step  $(n)$  to time step  $(n+1)$ ) and  $n^*$  ( porosity changes ratio) .Porosity changes are also a parabolic function of volumetric strain, as such the instability parameter is a function of coupling time-step ( $\Delta t_{coupling}$ ) as well as volumetric strain changes during  $\Delta t_{coupling}$ .

However as mentioned before, Equation (9-15) is only a guidance for selection of the pressure time steps. But the calculation of velocity fields at the end and beginning of each

coupling cycle as well as checking on the corrector step stability (Equation (9-15)), are both involved with additional computational costs, particularly for reservoirs with large number of grid cells. Therefore another approach suggested to check on the stability of the coupled system is to run different simulation cases with progressively increased coupling time-step sizes, and check on the convergence and stability of the solution, and come up with a general rule of thumb for selection of time step sizes (in terms of injected pore volume) at each coupling strategy.

A flow-geomechanical limiting parameter (stability criterion) on the time step sizes can still be designed to check on the velocity field updates at the end of large global coupling time steps (based on Equation (9-15),  $\Delta\lambda$ ). For instance if the global time steps are more than 400 days, and the reservoir rock is very stress sensitive (with low bulk and shear modulus) where a significant induced volumetric strain field is expected, a velocity field checking based on the Equation (9-15) is required. In this work, changes in gradient of solid bulk velocity have been neglected, as with reference to our work on large-scale streamline-based hydrogeomechanical problem of CO<sub>2</sub> storage (Koochmarch et al, 2013), it was shown that they are negligible compared to gradient of bulk fluid velocity. However for some wellbore vicinity class of scenarios such as sand production, the solid bulk velocity parameter cannot be neglected.

It is interesting to note that the velocity field in CFL condition for conventional simulation, is replaced with the change in velocity fields induced (cycle-end velocity minus initial velocity at the beginning of the cycle) , which means that the global time steps limits are much larger than conventional simulators. It must also be noted that where the value of  $((\vec{u} - \vec{u}_0) - (\vec{v}_s - \vec{v}_{s0}))$  is small, the CFL limit gives even greater computational benefits for increase in coupling time steps (compared to the scenario where solid bulk velocity is neglected). These processes occur when there is only very slight transverse flux (e.g. no capillary, no gravity), or for simulation of reservoir with incompressible fluid and the problems with a very small gradient of solid velocity (cemented rocks with a very small sand production tendency or solid velocity gradient). If the problem is highly compressible, the pressure time step is at the same level with saturation time steps. In streamline alone class of simulations, the saturation time steps can be much larger than time steps in conventional flow simulations because in streamline simulations, the CFL is defined on 1D the streamline grids, allowing larger time

steps compared to conventional simulation where the time steps are defined on 3D cell volumes. But it must be noted that in coupled streamline-geomechanics simulations, the modified developed CFL is defined on the underlying 3D grid cells (cell volumes), therefore the time steps are bound with number of grid cells. And the key factor that plays a role in the coupled simulation speed up is the change in velocity fields instead of the velocity alone (which can be 10-folds smaller than the initial or instantaneous velocities, leading to 10-folds reduction in CFL number). Therefore even for compressible class of problems, the workflow computational load will still be less compared to conventional flow-geomechanics coupling techniques.

On the geomechanical side, when the rock behavior is elastic, and geomechanics is implemented on a finite-difference approach (FLAC 3D, 2013), the stability parameter is only dependent on the cell-size and reservoir rock stiffness (bulk and shear moduli) :

$$\Delta t < \frac{\alpha \Delta x_{min} (K + \frac{4G}{3}) \Delta x^2_{max}}{3A} , \quad (9-25)$$

where  $\Delta x_{min}$  shows the minimum and maximum cell size,  $K$  and  $G$  show the bulk and shear modulus of the rock, and  $A$  represent the surface area of the grid block. Equation (9-15) shows that stiffer rock material will ensure more stable solutions. If the constitutive model of the reservoir is non-linear elastic where rock moduli will change with effective stress changes (in a power law fashion), the stable time step sizes will change in the course of sequentially coupled problem, and the convergence may occur faster in subsequent steps as we move forward along the cycles. In FLAC 3D the stability and convergence is controlled by a parameter called “mechanical ratio”.

The geomechanical processes in our workflow are stationary (time-independent) in each cycle interval, and therefore the solution is independent of the physical time step (i.e. global pressure updates of streamline simulation). However the parameter  $\Delta t$  (time) in the formulation is a pseudo-time parameter, which is mainly the numerical time steps required for converged mechanical solution, and should not be mistaken with real time. The optimum speed of convergence is when  $\Delta t = 1$  in Equation (9-25). In Streamline simulation however the parameter  $\Delta t$  is the real forward flow simulation time (global pressure time steps).



## Material Balance Error

Streamline simulations by their own are involved with material balance errors, mainly because of the remapping step when saturations are remapped from streamlines (after solution of Equation (9-13)) back to the underlying grid. This occurs because saturations of all the stream-tubes passing through the grid block are averaged and assigned to the underlying grid block. However, the volume of all stream-tubes passing through the grid block does not equal to the volume of the grid block and as such, some mass is expected to be gained or lost. To mitigate this type of material balance error, the grid blocks must be finer, and more streamlines must be launched and the number of TOF grids should be increased along each streamline.

In addition to the material balance error due to remapping, there is another source of material balance error that is due to dependence of mass on absolute pressure. When geomechanics is embedded into the streamline simulation workflow as a source of changing permeability and porosity, the pressure field will be even more disturbed, and therefore the material balance error will increase even more, leading to problems in the resolution of absolute pressure values. To mitigate this type of material balance error during forward time steps of coupling, the following workflow is proposed.

From a physical point of view, the total fluid volume responses (due to increase in volumetric strain) can be decomposed to two parts:

$$\Delta V_f = \Delta V_f^I + \Delta V_f^{II}, \quad (9-26)$$

where  $\Delta V_f$  is the total change in fluid volume (mass gained or loss),  $\Delta V_f^I$  is the volume of fluid changed due to compressibility effect (geomechanical effects on fluid flow), and  $\Delta V_f^{II}$  is the fluid volume change due to induced volumetric strain, and fluid exchange of a grid block with neighboring grid blocks (fluid flow effects on geomechanics), and are defined:

$$\begin{cases} \frac{\Delta V_f^I}{V_f} = -\frac{p}{K_f} \\ \frac{\Delta V_f^{II}}{V_f} = -\frac{\Delta V_f^{II}}{\phi V} = \frac{\zeta}{\phi} \end{cases}, \quad (9-27)$$

where  $p$  is the pore pressure changes,  $K_f$  shows the bulk modulus of fluid ( $\frac{1}{c_f}$ ),  $\xi$  is the volume of fluid gained or lost in a material element,  $\phi$  is porosity of the material element, and  $V_f$  is the total changes of pore space or fluid volume. The assumption for all the formula is that the entire pore volume is filled with fluid, and therefore  $\Delta V_f = \Delta V_p$ .

Two different correctors are suggested to mitigate the material balance issues involved with two different physical inconsistencies that form each part of Equation (9-27). Both correctors that are embedded in the streamline-based coupling technique (**Figure 9-1**) are focused on the updating and remapping of the pressure field. As discussed previously, in the course of sequential coupling porosity field changes. In a compressible system, the changes in pore volume of the porous rock lead to expansion or shrinkage of the compressible phase, and accordingly different phase density in a REV. Change in density (in each REV) calls for a different pressure field during/at the end of coupled forward simulation. Consequently, a fluid flow simulator will have difficulty with the new porosity and permeability values whereas the pressure used to re-initiate the next cycle is based on the old porosity and permeability (without inclusion of geomechanics). The material balance error is inevitable under these conditions.

Based on Ács et al. (1985) we have:

$$(C_f V_f + C_r V_p)^n (P^{n+1} - P^n) \Delta t = 0; \quad (9-28)$$

where  $n$  shows time step,  $P$  shows pressure,  $C_f$  shows the mixed fluid compressibility,  $C_r$  represents rock compressibility, and  $\Delta t$  shows the physical time step length. For the staggered approach when new porosity and permeability fields are updated before they are transferred to a fluid flow simulator to be resolved (path [4]) in Figure 9-1, a pressure field corrector should be used. The correctors are used to remove the material balance error and truncations committed by compressibility effects.

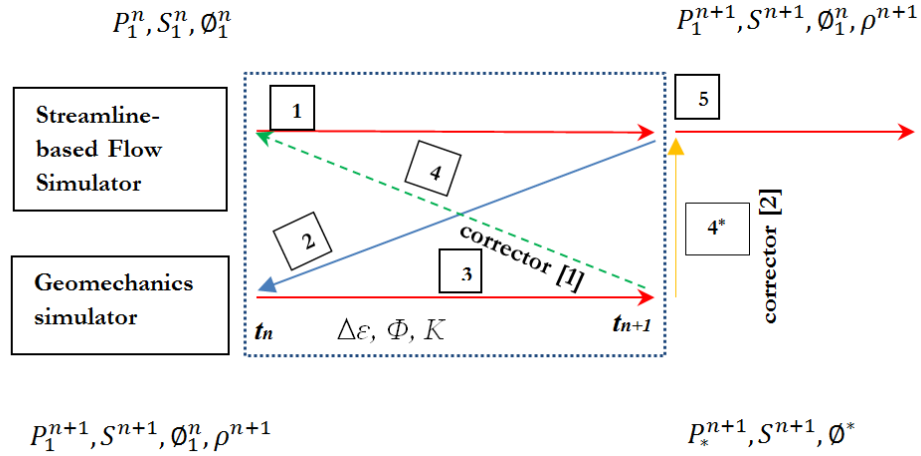


Figure 9-1-Representation of material balance error correction paths.

### Corrector 1

Assuming a multiphase fluid flow system, where one phase is compressible but the other phases are incompressible or slightly compressible, there must be a conservation of mass for the incompressible system. Equation (9-28) is derived from Equation (9-28) where  $V_f = V_p$  and  $C_r$  is constant.

$$\rho_1^n \phi^n = \rho_2^n \phi^* \quad (9-29)$$

Therefore in Figure 9-1 on path [4], where porosity and permeability is transferred to the beginning of the flow simulation run cycle, the pressure must be updated. Note that “corrector 1” is applied on time level ( $n$ ) at this step. To update pressure, we need to update phase density of the compressible phase as below:

$$\rho_2^n = \frac{\rho_1^n \phi^n}{\phi^*}; \quad (9-30)$$

where  $\rho_1^n$  and  $\phi^n$  are phase density and porosity before deformation of porous medium through geomechanical simulation, and  $\phi^*$  is the updated porosity after considering the geomechanical impacts into account. The adapted relation between density and pore pressure is as below, where density and pore pressure are calculated based on the reference values of density ( $\rho_0$ ) and pressure ( $P_0$ ).

$$\rho_2^n = \rho_0 \exp[-c_o(P_*^n - P_0)] \quad (9-31)$$

Therefore from Equation (9-31), the updated pressure field,  $P_*^n$ , which is computed before carrying out streamline simulation on path [1] for the next inner cycle, is defined as:

$$P_*^n = P_0 + \frac{1}{c_o} \ln\left(\frac{\rho_o}{\rho_2^n}\right). \quad (9-32)$$

As such, each time we go through path [4] to provide the flow simulator with new porosity and permeability we should change the pressure field from  $P^n$  to  $P_*^n$ . Similarly when we go through path [4\*], the pressure field requires to be updated with the same concept but at time step (n+1), by use of corrector [1].

It must be noted if convergence (in porosity, permeability, and pressure values) was achieved, there is no need to go through path [4\*]. But if there were no inner cycles carried out (staggered technique) or the convergence was not fully achieved, corrector [1] must be carried over on path [4\*] from the end of the geomechanical run to the beginning of the next cycle's streamline forward flow simulation. The use of developed corrector technique (pressure-remapping) not only leads to an increased convergence rate (less number of inner cycles to ensure convergence) but also must be applied in the coupling techniques to result in physically correct and consistent production rates.

## Corrector 2

As discussed corrector [2] was developed to account for the material balance errors resulting from geomechanical responses of the reservoir and the expulsion of fluid out of each material representative bulk volume. From two sets of equations below, which are basis of poroelasticity at each location in the reservoir and at a certain time we can write:

$$\varepsilon_v = \frac{-1}{K} (\sigma_t - \alpha p) \quad (9-33)$$

$$\zeta = \frac{-\alpha}{K} (\sigma_t - \frac{p}{B}) \quad (9-34)$$

where  $\alpha$  is the Biot's coefficient,  $K$  is the bulk modulus of medium,  $\sigma_t$  shows the total stress,  $p$  is pore pressure,  $B$  is Skempton factor,  $\varepsilon_v$  shows the volumetric strain, and  $\zeta$  shows the volume of fluid gained or lost. We can derive the equation below based on Equations (9-33) and (9-34),

$$p = M(\zeta - \alpha \varepsilon_v), \quad (9-35)$$

where  $M$  is the storage coefficient or Biot modulus, and under  $\pi$ -loading (where porosity remains constant) for a two phase system of fluid and rock can be defined as below:

$$\frac{1}{M} = \phi_0 c_f + (\alpha - \phi_0) c_r. \quad (9-36)$$

If we write the equation for one location in the reservoir but at two different time steps, where there is no volume of fluid lost or gained we can have:

$$p^{n+1} - p^n = -M\alpha(\varepsilon_v^{n+1} - \varepsilon_v^n) \quad (9-37)$$

$$p_*^{n+1} = p^n - M\alpha(\varepsilon_v^{n+1} - \varepsilon_v^n); \quad (9-38)$$

where  $p_*^{n+1}$  is the corrected updated pressure, and  $p^n$  is the pressure field at the beginning of cycle. The above-mentioned formulation could alternatively be obtained from Coussy (1995) poroelasticity equations, where the change in mass is considered zero ( $m - m_0 = 0$ ).

The above corrector technique is deployed on path [4\*] where porosity and permeability from mechanical problem are fed to the next cycle ( $n + 1$  to  $n + 2$ ). It must be noted that both correctors (1 and 2) are applied on all reservoir grid-blocks and therefore each time the correction is applied, volumetric strain and storage coefficient should be calculated for all cells. A test on a synthetic case showed that the pressure corrections can be slightly different if  $M$  is assumed constant compared to the case where  $M$  is calculated based on the average cycle porosity, as long as the correction on pressure field along path [4\*] is an average of the pressure values out of combined application of corrector [1] and corrector [2]. When the workflow is not iterative between streamline pressure updates and permeability updates and Approach 2 is carried out for forward streamline-geomechanics coupling, both pressure correctors [1 and 2] have to apply along path [4\*] before moving to the next cycle. Material balance error reduction helps also to achieve greater stability and convergence.

## Drained vs. Undrained

From a lab measurement perspective, a drained test is one where no excess pore pressure,  $\Delta p = 0$ , develops within a specimen under the application of a deviatoric stress change  $\Delta \sigma_d$  (i.e., the pore pressure remains at its initial condition). An initial consolidation stage under isotropic loading may induce some pore pressure in the rock (undrained), but in the course

of time, the pore pressure is dissipated and comes into equilibrium with the boundary. The undrained condition however, is the condition where no fluid is allowed to leave or enter the sample ( $\Delta m_f = 0$ ), and accordingly the pore pressure changes in a test specimen when subjected to loading whether isotropic or shear loading. Undrained condition in the reservoir generally occurs when porosity and permeability are too low (allowing no space for fluid to be exchanged with neighboring material elements), and drained responses occur when pore pressure can dissipate easily in the reservoir, usually due to high porosity and permeability of the reservoir rock.

Biot and Willis (1957), Brown (1975), Geertsma (1957), have shown that in a rock sample with homogenous mechanical properties, porosity remains constant during undrained responses of the rock (or reservoir). In such a reservoir rock response, compressibility of solid, pore and bulk are all the same, which means they all shrink or expand in size equally in a fashion, where porosity remains constant. Based on Equation (9-24) when porosity ratio remains constant and equal to one ( $\phi^{n+1} = \phi^n$ ) during inclusion of geomechanics into streamline-geomechanics workflow (from beginning of cycle ( $n$ ) to the beginning of ( $n+1$ )), the coupled problem remains stable, meaning that there is no transverse flux due to changes in void spaces in reservoir. Adapting equation (9-22) for permeability updates, there will also be no changes in absolute permeability values, since the porosity ratio has remained unchanged.

Hence, in the undrained split coupling processes of streamlines with geomechanics, Approach 2 is a sufficient approach to ensure converged solution and numerically stable coupled system, and there is no need to utilize Approach 3 any longer to ensure more stable results. In terms of material balance errors reduction, in undrained conditions where porosity and permeabilities are assumed constant in the course of each cycle interval (path [3] in Figure 9-1), there is no need to deploy corrector [1] (path [4] in Figure 9-1). However since the excess pore pressure has increased during explicit mechanical problem (in addition to the pore pressure changes from  $P_n$  to  $P_{n+1}$  in forward streamline solution), it has to be adjusted along path [4\*]. Based on Zienkiewicz (1999), the alternative form of poroelastic equation can be written as below, and as such the local changes in pore pressure due to mechanical solution of the problem, can be obtained from below equation where  $\phi^{n+1} = \phi^n$ .

$$\phi^{n+1} = \phi^n + \alpha(\varepsilon_v^{n+1} - \varepsilon_v^n) + \frac{1}{M}(P^{n+1} - P^n) \quad (9-39)$$

In Drained condition, on the other hand, since porosity and permeability values change in the coupling process, to reduce the material balance error undertaking path [4] on Figure 9-1 is recommended, but as mentioned before convective saturation equation can be skipped and be solved only once, and at a different level when the coupling between pressure and displacement solution variables are achieved. However for computational cost reductions, Approach 2 can be undertaken, provided that both pressure corrector-splitting steps are taken on path [4\*]. Since the reservoir condition can hardly be totally undrained or drained, the pressure corrector [2] can be interchangeably used for drained condition as well. Therefore the closer the reservoir rock volumetric responses are to “undrained” responses, the faster and numerically more stable the streamline-geomechanics coupling will be. The minimum changes in porosity and permeability values allow longer coupling time steps, and no (computationally) expensive iterative inner cycles are required for solution convergence. The other condition that the reservoir volumetric response is undrained is when the reservoir rock experiences an instant loading where pore pressure does not have the time to be dissipated to neighboring material elements in the reservoir. The convective fluid flow in the reservoir is also a condition that the time scale characteristic of the loading (of fluid on the reservoir rock skeleton in each grid block) is very short, and therefore denotes an undrained condition. The diffusive mass transport from a reservoir rock element to the neighboring elements in a long time period, on the other hand denotes a drained condition. Streamline simulations scale well for flow processes dominated by convective displacement, and as such undrained conditions with high instantaneous loading (due to large pressure gradients) are better suited for streamline class of simulations.

**Figure 9-2** shows the suggested optimized interactive coupled streamline-geomechanics system for both drained and undrained reservoir volumetric responses.

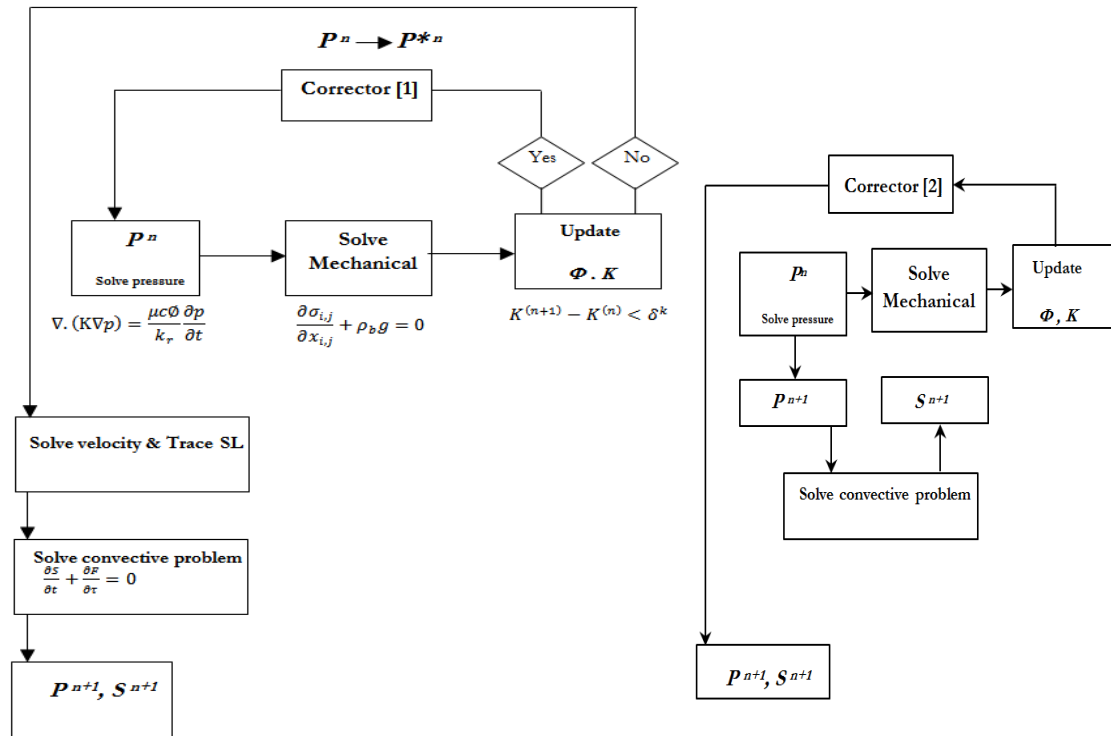


Figure 9-2-Representation of streamline-geomechanics coupling workflows; comparison of optimized coupling scheme for drained (left) versus undrained (right) split methods.

## Compressible vs. Incompressible

In streamline simulations, the more incompressible the fluid phases are the more linear the problem is, and the faster and more robust the solution of the problem is. Obviously for incompressible problems, the numerical solution to the pressure diffusivity equation in its matrix algebraic form ( $\Delta p = 0$ ) converges harder (due to singularity of matrix of Laplacian of pressure). However, when in place and injected fluids are incompressible, the velocity field remains almost constant due to problem linearity and as such there is no need to update streamline configuration nor to resolve pressure equation often. Therefore incompressible problem avoids excessive coupling time steps, allowing faster coupling system. And the solution of the pressure equation is independent of the absolute value of pressure, but only changes in pressure matters and also the flow rate along the streamline is constant, leading to a more efficient solution of the transport equation. In compressible problems however, streamlines can start or end in any grid blocks that have the nature of a volume source (fluid density decrease with pressure changes) or sink (fluid density increase with pressure increase) because of the compressible nature of the model. And since the fluid parameters (densities,



viscosities, etc.) are pressure dependent the problem is non-linear and successive update of streamlines pattern are required, leading to smaller global time steps.

The most ideal case is a one phase incompressible problem where the well configurations do not change in the course of streamline-geomechanics coupling, where pressure field needs to be solved only once, hence the coupling scheme is very fast. For streamline based compressible flow problems, both pressure and saturations time steps are at the same level. Even though still the problem is faster compared to FD or FEV flow simulations, the long global pressure time steps are not allowed and pressure field (in 3DSL) has to be resolved on the same frequency with saturation equation. Therefore, the coupled system is slower in a compressible case than an incompressible one where the coupling time steps (when pressure fields require to be updated) are large.

In terms of material balance error, standalone streamline simulations exhibit a larger material balance error in compressible problems than the incompressible ones, due to mass dependency on the absolute value of pressure. In streamline-geomechanics coupled system (either explicit or semi-fully coupled schemes), problem incompressibility does not allow undertaking path [4] in Figure 9-1. Therefore for incompressible problems Approach 3 (iterative inner cycles) is not allowed as Equation (9-29) cannot be satisfied in an incompressible problem ( $d\rho = 0$ ). Therefore streamline-based hydromechanical coupling can be alternatively performed through Approach 2, with application of corrector [2]. Skipping the iterative coupling inner cycles (coupling between decoupled pressure with displacements) as well as application of only one corrector (along path [4\*]) leads to a faster coupling scheme in incompressible problems than compressible ones. When reservoir rock is very stiff and reservoir fluid is incompressible, the hydromechanical parameters are on their upper bounds (based on poroelasticity equations):

$$B \rightarrow 1$$

$$K_u \rightarrow \infty$$

$$M \rightarrow \infty ,$$

where  $B$  is the Skempton pore pressure coefficient,  $K_u$  is the undrained bulk modulus of the rock. Skempton coefficient of unity means that if the reservoir volumetric response is

undrained, the change in pore pressure in each representative element is equal to the total stress exerted on the material element. Under condition of undrained system with incompressible flow, volumetric strain is almost zero based on definition of volumetric strain as below:

$$\varepsilon_v = \frac{-\sigma_t}{K_u} \quad (9-40)$$

Also, based on Equation (9-39), both portions of pore volume changes (due to pore pressure changes and volumetric strain changes) are zero, and consequently there is no change in porosity of porous medium. As such, based on what was discussed in the stability analysis section, the coupled streamline-geomechanics workflow is more robust and stable and better suited for incompressible displacement problems.

## Homogenous vs. Heterogeneous

Streamlines do a great job in capturing the effects due to geological heterogeneity. For strongly heterogeneous systems the streamlines pattern are dictated by the geology rather than by the displacement, and the more heterogeneous the geology of reservoir is, the less dependent the system nonlinearity will affect the streamlines. Therefore reservoirs with high level of geological heterogeneity (in porosity and permeability) mitigate the effect of problem non-linearity (e.g. capillary, gravity, transverse flux). From physical point of view the reason is that reservoirs dominated by heterogeneity (and unchanged well conditions) will allow streamline paths that change slightly over time. Therefore the negative effect of porosity and permeability updates (in inducement of transverse flux) during streamlines-geomechanics coupling cycles can be minimized by the increased time that global time steps (and accordingly coupling time steps) can have due to increased problem heterogeneity.

It must be noted that with fixed coupling time steps (e.g. 100 days), a homogeneous coupled system may (or may not) exhibit a lower computational efficiency than a heterogeneous one. However since the coupling time steps and hence the cycle lengths can be larger in highly heterogenous domains, the overall CPU efficiency of the system is expected to increase. The reason that coupled streamline-geomechanics strategies are best suited for highly heterogeneous reservoirs, is that longer coupling time steps are allowed and therefore excessive small time steps (to ensure a constant velocity field during inclusion of

geomechanics) are avoided. In the contrary, heterogeneities in FD or FV simulations of fluid flow and coupled flow-geomechanics result in lower CPU efficiency and excessive simulation run times.

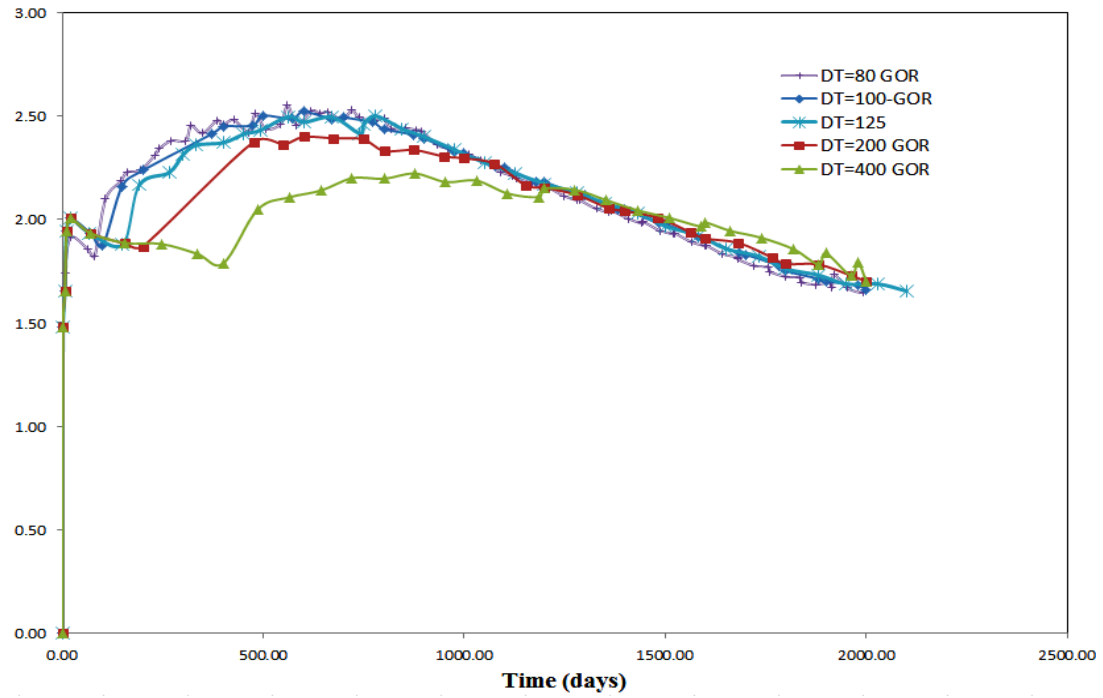
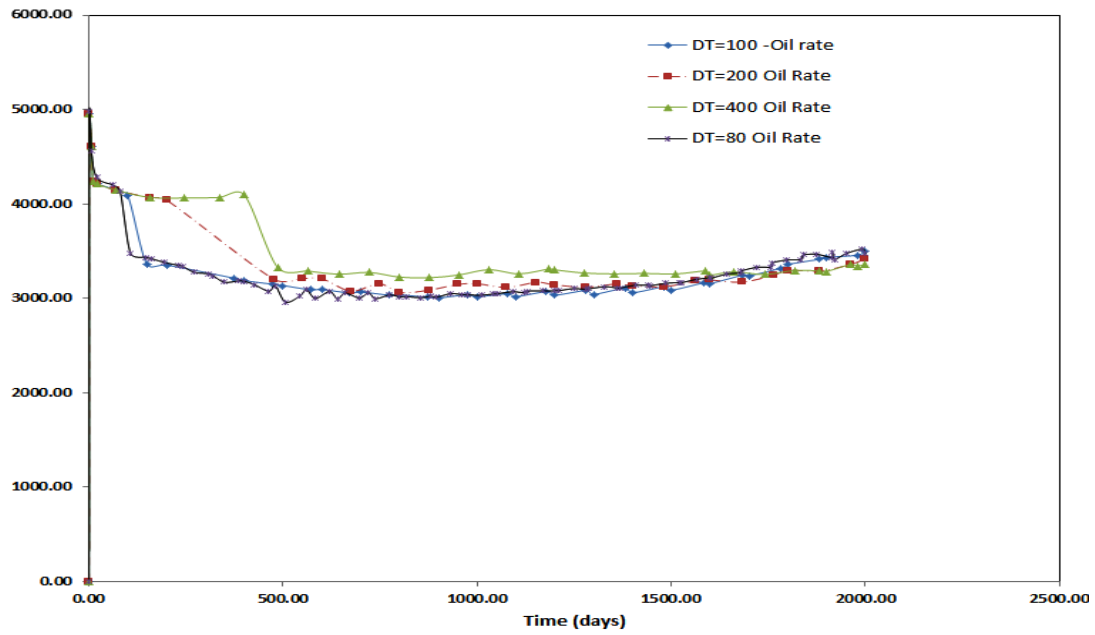
Convergence of poroelastic problems and CPU time however are not affected by porosity and permeability heterogeneities. The only input parameters heterogeneity that are influential on solution convergence rate and simulation speed as well as final stress and strain field values in (elastic) mechanical problems, are the heterogeneity of MEM properties (e.g. Poisson's ratio, Young Modulus, etc.). In plastic rock constitutive behavior however, porosity is an input parameter and is decisive on reservoir loading path (Roscoe, 1958). Therefore based on the discussion above, increased heterogeneity leads to a faster coupled streamline-geomechanics system, since larger coupling time steps are allowed in all discussed coupling strategies.

## **Results and discussions**

The simulation models are identical as the ones discussed in Chapter 8 (Case 1 and 2).

### **Case 1**

It must be noted that the suggested coupling time step is to ensure full convergence throughout production time (both early and late times after production); however the problem converges for late production times, even at time step sizes of more than 400 days (0.15 PVI).

**Mscf/stb****stb/d**

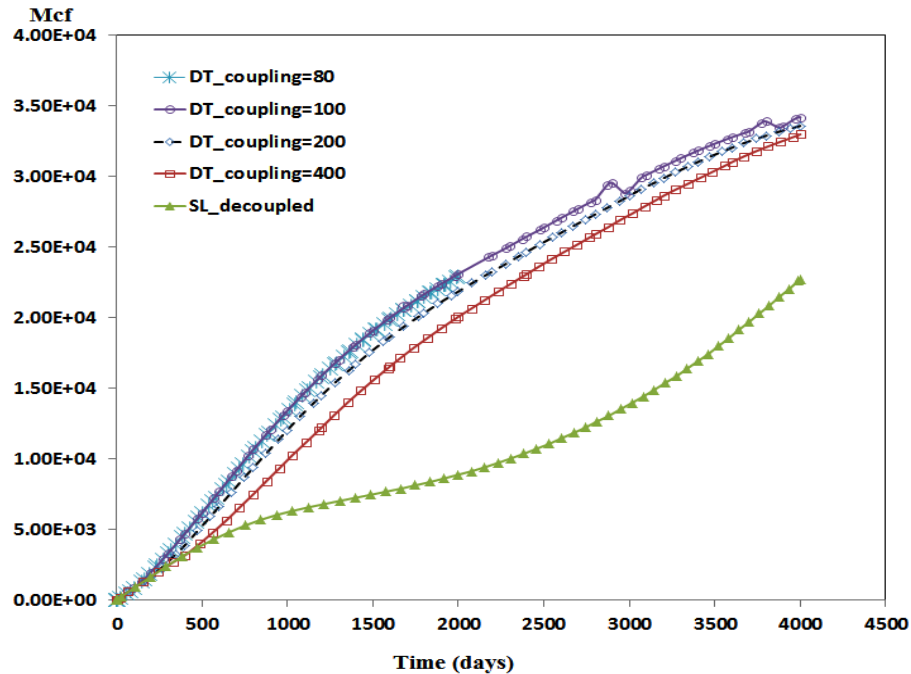


Figure 9-3-Rate surface GOR gas oil ratio (top), surface oil rate (middle), cumulative reservoir gas production (bottom). Convergence of the coupled system solution through Approach 2 appears to occur at around  $\Delta t_{\text{coupling}}=100$  days (0.036 PVI).

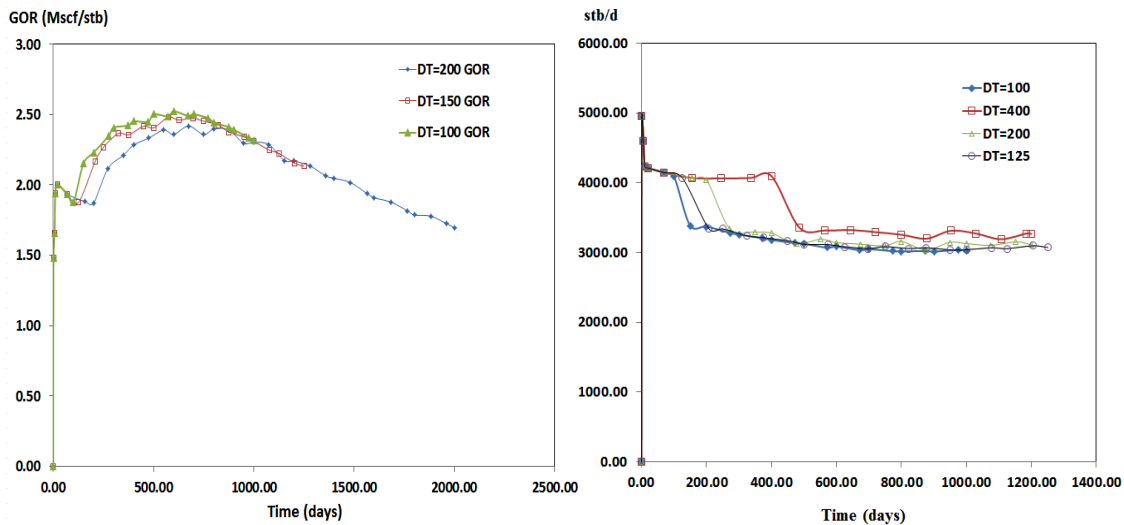


Figure 9-4-Convergence of the coupled system solution through Approach 3 appears to occur at around  $\Delta t_{\text{coupling}}=150$  days (0.05 PVI). Representation of field GOR (left) and field oil rate (right).

It must also be noted that even though Approach 3 can allow the user to undertake longer coupling time step (expecting faster simulation run time) compared to Approach 2, the

comparison on the total CPU run time over 1000 days of production shows that Approach 2 by 2832 *millisecond* of run time is ultimately faster than Approach 3 with 3202 *millisecond* CPU run time. Therefore depending on the problem size and problem compressibility one has to perform a comparison between Approach 2 and 3 on the run time and convergence before undertaking the simulation on the longer simulation time steps on the models with larger number of cells.

**Figure 9-5** illustrates how the convergence (on field oil production rate and water cut rate) occur through full flight cycles of Approach 4. Each cycle is longer in time-length compared to the previous cycle and predicts slightly different production rates due to geomechanical updates.

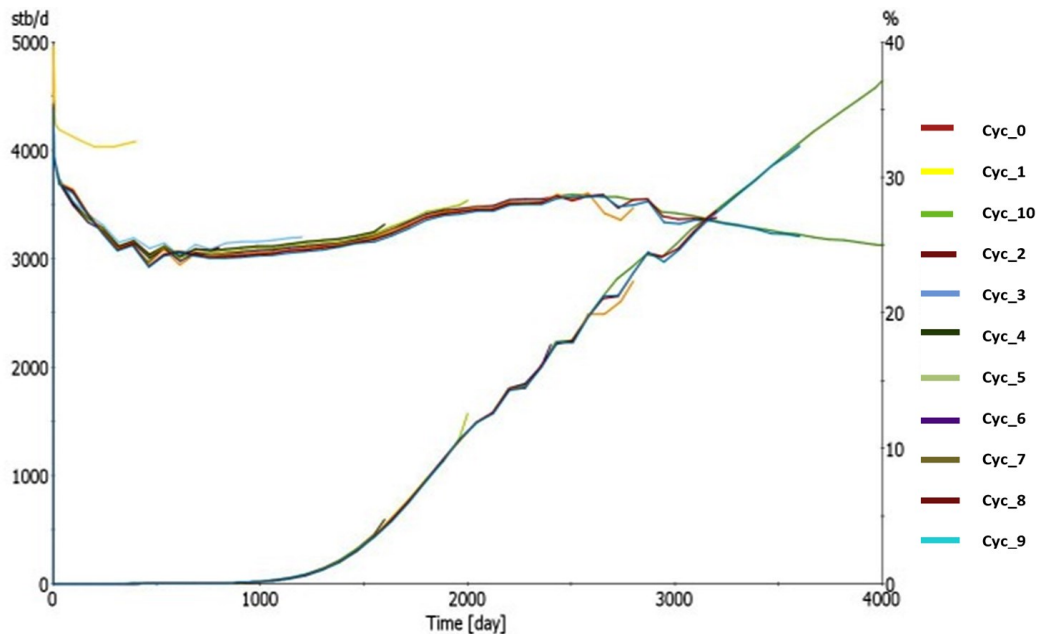


Figure 9-5-Convergence of field oil production and water cut rates by use of Approach 4 at 10 full flight cycles over 4000 days of coupled simulation. Each single cycle is illustrated by different color.

## Case 2

### Solution Stability and Convergence

Similar to case 1, the coupling time step sizes are progressively increased from 50 days to 400 days while the internal streamline global time steps (frequency of pressure updates) were kept constant and equal to 0.1 PVI.

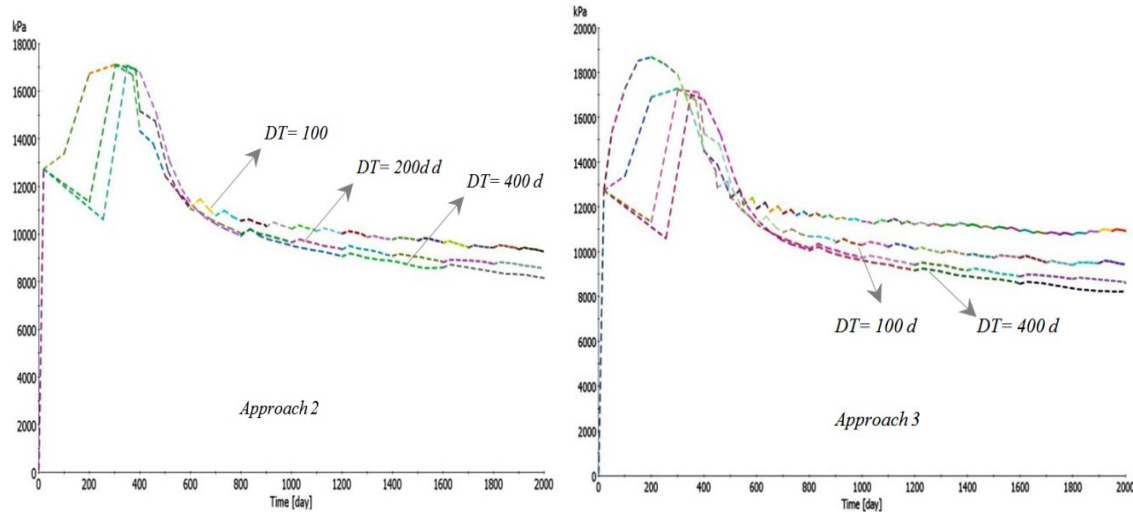


Figure 9-6- Convergence of Approach 2 (left) at  $DT=100$ ,  $200$ ,  $400$  days and convergence behavior of Approach 3 (right) at  $DT=50, 100, 200, 400$  on average reservoir pressure. Each color illustrates a coupling cycle.

**Figure 9-6** shows that Approach 2 and Approach 3 represent similar convergence on average reservoir pressure. Both show a converged solution at coupling time step size of 200 and 400 days. This time step is a very large time step size, which shows for incompressible problems the coupling time step can be larger (10 fold times) than streamline global time steps, and the computational efficiency loss due to inclusion of mechanical problem be mitigated significantly by large time step size of coupling that streamline-based reservoir geomechanics system offers.

Comparison of the stable coupling time step size for incompressible problems (0.6-4 PVI) with converged time step sizes of compressible problems such as case 1 (0.05 PVI), shows that the more incompressible the problem is the more stable the streamline-based geomechanics coupled system is.

Problem solution (average pressure) on coupling time step of 200 days was considered as an acceptable time step, since the uncoupled standalone streamline simulations shows a range of convergence tolerance on different time step sizes. **Figure 9-7** illustrates that even on streamline alone side of simulation the problem does not show a full convergence and similar behavior with only a small increase in time step (from 0.01 PVI to 0.05 PVI and 0.1) at even late stages of simulation (1000 days).

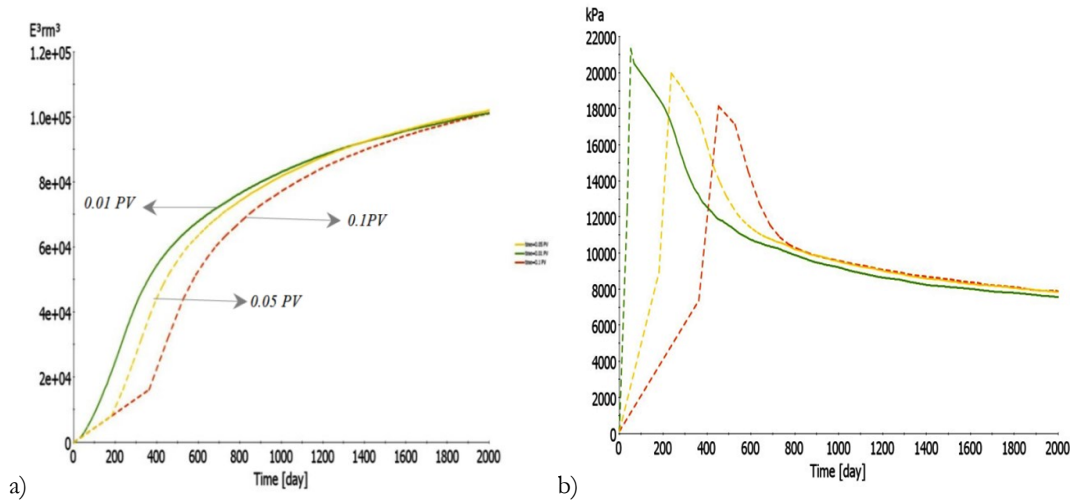


Figure 9-7-Uncoupled problem convergence study of model 2 on streamline standalone mode. a) in-place reservoir gas in time and b) average reservoir pressure. The comparison is performed on three progressive time steps equivalent to 0.01, 0.05 and 0.1 reservoir pore volume.

### Impact of Streamline Global Time Steps on Solution Stability and Convergence

By decreasing the global time step sizes on streamline side from 0.1 pore volume (Figure 9-8) to 0.05 pore volume (Figure 9-9), the convergence was attained at larger coupling time step sizes. That simply means that SL-based reservoir geomechanics coupling can be conducted through larger time steps when streamline global time steps (frequency of pressure updates) are well tuned and are chosen smaller which leads to avoiding excessive smaller coupling time steps, and yet ensure robust results. It must be noted that the added CPU run time of coupling by tuning the streamline time step is computationally much less crucial than performing the mechanical simulation runs more frequently (each time mechanical problem is solved three independent solution variables are solved, but streamline simulations solve only one solution variable which is pressure).



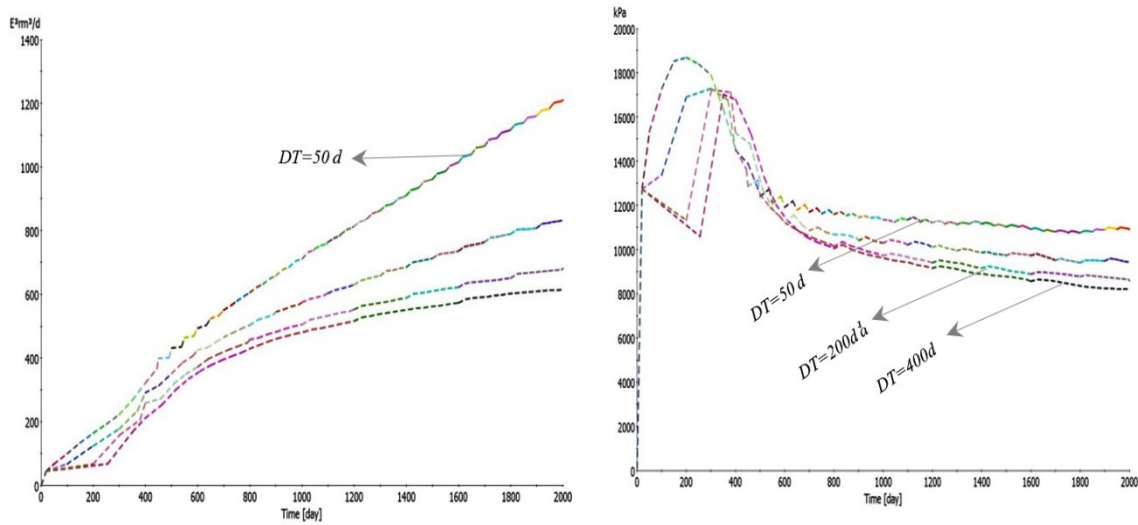


Figure 9-8-Convergence study of Approach 3 at progressive coupling time steps of 50, 100, 200 and 400 days when streamline global time steps are 0.1 pore volumes. Representation of reservoir gas injection rate (left) and average reservoir pressure (right).

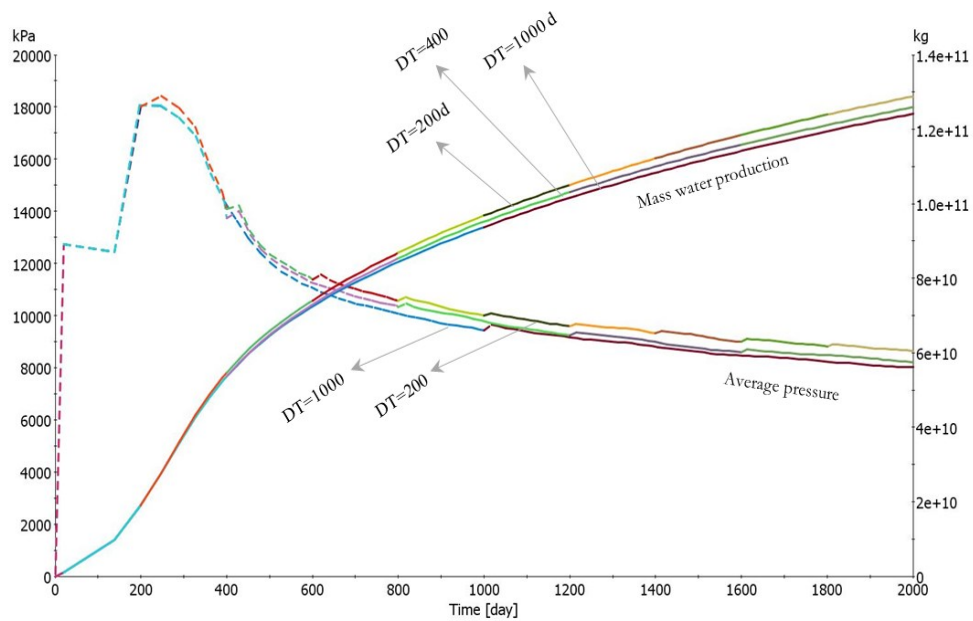


Figure 9-9-Convergence study of Approach 3 at progressive coupling time steps of 200, 400 and 1000 days when streamline global time steps are 0.05 pore volumes. Representation of average in place reservoir pressure and cumulative mass water production at the model boundaries due to injection of supercritical CO<sub>2</sub>. Different colors illustrate each coupling cycle.

The dynamic responses of reservoir when the reservoir rock was very stress sensitive ( $E=50 \text{ MPa}$ ) through Approach 2 were very different than the results through Approach 3. The problem solutions (average reservoir pressure and cumulative gas injection rate) did not

converge through either of approaches at even very small coupling time steps of 80 days.

**Figure 9-10** shows also how the problem converges in full flight coupling strategy from day 200 (first cycle) to the 2000<sup>th</sup> day (10<sup>th</sup> cycle).

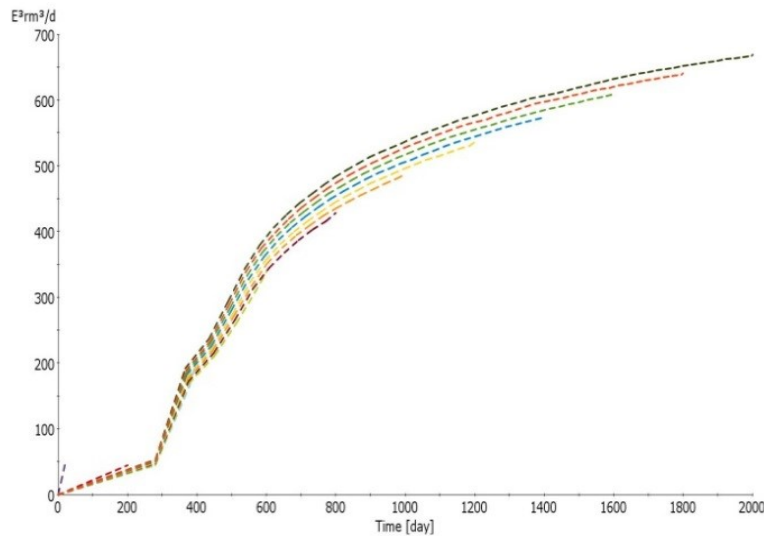


Figure 9-10-Convergence of reservoir gas injection rate by use of Approach 4 in 10 full flight cycles.

## Conclusions

The simulation results showed that for reservoirs with incompressible flow and undrained and linear elastic mechanical problems, there are almost no constraints on the coupling time step, and the coupled flow and geomechanical solutions of the problem can be output at desired user time step. Therefore if a reservoir has low permeability and porosity (undrained split) with an incompressible fluid dominated by convective displacement, the reservoir rock behavior is assumed linear elastic, and the flow displacement problem scales close to linear (such as tracer or immiscible water flood problem) only one cycle of coupling (between initial condition and simulation end time) is sufficient to ensure the converged solution. For the problem of incompressible injection of  $CO_2$  the coupling time step of 1000 days provided almost the same results as 200 and 100 days.

Conducting large number of simulations at progressively increased time steps on both compressible and incompressible fluid flow problems showed that by use of strategy 1, compressible problems report stable behavior and converged solutions at coupling time step of 0.05 PVI and incompressible problems converge at time steps of 0.6-4 PVI. Sensitivity on

the streamline global time steps showed that smaller streamline global time steps (around 0.1 PVI for incompressible problems) lead to larger coupling time step and faster coupled simulation.

A mathematical formulation was developed to provide a guideline for selection of proper SL-based geomechanics coupling time step to ensure solution stability. The mathematical developments showed that in coupled streamline-geomechanics simulations, incompressible undrained problems are unconditionally stable and for compressible drained problems the stability of the system is time dependent and it also depends on the stiffness of the rock matrix (changes in volumetric strain due to pressure changes).

Two different corrector steps within the streamline-geomechanics coupling framework for updating of pressure were developed to mitigate the material balance and enhancement of problem convergence at each coupling strategy. The use of corrector steps depend on the level of compressibility of the problem as well as proximity of reservoir behavior to undrained situation.

## Chapter 10 : Conclusion and Recommendations for Future Studies

### Conclusion

The main goal of this research was investigating the development of methodologies to include geomechanics on a full field scale into reservoir simulation studies of large fields. To meet this objective, three different potential approaches were utilized: 1) Development and use of analytical proxies 2) Development and application of numerical proxies 3) Inclusion of geomechanics into streamline simulation workflow. All three methodologies were developed and tested synthetically or on some case studies. The overall summary for the potential use of each technique in research and practice is as below:

#### 1. Analytical Proxy

- i. An analytical relation was found between temperature front and saturation front in three different scenarios. As saturation front position (or radius of saturated zone by hot water) was known from Buckley-Leverett equation, distance of heated zone was estimated. A numerical simulation of a hot water displacement (core flood) of oil was done and the result of which was in agreement with the developed analytical model.
- ii. As Equation (3-16) suggests, in a downward convective fluid flow ( e.g. hot water flooding in an inclined reservoir), a larger discrepancy between hot water saturation front and temperature front is expected; similarly in an upward convective flow of heat and hot water, the distance between these two fronts is less.
- iii. A domain decomposition approach was used to develop an analytical proxy for full-field geomechanical assessment of reservoir. The domain splitting technique was based on temperature front movement. Effect of geomechanics on frontal movements was assessed and it was shown that inclusion of geomechanics into the model simulation causes the discrepancy between temperature front and saturation front to increase. The mathematical model is exact, and a numerical flow-geomechanics model was made to show that the stress and strain field, out of analytical model is in close agreement with the numerical model. The output of proxy model is stress and strain field prediction in near field and far field as well as prediction of an approximate shape of steamed zone.

- iv. The main concepts behind the analytical model were: domain decomposition, and temperature and saturation frontal discrepancies. As far as to the knowledge of author, there has been no analytical model in literature to obtain the temperature shock frontal velocity and location, purely from heat transport equation, such as Buckley-Leverett for saturation forward convective transport equation. Instead, the temperature front from saturation front at each time during steam injection was obtained.
- v. The analytical model developed can also perform a failure analysis. The model can predict if for instance in ten years of injection with a suggested MOP, there will be any potential for failure in the reservoir or in the caprock or anywhere else (far field or near field in the reservoir).
- vi. The key advantages of the technique can be outlined as follow: the solution of the analytical model is space dependent and as opposed to the previous conventional analytical model (for prediction of geomechanical responses of the reservoir in thermal recovery techniques) , pressure and temperature are not inserted into the model as a domain bulk average value , but are space variant. The analytical model also can be applied to time sensitive scenarios (e.g. no-stationary dynamic models), and therefore can be applied in the cases where the well configuration or well rates and pressure change in time, or to the cases where the non-linear displacement process dictates finer resolution of (geomechanical) results in time. The model can also address the problem of caprock integrity in time and space. The same analytical model that was developed here, can be discretized and used in the development of numerical simulation codes in a three-dimensional space, in order to reduce the computational load and increase memory efficiency.
- vii. In this work, application of domain decomposition technique in the geomechanical domain, provided us the chance to predict displacement and stresses everywhere in the reservoir, based on the sensitive time-varying temperature and pressure fronts. Application of domain decomposition was in good agreement with the physics of the problem, as in reality at each domain different physical processes happen. The use of domain decomposition must be dynamic as the splitting interface moves in space with time.

## 2. Numerical Proxy

- i. A new reduced-order linear localized model (streamline-based proxy) was presented for a highly nonlinear multi-phase flow in underground formations. The proposed model took advantage of streamlines by using information gleaned from streamline trajectories.
- ii. In this work localization method was used to split and categorize the output (state variables) vector of reservoir model. Streamlines were used as an alternative to mathematical techniques to identify the effective region of each local model. A novel linearization method in reservoir modeling was presented based on the density of number of streamlines per grid cell. It was shown that the model which is highly nonlinear in Cartesian or Radial coordinates is linear in streamline-based coordinates, due to the linearity of local models along streamlines. The results of simulation on a synthetic case and comparison with a reference simulator verified the robustness of the method.
- iii. A workflow was suggested to embed geomechanics into the proxy workflow and reduce the order of reservoir-geomechanics coupled system. It was shown that localization can be applied when geomechanics exist, but wave advanced model cannot be applied on geomechanical part of the problem. However the use of localization in the coupled system can be quite helpful in rapid prediction of reservoir dynamic responses. The technique is most suited for the workflows that require successive forward flow and geomechanics simulation such as optimization, ranking, and history matching, or where the dimensions of the model are large.
- iv. Use of the developed proxy allowed to calculate the solution state vectors (pressure and saturation) of the full field reservoir by lunching only one streamline per time step, and as such the method had significant computational cost reduction compared to current reservoir simulators.

## 3. Inclusion of Geomechanics in Streamline Simulation Workflow

- i. Reservoir-geomechanics simulation of underground CO<sub>2</sub> injection in saline aquifers was studied. Geomechanics was introduced as an important piece of physics that is influential in the storage mechanism. Different existing strategies of coupling were introduced. Above that, a novel hydro-mechanical strategy was introduced. Initially we investigated the feasibility of the approach and if the coupling is doable. For that

- purpose, a geomechanical code was developed (based on an existing research open source code) and was linked to a FORTRAN based tool for streamline simulation. Streamline simulation was coupled to an elastic geomechanical code and was shown to be computationally robust and efficient especially for larger reservoirs.
- ii. The main disadvantages associated with streamline-based hydromechanical coupling, are the disadvantages in the streamline simulation, as they are approximate methods. For highly nonlinear systems such as compositional miscible flood simulations, gravity dominant systems, systems with rigorous capillary pressure effects, etc., streamline-based hydromechanical techniques are not expected to provide accurate results. It is expected that the CPU efficiencies achieved by inclusion of geomechanics in streamline simulation, would be reduced by increasing model non-linearity. Furthermore, since streamline simulation deals with a dual-grid system (Cartesian grids to solve pressure and streamline grid to solve saturation equation), the mapping in the streamline workflow between these two grids is associated with some material balance error. However the technique is not associated with numerical solution divergence during iterative simulation, in contrary to traditional coupling techniques. When porosity is significantly updated in traditional coupling schemes, the solution diverges, (forward simulation will be interrupted) and a divergence criterion must be defined for the simulation.
  - iii. The developed SL-based reservoir geomechanics coupling technique was compared to the sequentially coupled and fully coupled FV-FEM (Box method) technique. All three coupling schemes were tested on an underground CO<sub>2</sub> injection case. The comparisons were based on the precision and computational efficiency.
  - iv. Streamline-based hydromechanical coupling showed to be faster (in orders of magnitude) compared to the hydromechanical coupling technique we used for comparison for a model with 1000 grid-cells. The conventional reference approach for comparative study was a finite volume-finite element based hydromechanical technique. An approximate comparative study was performed to check on the robustness of the presented coupling technique. The comparisons showed the results are exact to a good acceptable extent. To generalize the results with respect to performance, one should of course, pursue a systematic investigation of different

- conventional coupling schemes in comparison with the streamline-based approach as proposed here. In either case, this paper showed that it is worth doing it.
- v. The authors expect that the new coupling technique provides even larger computational benefits and more efficient hydromechanical coupling, for larger models with larger number of grid-cells. Also for models with high heterogeneity in petrophysical properties (e.g. porosity and permeability), SL-based hydromechanical coupling is expected to be even more robust compared to conventional coupling approaches. Future sensitivity analysis on these two is required.
  - vi. Inclusion of geomechanics in streamline simulation workflow was shown to be effective in performing large-scale hydromechanical simulation of reservoirs within long simulation time windows. Several different coupling strategies were proposed and designed and advantage of each coupling strategy, its potential added value versus conventional coupling schemes and its application in petroleum engineering were discussed. All the proposed coupling approaches were developed on a QT platform (C++ based programming language) to sequentially or semi-fully implicitly couple 3DSL (streamline simulation tool) to FLAC3D (geomechanical tool). The developed schemes were tested and performed on two numerical cases of compressible and incompressible scenarios.
  - vii. The simulation results on a full-field case showed that inclusion of geomechanics into fluid flow physics processes changes the flow directionality (streamline configuration) as well as local and global stress tensor orientations and consequently may lead to a significant change in final cumulative produced oil (six million barrels of oil within 4000 days of production in the presented simulation case).
  - viii. In order to mitigate the material balance and enhancement of problem convergence, development of corrector steps within the streamline-geomechanics coupling framework for updating of pressure field at each coupling strategy was suggested. The use of corrector steps depend on the level of compressibility of the problem. Also, conducting large number of simulations at progressively increased coupling time steps was required to suggest a guideline for selection of time step sizes to ensure a converged and stable coupled solution on both compressible and incompressible fluid flow problems.



- ix. Approach 3 (staggered scheme) presented in **Chapter 8** exhibited the largest CPU run time compared to the other approaches, but resulted always in the converged solution. In both compressible and incompressible test cases, Approach 3 showed a converged solution after second inner cycle; therefore to avoid large CPU run time, increasing number of inner cycles (more than two or three) is not suggested. Approach 3 (with five inner cycles) and Approach 2 showed approximately close simulation results within 4000 days of coupled simulation, at a small coupling time step size of 100 days.
- x. All the coupling strategies showed almost the same reservoir stress path and displacement profile in time in the middle of the reservoir, but Approach 1 (one way coupling) exhibited slightly different stress path, but significant displacement profile. The latter conclusion signifies the use of coupled hydromechanical systems for prediction of dynamic and mechanical responses of the reservoir.
- xi. The scaling behavior of streamline-based reservoir geomechanics (Approach 2) CPU run time as a function of active grid blocks is close to linear. Therefore streamline-based geomechanics coupling is the method of choice for prediction of hydromechanical responses of large heterogeneous reservoirs with large number of cells (more than 250,000). The linear scaling behavior means the computational load for larger number of grid cells (e.g. multimillion cells) can be extrapolated from CPU run time of the coarse model with small number of cells. The other important conclusion is that the computational load is much less than the computational load of FD simulators that increase in a polynomial behavior with increasing number of active cells like  $N^{2 \rightarrow 3}$  where N is the number of active grid blocks.
- xii. The simulation results showed that for reservoirs with incompressible flow and undrained and linear elastic mechanical problems, there are almost no constraints on the coupling time step, and the coupled flow and geomechanical solutions of the problem can be output at desired user time step. Therefore if a reservoir has low permeability and porosity (undrained split) with an incompressible fluid dominated by convective displacement, the reservoir rock behavior is assumed linear elastic, and the flow displacement problem scales close to linear (such as tracer or immiscible water flood problem) only one cycle of coupling (between initial condition and simulation end time) is sufficient to ensure the converged solution. For the problem

- of incompressible injection of CO<sub>2</sub> the coupling time step of 1000 days provided almost the same coupling results as 200 and 100 days.
- xiii. Conducting large number of simulations at progressively increased time steps on both compressible and incompressible fluid flow problems showed that Approach 2, for compressible problems exhibits stable behavior and converged solution at the coupling time step of 0.05 PVI and for incompressible problems Approach 2 shows a converging time step of 0.6-4 PVI. Sensitivity on the standalone streamline global time steps showed that smaller global time steps on streamline side (around 0.1 PVI for incompressible problems) allows using larger coupling time steps and faster coupled simulation.
  - xiv. A mathematical formulation was developed to provide a guideline for selection of proper SL-based geomechanics coupling time step to ensure solution stability. The mathematical developments showed that in coupled streamline-geomechanics simulations, incompressible undrained problems are unconditionally stable and in compressible drained problems the stability of the system is time dependent. The stability of drained split SL-based coupling also depends on the stiffness of the rock matrix (leading to changes in volumetric strain due to pore pressure changes).
  - xv. Two different corrector steps within the streamline-geomechanics coupling framework for updating of pressure were developed to mitigate the material balance and enhancement of problem convergence at each coupling strategy. The use of corrector steps depend on the level of compressibility of the problem as well as proximity of the reservoir behavior to undrained situation.

### Suggestions for Future Studies

In this research, the scaling behaviour of the coupling system was assessed by increasing the number of grid cells for Approach 2 (described in **Chapter 8**) and was shown to be linear. However, the large and computationally crucial simulation runs could not be performed with increased number of cells (up to 2 millions) for other four coupling strategies. We therefore suggest doing investigation on the scaling behaviour of other coupled systems for future studies.

In **Chapter 4**, the analytical proxy was developed for a uniaxial geometry (with PDEs defined in a one-dimensional Cartesian coordinate), and the model was developed for rocks

with linear elastic constitutive rock behavior. To obtain the reservoir geomechanical responses with more precisions for more challenging scenarios, we suggest extending the model for plastic constitutive behaviors in radial geometry.

The findings of **Chapter 8** and **Chapter 9** can be used to develop a “geomechanical approach for streamline-based history matching problem”. This is a smart automated assisted history matching workflow for reservoirs with large number of cells and stress sensitive rocks. We suggest continuing the work of Caers (2004), and Wang and Kovscek (2000) to update petrophysical properties of the reservoir locally to match the observed data with history on both field and well level. The suggested workflow however suggests updating of reservoir MEM properties (stiffness and Poisson’s ratio) as well, to have a physically more meaningful history matching with more retainable predictive power.

## References

- 3DSL User Manual v.4.10, 2013, Calgary: StreamSim Technologies
- A.S.Emanuel and W.J.Milliken, 1998, “History Matching Finite Difference Models with 3D streamlines”, paper SPE 4900, SPE ATCE, and New Orleans 27-30 September.
- Ács, G., Doleschall, S., and Farkas, E. 1985, “General Purpose Compositional Model,” SPE J.,25 (4), 543–553. SPE-10515-PA, doi: 10.2118/10515- PA.
- Atkin, R.J. and Craine, R.E., 1976, “Continuum theories of mixtures: basic theory and historical development”, Q. J. Mech. Appl. Math., 29, 209-244.
- Bachu S., Bennion DB. 2009, “Experimental assessment of brine and/or CO<sub>2</sub> leakage through well cements at reservoir conditions,” Int J Greenh Gas Control 3:494–501.
- Bachu S., Bonijoly D., Bradshaw J., Burruss R., Holloway S., Christensen N.P., Mathiassen O.M. 2007, “CO<sub>2</sub> storage capacity estimation: Methodology and gaps,” International Journal of Greenhouse Gas Control 1: 430-443.
- Batycky, R. P., Blunt, M. J., and Thiele, M. R., 1997, “A 3D Field-Scale Streamline-Based Reservoir Simulator,” SPE Reservoir Engineering, 12(4):246–254.
- Batycky, R. P.; Blunt, M. J. and Thiele, M.R., 1996 “A 3D Field-Scale Streamline Simulator With Gravity and Changing Well Conditions”, paper SPE 36726 proceedings of the 1996 SPE Reservoir Simulation Symposium, Denver, Colorado, U.S.A., Feb 6-9.
- Batycky, R.P., 1997, “A Three-dimensional Two-phase Scale Streamline Simulator,” PhD dissertation, Department of Petroleum Engineering, Stanford University, Stanford, California (January 1997)
- Datta-Gupta, A. and King, M.J., 2007,”Streamline simulation: theory and practice,” Textbook Series, SPE, Richardson, Texas.
- Datta-Gupta, A., Lake, L. W., Pope, G. A. and King, M. J., “A Type Curve Approach to Analyzing Two-Well Tracer Tests, “ SPE Formation Evaluation, 10 (1), .40-48, 1995.
- Drucker, D. C. and Prager, W. 1952, “Soil Mechanics and Plastic Analysis for Limit Design,” Quarterly of Applied Mathematics, vol. 10, no. 2, pp. 157–165.

- Batycky, R.P., Blunt, M. J., and Thiele, M. R., 1997, "A 3D Field – Scale Streamline-Based Reservoir Simulator," SPE Reservoir Engineering, pp.246-254, Volume 12, Number 4.
- Bear J. 1972, "Dynamics of Fluids in Porous Media," American Elsevier Publishing Company.
- Bedrikovetsky, P., 1993 "Mathematical Theory of Oil and Gas Recovery: With applications to ex-USSR oil and gas fields", ISBN:0792323815.
- Benson S.M., Cole D.R. 2008 , "CO<sub>2</sub> sequestration in deep sedimentary formations," Elements 4:325–331.
- Beraldo, V. T.; Blunt, M. J. and Schiozer, D. J., 2006 "Development of a 2D Streamline Simulator for Incompressible Fluids with Horizontal Variation on Oil Density", proceedings of the Rio Oil & Gas Expo and Conference 2006, Rio de Janeiro, Brazil, Sep 11-14.
- Bickle M.J. 2009, "Geological carbon storage," Nature Geosci2:815–819.
- Biot, M., A. 1940 "General Theory of Three-Dimensional Consolidation," J. Appl. Phys., Vol. 12, 155-164.
- Biot, M.A., 1955, "Theory of Elasticity and Consolidation for a Porous Anisotropic Solid," J. Appl. Phys. 26, 182-185.
- Boberg, T.C. and Lantz, R.B. 1966, "Calculation of the Production Rate of a Thermally Stimulated Well," Journal of Petroleum Technology, 1613-23.
- Bommer, M.P. and Schechter, R.S. 1979, "Mathematical Modeling of In-Situ Uranium Leaching," SPE Journal, 393.
- Bower KM, Zyvoloski.G 1997, "A numerical model for thermohydro- mechanical coupling in fractured rock," Int J Rock Mech Min Sci 34:1201–1211
- Buckley, S.E., and Leverett, M.C., 1942, "Mechanism of Fluid Displacement in Sands," SPE 942107-G, 1942 .Petroleum Transactions, AIME, Volume 146, pages 107-116.
- Butler, R.M., 2004. Thermal Recovery of Oil and Bitumen, 4th Printing. Calgary: GravDrain Inc.

- Caers, J. 2005, "Petroleum Geostatistics," SPE Textbook Series, Society of Petroleum Engineers, 104 pp, ISBN: 978-1-55563-106-2.
- Caers, J., Gross, H., and Kovscek, A.R., 2004, "Direct sequential Simulation Approach to Streamline-Based History Matching," Stanford University, CA., 2004
- Caers, J., Krishnan, S., Wang, Y., and Kovscek, A. R., 2002, "A geostatistical Approach to Streamline- Based History Matching," SPE Journal, 7(3):250–266.
- Caers, J. 2003, "Efficient gradual deformation using a streamline-based proxy method," 2003, Journal of Petroleum Science and Engineering 39, 57– 83
- Cardoso, M.A., Durlofsky, L.J., and Sarma, P., 2009, "Development and application of reduced-order modeling procedures for subsurface flow simulation," International journal for numerical methods in engineering, Volume 77, pp.1322-1350.
- Cardoso, M.A., Durlofsky, L.J., 1959" Linearized reduced-order models for subsurface flow simulation," Journal of Computational Physics, Volume 229, pp.681-700, (2010).
- Carslaw, H.S., Jaeger, J.C., Conduction of Heat in Solids, Oxford University Press.
- Cassis, R., Fuller, N., et al., 1985 "Specific Heat Capacities of Bitumens and Heavy Oils, Reservoir Minerals, Clays, Dehydrated Clays, Asphaltenes and Cokes.," AOSTRA Journal of Research, 1(3) pp.163-173.
- Chalaturnyk R.J., 2007, "Geomechanical characterization of the Weyburn field for geological storage of CO<sub>2</sub>," 1st Canada-US rock mechanics symposium Vancouver, Canada, 27– 31 May 2007.
- Chalaturnyk, R.J. 1996, "Geomechanics of the steam-assisted gravity drainage process in heavy oil reservoirs," Ph.D. dissertation. University of Alberta, 576p.
- Chalaturnyk, R.J., and Li, P. 2004, "When is it important to consider geomechanics in SAGD operations?" Journal of Canadian Petroleum Technology. 43(4): 53-61.
- Chandra, S. and Mamora, D.D. 2005, "Improved Steamflood Analytical Model," SPE/PS-CIM/CHOA International Thermal Operations and Heavy Oil Symposium, Calgary, Alberta, Canada.

- Chi-tsong Chen, 1999, "Linear System Theory & Design," 3d ed., Oxford university press, pp.76-77.
- Coussy O. ,1995," Mechanics of Porous Continua," Chichester, England: John Wiley & Sons
- Cristescu, N. (Ed.), 1989 "Rock Rheology," Dordrecht; Boston; London: Kluwer Academic Publishers, Mechanics of Elastic and Inelastic Solids, 7 Series.
- Crochet, M.J. and Naghdi, P.M., 1966, "On constitutive equations for flow of fluid through an elastic solid", Int. J. Engng. Sci., 4, 383-401.
- Dake, L.P., 1998 "Fundamentals of Reservoir Engineering," Elsevier Science B.V., ISBN 0-444-41830-X.
- Darcis, M., 2012, "Coupling Models of Different Complexity for the Simulation of CO<sub>2</sub> Storage in Deep Saline Aquifer," Mitteilungsheft des Instituts für Wasserbau Nr. 218-Institut für Wasser- und Umweltsystemmodellierung, Universität Stuttgart.
- Datta-Gupta, A., 2000, "Streamline simulation: A Technology Updated," SPE Distinguished Author Series, Journal of Petroleum Technology, pp.68-73.
- Datta-Gupta, A. and King, M.J. 2007, "Streamline simulation: theory and practice," Textbook Series, SPE, Richardson, Texas.
- David Gratton, Reduced order, trajectory piecewise-linear models for nonlinear computational fluid dynamics, Master of Science thesis, Massachusetts Institute of Technology, (2004).
- Detournay, E. and Cheng, A.H-D., 1991, "Plane strain analysis of a stationary hydraulic fracture in a poroelastic medium", Int. J. Solids Struct., 37, 1645-1662.
- Detournay, E., Cheng, A.H-D., Roegiers, J-C., McLennan, J.D., 1989, "Poroelasticity considerations in in situ stress determination by hydraulic fracturing," Int. J. Rock Mech. Mining Sci. Geomech. Abstr., 26, 507-513.
- Doyen, P.M. 2007, "Seismic Reservoir Characterization: An earth modeling perspective," Houten, Netherlands, EAGE publication, BV, 255 p.

- Due, H., Chang, Y., Yu, J., Wang, X., Ma, Y., 2007, "A New Mathematics Model and Theory for Heavy-Oil Reservoir Heating by Huff'n' Puff," SPE 106234, Latin America and Caribbean Petroleum Engineering Conference, Buenos Aires, Argentina, 15-18 Nov.
- Elkin Arroyo-Negrete, Deepak Devegowda, and Akhil Datta-Gupta, 2006 "Streamline Assisted Ensemble Kalman Filter for Rapid and Continuous Reservoir Model Updating", SPE 104255.
- Farouq, A., et al., 1970 "Oil Recovery by Steam Injection," Bradford PA: Producers Publication Co. Inc.,.
- Fenwick, D., Batycky, R., and Thiele, M. 2007, "Streamline-Based History Matching." 9th International Forum on Reservoir Simulation, Abu Dhabi, United Arab Emirates, Dec. 9th-13th, 2007.
- Fjær, E., Horsrud, P., Raaen, A.M., Risnes, R., Holt A.M., 2008 "Petroleum Related Rock Mechanics," (Developments in Petroleum Science), Elsevier Publication.
- FLAC 3D v.5.0 (Fast Lagrangian Analysis of Continua in 3 Dimensions), 2013, Minneapolis, Itasca Consulting Group.
- FrontSim Technical Description, v.2008.1, 2008, Abingdon, Schlumberger.
- Geertsma, J. 1957, "The Effect of Fluid Pressure Decline on Volumetric Changes of Porous Rocks," Trans. AIME 210, 331-340.
- Goerke U.J., Park C.H., Wang W., Singh A.K., Kolditz O. 2011, "Numerical simulation of multiphase hydromechanical processes induced by CO<sub>2</sub> injection into deep saline aquifers," Oil Gas Sci Technol Rev IFP 66:105–118
- Gorell, S., and Bassett, R. 2001, "Trends in Reservoir Simulation: Big Models, Scalable Models? Will you please make you Mind?" paper SPE #71596 in proceedings of the 2001 ATCE, New Orleans, LA.
- Gross H., 2003, "History Matching Multiple Attributes with Streamlines and Statistics," SPE.
- Gross, H., Thiele, M.R., Alexa, M.J., Caers, J., and Kovscek, A.R. 2004, "Streamline-Based History Matching Using Geostatistical Constraints: Application to a Giant, Mature Carbonate Reservoir," Society of Petroleum Engineers."



- Gunter W.D., Bachu S., Benson S.M. 2004, "The role of hydrogeological and geochemical trapping in sedimentary basins for secure geological storage for carbon dioxide," In: Baines SJ, Worden RH (eds) Geological storage of carbon dioxide.
- Gunter W.D., Bachu S., Benson S.M. 2004. The role of hydrogeological and geochemical trapping in sedimentary basins for secure geological storage for carbon dioxide. In: Baines SJ, Worden RH (eds) Geological storage of carbon dioxide.
- Gutierrez.M., and Lewis. R. W., 1998."The Role of Geomechanics in Reservoir Simulation," SPE/IRSM 47392, Proc. Eurock 98 (2) 439–448, Trondheim.
- Haimson, B.C. and Fairhurst, C. 1969, "Hydraulic fracturing in porous-permeable materials," J. Pet. Tech., July, 811-817.
- Jaeger, J.C., Cook, N.G.W., Zimmerman, R.W., 2007" Fundamentals of Rock Mechanics," fourth ed. Blackwell Publishing
- Jesmani M., Koohmarch Hosseini, B., and Chalaturnyk J. 2012, "A Streamline Approach to Linearize and Reduce the Order of Reservoir Model," Ninth International Geostatistics Congress, Oslo, Norway.
- Jones, J. 1981, "Steam Drive Model for Hand-Held Programmable Calculators," J. Pet. Tech. 1583-1598.
- K. Aziz, A. Settari, 1986 "Fundamentals of Reservoir Simulation", Elsevier Applied Science Publishers.
- Kelkar, M., and Prez, G. 2002, "Applied Geostatistics for Reservoir Characterization,"
- Kim J., Tchelepi H.A. and Juanes R. 2011, "Stability, Accuracy, and Efficiency of Sequential Methods for Coupled Flow and Geomechanics," SPE Journal, 119084-PA.
- Kirsch, 1898 "Die Theorie der Elastizität und die Bedürfnisse der Festigkeitslehre," Zeitschrift des Vereines deutscher Ingenieure 42,797–807.
- Koohmarch Hosseini, B., Ardali, M., Chalaturnyk, R.J., Mamora, D., 2011" A New Analytical Approach To Investigate Heated Area in Thermal Recovery Techniques," SPE CSUG/SPE 148836 presented at Canadian Unconventional Resources Conference, Calgary, Alberta, Canada, 15-17 November 2011.

- Koohmarch Hosseini, B., Chalaturnyk, R.J. 2012, "Effect of reservoir local heterogeneity on viscous fingering of heavy oil reservoirs," World Heavy Oil Congress 2012, Aberdeen, Scotland, WHOC12-323.
- Koohmarch Hosseini, B., Chalaturnyk, R.J., 2014, "Streamline-based Reservoir Geomechanics Coupling Strategies for Full Field Simulations", presented at ECMOR-XIV 2014, Catania, Italy.
- Koohmarch Hosseini, B., Chalaturnyk, R.J. 2013, "Streamline Based Coupled Geomechanics and Reservoir Simulation for Hydromechanical Modeling of CO<sub>2</sub> Storage in Saline Aquifers", SPE Heavy Oil Conference - SPE-165409., Canada, Jun 11 - 13, 2013.
- Koohmarch Hosseini, B., R.J. Chalaturnyk, University of Alberta, 2014, "A Domain Splitting-Based Analytical Model for Rapid Assessment of Hydro-thermo-geomechanical Responses of Large Scale Heavy oil Reservoirs: Steamflood Application", 14HOCC- SPE-170193 2014 SPE Heavy Oil Conference – Canada.
- Koohmarch Hosseini, B., Chalaturnyk, R.J., 2013, "On Use of Streamlines for Reservoir Fluid Flow-Geomechanics Coupling: Current Technical Evolutions, and Future Opportunities," international workshop on geomechanics and energy, EAGE, Switzerland, DOI: 10.3997/2214-4609.20131968, Nov 2013.
- Koohmarch Hosseini, B., R.J. Chalaturnyk, University of Alberta, 2013, "Inclusion of Geomechanics in Streamline Simulation for Full-Field Hydromechanical Modeling of Underground CO<sub>2</sub> Storage", presented at ARMA-47th U.S. Rock Mechanics Geomechanics Symposium, June 2013 San Francisco, US . Paper ID No. 631.
- Kovscek, A. R. and Y. Wang. 2005, "Geologic Storage of Carbon Dioxide and Enhanced Oil Recovery I: Uncertainty Quantification Employing a Streamline-Based Proxy for Reservoir Simulation," Energy Conversion and Management, 46(11-12), 1920-1940
- Kovscek, A. R. and Y. Wang. 2005. "Geologic Storage of Carbon Dioxide and Enhanced Oil Recovery I: Uncertainty Quantification Employing a Streamline-Based Proxy for Reservoir Simulation," Energy Conversion and Management, 46(11-12), 1920-1940.
- Lake, L.W., 1989 , "Enhanced Oil Recovery," first edition Prentice Hall, Englewood Cliffs, New Jersey.

- Lee, W.J. 1982, "Well Testing," Dallas, Texas: Textbook Series, SPE.
- Lewis, R.W. and Schrefler, B.A., 1978, "The Finite Element Method in the Deformation and Consolidation of Porous Media, Wiley.
- Li, X.S. 2005, "An Overview of SuperLu: Algorithms, Implementation, and User Interface," ACM Transactions on Mathematical Software (TOMS) 31 (3): 302–325. doi: 10.1145/1089014.1089017.
- Longuemare, Mainguy, P., Lemonnier, P., Onaisi, A., Gérard, .Ch and Koutsabeloulis, N., 2002, "Geomechanics in Reservoir Simulation: Overview of Coupling Methods and Field Case Study," Oil and Gas Science Technology
- Maciejowski, J.M., 1989, "Multivariable Feedback Design," Addison Wesley, pp-76-80.
- Mainguy, M., Longuemare, P., 2002, "Coupling fluid flow and rock mechanics: formulations of the partial coupling between reservoir and geomechanical simulators" Oil Gas Sci. Technol. 57 (4), 355–367.
- Mandl, G. and Volek, C.W., 1969, "Heat and Mass Transport in Steam Drive Processes," SPE. J. 59-79; Trans, AIME, 246.
- Marx, J.W., Langenheim, R.H. 1959, "Reservoir Heating by Hot Fluid Injection," SPE 312315, AIME,.
- Minkoff, S. Mike Stonez, C., Bryant, S. and Peszynska, M. 2004, "Coupled geomechanics and flow simulation for time-lapse seismic modeling." Geophysics, Vol. 69, No. 1, January pp. 200–211
- Myhill, N.A. and Stegemeier, G.L. 1978, "Steam-Drive Correlation and Prediction," J. Pet.Tech, 173-182, February.
- Nævdal, G., Johnsen L.M., Aanonsen S.I., Vefring E.H., 2005, "Reservoir monitoring and continuous model updating using ensemble Kalman filter", SPE Journal, Volume 10, Number 1, pp. 66-74.
- Norton, J.P., 1986, "An introduction to identification," ACADEMIC PRESS INC., Orlando, Florida.

- Nukhaev M., Pimenov V., Shandrygin A., Tertychnyi V., 2006, “A New Analytical Model for the SAGD Production Phase,” SPE 102084, ATCE held in San Antonio, USA, 24-27.
- Ojagbohunmi, S., Chalaturnyk, R.J., Leung, J., 2012., “Coupling of Stress-Dependent Relative Permeability and Reservoir Simulation,” SPE 154083-MS.
- Osako, I., Datta-Gupta, A. and King, M.J. 2004 “Timestep Selection During Streamline Simulation Through Transverse Flux Correction.” SPEJ 9, No.4, 459-464.
- Ouellette A, Be'rard T., Desroches T.J., Frykman P., Welsh P, Minton P.J., Pamukcu Y., Hurter S., Schmidt Hattenberger C. 2011,”Reservoir geomechanics for assessing containment in CO<sub>2</sub> storage: a case study at Ketzin, Germany,”. Energy Procedia 4:3298–3305.
- Peir’o, J., Sherwin, S. 2005, “Finite difference, finite element and finite volume methods for partial differential equations,” Department of Aeronautics, Imperial College, London, UK, Handbook of Materials Modeling. Volume I: Methods and Models, 1–32.\_c 2005 Springer.
- Qi. R., LaForce., T.C., Blunt., M. 2009, “A three-phase four component streamline-based simulator to study carbon dioxide storage,” Computational Geosciences , Volume 13, Issue 4, pp 493-509
- Reis L. C., 1992, “A steam Assisted Gravity Drainage Model for Tar Sands: Linear Geometry,” JCPT 13(10), December 1992.
- Renato Markovinovi’c, 2009,”System-Theoretical Model Reduction for Reservoir Simulation and Optimization”, PhD thesis, Delft University.
- Rewienski, M., 2003, “A Trajectory Piecewise Linear Approach to Model Order Reduction of Nonlinear Dynamical Systems,” PhD Thesis, Dep. Of Electrical Engineering and Computer Science, MIT.
- Risnes, R., Bratli, R., Horsrud, P. “Sand stresses around a borehole” 1982, SPE. J. 22, 883–898.
- Roscoe, K.H., Schofield. A.N., and Wroth A.N, 1958, “On the yielding of soil,” Geotechnique 8, 22-53.

- Rothenburg, L., Obah, A., 1995, "Horizontal ground movements due to water abstraction and formation of earth fissures", Fifth International Symposium on Land Subsidence, IAHS Publ no. 234, 1995.
- Rudnicki, J.W. and Hsu, T.-C., 1988, "Pore pressure changes induced by slip on permeable and impermeable faults", *J. Geophys. Res.*, 93, 3275-3285, 1988.
- Ruina, A., 1978, "Influence of coupled deformation-diffusion effects on the retardation of hydraulic fracture", *Proc. 19th U.S. Rock Mech. Symp.*, 274-282, 1978.
- Rutqvist J., 2012, "The Geomechanics of CO<sub>2</sub> Storage in Deep Sedimentary Formations," *Geotech Geol Eng.* DOI 10.1007
- Rutqvist, J., Stephansson, O., 2003, "The role of hydromechanical coupling in fractures rock engineering," *Hydrogeol. J.* 11, 7–40.
- Rutqvist, J., Tsang, C. 2002, "A study of caprock hydromechanical changes associated with CO<sub>2</sub>-injection into a brine formation". *Environmental Geology*, 42:296–305.
- Rutqvist, J. 2011," Status of the TOUGH-FLAC simulator and recent applications related to coupled fluid flow and crustal deformations" *Comput Geosci* 37:739–750
- Settari, A. and Nghiem, L. 2004, "New Iterative Coupling Between a Reservoir Simulator and a Geomechanics Module," paper SPE 88989.
- Settari, A., Walters, D.A., 1999, "Advances in coupled geomechanical and reservoir modeling with applications to reservoir compaction," *SPE Reservoir Simulator Symposium*, Houston, Texas.
- Spivak, A., Coats, K.H., 1970," Numerical Simulation of Coning Using Implicit Production terms," *SPEJ* 10, No.3, 257-267.
- Stüben, K. 2001, "An Introduction to Algebraic Multigrid," In *Multigrid*, ed.U. Trottenberg, C.W. Oosterlee, and A. Schüller, Appendix, 413–532. , London: Academic Press.
- T.A. Johansen and B.A. Foss, "Empirical modeling of a heat transfer process using local models and interpolation", *Journal of American control conference* Seattle, 1995. - 3654-3658.
- Thiele, M.R., Batycky, R.P., Blunt, M.J., and Orr, F.M. Jr.; "Simulating Flow in Heterogeneous Media Using Streamtubes and Streamlines," *SPERE* (February 1996) 5.

- Thiele, M. R.: 2001 , “Streamline Simulation”, proceedings of the 6th International Forum on Reservoir Simulation, Schloss Fuschl, Austria, Sep 3-7.
- Thiele, M.R., Batycky, R.P., and Fenwick, D.H. 2010, “Streamline Simulation for Modern Reservoir-Engineering Workflows.”
- Thiele, Marco R., Batycky, Rod P., Blunt, Martin J, 1997 “A Streamline-Based 3D Field-Scale Compositional Reservoir Simulator” SPE Annual Technical Conference and Exhibition, San Antonio, Texas, 5-8 October 1997.
- Toselli A., Widlund O.B., 2005 “Domain Decomposition Methods Algorithms and Theory,” Springer Series in Computational Mathematics 34.,
- Touhidi-Baghini, A. 1998, ”Absolute permeability of McMurray formation oil sands at low confining stresses.” *Ph.D* dissertation. Department of Civil Engineering, University of Alberta, 339 p.
- Tran, D., Settari, A., Nghiem, L., 2004, ”New iterative coupling between a reservoir simulator and a geomechanics module,” in SPE Journal, SPE/ISRM Rock Mechanics Conference, Irving, Texas, USA, October 20–23.
- Van Genuchten., M.Th., 1980, “A closed-form equation for predicting the hydraulic conductivity of unsaturated soils” *Soil Sci. Soc. Am. J.*, 44:892–898.
- Vasilyev,D., Rewienski,M., and White,J., 2003 “A TBR-based Trajectory Piecewise Linear Algorithm for Generating Accurate Low-Order Models for Nonlinear Analog circuits and MEMS”, *Chemical Engineering Science*, DAC, pp.490-495.
- Veil, J.A., Quinn, J.J., 2008, “Water Issues Relating to Heavy Oil Production,” SPE Americas E&P Environmental and Safety Conference, 23-25 March 2009, San Antonio, Texas.
- Vosteen, H-D., Schellschmidt, R., 2003, “Influence of temperature on thermal conductivity, thermal capacity and thermal diffusivity for different types of rock,” *Physics and Chemistry of the Earth* 28 (2003) 499–509.
- Wang, H.F., 2000, “Theory of Linear Poroelasticity. Princeton University Press, Princeton.”
- Wang, Y., and Kovscek, A. R. 2000, “Streamline Approach for History Matching Production Data,” *SPE Journal*, 5(4):353–362.

- White D., 2009, "Monitoring CO<sub>2</sub> storage during EOR at the Weyburn-Midale field," *Lead Edge* 28:838–842.
- Willien, F., Faille, I., Shneider, F., 1996 "Domain decomposition methods applied to sedimentary basin modelling," *ECMOR*.
- Witelski, T., Bowen, M., 2009, "Singular perturbation theory," *Scholarpedia*, 4(4):3951.
- Zienkiewicz, O.C., Chan, A. H. C., Pastor, M., Schrefler, B. A. and Shiomi, T. 1999,"*Computational Geomechanics with Special Reference to Earthquake Engineering*," John Wiley and Sons.

### Appendix 3-A: Development of Equation (3-15), and (3-16) for Gravitational Flow of Heat and Hot Water

Transport equation in gravitational form is as follow:

$$\frac{\partial S_w}{\partial t} + U_w \frac{\partial G(S_w)}{\partial z} = 0 \quad (3-33)$$

where  $z$  is the distance and  $G(S_w)$  is the gravitational fractional flow function. The equation of fractional flow when gravity is included in the model can be written as:

$$G(S_w) = F(S_w) + \beta R(S_w) = F(S_w)(1 + \beta k_{r0}), \quad (3-34)$$

where  $F(S_w)$  is the same as Equation (2-12) for fractional flow for horizontal case,  $k_{r0}$  is oil relative permeability and  $\beta$  is the gravity number which can be defined as :

$$\beta = \frac{gk(\rho_w - \rho_o)\sin\alpha}{\mu_o V}, \quad (3-35)$$

and  $R(S_w)$  is a function which represent the contribution of gravity to flow and is expressed as:

$$R(S_w) = F(S_w)k_o \quad (3-36)$$

The (+) sign in Equation (2-35) is applied for descending flow and (-) is for ascending flow. By writing the mass balance at the hot water saturation front and imposing Hugoniot-Rankin condition, the water front velocity can be obtained and is written as:

$$U_{f_{sw}} = U_f F'(S_w)(1 \pm \beta k_o) \quad (3-37)$$

### Appendix 3-B: Development of Equation (2-14) for a Radial Geometry

For a radial, horizontal system where the wetting phase is displacing non-wetting fluid towards the periphery of the system, we can write the equation of Buckley-Leverett as:

$$\emptyset \pi h [r^2(t) - r^2(0)] = [Q(t) - Q(0)] \frac{dF_w}{dS_w}, \quad (3-38)$$

where

$r(t)$  : radius of saturated zone by hot water at time  $t$

$Q(t)$  : the cumulative injected volume into the reservoir at time  $t$  .Assuming:



$$r(0) = r_w \quad (3-39)$$

$$Q(0) = 0,$$

then

$$r^2(t) = r_w^2 + \frac{Q(t)}{\phi \pi h} \frac{dF_w}{ds_w} \quad (3-40)$$

Combining Equation (3-40) and Equation (3-8) leads to the following relation:

$$\frac{(r^2(t) - r_w^2)\xi}{r^2(t)F'(s_w)} = U_T \quad (3-41)$$

### Appendix 3-C: More Detailed Calculation of Temperature Front (Extension to (3-7))

The more detailed version of Equation (3-7) can be written as follow:

$$\frac{\partial[\rho_w E_w \phi S_w + \rho_o E_o \phi S_o + \rho_s E_s (1 - \phi)]}{\partial t} = -\frac{1}{A} \frac{\partial}{\partial x} (\rho_w E_w q_T F_w + \rho_o E_o q_T F_o) \quad (3-42)$$

Under the assumption of no-dispersion and incompressible linear displacement ( $\rho, q_T = \text{cte}$ ), and assuming enthalpy is linear in temperature, Equation (3-42) can be rearranged to :

$$[\rho_w E_w \phi S_w + \rho_o E_o \phi S_o + \rho_s E_s (1 - \phi)] \left( \frac{dL_T}{dt} \right) = -\frac{q_T}{A} (F_w E_w + F_o E_o) \quad (3-43)$$

; and

$$\frac{dL_T}{dV} = \frac{\phi(F_w C_{pw} + F_o C_{po})}{\phi(C_{pw} S_w + C_{po} S_o) + C_{ps}(1 - \phi)} \quad (3-44)$$

; where  $V$  is the volume injected and  $L(X)$  is the pore volume (travelled by fluid) and are defined as follow :

$$V(t) = \int q_T dt, \quad X(x) = \int A \phi dx. \quad (3-45)$$

Therefore with uniform initial condition and water injection at  $x = 0$  (wellbore):

$$X(x) = V(t)F'_w(S_w). \quad (3-46)$$

By treating  $S_w$  as the independent variable and taking derivation of Equation (3-46) with respect to  $V(t)$ , we can obtain the solution to Equation (3-44) (considering that  $X = L_T(V)$ , which is the distance travelled by injected volume  $V$ ) :

$$\frac{dL_T}{dV} = F'_w(S_w) + V(t)F''_w(S_w) \frac{dS_w}{dV} = \frac{\phi(F_w C_{pw} + F_o C_{po})}{\phi(C_{pw} S_w + C_{po} S_o) + C_{ps}(1-\phi)} \quad (3-47)$$

And alternatively:

$$\frac{dS_w}{d(\ln V)} F''_w = -F'_w + \frac{\phi(F_w C_{pw} + F_o C_{po})}{\phi(C_{pw} S_w + C_{po} S_o) + C_{ps}(1-\phi)}. \quad (3-48)$$

For the case of two-phase convective tracer equation, (where concentration  $C(x, t)$  is replaced with  $T(x, t)$  in the general form of transport equation), the form of the solution to Equation (3-48) is as below:

$$\frac{dS_w}{d(\ln V)} F''_w = -F'_w + \frac{F_w}{S_w} \quad (3-49)$$

; where  $\frac{F_w}{S_w}$  is the derivation of the fractional flow at saturation shock front. If tracer is introduced late in the flood (where  $-F'_w$  is small), then tracer jump moves faster than saturation front, and when tracer is introduced with initial water, derivation of fractional flow is large and  $F'_w > \frac{F_w}{S_w}$ , and therefore tracer front falls back from the saturation shock front.

With the same analogy to temperature equation, when the change in temperature is introduced in the early stage of flooding with the hot water injection (as it is the case in hot waterflooding), then temperature front falls back from the saturation front as the right-hand-side of Equation (3-48) is negative.

#### Appendix 4-A: Why $\epsilon$ (if $\epsilon \rightarrow 0$ ) Can Be Omitted from an Equation?

Consider the following equation:

$$\epsilon x^2 + x + 1 = 0; \quad (4-50)$$

where  $\epsilon$  is a very small number close to zero. The general form of the solution is:

$$x_{1,2} = \frac{-1 \pm \sqrt{1-4\epsilon}}{2\epsilon}. \quad (4-51)$$

One of the roots of the equation is  $x = -1$ , if  $\epsilon$  is a very small number can be neglected under square root of the term  $(1 - 4\epsilon)$ . Obviously if we had omitted  $\epsilon$  from the original

form of the equation, the solution to the problem of  $x + 1 = 0$  would have been  $x = -1$ . Now one can replace  $\varepsilon$  back into the equation, and obtain the second root of the equation as below:

$$\frac{\varepsilon x^2 + x + 1}{(x+1)} = (\varepsilon x - \varepsilon + 1) + \frac{\varepsilon}{x+1}. \quad (4-52)$$

Therefore another root of the problem is approximately  $(\varepsilon x - \varepsilon + 1)$  which was obtained by replacing  $\varepsilon$  back into the original form of the equation, even though it was initially an infinitesimal number and was omitted from the equation.

#### **Appendix 4-B: How Boundary and Initial Conditions Can be Applied after Solution of ODE?**

Consider an ordinary second order differential equation of the form below:

$$y'' + \alpha y' + \beta y = f; \quad (4-53)$$

where  $f$  is the boundary value of the equation( equivalent to body force in equilibrium equation), and the initial conditions of the problem are known :

$$\begin{cases} y'(0) \\ y(0) \end{cases}. \quad (4-54)$$

In order to solve the problem, the equation can be split to two parts: 1) where only boundary value is applied

$$\begin{cases} y'' + \alpha y' + \beta y = 0 \\ y(0), y'(0) \neq 0 \end{cases} \gg \text{Solution to the problem is } y_1, \text{ and} \quad (4-55)$$

2) where only initial conditions are applied, and based on superposition, the solution of the problem is the overall sum of the individual solutions

$$\begin{cases} y'' + \alpha y' + \beta y = f \\ y(0) = 0, y'(0) = 0 \end{cases} \gg \text{Solution to the problem is } y_2 \quad (4-56)$$

By applying superposition we have:

$$y = y_1 + y_2. \quad (4-57)$$

Therefore,

$$y''_1 + \alpha y'_1 + \beta y_1 + y''_2 + \alpha y'_2 + \beta y_2 = 0 + f = f. \quad (4-58)$$

Applying the boundary condition on a superposition basis yields:

$$y(0) = y_1(0) + y_2(0) = y(0) + 0. \quad (4-59)$$

$$y'(0) = y'_1(0) + y'_2(0) = y'(0) + 0 = y'(0). \quad (4-60)$$

As it was shown, both boundary condition and initial values satisfy the overall solution of  $y = y_1 + y_2$ , and therefore the solution to  $y$  is equivalent to individual solutions of  $y_1$  and  $y_2$ . As such the problem can be solved without the initial and/or boundary conditions and then the individual effects of boundary ( $y_2$ ) and initial condition ( $y_1$ ) be applied.

#### Appendix 4-C: Failure Analysis Formulations Based on the Presented Analytical Model

The yield function is defined as below:

$$F = q' - Mp' - C\beta; \quad (4-61)$$

where  $q'$  is the deviatoric stress, and  $p'$  shows the mean effective stress, and  $M$  represents the slope of yield envelope ( $q'$  vs  $p'$ ), and  $C$  is the cohesion factor. Both  $\beta$  and  $M$  are stress dependent parameters and  $q$  and  $p'$  are defined as:

$$q = \frac{\sigma'_1 - \sigma'_3}{2} \quad (4-62)$$

$$p' = \frac{\sigma'_1 + \sigma'_2 + \sigma'_3}{3} = \frac{\sigma_1 + \sigma_2 + \sigma_3}{3} - p; \quad (4-63)$$

where  $\sigma'_1, \sigma'_2, \sigma'_3$  are the effective principal stresses, and  $p$  is the pore pressure. For compression ( $\sigma_1 > \sigma_2 - \sigma_3$ )  $M$  and  $\beta$  can be written as below:

$$M = \frac{3\sin(\varphi)}{3 - \sin(\varphi)} \quad (4-64)$$

$$\beta = \frac{3\cos(\varphi)}{3 - \cos(\varphi)}; \quad (4-65)$$

where  $\varphi$  is the rock internal friction angle.

$F < 0$ , denotes elastic rock behavior, and therefore is a safer margin for the reservoir or caprock to be during steam injection. With the same analogy for a two-dimensional model, the above equations can be written for our problem as below, assuming the initial stress state in the reservoir is close to a normal fault regime; initial stress field displays a greater vertical stress than horizontal stress:

$$\sigma_z',^{initial} = \sigma_z^{initial} - p = (\rho_r - \rho_w)gh \quad (4-66)$$

$$\sigma_x',^{initial} = \frac{\vartheta}{1-\vartheta} \sigma_z',^{initial} = \left(\frac{\vartheta}{1-\vartheta}\right)(\rho_r - \rho_w)gh; \quad (4-67)$$

where  $h$  is the depth of zone of study from surface. Obviously for sequence of lithologies,  $\sum(\rho_i - \rho_w)h_i$  should be replaced with  $(\rho_r - \rho_w)h$

$$q = \frac{\sigma_x - \sigma_z}{2} = \frac{\Delta\sigma_x + \sigma_x^{ini} - (\sigma_z^{ini} + \Delta\sigma_z)}{2} = \frac{\left(\frac{\vartheta}{1-\vartheta} - 1\right)\Delta\rho gh + \Delta\sigma_x}{2}. \quad (4-68)$$

Depending on the location of temperature front,  $\Delta\sigma_x$  formulation will be different. Here, we write the deviatoric term for near field domain:

$$q = \frac{\left(\frac{\vartheta}{1-\vartheta} - 1\right)\Delta\rho gh - \frac{\alpha_T E \Delta T^I}{1-\vartheta^2} + \frac{1+2\vartheta}{1-\vartheta^2} \Delta P^I}{2} \quad (4-69)$$

$$p' = \frac{(1+\vartheta)\left[\left(\frac{\vartheta}{1-\vartheta} + 1\right)\Delta\rho gh + \Delta\sigma_x\right]}{3} - p. \quad (4-70)$$

It must be noted that  $p'$  shows the mean effective stress (tensor) and  $p$  shows local reservoir pore pressure (scalar). Therefore, to check the failure and stress state at a certain time after start of steam injection and at a particular location in the reservoir,  $q$  and  $p$  need to be calculated from the formula above, and if the below condition is satisfied, the reservoir rock behavior is in elastic state, and the injection process can be safely continued with the same constraints on the injection well, and under the same operating pressure and temperature:

$$q' < Mp' + C\beta. \quad (4-71)$$

## Appendix 6-A: Development of Coupling Interface/Tool

The main interface that was developed is a C++ based interface which links the decoupled geomechanical code (in Dumux and on the Dune platform) to the fluid flow code. This interface, unlike the interface between commercial software packages, does not work with “restart files” as an exchangeable file for initialization step of next sequential time steps. The interface exchanges properties between flow and geomechanics code by solution vectors within the frame of the code. Therefore a C++ routine has to be written in Dumux\_Geomechanics to output the vectors for Dumux\_Flow, and at the same time a routine was developed to read the solution vectors outputted by Dumux\_Geomechanics ( $\emptyset$ ,  $K$ ). **Figure 10-1** represent a snapshot of the interface developed for hydro mechanical purposes.

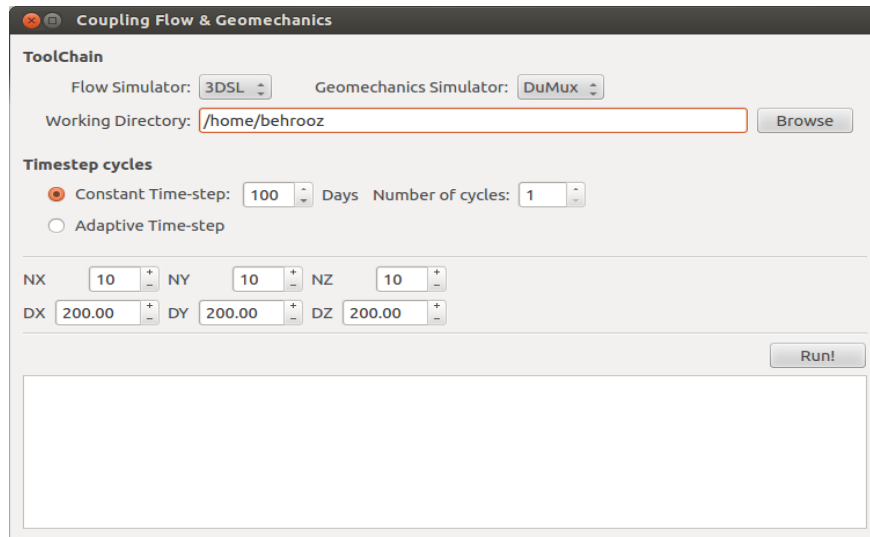


Figure 10-1- Graphical User Interface developed by QT programming language for hydromechanical coupling of streamline simulation with C++ geomechanical code.

The interactive structures of the sequentially coupled interface between streamline simulation and the C++ geomechanical codes, as well as the exchange parameters, are explained in the **Figure 10-2**. **Figure 10-3** shows the structure of the interface between geomechanical code and fluid flow code that are all developed in C++ platform (based on Box-Method discretization scheme) and are linked by QT and Matlab programming language.

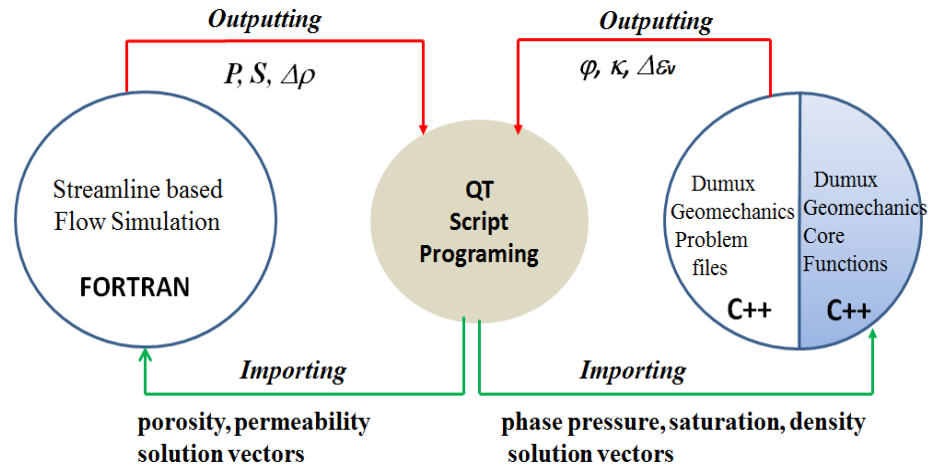


Figure 10-2-Schematic of interactive coupling between streamline simulation and geomechanical code.

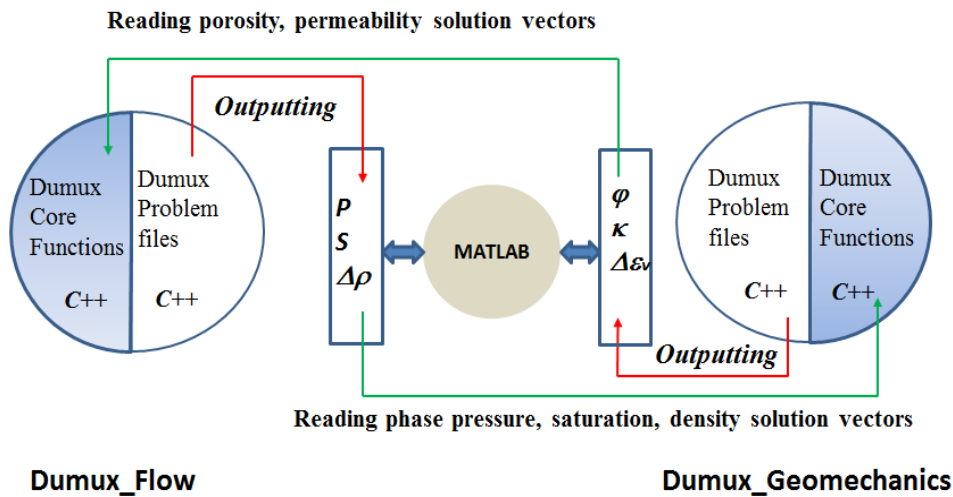



Figure 10-3-Schematic of interactive coupling between fluid flow simulation (FVE and FEM) and geomechanical code.

## Appendix 8-A: Development of Software for Reservoir-Geomechanics Coupling

The software was developed by QT (C++ based programming language) with a source code of almost 7000 lines. The tool is designed to implement all the methodologies in **Chapter 8** and **Chapter 9**. The GUI in the software can help one visually link the streamline simulator (3DSL) to the geomechanical engine (FLAC 3D). The software has the capabilities of adding/saving projects, selection the model directory and running all the five individual strategies on any desired model, illustrating pressure and dynamical petrophysical properties on each grid-cell at each coupling time step, and outputting individual CPU run times. The

user only requires making a source folder (0) with data file for initialization of each simulator; the rest of the workflow is fully automated. Pressure field and petrophysical data are read/mapped on the grid cell centers. Below is a brief introduction and run procedure of the developed tool:

- 1- Click on File > New Project 
- 2- Insert the project name and select path(directory) of project by Browse Button and Click OK.

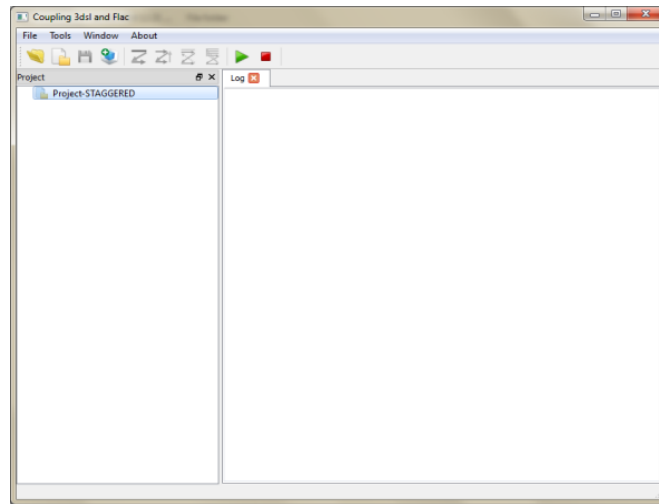



Figure 10-4-Illustration of step 1 and 2.

- 3- In the toolbar click on Add Model icon 
- 4- Insert the name of the model and select path of 3DSL Data File and Flac Data File using Browse buttons and then click OK.



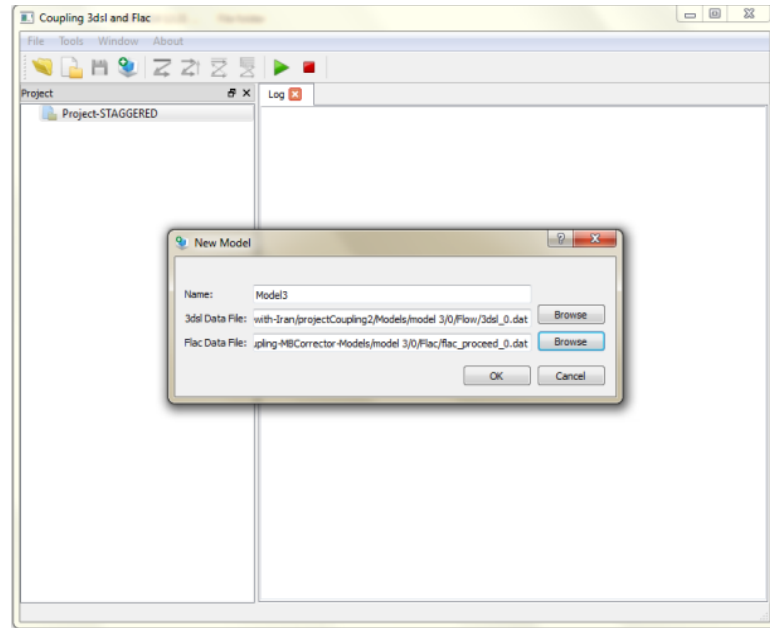
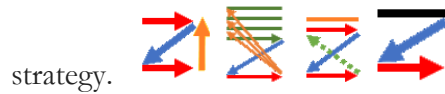


Figure 10-5- Illustration of steps 3 and 4.

- 5- From The Toolbar click on one of the “Coupling Icons” to select a coupling



strategy.

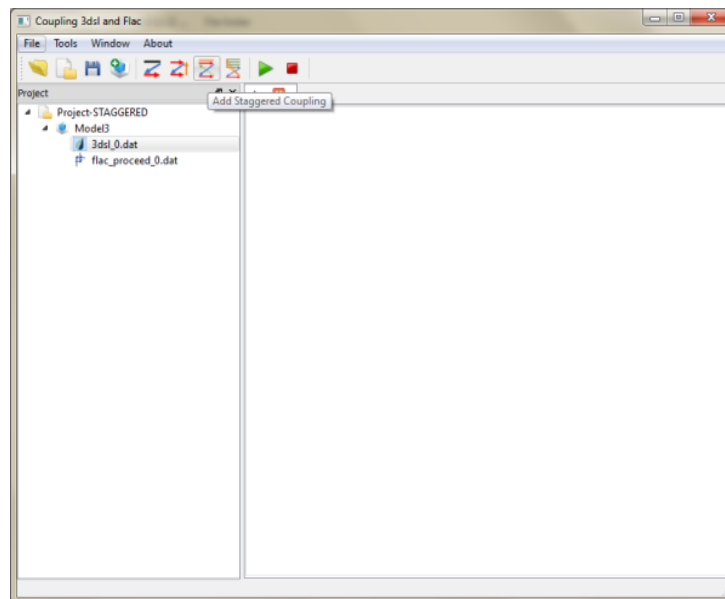


Figure 10-6-Representation of Step 5.

- 6- In the Coupling dialog box insert the values of run parameters and then click OK.
- 7- Double click on the name of coupling in Project panel to view/change the parameters in the Coupling Setting panel.

- 8- To perform the selected coupling strategy click on the Run Icon. 

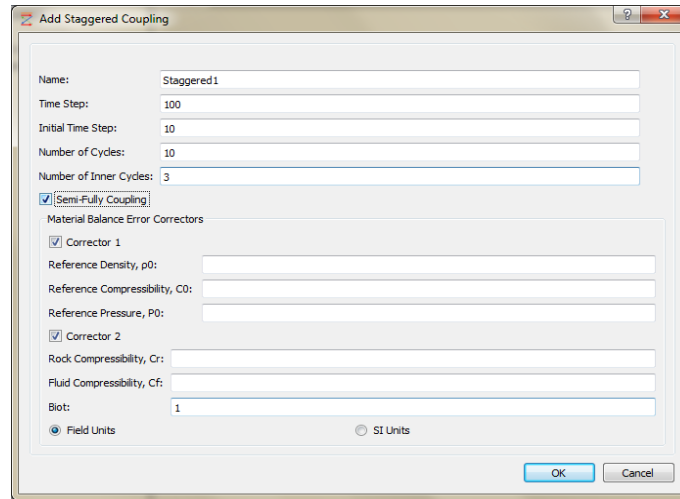



Figure 10-7- Illustration of steps 6, 7, 8.

- 9- If the path of \*.exe files are not set yet an error message box will display. To resolve this go to the Tools > Settings  and select the path of simulator executives and then click OK.
- 10- By clicking the Run button the Log tab will show the details (cycle directory, number, CPU time of each component of coupling, etc.) of coupling.

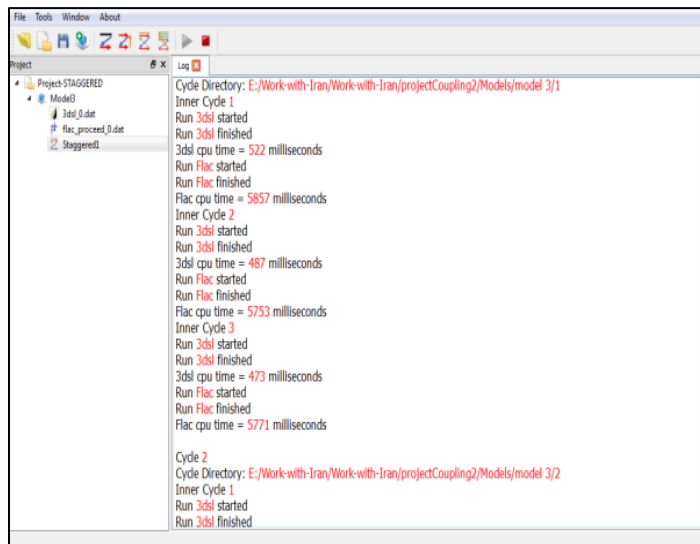
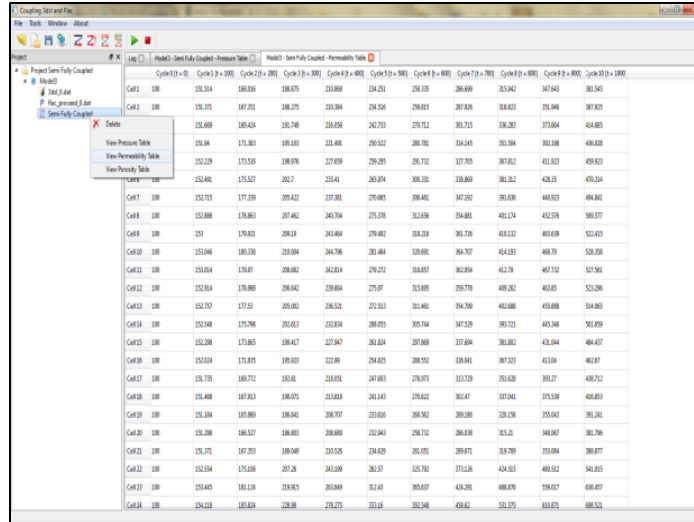



Figure 10-8-Illustration of Step 10.

- 11- One can select the View Porosity /View Permeability table by right click on the project , and displays all cell-based input output data (i.e. pressure, porosity , and permeability).



		Cycle 1 (3 = 300)	Cycle 2 (3 = 300)	Cycle 3 (3 = 300)	Cycle 4 (3 = 400)	Cycle 5 (3 = 500)	Cycle 6 (3 = 600)	Cycle 7 (3 = 700)	Cycle 8 (3 = 800)	Cycle 9 (3 = 900)	Cycle 10 (3 = 1000)
Cell 1	100	126.514	180.836	188.875	210.869	224.251	236.135	246.689	255.942	267.663	281.545
Cell 2	100	126.375	187.251	188.275	210.364	224.538	236.853	247.835	258.633	270.844	285.825
Cell 3	100	126.869	189.424	191.748	214.559	228.733	239.732	251.715	263.263	275.684	291.485
Cell 4	100	126.58	179.383	195.183	221.465	246.552	266.785	284.545	299.584	312.588	328.638
Cell 5	100	125.229	175.559	196.976	227.859	259.295	285.732	317.745	347.622	371.823	399.923
Cell 6	100	122.402	175.527	202.7	233.41	265.674	298.335	330.869	361.323	389.15	419.534
Cell 7	100	125.753	177.339	205.422	237.381	270.885	304.402	347.292	389.636	430.923	464.841
Cell 8	100	125.888	178.863	207.462	240.754	275.238	312.638	354.851	401.274	452.578	505.577
Cell 9	100	125	179.823	208.18	244.664	279.482	318.238	361.738	412.132	463.638	522.453
Cell 10	100	125.048	180.338	215.094	244.796	281.484	324.886	364.707	414.133	466.79	526.358
Cell 11	100	125.034	179.87	208.682	242.814	279.272	318.887	362.894	412.78	467.732	527.361
Cell 12	100	125.034	179.866	208.642	239.664	279.87	323.689	369.778	419.262	463.63	522.284
Cell 13	100	125.757	177.33	205.502	236.525	272.513	311.462	354.769	402.688	455.888	514.365
Cell 14	100	125.248	175.798	202.613	232.834	268.025	305.744	347.529	393.721	443.348	501.659
Cell 15	100	125.288	173.865	198.417	227.347	263.824	307.889	357.694	401.882	451.644	504.457
Cell 16	100	125.028	173.855	195.937	222.89	254.825	298.352	338.841	387.323	433.88	485.67
Cell 17	100	126.735	180.772	192.61	218.951	247.883	278.873	313.739	351.638	393.27	438.732
Cell 18	100	126.488	187.823	196.071	213.819	242.143	274.622	312.47	357.041	395.538	438.853
Cell 19	100	126.284	185.889	198.641	208.707	233.658	266.362	303.386	338.138	375.663	416.241
Cell 20	100	126.288	186.527	198.883	208.889	232.943	266.732	303.638	343.15	384.867	426.796
Cell 21	100	126.375	187.251	198.549	210.538	234.629	265.076	299.671	338.799	375.884	416.877
Cell 22	100	125.534	175.688	207.18	241.336	282.57	325.762	373.216	424.515	480.512	542.815
Cell 23	100	125.645	181.118	218.915	263.849	312.43	365.657	424.261	488.876	558.857	636.457
Cell 24	100	124.118	183.824	228.36	278.271	333.145	392.548	458.61	531.575	613.871	698.521

Figure 10-9-Illustration of Step 11.

12- One can save the project by clicking on the Save Icon 

13- One can open the saved project through File > Open Project. 